DIRECT MEASUREMENT OF PORE FLUID SUCTION IN GOLD MINE TAILINGS

JACOBUS HENDRIK FRANCOIS VAN HEERDEN

A dissertation submitted in partial fulfilment of the requirements for the degree of

MASTER OF ENGINEERING (GEOTECHNICAL ENGINEERING)

in the

FACULTY OF ENGINEERING, BUILT-ENVIRONMENT AND INFORMATION TECHNOLOGY

UNIVERSITY OF PRETORIA

October 2002

DISSERTATION SUMMARY

DIRECT MEASUREMENT OF PORE FLUID SUCTION IN GOLD MINE TAILINGS

JACOBUS HENDRIK FRANCOIS VAN HEERDEN

Supervisor: Professor E Rust
Department: Civil and Biosystems Engineering
University: University of Pretoria
Degree: Master of Engineering (Geotechnical Engineering)

A vast amount and variety of mine tailings are produced around the world each day. In the gold-mining industry in South Africa the residue of crushed ore is disposed of in large tailings or hydraulic fill dams. The outer walls of these dams are built up of layers of material, each of which is allowed to dry before the next layer is placed. In order to study the stability of these walls, the appropriate engineering properties of the tailings must be ascertained.

Due to the construction technique used in tailings dam construction, the outer walls are in an unsaturated state, which also means that suctions are generated within the tailings. Various techniques exist to measure suction, most of which are indirect methods. The recent development of the mid-plane suction probe at the University of Pretoria created the opportunity of measuring suctions directly on desiccating samples of gold mine tailings.

A test method has been developed from which soil mechanics parameters can be derived from suction measurements. The experimental programme consisted of a series of these newly developed tests on fine and coarse samples of gold mine tailings, as well as on different particle size ranges. The experimental results were used in the development of a new method of predicting the air-entry value, with only the grading of the tailings known. A new method of predicting the soil-water characteristic curve up to the air-entry value was also proposed.

The results of the research showed that the tailings remain saturated up to the air-entry value. The clay, fine silt and medium silt sized tailings was found to be the controlling particle size ranges in the development of suctions. The vast amount of parameters and information gained through the use of

the proposed test method clearly indicates its effectiveness in studying the performance and characteristics of a material drying from saturation. The results also indicated the effectiveness of the mid-plane suction probe for the direct measurement of suction.

Keywords: air-entry value, desiccation, gold mine tailings, particle size ranges, shrinkage, soil-water characteristic curve, suction, suction probe, unsaturated soils, water retention curve

ACKNOWLEDGEMENT

I wish to express my appreciation to the following organisation and persons who made this dissertation possible:

- Metago Environmental Engineers for their financial support.
- Professor E Rust, my supervisor, for his guidance and support.
- Mr J van Staden for his support in the laboratory.
- Dr N Vermeulen for the use of his samples.
- My family and friends for their encouragement and support during the study.
- Miss M Irving for her continuous motivation and confidence in my abilities.

TABLE OF CONTENTS

LIST OF TABLES

LIST OF FIGURES

LIST OF SYMBOLS

A	Area
c'	Effective cohesion
D	Depth/Diameter
D_{10}	Effective grain size
e	Void ratio
ϕ'	Effective angle of internal friction
g	Acceleration due to gravity
G_s	Specific gravity
H	Height
η	Dynamic viscosity
L	Length
M	Mass
$\dot{n}$	Porosity
π	Osmotic suction
θ	Volumetric water content
r	Radius
R_s	Radius of curvature
ρ	Density
S	Degree of saturation
σ	Total normal stress
σ'	Effective normal stress
T_s	Surface tension
τ	Shear stress
u	Pore pressure
u_a	Pore air pressure
u_w	Pore water pressure
(u_a-u_w)	Matric suction
υ	Terminal velocity
V	Volume
w	Moisture/water content (gravimetric)
ψ	Total suction

CHAPTER 1:

INTRODUCTION

1.1 Background

South Africa is one of the world's largest gold producing countries. The extraction and processing of gold ores result in the generation of large volumes of fine-grained powder-like residues, known as tailings. Tailings are disposed of into structures called tailings dams. Many catastrophic failures of these dams have occurred in the past, not only in South Africa, but also across the world. These failures can easily lead to the loss of human life and have a negative impact on the environment.

Due to the climatic conditions in South Africa, the upper layers and walls of tailings dams are in an unsaturated state. Negative pressures or suctions are generated within the soil, resulting in an increase in strength. Many researchers have worked on unsaturated soils in the past, which has resulted in the development of a conceptual framework for unsaturated soils. The measurement of suctions has traditionally been made using indirect methods. These methods are unable to accurately represent, for example, the actual drying process of a soil. Only a few methods of measuring suctions directly exist, mainly due to the problem caused by cavitation.

The recent development of the mid-plane suction probe at the University of Pretoria presented the opportunity to conduct laboratory tests on gold tailings samples using a direct method of measuring suctions. Few test methods have been developed which incorporates the suction probe, each with its own difficulties and shortcomings. There thus exists the need for a new test method that overcomes the difficulties and shortcomings encountered in the previous methods. Very little research has been performed in the past to investigate the effect that different particle size ranges will have on suctions within whole tailings samples.

1.2 Objectives

- Investigate the correct use of the mid-plane suction probe and perform a calibration.
- Develop an appropriate test method of obtaining the various soil mechanics properties of gold tailings samples at different suctions.
- Investigate the effect that different gradings of gold tailings will have on suction.

- Investigate the effect that different particle size ranges will have on suction.

1.3 Scope

- The material tested comprised of gold tailings from Vaal River Operation's Pay Dam and Mizpah tailings dams. The results obtained might thus not be applicable to all gold tailings.

- Measurements of suction were made using a mid-plane suction probe with a capacity of measuring suctions directly up to about 350 kPa due to the type of ceramic used.

- The experimental work was only carried out on gold tailings undergoing air-drying from saturation.

- The manner in which particle size ranges were separated does in no way guarantee that the process was accurate.

1.4 Methodology

- Select a proper method of measuring suctions directly. Investigate the proper use and performance of the mid-plane suction probe and perform a calibration.

- Develop a test procedure from which relevant soil mechanics parameters on desiccating samples of slurried gold tailings can be gained, together with suction measurements.

- Perform experimental work on different types of gold mine tailings using the developed test method.

- Draw meaningful conclusions from the test results.

1.5 Organisation of the Report

The report consists of the following chapters and appendices:

- Chapter 1 serves as an introduction to the report.
- Chapter 2 contains a technical introduction to suctions and gold mine tailings based on a literature study.
- Chapter 3 discusses the development of a test method to relate various soil mechanics parameters to suctions.
- Chapter 4 contains the laboratory data obtained from experimental work on the selected samples of gold mine tailings.
- Chapter 5 serves as a discussion on the results obtained from the experimental work.
- Chapter 6 contains the conclusions of the study.
- The list of references follows at the end of the report.
- Appendix A serves as an extension to Chapter 4.

CHAPTER 2:

LITERATURE STUDY

2.1 Introduction

Soil mechanics in the past has been mainly concerned with saturated soils. In recent times it has been realised that attention should also be given to soils in an unsaturated state. Problem soils encountered in engineering practise usually do not behave consistently with the principles and concepts of classical, saturated soil mechanics, due to the presence of more than two phases.

The general field of soil mechanics can thus be subdivided into two categories: Saturated soil mechanics and Unsaturated soil mechanics due to their differences in behaviour and nature. An unsaturated soil has more than two phases, and the pore-water pressure is negative relative to the pore-air pressure. In a relatively dry environment, any soil near the ground surface will be subjected to negative pore pressures.

An unsaturated soil has three phases, namely solid, water and air phases. Fredlund and Morgenstern (1977) found that it might be more correct to add a fourth phase, namely the air-water interface or contractile skin. Water and the soil particles are assumed to be incompressible, whereas the presence of even a small volume of air will result in a compressible unsaturated soil sample due to the compressibility of air.

Climate plays an important role in whether a soil is saturated or unsaturated. Evaporation and evapotranspiration results in the removal of water from soil near the ground surface. However, precipitation will result in the addition of water to the soil. The difference between these processes will govern the pore-water pressure conditions in the soil.

The changes in pore-water pressures will result in changes in the volume and shear strength of the soil. Upon wetting, some soils will swell or expand, and some soils will show a loss in shear strength. Examples of this are seen on a relatively frequent basis when heavy rains causes houses to crack and slopes to fail.

Examples of the types of problems encountered in unsaturated soil mechanics are:

- Construction and Operation of Earth and Tailings Dams
- Natural Slopes Subjected to Environmental Changes
- Stability of Vertical or Steep Excavations
- Ground Movements Involving Expansive Soils

There are many practical situations involving unsaturated soils that require the understanding of the seepage, volume change and shear strength characteristics.

2.2 Phase Properties

An unsaturated soil consists of four phases: soil particles, water, air and the contractile skin (Fredlund and Morgenstern, 1977). When the air phase is continuous, the contractile skin interacts with the soil particles and provides an influence on the mechanical behaviour of the soil. An element of unsaturated soil with a continuous air phase is idealised in Figure 2.1.

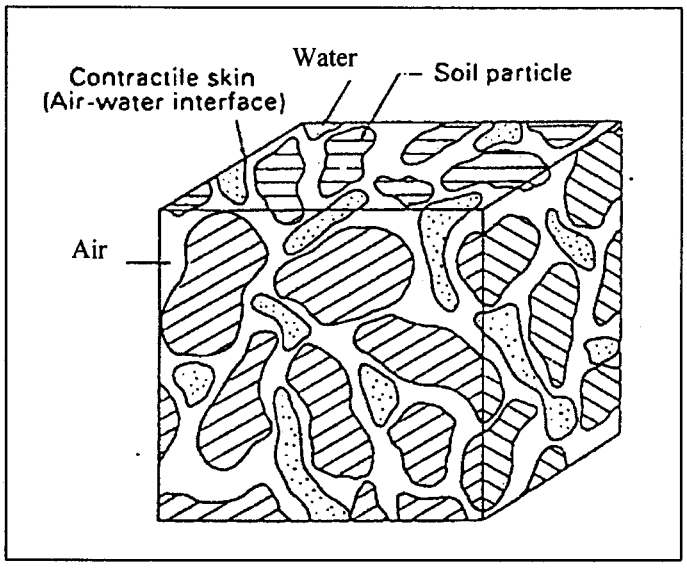

Figure 2.1: An element of unsaturated soil with a continuous air phase (after Fredlund and Rahardjo, 1993)

The thickness of the contractile skin is in the order of a few molecular layers; therefore the physical subdivision of the contractile skin is unnecessary when establishing volume-mass relations for an unsaturated soil. The most important property of the contractile skin is its ability to exert a tensile pull, which is referred to as surface tension.

2.2.1 Surface Tension

The contractile skin encountered in an unsaturated soil possesses a property called surface tension. This phenomena result from the intermolecular forces acting on molecules in the contractile skin. A

molecule in the interior of the water experience equal forces in all directions, while a molecule in the contractile skin experiences an unbalanced force towards the water (Figure 2.2(a)). In order for the contractile skin to stay in equilibrium, a tensile pull is generated. This property is called surface tension, T_s. Surface tension is tangential to the contractile skin surface. The contractile skin acts as an elastic membrane and assumes a concave curvature towards the larger pressure (also referred to as a meniscus). The pressure difference across the curved surface can be related to the surface tension and the radius of curvature of the surface by considering equilibrium across the contractile skin (Figure 2.2(b)).

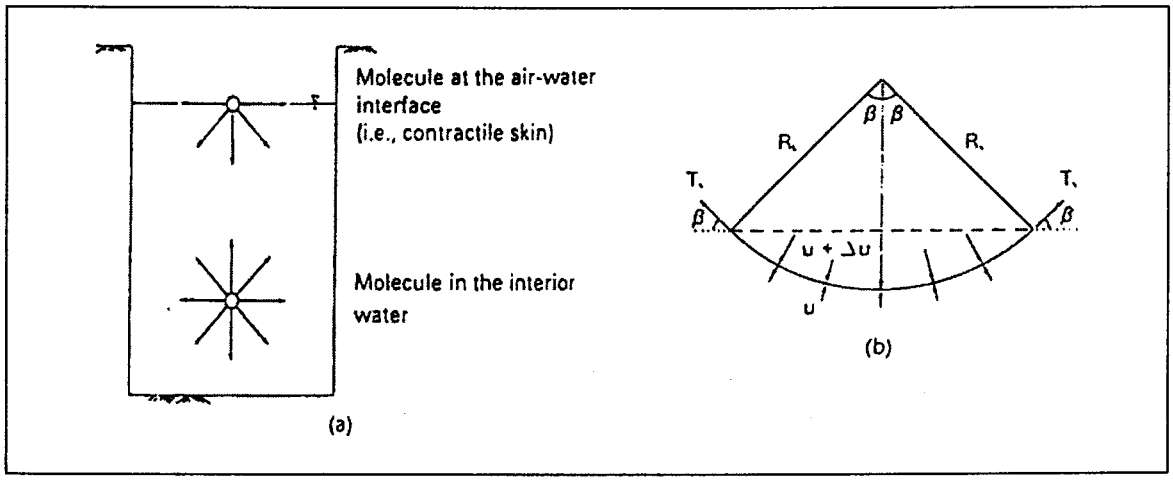

Figure 2.2: Surface tension phenomenon at the contractile skin. (a) Intermolecular forces on contractile skin and water; (b) pressures and surface tension acting on a curved two-dimensional surface (after Fredlund and Rahardjo, 1993)

The pressures acting on the contractile skin are u and (u + Δu), it has a radius of curvature of R_s, and a surface tension, T_s. Horizontal forces along the membrane are balanced, and thus force equilibrium in the vertical direction requires that

$$2.T_s.\sin\beta = 2.\Delta u.R_s.\sin\beta \qquad [2.1]$$

Where:

Δu = pressure difference across a two-dimentional curved surface

$2\ R_s \sin\beta$ = length of the contractile skin projected onto the horizontal plane

Equation 2.1 can be rearranged to give

$$\Delta u = \frac{T_s}{R_s} \qquad [2.2]$$

Equation 2.2 can be extended to a three-dimensional membrane using the Laplace equation. If the radius of curvature is the same in all directions, Equation 2.2 becomes

$$\Delta u = \frac{2T_s}{R_s} \qquad [2.3]$$

In an unsaturated soil, the contractile skin would be subjected to an air pressure, u_a, and a water pressure, u_w. The air pressure would be greater than the water pressure, and the difference, $(u_a - u_w)$, is referred to as matric suction. Equation 2.3 now becomes

$$(u_a - u_w) = \frac{2T_s}{R_s} \qquad [2.4]$$

Where:

$(u_a - u_w)$ = matric suction acting on the contractile skin

Equation 2.4 is referred to as Kelvin's capillary model equation. As the matric suction of a soil increases, the radius of curvature decreases. As the matric suction of a soil decreases, the radius of curvature increases.

2.2.2 Capillarity

The maximum negative pressure (u_w) that can be attained in large tubes is limited by the vapor pressure of water, which is about 99 kPa gauge pressure at 20 °C. When the pressure goes below this value, water will cavitate and measurement of the pressure becomes quite difficult due to the phase change from liquid to gas. The equivalent capillary tube diameter at the vapour pressure is about 3 μm (Holtz and Kovacs, 1981). If the tube is smaller than this diameter, then the water cannot cavitate because the surface tension is too high and a bubble cannot form. In this case the pore-water tension can be much greater than 100 kPa.

Even though soils are random assemblages of particles and the resulting voids are similarly random and irregular, Taylor's capillary tube analogy helps explain capillary phenomena observed in soils. In principle, capillary or negative pressures and capillary rise will be similar in soils and in glass tubes. Figure 2.3 shows a series of capillary tubes.

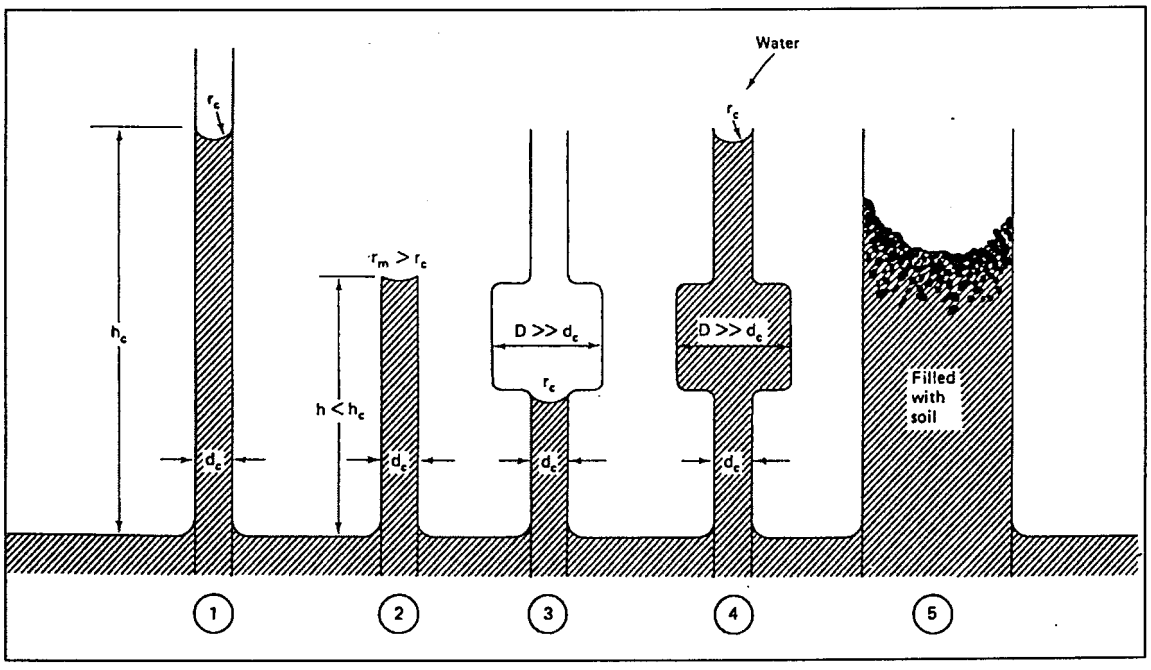

Figure 2.3: Capillary rise in tubes of different shapes (after Taylor, 1948)

Tube 1 has a diameter, d_c, a corresponding height of capillary rise, h_c, and radius of curvature, r_c. in tube 2 the height of the tube is h which is smaller than the height of tube 1, h_c. The water will try to rise to h_c but cannot. Thus the radius of curvature in tube 2 will be greater than r_c since it is impossible for the corresponding capillary pressure to develop (Equation 2.4). In tube 3 a large void exists, and there is no way for the water to be pulled above a void with a diameter greater than d_c. However, if as is shown in tube 4 water infiltrates from the top, then it is possible for the contractile skin to support the entire column of water. Tube 5 is filled with soil, and the water would rise to the surface of the soil since the average pore diameter is much less than d_c. The contractile skin hangs on the particles, which increases the contact forces between the particles. An illustration of two soil particles connected by contractile skins is shown in Figure 2.4.

In soils, it is common to assume the effective or average pore diameter is about 20 % of the effective grain size, D_{10} (Holtz and Kovacs, 1981). Using this assumption it is possible to estimate a theoretical capillary pressure for a soil. This assumption shows the importance of pore size, and not grain size, as the controlling factor.

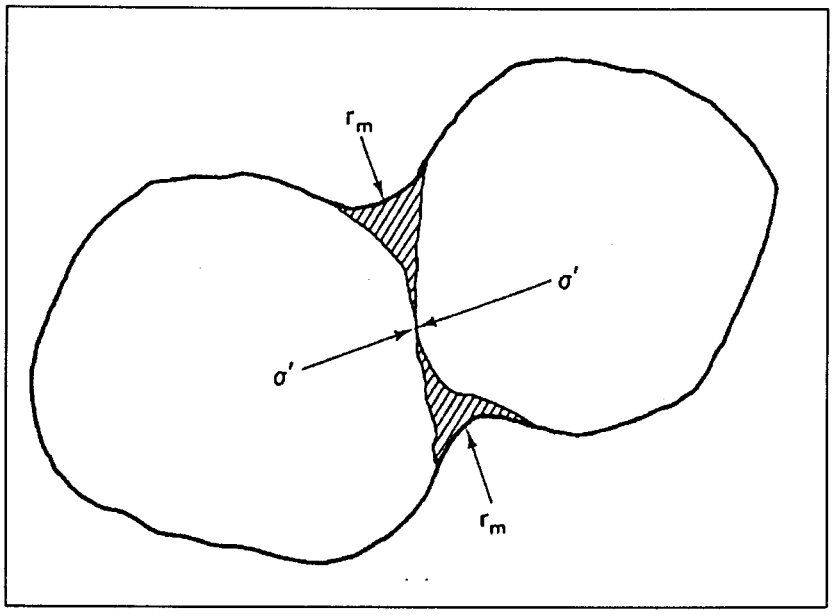

Figure 2.4: Two soil particles held together by a capillary film (after Holtz and Kovacs, 1981)

The effective stress, σ', is defined as the total stress σ minus the pore-water pressure u.

$$\sigma' = \sigma - u \qquad [2.5]$$

When a soil sample is allowed to dry out on its own, the sample is acted on by atmospheric pressure. The total stress σ = 0 (zero gauge pressure). Then the effective stress σ' = - u. In unsaturated soils the pore-water pressure is negative, thus σ' = u.

Capillarity is an important phenomenon in unsaturated soil mechanics. It should however be noted that some of the voids in natural soils are large enough that the water can vaporise and bubbles can form. Thus, menisci or contractile skins are destroyed and the actual height of capillary rise is reduced.

At the top of the soil-water column, the tension in the water pulls the grains of soil together. The greater the capillary tension or suction, the greater the inter-particle contact stress, and therefore a higher frictional resistance develops between the particles.

An example of capillarity can be seen when excavations are made in silts and very fine sands. These materials would readily fall to their natural angle of repose if they were dry. Below the ground water table, excavations in granular soils will collapse since the menisci do not exist there. Above the

ground water table and within the zone of capillarity, capillary menisci at the surface of the excavation provide the stability for the cut. However, such excavations are extremely unstable. They can collapse due to even very slight vibrations or the rising of the water table.

2.2.3 Shrinkage

Terzaghi (1927) introduced an analogy to explain how capillary stresses cause shrinkage in clay soils. The analogy involves a horizontal tube with compressible elastic walls shown in Figure 2.5. In (a) the tube at the start is completely filled with water and the radius of the contractile skin is very large. As evaporation occurs, pressure in the water decreases and the radius also start to decrease as is shown in (b). As evaporation continues, the radius becomes smaller and smaller, the compression in the compressible walls of the tube increases, and the tube shrinks in length as well as in diameter. The limiting case, shown in (c), is when the radius of the contractile skin is at a minimum, which is one-half of the tube diameter. The negative pressure or the suction in the tube is then equal to the value computed in Equation 2.4, and the walls of the tube have shrunk to an equilibrium condition between the rigidity of the walls and the capillary forces. If the tube is immersed in water, the contractile skin is destroyed and the tube can expand because the suction acting on the tube walls is destroyed.

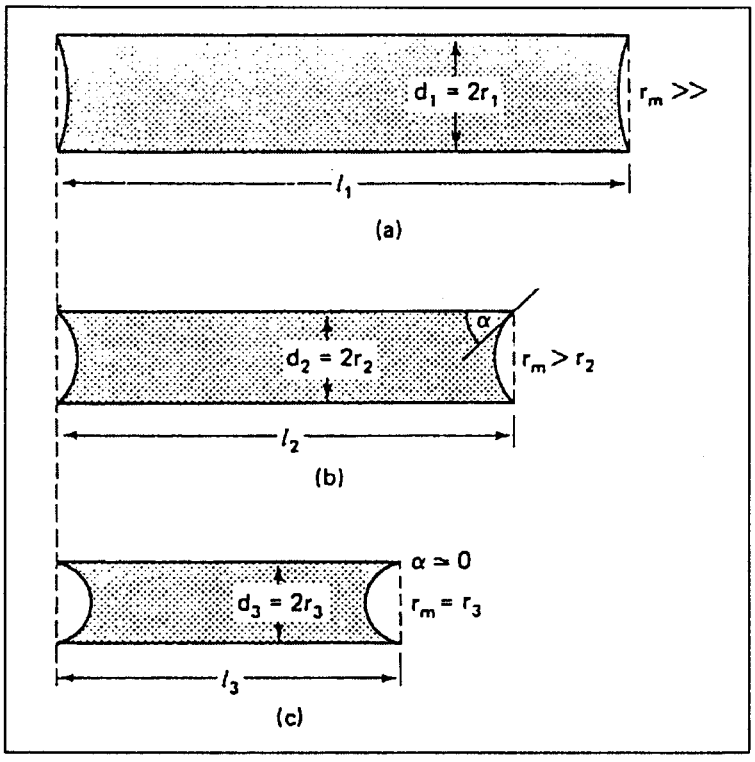

Figure 2.5: Compressible elastic capillary tube shrinkage due to evaporation and surface tension (after Terzaghi, 1927)

A soil sample slowly drying (undergoing desiccation) will form contractile skins between the individual soil particles. As a result the effective stresses will increase and the soil will decrease in volume. As shrinkage continues, the contractile skin radius becomes smaller and the suction will increase, with a further reduction in volume. A point is then reached where no further volume reduction occurs, but with the degree of saturation still essentially at unity. The water content at which this occurs is defined as the shrinkage limit (SL). At this point the contractile skin just start to retreat below the soil surface, and the colour of the surface changes from a shiny one to a dull appearance. The suction value at which the SL is reached, corresponds to the air-entry value of the material.

The shrinkage limit is calculated from

$$SL = \left(\frac{V_{dry}}{M_s} - \frac{1}{\rho_s} \right) \rho_w \times 100 \qquad [2.6]$$

Where:

V_{dry} = Dry volume of the soil sample
M_s = Oven dry mass of soil sample
ρ = Density

Equation 2.6 corresponds to Figure 2.6.

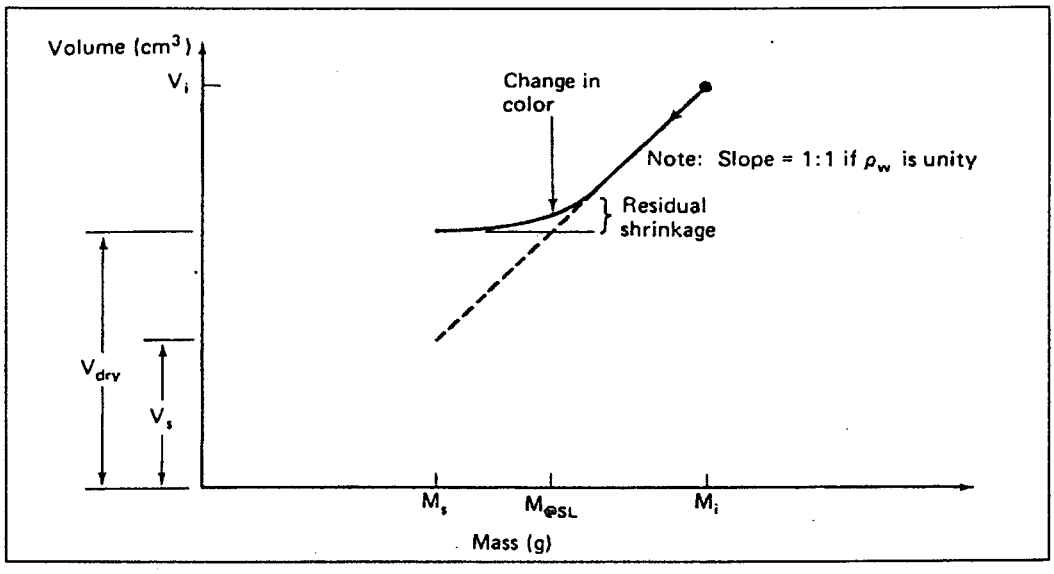

Figure 2.6: Determination of the shrinkage limit based on total mass (after Holtz and Kovacs, 1981)

2.3 Suction

The total suction, ψ, of a soil is made up of two components, namely, the matric suction, $(u_a - u_w)$, and the osmotic suction, π:

$$\psi = (u_a - u_w) + \pi \qquad [2.7]$$

Any change in suction affects the overall equilibrium of the soil mass. Changes in suction may be caused by a change in either one or both components of soil suction.

2.3.1 Matric suction

Matric suction is closely related to the surrounding environment. The in-situ profile of pore-water pressures (and thus matric suction), may vary from time to time. The variation in the soil suction profile is generally greater than variations commonly occurring in the net normal stress profile. Variations in the suction profile depend upon several factors, as illustrated by Blight (1980).

- **Ground surface condition.** The matric suction profile below an uncovered ground surface is affected significantly by environmental changes. The opposite is true for a covered ground surface.

- **Environmental conditions.** The matric suction in the soil increases during dry seasons and decreases during wet seasons.

- **Vegetation.** Vegetation on the ground surface has the ability to apply a tension to the pore-water of up to 2 MPa through the evapotranspiration process. This process removes water from the soil thus increasing the matric suction.

- **Water table.** The depth of the water table influences the matric suction. The deeper the water table, the higher the possible matric suction.

- **Permeability of the soil.** The permeability of a soil represents its ability to transmit and drain water. This, in turn, indicates the ability of the soil to change matric suction as a result of environmental changes.

2.3.2 Osmotic suction

Osmotic suction is related to the salt content in the pore-water, which is present in both saturated and unsaturated soils. Osmotic suction changes have an effect on the mechanical behaviour of a soil. If the salt content in a soil changes, there will be a change in the overall volume and shear strength of the soil.

Most engineering problems involving unsaturated soils are commonly the result of environmental changes. These changes primarily affect the matric suction component. Osmotic suction changes are generally less significant. Generally osmotic suction is ignored, and a change in matric suction is equivalent to a change in total suction. In the case where the salt content of the soil is altered by chemical contamination, the effect of the osmotic suction change on the soil behaviour may be significant. In this case, it is necessary to consider osmotic suction as part of the stress state.

2.3.3 Conventional measurement of suction

Soil suction is commonly referred to as the free energy state of soil water (Edlefsen and Anderson, 1943). The free energy of the soil water can be measured in terms of the partial vapour pressure of the soil water (Richards, 1965). The soil suction as quantified in these terms is commonly called total suction and is the sum of both the matric and osmotic suction components. There exists various techniques and methods of measuring total suction, matric suction and osmotic suction separately. Table 2.1 lists the more common methods of suction measurement together with their measurement ranges and response times.

The suction range of filter paper covers the whole spectrum of measurable suction. They are suitable for both laboratory and in-situ applications. However, their response or equilibrium time is much too long. Problems have also been experienced with the accuracy of this method.

The psychrometer can reach equilibrium within a couple of minutes. Its suction range is fairly large, although the lower limit is at 100 kPa. The instrument is extremely fragile, has bad conformance and may only be used in the laboratory.

Thermal blocks have the advantage that they are able to measure matric suction in-situ. However, the response time of this method varies from 1 day to 3 weeks, which is unsuitable in a rapid moisture-

changing environment. They are fragile instruments, susceptible to failure and are adversely affected by saline effects.

Table 2.1: Common Suction Measurement Devices

Instrument	Suction Component	Suction Range (kPa)	Response Time
Filter Paper (Ho, 1979; McKeen, 1981; Chandler and Gutierrez, 1986)	Total and Matric	10 to 30 000	7 days
Psychrometer (Richards, 1965; Rawlins and Dalton, 1967)	Total	100 to 8 000	Minutes
Suction Plate (Ridley, 1993)	Matric	0 to 90	Several hours
Pressure Plate (Schofield, 1935)	Matric	0 to 1 500	Several hours
Thermal Blocks (Sattler and Fredlund, 1989)	Matric	0 to 400	24 hours to 3 weeks
Gypsum Blocks (Aitchison et al, 1950)	Matric	100 to 1 000	2 to 3 weeks
Tensiometer (Ridley et al, 1998)	Matric	0 to 90	Up to 2 hours
Imperial College Suction Probe (Ridley and Burland, 1993)	Matric	0 to 1 800	1 to 3 hours

Gypsum blocks are cheap and easy to use. They are able to measure a large range of suctions, but with a lower limit of 100 kPa. Their response time is extremely long, which makes them unsuitable instruments in an environment where moisture changes occur. Measurements are also influenced by salinity.

The suction plate has a response time of a few hours. It is also unaffected by salinity and may only be used in the laboratory. The apparatus can only measure suctions up to 90 kPa, which is its main limitation.

The pressure plate uses axis translation to measure suctions above 90 kPa to about 1 500 kPa. It is very similar to the suction plate. The effect that axis translation has on measurements of suction has not yet been determined.

The tensiometer may be used in-situ as well as in the laboratory, and is unaffected by salinity. The response of the instrument is fairly good, although it can only measure suctions up to 90 kPa.
The Imperial College suction probe is applicable to both laboratory and in-situ measurements and is unaffected by salinity. The response time for laboratory measurements is one hour, while the response time for in-situ measurements is 3 hours. It must however be noted that 90 % of the final suction is reached within a few minutes.

2.3.4 The mid-plane suction probe

The mid-plane suction probe was designed and constructed by Theron (2000). The probe incorporates a sub miniature Kyowa PS 2KA pressure transducer (Figure 2.7). The pressure transducer is embedded in a cavity leaving a gap of 0.1 mm for the water reservoir between the surface of the transducer and a 3 bar (300 kPa) ceramic. The body of the probe is machined from stainless steel. The water reservoir has a volume of 2.8 mm^3 that will inhibit the formation of air bubbles in the reservoir (cavitation), thereby increasing the range of suction measurement beyond 90 kPa (Ridley and Burland, 1993).

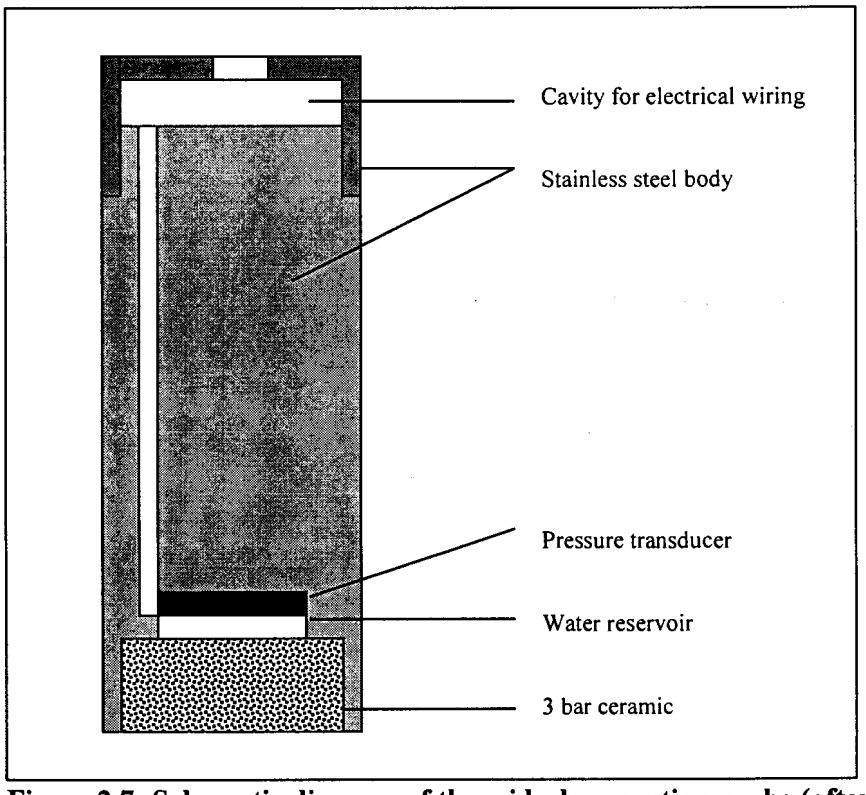

Figure 2.7: Schematic diagram of the mid-plane suction probe (after Theron, 2000)

Placing the probe in a volumetric flask partly filled with de-aired water and applying a vacuum for two hours de-aired the probe after it was constructed. The probe was then placed in a triaxial cell and cyclic pressures from 50 to 350 kPa were applied to the cell water for 24 hours to saturate the probe. The probe is able to measure suctions up to the air-entry value of the ceramic, which is between 350 and 400 kPa. Theron (2000) made no mention of the response time of the probe, but as it is very similar to a tensiometer and the Imperial College suction probe, it is assumed that the response time will be in the same order.

Theron (2000) used the mid-plane suction probe to measure suctions in gold mine tailings. Tests were developed to obtain soil-water characteristic curves for the tailings samples, but failed due to inaccurate measurements of volume change. The research, however, showed that the mid-plane suction probe is a useful and effective instrument for the direct measurement of suctions.

2.4 The Soil-Water Characteristic Curve

2.4.1 Introduction

The soil-water characteristic curve (SWCC), also commonly known as the water retention curve, may be defined as the variation of suction with the water storage capacity within the macro and micro pores of a soil. The curve is generally plotted as the variation of gravimetric water content, w, or volumetric water content, θ, or degree of saturation, S, with suction. The volumetric water content is calculated from:

$$\theta = n.S \qquad [2.8]$$

Where:

n = porosity

S = degree of saturation

The SWCC provides a conceptual framework in which the behaviour of unsaturated soils can be understood (Barbour, 1998). The suction may be either matric or total suction. Figure 2.8 (a) shows a typical soil-water characteristic curve plotted as the degree of saturation versus matric suction. The

air-entry value of the soil and the residual degree of saturation, S_r, are also shown. Beyond the air-entry value the soil starts to desaturate. The suction increases as desaturation continues. The rate of desaturation considerably decreases beyond a particular level of suction. The degree of saturation at this value of suction is called the residual degree of saturation, S_r. The SWCC can also exhibit hysteresis; however, this feature is not discussed within this paper. The reader is referred to more detailed descriptions of hysteretic behaviour provided by Fredlund and Rahardjo (1993). The SWCC plays a role for unsaturated soils similar to that played by the consolidation curve for saturated soils.

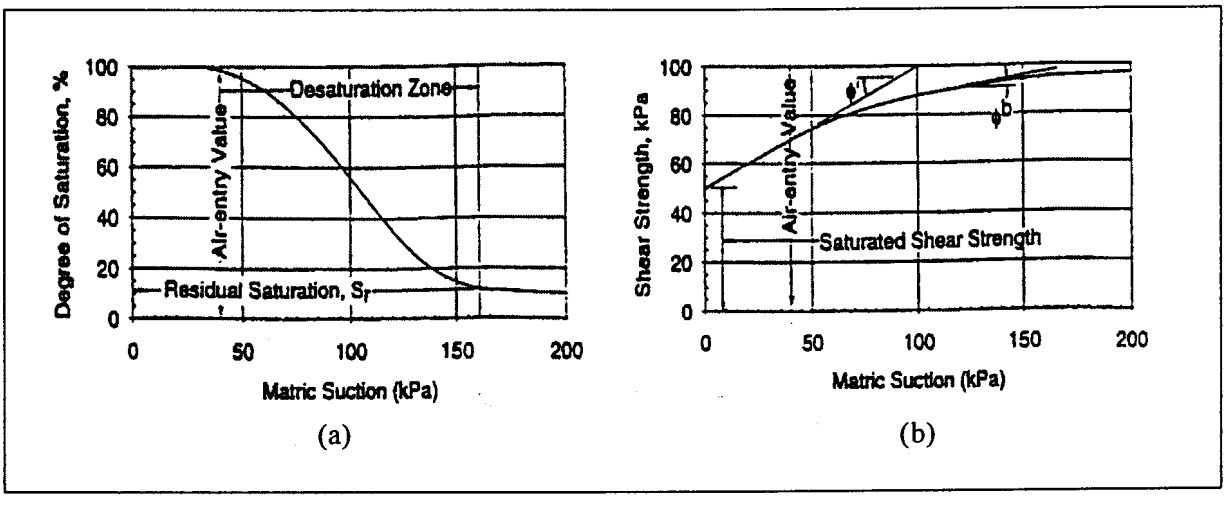

Figure 2.8: Relationship between soil-water characteristic curve and shear strength. (a) Matric suction versus degree of saturation; (b) Matric suction versus shear strength (after Fredlund et al, 1995)

Figure 2.8 (b) shows a typical relationship between shear strength and increasing soil suction. The relationship between the shear strength and the soil-water characteristic curve can be seen by comparing Figure 2.8 (a) and (b). The rate of desaturation with respect to an increase in matric suction, (i.e. $dS/d(u_a - u_w)$) is greatest between the air-entry value and residual suction.

The shear strength contribution due to matric suction is primarily through the water inter-aggregate contact area. As there is little change in water content of the soil below the air-entry value, suction as a stress state variable is as effective as net normal stress in mobilizing the shearing resistance along all the contact area points. This implies that ϕ^b is equal to ϕ'. Above the air-entry value, the contribution of shear strength by suction decreases with the desaturation of the soil and results in a nonlinear variation of shear strength with respect to suction. Thus, there is a strong correlation between the shear strength behaviour of an unsaturated soil and the soil-water characteristic curve.

A general characterization of the SWCC can be illustrated using a series of SWCCs as shown in Figure 2.9. It is evident that as we move from a uniform sand to a clay (Figure 2.9 (a)), the decrease in grain size and the increase in gradation lead to an increase in the air-entry value and a flattening of the slope of the curve. Consolidation of a slurried silt sample leads to a decrease in the size of the largest pores, resulting in an increase in the air-entry value (Figure 2.9 (b)), although the curves for the silt under various loads become coincident at higher suctions, where the pore sizes are relatively unaffected by consolidation (Lapierre et al, 1989). Figure 2.9 (c) shows that the compaction of a fine-grained, clay soil at dry of optimum water contents leads to a lower air-entry value than compaction wet of optimum due to the more open macropores provided by the more aggregated structure in the sample compacted dry of optimum (Benson and Daniel, 1990).

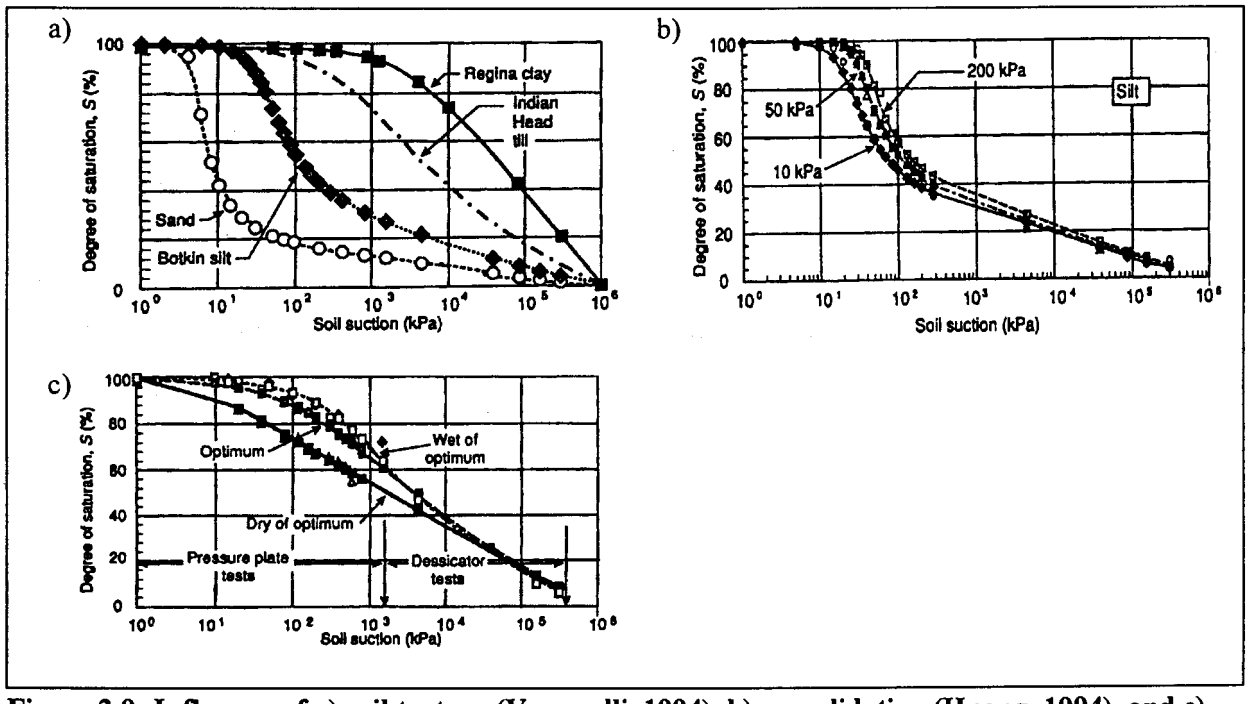

Figure 2.9: Influence of a) soil texture (Vanapalli, 1994), b) consolidation (Huang, 1994), and c) compaction (Vanapalli, 1994) on the SWCC

2.4.2 The air-entry value

One of the main parameters that can be obtained from the SWCC is the air-entry value (AEV), which represents the matric suction, $(u_a - u_w)$, at which the largest pores in the material start to drain (Aubertin et al, 1998). This point corresponds to the shrinkage limit (SL) of the soil as discussed in

Section 2.2.3. In general, it is expected that the AEV fall within the following range (e.g. Kovacs, 1981):

- 0.2 to 1 kPa for coarse sands
- 1 to 3.5 kPa for medium sands
- 3.5 to 7 kPa for fine sands
- 7 to 25 kPa for silts
- More than 25 kPa for clays

The most common method for the determination of the AEV is the one proposed by Brooks and Corey (1964). This method incorporates the effective volumetric water content, θ_e:

$$\theta_e = \frac{(\theta - \theta_r)}{(\theta_s - \theta_r)} \qquad [2.9]$$

Where:

θ_r = the residual value of θ

θ_s = the value of θ at saturation, which is equal to the porosity, n, of the material

This method is based on the assumption that the θ_e - $(u_a - u_w)$ relationship (in a semi-logarithmic plot) can be idealized by two straight lines, one horizontal and one inclined. The intersection between these two lines gives the suction corresponding to the start of desaturation (AEV (BC)), as shown in Figure 2.10. However, some adjustments may be required for the θ_r-value to ensure that the results obey this idealized representation of the SWCC; the moved points in Figure 2.10 represent such adjustments.

Another method of obtaining the AEV was proposed by Aubertin et al (1998). It is based on the fact that around the AEV, some continuous air channels are created within the material (Kovacs, 1981). This often occurs for a saturation ratio S of about 90 %. Thus the AEV is the suction where θ is equal to $0.9\theta_s$ (AEV(90)). The main advantage of this method is its simplicity, as it does not require any calculations or adjustments of results.

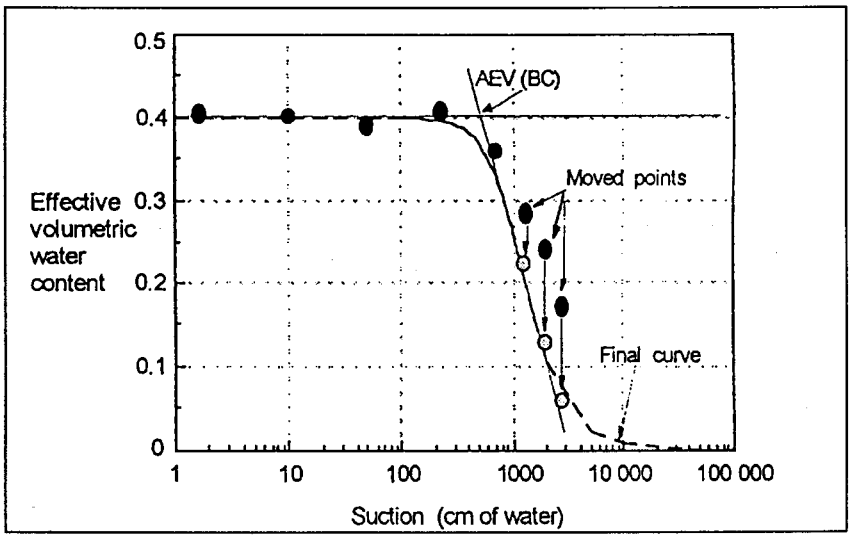

Figure 2.10: Determination of the air-entry value (AEV) according to the procedure proposed by Brooks and Corey (1964)

In many situations, it may be useful to have an estimate of the AEV, knowing only some basic properties of the material. Aubertin et al (1998) found that a generalization of the Polubarinova-Kochina equation, presented in Bear (1972), represents the data fairly well. This simple expression is written as follows:

$$AEV = \frac{b}{e.D_{10}} \qquad [2.10]$$

Where:

b = a constant that varies according to the method used to determine the AEV. For AEV (BC) the average value of b is 2.5 mm^2, whereas it is 4 mm^2 for AEV (90)

e = the void ratio of the soil

D_{10} = the diameter for which 10% by weight passed the sieve having an opening size D (in mm)

2.4.3 Prediction of the soil-water characteristic curve

Many models have been proposed to describe the SWCC. Fitting empirical functions to experimental data developed most of these. Several early methods were developed to determine the SWCC, such as Brooks and Corey (1964), Van Genuchten (1980) and Kovacs (1981). Most of these methods are only

applicable to certain suction ranges and soils. Fredlund and Xing (1994) proposed an equation that is based on the assumption that the shape of the SWCC is governed by the pore-size distribution of the soil. The method is applicable to the entire suction range and provides a good fit for soil types such as sand, silt and clays.

$$\theta = C(\psi)\frac{\theta_s}{\left(\ln\left(e+\left(\frac{\psi}{a}\right)^n\right)\right)^m} \qquad [2.11]$$

With:

$$C(\psi) = 1 - \frac{\ln\left(1+\frac{\psi}{\psi_r}\right)}{\ln\left(1+\frac{10^6}{\psi_r}\right)} \qquad [2.12]$$

Where:

a, m, n = fitting parameters

ψ = soil suction

ψ_r = soil suction corresponding to the residual volumetric water content, θ_r

$C(\psi)$ = a correcting function which forces the SWCC through 10^6 kPa at zero water content

Recently Aubertin et al (1998) proposed a modified Kovacs model that takes into account some of the aspects of the Fredlund and Xing approach. Good agreement was achieved between observed and calculated results. The model makes use of a saturation ratio (S_r or θ/θ_s) and incorporates both the capillary (S_c) and absorption (S_a) forces. The equations are:

$$S_r = S_c + S_a(1 - S_c) \qquad [2.13]$$

$$S_c = 1 - \left[\left(\frac{h_{co}}{\psi}\right)^2 + 1\right]\exp^{-m\left(\frac{h_{co}}{\psi}\right)^2} \qquad [2.14]$$

$$S_a = C_\psi\left(\frac{a}{e^{1/3}.\psi^{1/6}}\right)\psi_{90} \qquad [2.15]$$

$$C_\psi = 1 - \frac{\ln\left(1+\frac{\psi}{\psi_r}\right)}{\ln\left(1+\frac{\psi_o}{\psi_r}\right)} \qquad [2.16]$$

Where:

h_{co} = a representative water rise taken as an intermediate value between the Brooks and Corey AEV (ψ_{BC} or AEV (BC)) and ψ_r

m = controls the slope of the inclined portion of the SWCC

Aubertin et al (1998) proposed that h_{co} should equal AEV (90) and that parameter a is equal to 0.006 for a draining curve. The parameter m may be obtained by adjusting the theoretical curve to experimental data.

2.5 Effective Stress Concept

The mechanical behaviour of a soil (the volume change and shear strength behaviour) can be described in terms of the state of stress in the soil. The state of stress in a soil consists of certain combinations of stress variables that can be referred to as stress state variables (Fredlund and Rahardjo, 1993). These variables should be independent of the physical properties of the soil (Fung, 1977). The number of stress state variables required for the description of the stress state of a soil depends primarily upon the number of phases involved.

For saturated soils the effective stress (σ - u_w) is given by Equation 2.5, and has often been regarded as a physical law. The effective stress is a stress state variable that can be used to describe the behaviour of a saturated soil.

Acceptable stress state variables for an unsaturated soil have been considerably more difficult to establish. Only recently has there been some agreement on the most acceptable stress state variables to use in practise. The use of a single-valued effective stress state variable for unsaturated soils has encountered many difficulties, and has led to the recognition that two independent stress state variables should be used. Consideration of the contractile skin as a fourth phase lends support to the theoretical justification for two independent variables (Fredlund and Morgenstern, 1977).

Fredlund and Morgenstern (1977) presented a theoretical stress analysis of an unsaturated soil on the basis of multi-phase continuum mechanics. The unsaturated soil was considered as a four-phase system. The soil particles were assumed to be incompressible and the soil was treated as though it was chemically inert. The analysis concluded that there are three possible combinations, which can be used as stress state variables for an unsaturated soil. These are:

1) $(\sigma - u_a)$ and $(u_a - u_w)$
2) $(\sigma - u_w)$ and $(u_a - u_w)$
3) $(\sigma - u_a)$ and $(\sigma - u_w)$

The stress state variables can then be used to formulate constitutive equations to describe the shear strength behaviour and the volume change behaviour of unsaturated soils. It was found by Fredlund (1979) and Fredlund and Rahardjo (1987) that combination (1) is the most satisfactory in engineering practise. This combination is advantageous because the effects of change in total normal stress can be separated from the effects caused by a change in the pore-water pressure. In addition, the pore-air pressure is atmospheric (i.e., zero gauge pressure) for most practical engineering problems. The difference between the pore-air and the pore-water pressures, $(u_a - u_w)$, is known as the matric suction of a soil.

2.5.1 Limiting stress state conditions

There is a hierarchy with respect to the magnitude of the individual stress components in an unsaturated soil:

$$\sigma > u_a > u_w \qquad [2.17]$$

This must be maintained in order to ensure stable equilibrium conditions. Limiting stress state conditions occurs when one of the stress state variables becomes zero. For example, if the pore-air pressure, u_a, is momentarily increased in excess of the total stress, σ, an explosion of the sample may occur. In saturated soils a limiting condition may also be reached when the effective stress, $(\sigma - u_w)$, reaches zero. At this point the soil is in a quick condition.

2.5.2 Stress analysis

The stress state variables for unsaturated soils can be used in engineering practice in a manner similar to which the effective stress variable is used for saturated soils. The distribution of the stress components allows the computation of in-situ profiles for the net normal stress, $(\sigma - u_a)$, and matric suction, $(u_a - u_w)$. Their variation with depth and time is required for analysing shear strength or volume change problems. As the soil becomes saturated, the two profiles revert to the classic effective stress, $(\sigma - u_w)$, profile.

The total normal stress in a soil is a function of the density or the total unit weight of the soil. The magnitude and distribution of the total normal stress is also affected by the application of external loads.

2.5.3 Air-drying

Air-drying a soil or evaporation from a soil will bring the soil to a dry condition. As the soil dries, the matric suction will increase. Numerous experiments by Fredlund (1964) have shown that the matric suction of a soil tends to a limiting value in the range of 620-980 MPa as the water content reaches 0%.

The relationship between the water content and the suction of a soil is referred to as the soil-water characteristic curve. Figure 2.11 shows the relationship between the volumetric water content, θ, and suction for various Dutch soils. In can be seen that the soils reaches a limiting value of 980 MPa when the water content reaches 0 %. The plot also shows the continuous nature of the water content versus suction relationship.

The effects of a change in matric suction on the mechanical behaviour of a soil may become negligible as the soil approaches a completely dry state. For these dry soils, the net normal stress, $(\sigma - u_a)$, may become the only stress state variable controlling their behaviour.

The effect of a matric suction change on the volume change of Regina clay is shown in Figure 2.12. As the matric suction of the soil increases, the water content of the soil is reduced and the volume of the soil decreases. However, before the soil becomes completely dry, the volume of the soil remains constant in spite of the increase in matric suction.

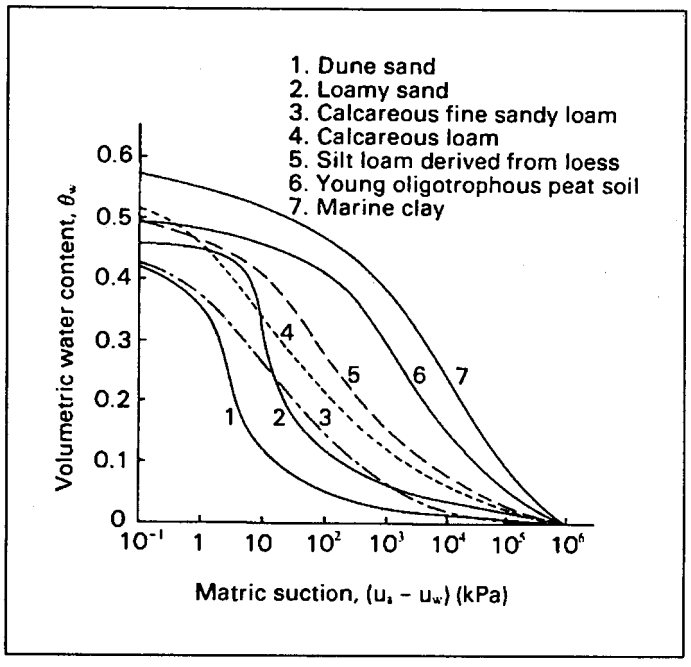

Figure 2.11: Soil-water characteristics curve for some Dutch soils (after Koorevaar et al, 1983)

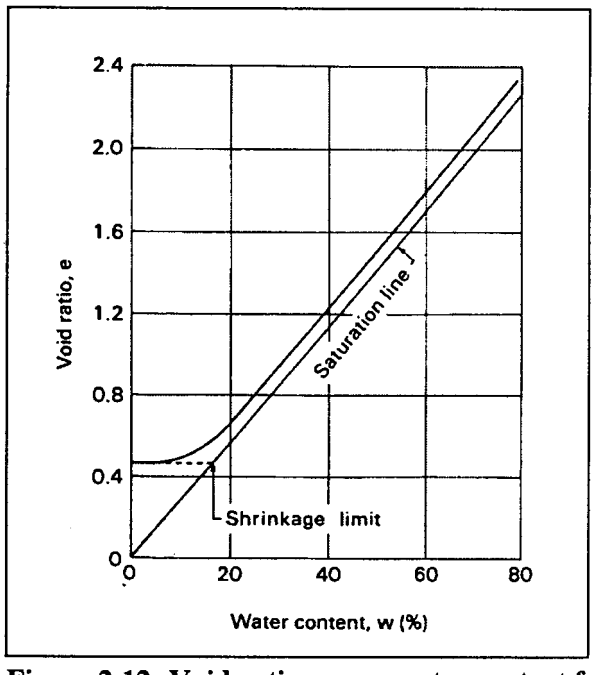

Figure 2.12: Void ratio versus water content for Regina clay (after Fredlund, 1964)

2.6 Shear Stress Theory

Many geotechnical problems are related to the shear strength of a soil. The shear strength of a soil can be related to the stress state in the soil. As discussed above, the stress state variables used in unsaturated soils are the net normal stress, $(\sigma - u_a)$, and the matric suction, $(u_a - u_w)$.

The shear strength of a saturated soil is described using the Mohr-Coulomb failure criterion and the effective stress concept (Terzaghi, 1936).

$$\tau_{ff} = c' + (\sigma_f - u_w)_f \tan \phi' \qquad [2.18]$$

Where:

τ_{ff} = shear stress on the failure plane at failure

c' = effective cohesion, which is the shear strength intercept when the effective normal stress is zero

$(\sigma_f - u_w)_f$ = effective normal stress on the failure plane at failure

σ_{ff} = total normal stress on the failure plane at failure

u_{wf} = pore-water pressure at failure

ϕ' = effective angle of internal friction

Equation 2.18 defines the failure envelope on a Mohr circle plot for saturated soils. The shear strength envelope is a measure of the ability of a soil to withstand applied shear stresses. The soil will fail when the applied shear stress exceeds the shear strength of the soil.

2.6.1 Shear strength for unsaturated soils

Equation 2.18 is the shear strength equation for a saturated soil. The shear strength equation for an unsaturated soil at failure is written as follows:

$$\tau_{ff} = c' + (\sigma_f - u_a)_f \tan \phi' + (u_a - u_w)_f \tan \phi^b \qquad [2.19]$$

Where:

u_{af} = pore-air pressure on the failure plane at failure

$(u_a - u_w)_f$ = matric suction on the failure plane at failure

ϕ^b = angle indicating the rate of increase in shear strength relative to the matric suction, $(u_a - u_w)_f$

In the case of an unsaturated soil, the Mohr circles corresponding to failure conditions can be plotted in a three-dimensional manner, as illustrated in Figure 2.13. The plot has the shear stress, τ, as the ordinate and the two stress state variables, $(\sigma - u_a)$ and $(u_a - u_w)$, as abscissas. The frontal plane represents as saturated soil where the matric suction is zero. On the frontal plane, the $(\sigma - u_a)$ axis reverts to the $(\sigma - u_w)$ axis since the pore-air pressure becomes equal to the pore-water pressure at saturation.

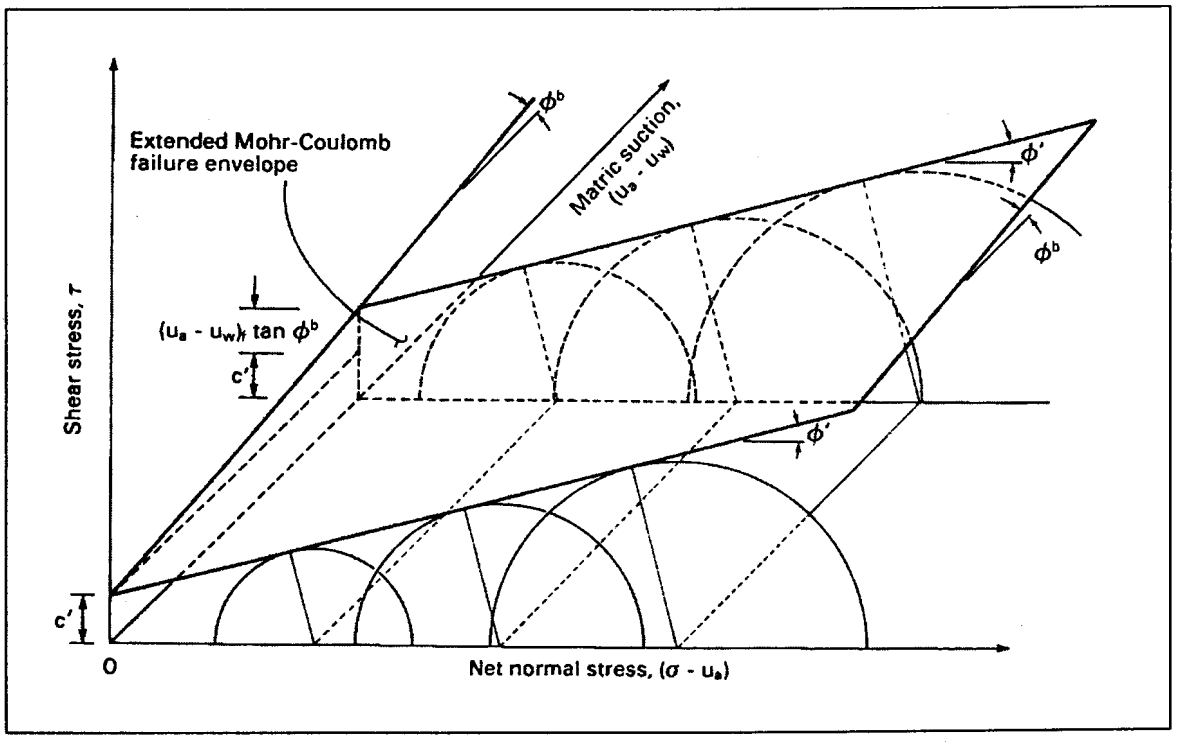

Figure 2.13: Extended Mohr-Coulomb failure envelope (after Fredlund and Rahardjo, 1993)

The Mohr circles for an unsaturated soil are plotted with respect to the net normal stress axis, $(\sigma - u_a)$, in the same manner as the Mohr circles are plotted for saturated soils with respect to effective stress axis, $(\sigma - u_w)$. However, the location of the Mohr circle plot in the third dimension is a function of

the matric suction. The surface tangent to the Mohr circles at failure is referred to as the extended Mohr-Coulomb failure envelope for unsaturated soils.

2.7 Gold Mine Tailings

2.7.1 Tailings

Tailings can be defined as the waste product of mining, industrial and chemical processes. Tailings consist of sand and silt-size particles of milled rock from which the mineral value has been removed. Normally tailings contain hardly any clay-size particles and, when sheared, behave as frictional, cohesionless materials with angles of shearing resistance in the range of 29-35° (all, not just gold).

2.7.2 Tailings dams

Gold slimes (tailings) dams in South Africa are usually of the ring-dyke type constructed using the 'upstream semi-dry paddock' method (Figure 2.14). In this method, the outer or 'daywall' of the tailings dam is raised by constructing a paddock varying between 10 m and 50 m wide to form the perimeter of the dam. The paddock is filled with 150 mm to 200 mm of slurry placed at a relative density (RD) of between 1.20 and 1.45. Once the slurry has settled out, the excess water is decanted through temporary pipes built into the internal wall of the day paddock and flows to a pool in the body of the dam.

After a section of the daywall paddock dries out sufficiently to become trafficable, the paddock walls are built up by hand, using a shovel, or by tractor and plough, ready to receive the next batch of slurry. This wall-building operation takes place under supervision during the day, hence the name 'daywall'. Discharge of the slurry into the body of the dam where supervision is not required takes place at night; hence the body or basin of the dam is known as the nightpan. Slurry discharged into the nightpan runs along the concave surface or 'beach' of the dam towards the penstock outlet tower. The penstock outlet is ideally located centrally in the dam and is used to decant return water and storm water from the dam.

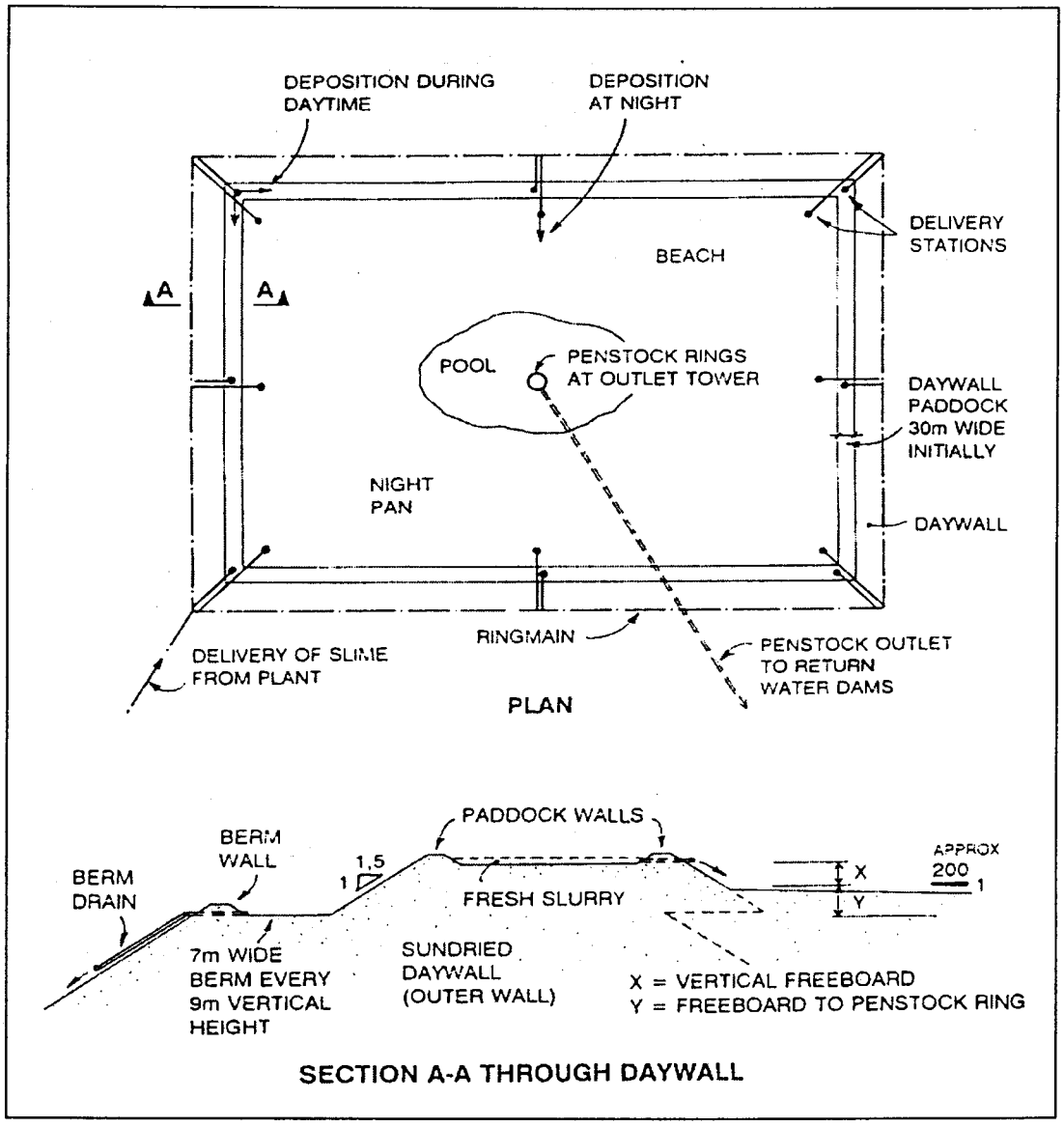

Figure 2.14: Upstream semi-dry paddock method of constructing a gold slimes dam (after Wagener, 1997)

On a large dam one complete cycle of deposition in the daywall takes 10 to 14 days to complete. Between successive depositions of slime the surfaces of the daywall and upper reaches of the beach of the nightpan would be subjected to sun drying, which has the effect of cracking and consolidating the material. A dense, sun-dried wall of slime thus surrounds a correctly constructed and operated gold tailings dam.

It should be noted that when slurry is delivered in the daywall or nightpan, the coarser particles of the slime settle out closest to the point of deposition. The deposited material gets progressively finer

along the daywall away from the delivery point and in the nightpan towards the pool. The material in the pool area could remain under water and not be sun-dried. It could remain a loose, low-density, low-strength material and could be subject to liquefaction.

The tailings are often distributed around the circumference of the dyke partly by open channel flow and the crest must be graded to cause the tailings slurry to flow (Blight, 1997). Also, deposition does not take place simultaneously around the entire perimeter. As a result of these two factors, the crest elevation and the free-board usually vary around the dyke perimeter. Because of low spots on its perimeter a ring-dyke may be at greater risk of overtopping during unusually wet weather. Overtopping is a particular danger if there is poor control over the operation of the impoundment or if the principles of tailings dam operation are not appreciated by mine management, and excessive volumes of water are stored in the basin of the tailings impoundment, thus reducing the free-board to a dangerous level.

Ring-dykes may also be susceptible to shear or slip failure if, as a result of poor operational control, rates of rise become excessive so that the phreatic surface rises, or the outer slopes of the dyke are built over-steep so that the factor of safety against shear failure is reduced.

Figure 2.15 shows a typical vane shear strength profile measured in a gold tailings impoundment. In the diagram, the 'predicted' strength line is given by

$$\tau = \sigma_v' \tan \phi' \qquad [2.20]$$

Note that the strength vs depth lines in Figure 2.15 do not pass through the origin because the effective stress at surface is equal to a capillary pore pressure of 10m of water (100 kPa → Water table at 10m).

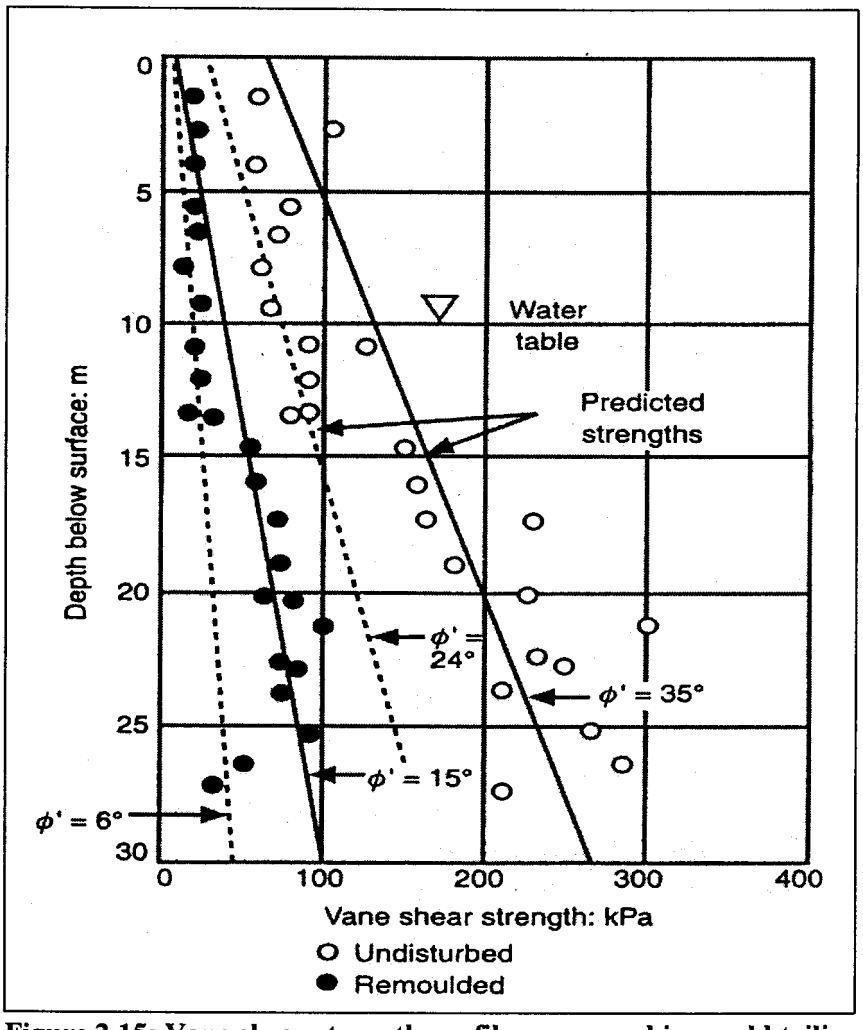

Figure 2.15: Vane shear strength profiles measured in a gold tailings dam (after Blight, 1997)

2.8 Discussion

It is clear from Section 2.7 that a tailings dam consists of a soft inner part (night pan) and a consolidated stronger outside (daywall) part that keeps the tailings dam stable. A tailings dam is much like an earth retaining dam, where the daywall corresponds to the earth dam wall, and the nightpan corresponds to the water inside the dam. The stability of a tailings dam thus depends on the strength of the daywall.

The method used to construct a tailings dam's daywall was discussed in Section 2.7. In order for the daywall to provide sufficient strength to the tailings dam, successive layers of deposition needs to be allowed adequate time to dry out and to consolidate to gain strength. This time interval is termed rate of rise. There are no codes of practise that defines an accurate method of determining the rate of rise

of a tailings dam. The rate will depend on several factors including environmental conditions, moisture content of the deposited slurry, the grading of the tailings and the depth of the water table. An increase in the rate of rise for a tailings dam would be beneficial to the operation of a mine.

Section 2.3 dealt with suctions in soil. It is clear that matric suction, $(u_a - u_w)$, will be the primary component of suction in gold mine tailings. It is assumed from the literature that matric suctions are exclusively controlled by the grading and hence the pore size of the tailings. Section 2.3 compared various methods of measuring suction and it was shown that the mid-plane suction probe is an effective instrument for the measurement of suctions, and is probably superior to the conventional methods of suction measurement.

The soil-water characteristics curve was shown in Section 2.4 to be able to provide a conceptual framework in which the behaviour of unsaturated soils can be understood. It was shown that the behaviour of the shear strength of a soil remains the same as if it is saturated up to the air-entry value for the particular soil. Various ways of predicting the air-entry value as well as the soil-water characteristic curve for a particular soil was also discussed. All of these methods, however, require the input of fitting parameters into the model. These parameters can only be obtained by fitting the curves to experimental data, or by using fitting parameters used for the representation of similar soils. Clay and silt was shown to control the suctions in a soil. Thus it seems reasonable to assume that if the amount of clay and silt in a soil sample is known, a reasonable estimate can be made of the suctions in the soil. This dissertation attempts to justify this assumption.

It was shown in Section 2.4 that the air-entry value of a soil corresponds to the shrinkage limit. Thus when the air-entry value is reached during a drying process (deposited tailings on a daywall), the tailings (soil) has reached a limiting volume and thus void ratio. At this point the soil has consolidated completely and further drying will result in an increase in shear strength due to rising suctions. This dissertation attempts to develop a new method of determining the air-entry value of tailings by knowing only the grading for the particular tailings.

CHAPTER 3:

EXPERIMENTAL METHOD

3.1 Introduction

The soil-water characteristics curve (SWCC) was shown in the previous chapter to be the single most important element of unsaturated soil mechanics. With the SWCC known for a specific soil, as well as certain saturated properties of the same soil, an estimate can be made for the shear strength, permeability and volume change for the same soil in an unsaturated state.

The SWCC relates the water content of a soil to suction. Matric or total suction may be used, but as discussed in the previous chapter, the choice between the two will have no significant effect on the SWCC for gold mine tailings. A test method therefore needs to be developed to relate the volumetric and gravimetric moisture content of a sample of gold tailings to the suction present in the sample.

The material to be tested is gold tailings obtained from Dr. N.J. Vermeulen. The tailings were taken from two tailings dams at Vaal River Operations in the North West Province of South Africa. Pay Dam is the oldest impoundment on the mine, while Mizpah is one of the more recent additions.

3.2 Previous Attempts

Students at the University of Pretoria previously developed two methods of obtaining the SWCC for a sample of gold mine tailings using the mid-plane suction probe. The very first attempt was made by Ms. M. Theron with her dissertation titled: "Soil Suction in Mine Tailings" (Theron, 2000). She was also responsible for the development of the mid-plane suction probe. Mr. A. Luyt developed the second method in his project report titled: "Measurement of Suction Pressures in Mine Tailings" (Luyt, 2001). Both of these students used fine and coarse graded tailings from Pay Dam. The main problems encountered in both methods were the accurate measurement of volume of the desiccating tailings, and correct use of the mid-plane suction probe.

Theron (2000) filled a glass container with tailings slurry with a height of 32.4 mm and a diameter of 67.9 mm. The volume of the tailings was then calculated by measuring the decreasing height of the sample inside the glass container. This proved to be unsuccessful. As the tailings dried out, the sample not only changed in height, but also in diameter. This was not taken into account during volume calculations. The tailings also showed cracking, which was also not incorporated in the volume calculations. Although measurements of moisture content, w, were accurate, calculations of void ratio,

e, degree of saturation, S, and volumetric water content, θ, were not due to inaccurate volume measurements. Because of the fairly thick sample, the tailings at the top will be drier than the tailings at the bottom of the container. Measurements of suction were made by placing the probe on the top surface of the tailings sample. Thus the measured suction was then incorrectly compared to the current water content of the whole sample (suctions too high at calculated water content). Theron (2000) made no mention of the response of the probe. Figure 3.1 shows shrinkage curves for both the fine and the coarse Pay Dam gold tailings. It is clear from the shapes of the curves that the measurement of volume change was inadequate. Figure 3.2 shows the SWCCs for both the fine and coarse tailings. The curves do show promise regarding their shape, but they lack in detail and do not show the air-entry value.

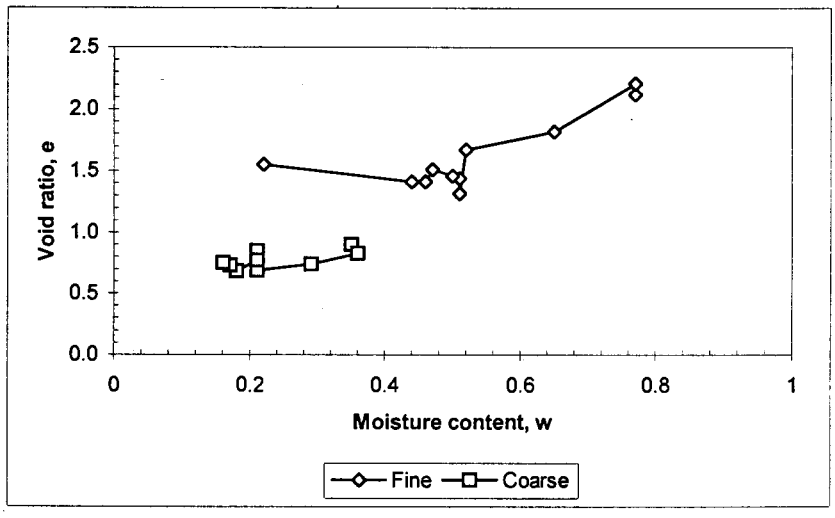

Figure 3.1: Shrinkage curves for Pay Dam tailings developed by Theron (2000)

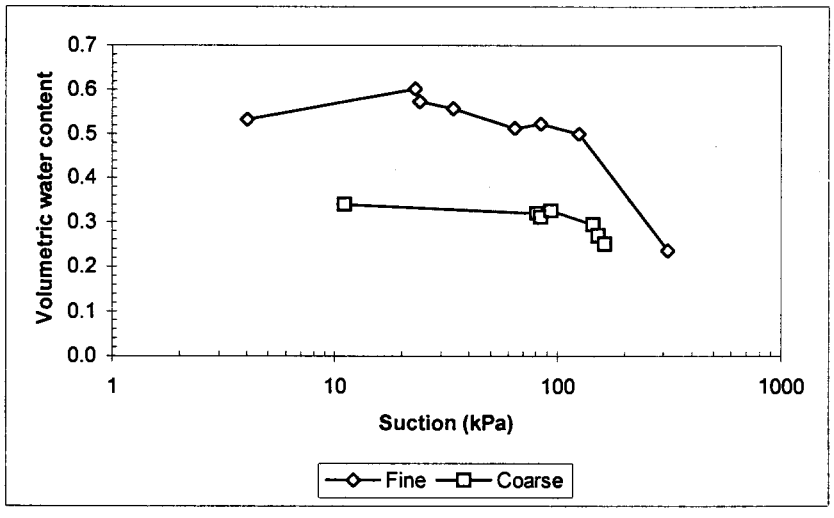

Figure 3.2: SWCCs for Pay Dam tailings developed by Theron (2000)

Luyt (2001) developed a test method that aimed at correcting the mistakes regarding volume measurement that was encountered in the previous method. The apparatus consists of a copper ring placed on top of a glass disk, which together forms a container 19 mm high with a diameter of 76 mm. The tailings slurry is poured inside this mould and may be dismantled for measurement of volume. The change in height of the sample is measured using a dial gauge. When the sample starts to decrease in diameter, the copper ring can be removed and the diameter of the sample measured using vernier callipers. This method showed improved results. Luyt (2001) recognised the fact that the probe must be allowed sufficient time to ensure that the moisture content near the probe reaches the moisture content of the whole sample. However, he also made no comment on the response time of the probe. Figure 3.3 shows shrinkage curves for both the fine and the coarse Pay Dam gold tailings. It is clear from the shapes of the curves that the measurement of volume change was improved. Figure 3.4 shows the SWCCs for both the fine and coarse tailings. Improvement is apparent.

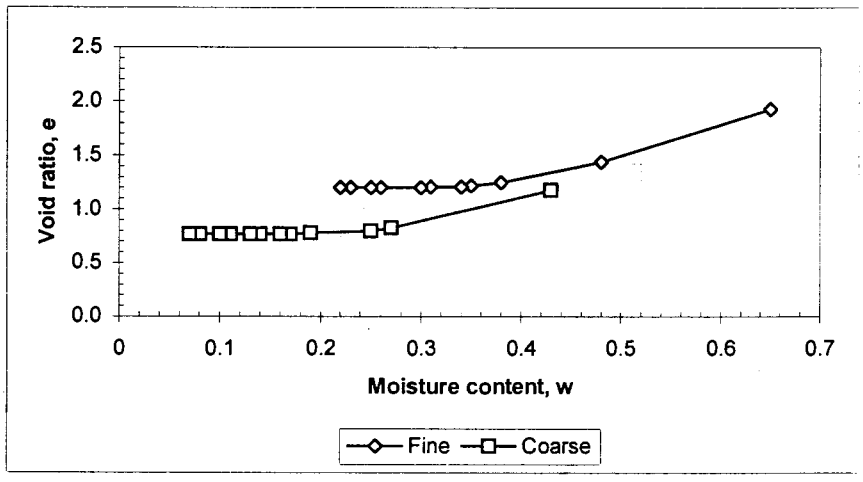

Figure 3.3: Shrinkage curves for Pay Dam tailings developed by Luyt (2001)

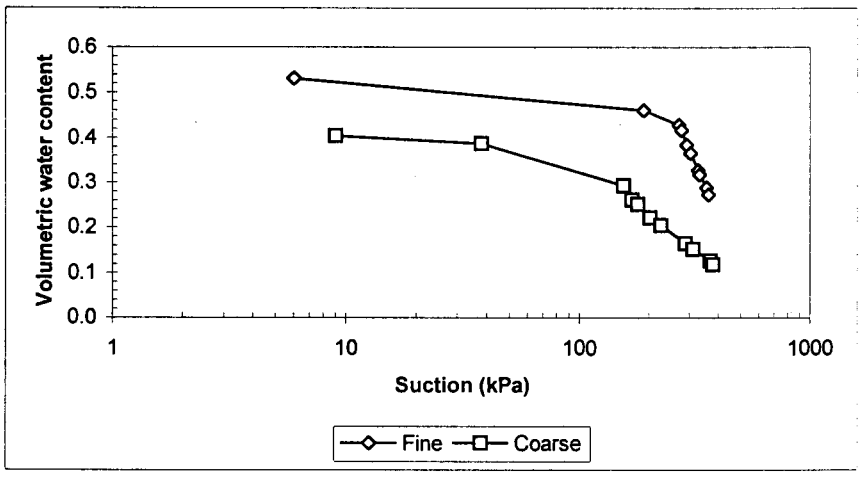

Figure 3.4: SWCCs for Pay Dam tailings developed by Luyt (2001)

It is clear from the above that the test method developed by Luyt (2001) is far superior to the method proposed by Theron (2000). However, the method proposed by Luyt (2001) does have some disadvantages, the first of which is the time necessary for the sample to dry out sufficiently to reach 350 kPa suction. It took both the fine and the coarse samples almost 12 days to reach the probe's limiting suction value. This is regarded as totally unacceptable. The second criterion is the unnecessary removal and replacement of the various components of the container each time volume measurements are taken. Thus a new test method needs to be developed that improves the above two methods.

3.3 Reasoning behind Test Method

A practical test method needs to be developed to relate the volumetric and gravimetric moisture content of a sample of gold tailings to the suction present in the sample (SWCC). The following are of importance in developing such a test method:

- The tailings should be mixed with water into a slurry to attempt saturation
- The mixture should be allowed to dry from saturation
- The container which will hold the tailings as it dries out should be of such a shape that the volume change can be easily measured during the drying process, as well as measurements of mass to determine the water content of the tailings at any given time
- The container should have a depth small enough to ensure that the material is at the same moisture content throughout, i.e. the tailings at the surface should not be dryer than the tailings at the bottom of the container
- The container should have sufficient width to allow for the mid-plane suction probe to be placed on the tailings for direct suction measurements

With a small enough container depth, the tailings will thus only be subjected to pore-water pressures (the overburden pressure will be negligible). The pore-air pressure, u_a, will be zero (atmospheric

pressure). Thus the probe, which measures pore-water pressure, u_w, will in actual fact also measure matric suction, $(u_a - u_w)$.

As discussed in the previous chapter (Section 2.3.4), the mid-plane suction probe can only measure suctions up to about 350 kPa. The face of the probe's ceramic tip needs to be in good hydraulic contact with the material to obtain reliable and fast readings. A method also needs to be developed for the correct usage and operation of the suction probe.

In order to relate volumetric and gravimetric moisture content to suction in the material, measurements of moisture loss, volume change and suction must be taken selectively over time. The mass of the material (moisture content) will continue to decrease throughout the test until a state of complete dryness is reached which will correspond with the end of the test. When the moisture content of a fine-grained soil is reduced below the plastic limit, shrinkage of the soil mass continues until the shrinkage limit (Section 2.2.3) is reached. At that point the solid particles are in close contact and the water contained in the soil is just sufficient to fill the voids between them. A further reduction in moisture content will not decrease the volume of the soil mass any further. This state is referred to as the shrinkage limit (SL). Thus unlike the measurements of mass which continues throughout the test, measurements of volume change only needs to be carried out until the SL is reached. Measurements of suction, however, also need to be carried out throughout the test. Thus the container must facilitate easy mass and volume measurements in conjunction with suction measurements.

3.4 Shrinkage Troughs

3.4.1 Volume change

As mentioned in Section 3.3 and in Section 2.4.2, the shrinkage limit of a soil corresponds to the moisture content at which the soil reaches its air-entry value. Thus a container should be designed to facilitate easy measurement of the shrinkage limit. BS1377: Part 2:1990:6.5 describes the use of non-corrodible moulds for the determination of linear shrinkage. The shrinkage limit is not the same as linear shrinkage, but the shrinkage limit corresponds to the point where linear shrinkage ceases. Furthermore, if the volume of soil within the mould can be measured in some way, the void ratio at any time can be calculated as the soil dries and the volume decreases up to the shrinkage limit from where the volume and thus also void ratio will remain constant.

It was decided to incorporate the same method used in shrinkage limit calculations namely the shrinkage mould, which allows for easy measurements of shrinkage, i.e. volume change. Shrinkage troughs were made from 25mm uPVC conduit of about 200mm lengths cut in half along the length. Figure 3.5 shows the shrinkage troughs that were made. The shrinkage of the material in the troughs could easily be measured as it dried out. This involved measurements of the changes in length and also in depth using a vernier. Figure 3.6 shows a trough and the tools used to measure volume change. With these changes measured the volume changes could be calculated with respect to time.

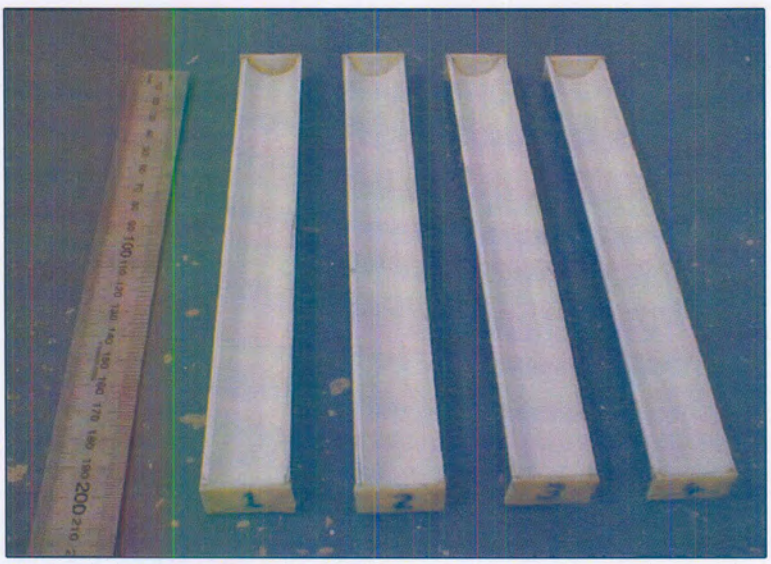

Figure 3.5: Shrinkage troughs

Figure 3.6: Tools used to measure volume change

The four troughs shown in Figure 3.5 were measured to obtain the following dimensions for each trough:

- Length (L_o)
- Radius (r_o)
- Depth (H_o)

These initial dimensions were then used in the volume calculations. The soil placed inside the troughs will have a cross-sectional area corresponding to the segment of a circle. If this area can be calculated and multiplied with the length of soil inside the trough, the volume can easily be calculated. Figure 3.7 represents the method used in calculating the cross-sectional area of the soil.

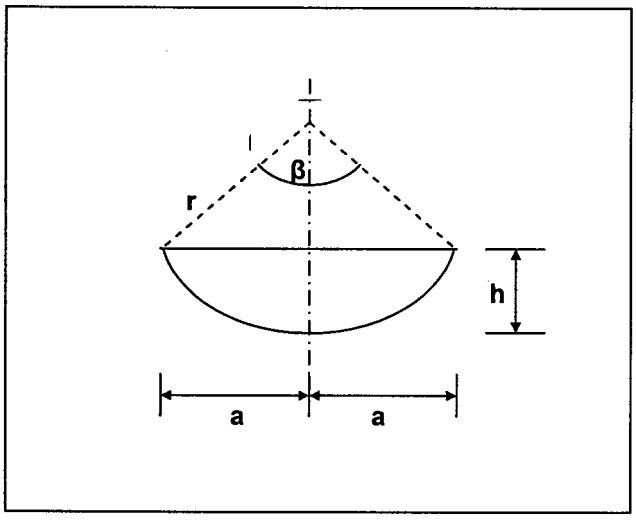

Figure 3.7: Segment of a circle

The area of the circle segment represented in Figure 3.7 is:

$$A = \frac{\pi . r^2 . \beta}{360} - a(r - h) \qquad [3.1]$$

It was decided to measure the volume change of the soil inside the troughs in the following manner:

- Measuring the linear shrinkage at both ends of a trough using a vernier (L). The length of the sample is thus the initial length of the trough minus the sum of the shrinkage at both ends.

- Measuring the change in depth of the sample at six positions along the length of the trough using a vernier and a spatula. The reduction in depth is taken as the average of the six depth measurements (D). The height of the sample is thus the initial depth, H_o, minus the average reduction in depth, D ($h = H_o - D$).

- The radius of each trough is calculated in the following manner:

$$r = r_o \frac{(L_o - L)}{L_o} \qquad [3.2]$$

- The angle β in Figure 3.7 can now be calculated using the following equation:

$$\cos\left(\tfrac{1}{2}\beta\right) = \frac{(r - H_o + D)}{r} \qquad [3.3]$$

- The dimension a in Figure 3.7 can now be calculated using the following equation:

$$a = r.\sin\left(\tfrac{1}{2}\beta\right) \qquad [3.4]$$

- The volume of the sample inside a trough may now be calculated using the following equation:

$$V = (L_o - L)\frac{\pi.r^2.\beta}{360} - a(r - H_o + D) \qquad [3.5]$$

It is thus now possible to calculate the volume of a sample inside each trough at any given time. It is also expected that the volume change or shrinkage of sand and clay will not be the same. A sand will have zero volume change, whereas a clay will have a large volume change. The effectiveness of the method of volume change measurement described above will be seen during testing on various materials with differing particle sizes.

3.4.2 Moisture loss

The calculation of the moisture content of each sample is also very standard. Before a sample is placed inside a trough, a thin film of Vaseline is applied to the inside of the trough to prevent material from sticking to the surface of the trough and thus helping the material to undergo volume change without any interference. The mass of the trough is then measured (M_{trough}). After the trough has been filled with material, the initial mass is measured of the trough and material (M_i). Throughout the drying process, consecutive measurements are made of the mass of the trough and material, M, until the material has dried up completely having mass M_{end}. The water content of the material at placement, w_o, may now be calculated with the following equation:

$$w_o = \frac{(M_i - M_{trough})}{(M_{end} - M_{trough})} - 1 \qquad [3.6]$$

The mass of the solids, M_s, may be calculated with:

$$M_s = \frac{(M_i - M_{trough})}{(1 + w_o)} \qquad [3.7]$$

The moisture content of the sample, w, may be calculated during any stage of the drying process with the following equation:

$$w = \frac{M}{M_s} - 1 \qquad [3.8]$$

3.5 Suction Probe

3.5.1 Introduction

The direct measurement of soil suction was done using a similar probe to the mid-plane suction probe that was designed by Theron (2000). The only changes made from the original probe was the incorporation of a 1 MPa pressure transducer as opposed to the 200 kPa transducer used in the original probe, as well as a few changes in dimensions of the probe body. The new probe has a larger cavity at the back to facilitate with the possibility of maintenance of the electrical wiring, and the water reservoir is a bit smaller. Figure 2.7 shows a schematic diagram of the mid-plane suction probe.

The suction probe is discussed in Section 2.3.4. It was shown that the suction probe measures suctions directly by actually measuring the negative pore water pressure inside a sample. This is done by simply placing the face of the ceramic tip of the probe against the sample and obtaining a readout using an amplifier. For the probe to work properly, the 3 bar ceramic and the small water reservoir needs to be completely saturated and calibrated.

3.5.2 Saturation

It is vitally important for the probe to be completely saturated before use. Saturation will improve the response time of the probe tremendously. The probe incorporates a 3 bar (300 kPa) ceramic tip. The air-entry value of the ceramic is not precisely known, but should lie somewhere between 300 and 400 kPa. In order for the probe to be saturated, the probe is placed inside a triaxial cell completely filled with de-aired water. The pressure inside the triaxial cell is controlled with a GDS pressure controller. The same method used by Theron (2000) was incorporated for the saturation of the probe, albeit at higher pressures. The pressure inside the triaxial cell was continuously cycled between 500 and 1000 kPa for a few days. This ensured complete saturation of the ceramic tip and the water reservoir. The extent of saturation will also be seen during calibration. Complete saturation will result in an immediate response from the probe. Figure 3.8 shows the saturation set-up with the GDS pressure controller and the triaxial cell with the probe inside.

In order for the probe to be maintained in a saturated state, the probe is stored in a container with water. If the probe is allowed to dry out, the air-entry value of the ceramic will be reached and air will enter the ceramic and subsequently also the water reservoir. The probe will then have to be re-

saturated due to the fact that the readings will be incorrect. When the probe is in use, the suctions that are measured should never exceed the air-entry value of the ceramic to keep the probe saturated.

Figure 3.8: Saturation of the suction probe

3.5.3 Calibration

Calibration of the suction probe is necessary to ensure a 1:1 relationship between the measured and the "real" suctions within a sample. It was decided to incorporate the GDS pressure controller for the calibration procedure. The suction probe was connected to the GDS controller and a watertight connection ensured. Figure 3.9 shows the calibration set-up.

One unused line from the GDS controller was opened to dissipate all pressures inside the lines. This pressure was taken as the zero or atmospheric pressure and both the GDS and the suction probe was zeroed. The GDS can apply positive water pressures well beyond 350 kPa (assumed to be the maximum suction that may be measured with the suction probe), but can only apply negative pressures to a maximum of –60 kPa due to cavitation. It is assumed, however, that the calibration for

the probe transducer derived between 350 and –60 kPa could be extrapolated to –350 kPa (suction). The calibration procedure involved raising the pressure using the GDS in increments of 50 kPa to 350 kPa and lowering the pressure to zero in increments of 50 kPa while taking measurements of the pressure from the probe at each target value. At zero GDS pressure, the probe was again zeroed if there was excessive drift and the GDS pressure lowered to –60 kPa in increments of 20 kPa and raised again to zero. Figure 3.10 shows a graph representing the calibration of the suction probe at a k factor of 0.39.

From Figure 3.10 it is clear that the probe has a 1:1 relationship to the "real" value. It was also seen throughout the calibration process that the probe was fully saturated. The response of the probe was instantaneous. The ceramic tip of the probe was also in a perfect hydraulic bond with the GDS, which also explains the immediate response time.

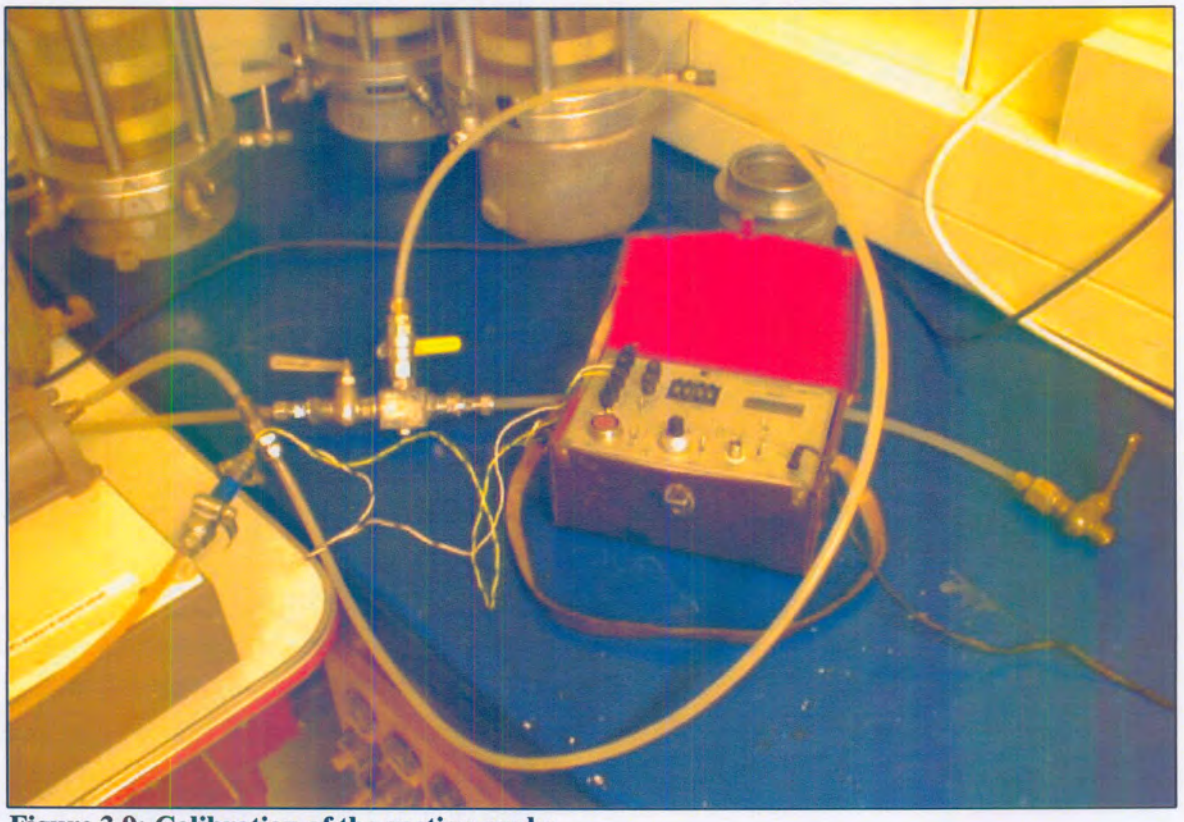

Figure 3.9: Calibration of the suction probe

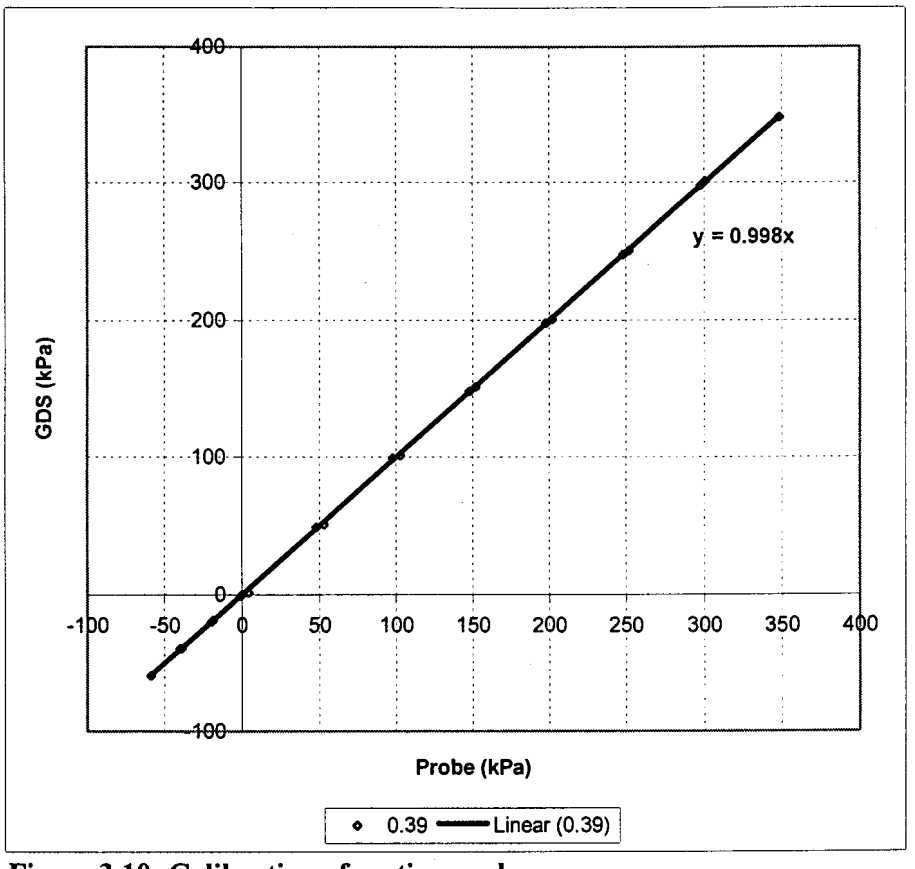

Figure 3.10: Calibration of suction probe

3.5.4 Placement

After the probe has been saturated and calibrated, the probe is ready to measure suctions. As discussed in Section 3.4, troughs shall be used during the testing of the material. It was shown above that there are two requirements that need to be met to ensure a fast response time. The first is complete saturation of the probe, and the second is a good hydraulic contact between the probe's ceramic tip and the material being measured. The first requirement is met during the saturation process and confirmed during the calibration process. It is the second requirement that will eventually control the response time and accuracy of the suction probe. Thus the correct placement of the probe is very important.

When the probe is brought in contact with the material, there should be a proper bond to ensure good hydraulic contact. This is fairly easy when the material is still moist and soft. The probe will have a good hydraulic contact with the material. It however becomes increasingly difficult to obtain a good bond as the material dries out and becomes progressively harder.

When the material is still soft, the probe is allowed to stand on its own on the surface of the material inside the trough. Proof of a good hydraulic bond can be seen in Figure 3.11. The probe can lift the whole trough; this is only due to the suctions generated between the probe and the material surface. This is not possible when the material becomes too dry. It was decided to use a stand to support the probe during measurement and also to apply some downward pressure onto the probe to improve the hydraulic contact. The stand with the probe is shown in Figure 3.12. The stand cannot always be used, the material must firstly achieve sufficient strength to stop the probe from plunging through the surface and it must not compact the material locally. As mentioned earlier, a good hydraulic contact will improve the suction probe response, which will result in more accurate measurements.

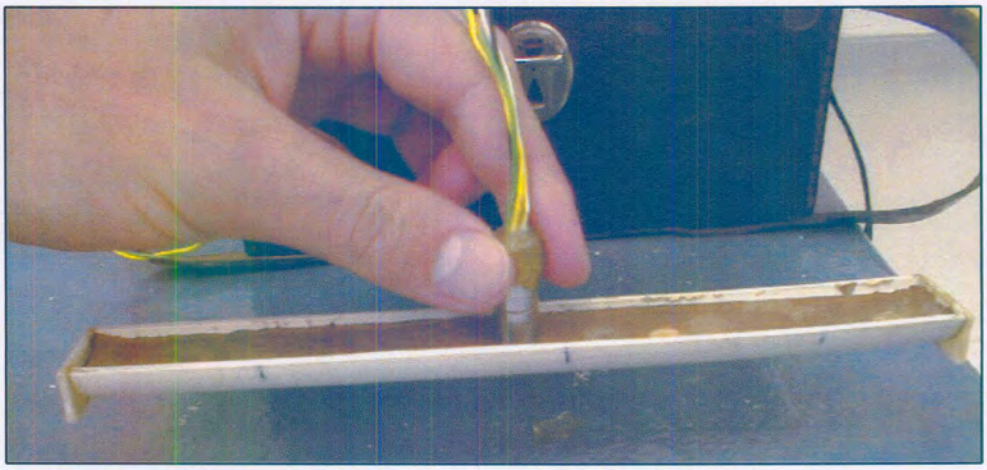

Figure 3.11: Trough lifted with good hydraulic contact

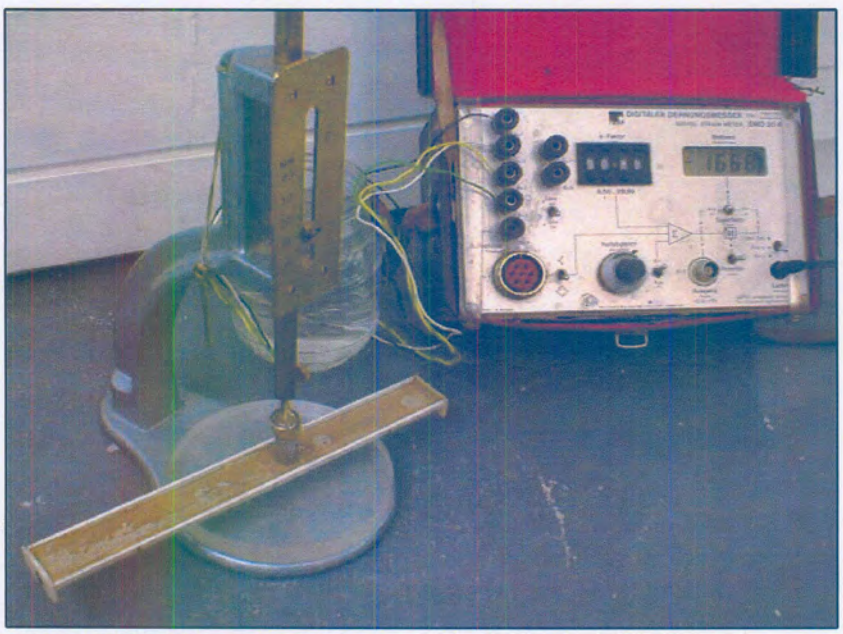

Figure 3.12: Stand used for measurement of suctions

The position of the probe on the material surface should also be investigated so that the suctions measured are representative of the whole sample. Different measurement positions were used throughout the drying process on a sample of mine tailings. It was found that the position of the probe relative to the material surface should not affect the readings. It was decided to take measurements of suction alternately just to the left and to the right of the midpoint of the samples. The reason for this is to allow any excess moisture that was left behind by the probe to dissipate. Figure 3.13 show that measurements at different positions on the material surface do not influence the readings.

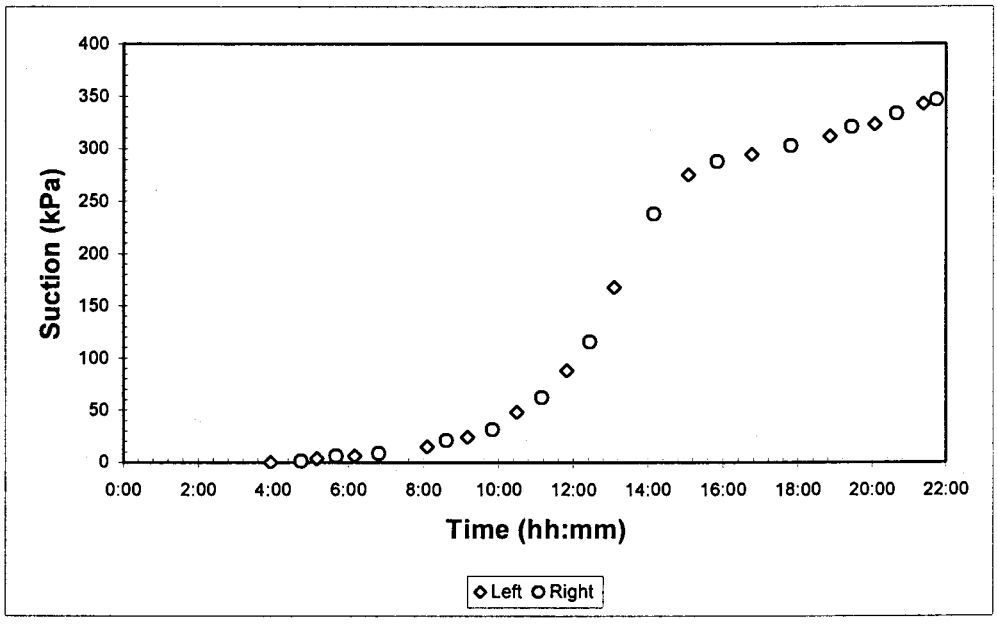

Figure 3.13: Graph showing insensitivity of position of probe on material surface

3.5.5 Response

As mentioned above, probe response is dependent on a good hydraulic contact between the suction probe's ceramic tip, and the material surface. It is important for the response of the probe to be known, otherwise measurements taken after too short or too long a time will be inaccurate. The response of the probe depends on several factors:

- The amount of water on the surface of the probe's ceramic tip. If a large droplet of water covers the tip, placement of the probe on the material will result in a local increase in moisture content. This will cause a drop in the suction of the material surrounding the probe. It will take much longer for the excess moisture to dissipate throughout the whole sample, and it may

change the suction of the whole sample. It is thus important to ensure that the tip is fairly dry before placement. Wiping the tip of the probe across the back of the hand a few times before bringing the probe in contact with the sample will ensure that the tip is fairly dry.

- The saturation of the probe. As mentioned earlier, saturation of the probe is important to minimise response time. To maintain the probe in a saturated condition, it is important to store the probe in water when it is not in use, and not to measure suctions above the air-entry value of the ceramic tip, which is assumed to be around 350 kPa.

- The effectiveness of the hydraulic contact between the probe's ceramic tip and the material surface. During calibration, the response time of the probe should be instantaneous when the probe is fully saturated. This is because there is a perfect hydraulic contact between the probe and the de-aired water from the GDS pressure controller. It is more difficult to obtain a good hydraulic contact between the probe and sample. When the material is still fairly wet, a relatively good bond can be achieved, which will result in a shorter response time. The opposite is true when the material has dried and hardened. Now the ceramic may be in contact with the atmosphere as well as the material. This will result in erroneous measurements.

- The particle sizes of the material measured. A sample with a fairly coarse grading will result in a much quicker response than a fairly fine material. This is due to the fact that the slight increase in moisture content at the place of contact between the probe and sample will dissipate much quicker in a coarser material (higher permeability).

- The volume of the water reservoir behind the ceramic tip inside the probe. A very small volume inhibits the formation of air bubbles in the reservoir, thereby increasing the range of direct measurement of suction beyond the pressure at which cavitation normally occurs.

The response of the probe may vary from as short as 30 seconds to as long as 10 minutes, depending on the factors described above. Figure 3.14 shows the typical response of the suction probe on fine tailings from Pay Dam. It is safe to assume that the readings will be accurate when the slope of the response curve remains constant. The slope cannot flatten out (slope is zero) because the material is in the process of drying out. The response curve will follow the true suction path once the slope reaches a constant. When the material is still fairly wet (low suction), the response time is 5 minutes, while 80 percent of the suction was reached within 1 minute. When the material is fairly dry (high suction), the response time has risen to 10 minutes, while 90 percent of the suction was reached within 1 minute.

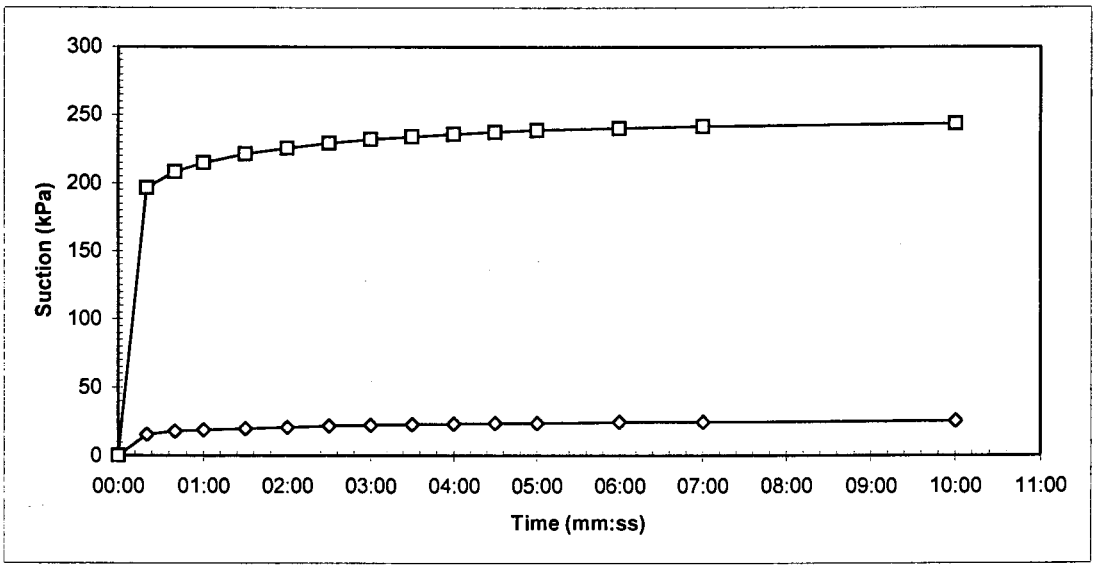

Figure 3.14: Probe response on fine tailings from Pay Dam

Figure 3.15 shows the typical response of the suction probe on coarse tailings from Pay Dam. When the material is still fairly wet (low suction), the response time is 2 minutes, while 95 percent of the suction was reached within 1 minute. When the material is fairly dry (high suction), the response time has risen to 6 minutes, while 95 percent of the suction was reached within 1 minute.

Figure 3.14 and 3.15 clearly shows the effect that grading of the material has on the response of the suction probe. The effect that a good hydraulic bond has is shown in Figure 3.15. When the material is fairly wet the bond is better, which results in a shorter response time.

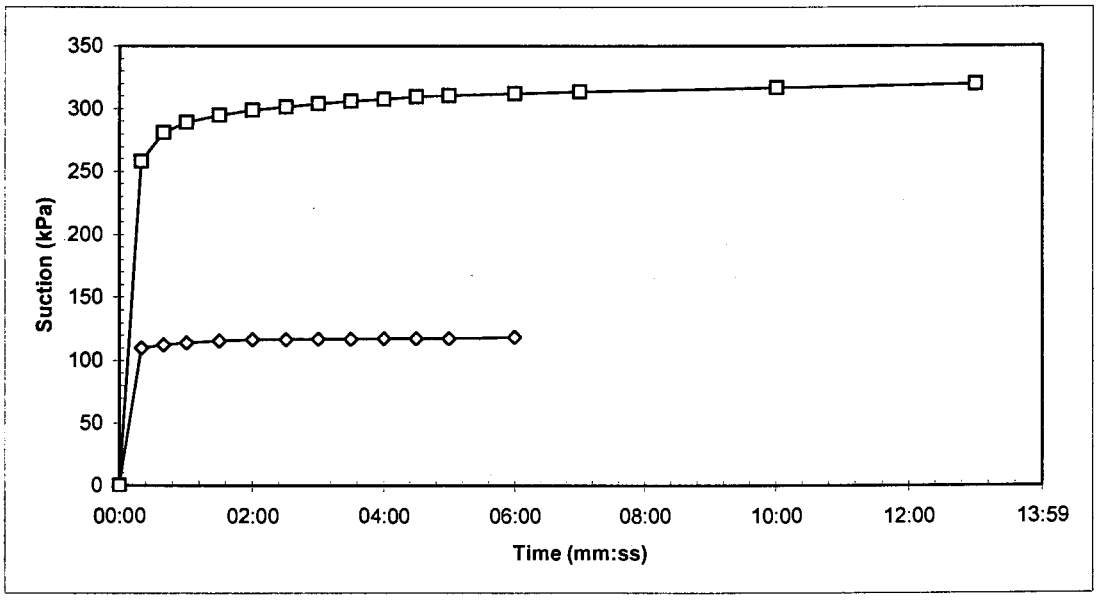

Figure 3.15: Probe response on coarse tailings from Pay Dam

3.6 Material Tested

3.6.1 Introduction

The study mainly focuses on gold tailings obtained from Vaal River Operations situated on the Vaal River between Potchefstroom and Klerksdorp. The mine forms part of Anglo Gold. Vaal River Operations has two tailings dams, Pay Dam and Mizpah. Both these dams gather their tailings from the same extraction plant. The samples were obtained from Dr. N.J. Vermeulen whom has done extensive research on the composition and state of gold tailings (Vermeulen, 2001). Three different materials were used in the experimental work, namely Pay Dam fine and coarse, as well as Mizpah whole tailings, which were obtained from Mizpah's delivery system's exit. Grading curves for the three materials are represented in Figure 3.16. Included in Figure 3.16 is the grading curve for BE tailings taken from Aubertin et al (1998).

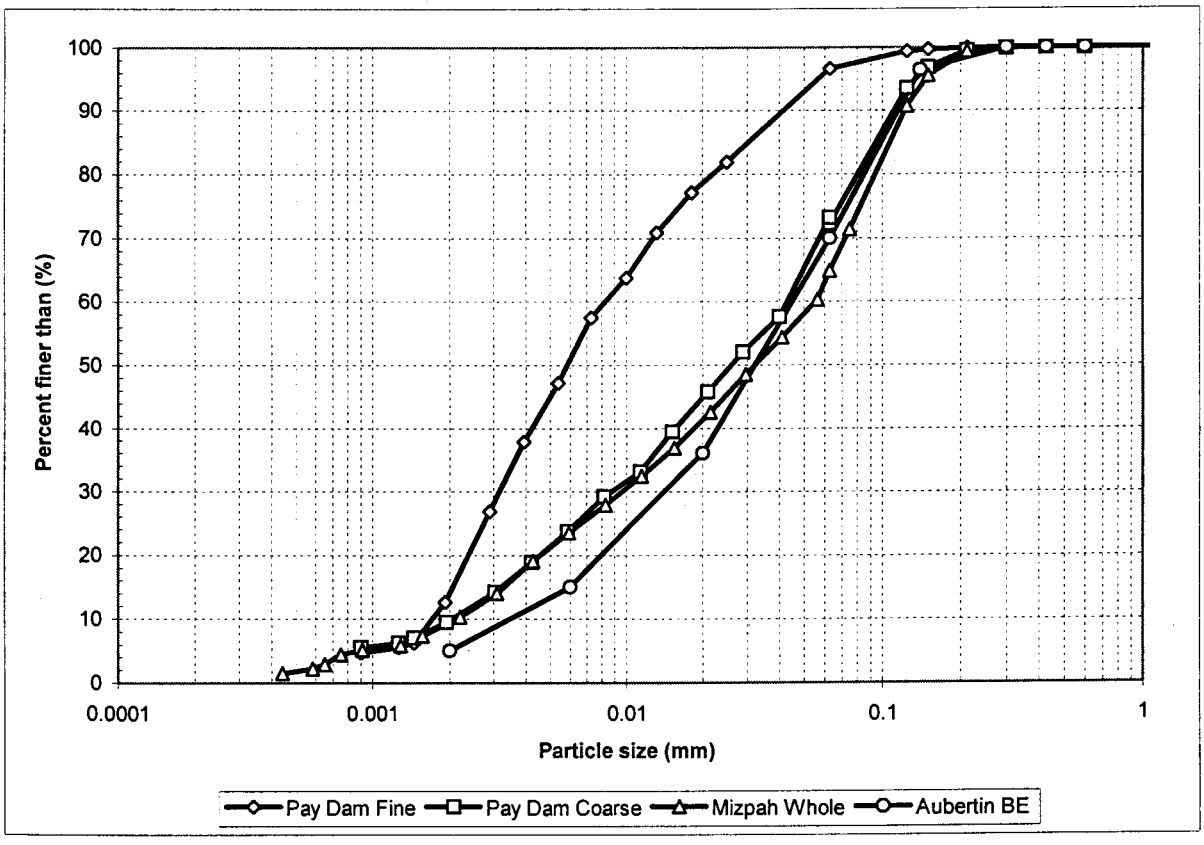

Figure 3.16: Grading curves for the three gold tailings samples (after Vermeulen, 2001 and Aubertin et al, 1998)

Desiccation tests using the troughs described in Section 3.4 as well as suction measurements using the suction probe were used to obtain soil-water characteristics curves for both the fine and coarse tailings from Pay Dam. The whole tailings obtained from Mizpah, were separated into different size ranges. Soil-water characteristics curves (SWCCs) were then also obtained for the different size ranges using the same method. The aim of this dissertation was then to investigate the possibility of combining the data for the different particle size ranges and comparing them to the SWCC data for the fine and coarse tailings from Pay Dam and also to new samples created to replicate Pay Dam coarse and Aubertin BE tailings.

3.6.2 Obtaining the different particle size ranges

The whole tailings from Mizpah were used in this part of the experimental work. Gold tailings may be classified as a fine, hard and angular rock flower, with generally 0-15 % fine sand, 80 % silt and 0-10 % clay sized particles slurried with process water (Vick, 1983; McPhail and Wagener, 1989). It is thus evident that the majority of gold tailings are of silt-sized particles. It was therefore decided to investigate the effects that the following particle size ranges will have on the SWCC of the whole sample (The letters given next to each size range shall from here on end refer to the particular range):

A: Sand sized particles ⇒ > 63 μm

B: Coarse silt sized particles ⇒ 20 to 63 μm

C: Medium silt sized particles ⇒ 6 to 20 μm

D: Fine silt sized particles ⇒ 2 to 6 μm

E: Clay sized particles ⇒ < 2 μm

Figure 3.17 shows the location of these ranges on the grading curves given in Figure 3.16.

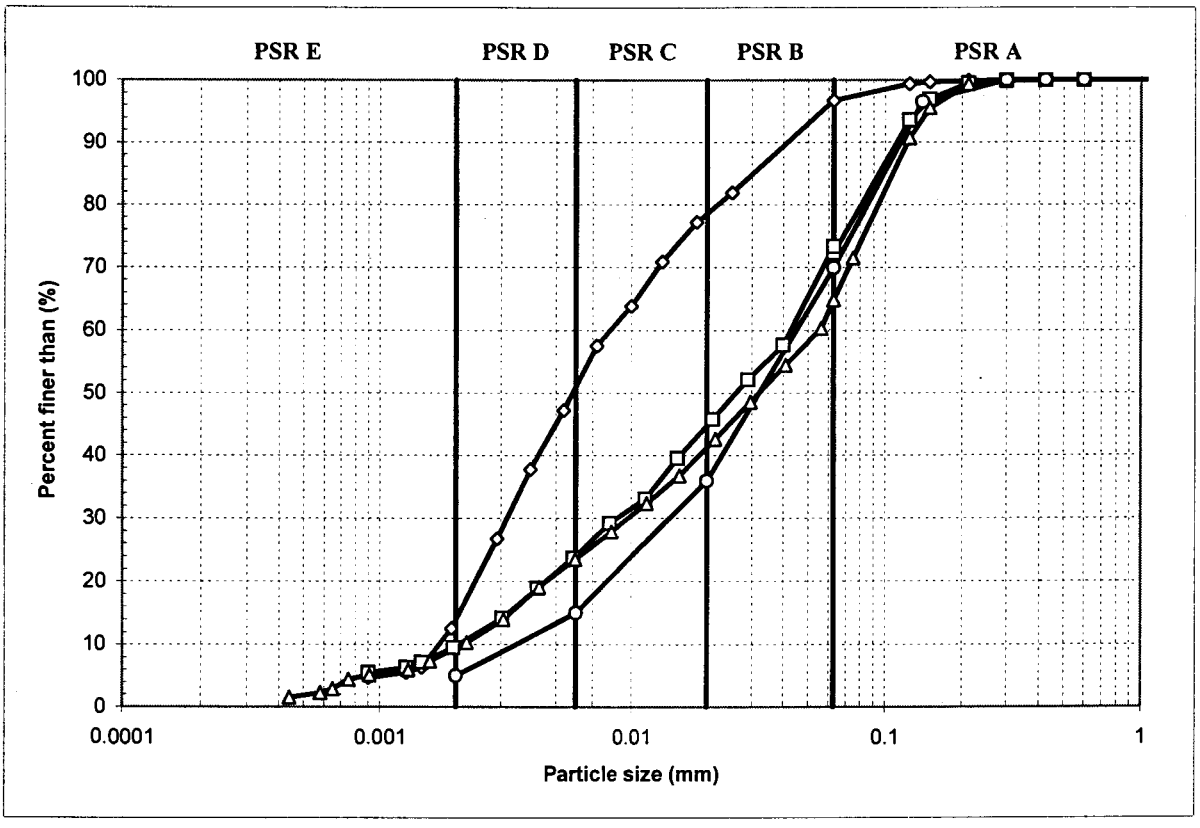

Figure 3.17: Particle size ranges used

The tailings sample was flocculated during the extraction and sample catchment process. For the separation of the different sizes, a dispersing agent needs to be used (Head, 1984). A small quantity of soluble chemical is added before the sedimentation test, usually in the form of a measured quantity of a prepared stock solution. The stock solution recommended by the British Standard and used in this study is made up of:

35 g sodium hexametaphosphate
7 g sodium carbonate
Distilled water to make 1 litre of solution

This stock solution is referred to as the standard dispersant, and is added to the water used for sieving or sedimentation. British Standard specifies using 50 ml of standard dispersant per litre of the material and water mix.

Wet Sieving:

If a soil contains silt or clay, it is necessary to carry out a wet-sieving procedure. Even when dry, fine particles of silt and clay can adhere to larger sand-sized particles and cannot be separated by dry sieving. Washing is the only practicable means of ensuring complete separation of fines (Head, 1984). The whole tailings sample was covered with distilled water containing 50 ml of the standard dispersant per litre of water and left for a few hours. The whole sample was washed through a 63 μm sieve using distilled water and the standard dispersant as described by Head (1984). The water that ran through the sieve were caught in buckets and dried in an oven at about 50 °C. The material retained on the sieve were washed from the sieve and oven dried in buckets at the same temperature (Sample A).

Sedimentation:

The theory of sedimentation is based on the fact that large particles in suspension in a liquid settle more quickly than small particles, assuming that all particles have similar densities and shapes. The standard test procedure according to BS1377 was modified for the purpose of this study. The principal of sedimentation was applied to extract samples B through E, simply because the smallest sieve available is the 63 μm sieve.

According to Stokes' Law (Stokes, 1891), the terminal velocity υ of a spherical particle falling freely in a fluid is given by:

$$\upsilon = \frac{D^2.g.(\rho_s - \rho_l)}{18\eta} \qquad [3.9]$$

Where:

D = Diameter of particle

ρ_s = Mass density of the solid particle

ρ_l = Mass density of the fluid

η = Dynamic viscosity of the fluid

g = Acceleration due to gravity

The application of Stokes' Law to the process of sedimentation is based on the following simplifying assumptions:

- The condition of viscous flow in a still liquid is maintained
- There is no turbulence – the concentration of the particles is such that they do not interfere with one another
- The temperature of the liquid remains constant
- Particles are small spheres
- The terminal velocities of the particles are small
- All particles have the same density
- A uniform distribution of the particles of all sizes is formed within the liquid

Stokes' Law may then be rewritten as follows with g = 9.81 m/s^2 and ρ_w = 1000 kg/m^3:

$$t = \frac{\eta.H}{(G_s - 1)\left(\frac{D}{0.005531}\right)^2} \qquad [3.10]$$

Where:

t = Settling time (min)

η = Dynamic viscosity of the fluid = 1.0019 m.Pa.s (at 20 °C)

H = Settling height (mm)

G_s = Specific gravity of particle = 2.74 (Vermeulen, 2001)

D = Diameter of particle (mm)

With the above equation, it was possible to determine the time it would take a particle with a certain diameter to drop to a certain depth in a solution of distilled water and standard dispersant.

The material that passed the 63 μm sieve and oven dried at 50 °C were used in the sedimentation process. The following were the steps taken in obtaining samples B through E:

1) Fill a 1-litre glass cylinder with 1 litre of distilled water and add 50 ml of the standard dispersant.

2) Add about 50 g of the material that passed through the 63 μm sieve.

3) Rotate the cylinder several times end over end and let stand for at least an hour.

4) Rotate the cylinder 60 times end over end and start the timer immediately when the cylinder is returned to the table surface.

5) Keep an eye on the level of material that deposits at the bottom of the cylinder. Calculate the approximate time it would take for a particle with a diameter of 20 μm to drop from the surface of the solution to a level just above the perceived deposit level.

6) Insert one end of a thin plastic tube into the cylinder, and let the other end hang over an empty bucket. Re-calculate the time it would take a particle with a diameter of 20 μm to drop to a level just above the current level of deposited material.

7) Start draining the material above the deposition level by sucking on the one end of the pipe and letting the solution flow into the bucket by gravity flow. The submerged end of the pipe should stay just below the solution's surface and must follow the receding surface up to the level of deposition.

8) The solution should be completely drained when the timer reaches the calculated time in step 6. The bucket with the drained solution is then oven dried at 50 °C.

9) The deposited material retained in the glass cylinder now should have particle diameters between 20 and 63 μm (Sample B). The sample is removed and oven dried at 50 °C.

10) Steps 1 through 9 are repeated several times to ensure that enough material is drained in the solution for the smaller samples.

The above steps are repeated to obtain samples C through E. For sample C, the diameter used in the calculations in steps 5 and 6 are 6 μm (6 to 20 μm), and for sample D it is 2 μm (2 to 6 μm). For sample E, the solution drained when obtaining sample D is used (smaller than 2 μm). Figure 3.18 shows the separation procedure.

Figure 3.18: Separation of particle size ranges

3.6.3 Creating new samples using particle size ranges

The opportunity arose for the creation of new samples using the particle size ranges discussed above. It was decided to replicate the Pay Dam coarse (NS C) and Aubertin BE (NS A) samples, and comparing the experimental results for NS C to results for Pay Dam coarse, and comparing results for NS A to results from Aubertin et al (1998). Table 3.1 lists the particle size range (PSR) percentages used to create NS A and NS C. Refer also to Figure 3.17.

Table 3.1: Particle Size Range Percentages used to create NS A and NS C

New Sample -	PSR A (%)	PSR B (%)	PSR C (%)	PSR D (%)	PSR E (%)	Total (%)
NS A	30	34	21	10	5	100
NS C	27	28	21	15	9	100

3.7 Test Method

All the steps necessary in devising a test method for the determination of soil water characteristic curve data on different gradings of gold mine tailings have been discussed in the preceding sections. All these steps need to be placed in the correct order and the method should be described in detail.

3.7.1 Preparing the material and starting the test

The material is thoroughly mixed with distilled water into a slurry consistency and left to stand for a few minutes. A shrinkage trough as described in Section 3.4 is cleaned and lightly wiped with Vaseline on the inside. The trough is now weighed, M_{trough}. The material is now thoroughly mixed again and poured into the trough. To increase the density of the material, the trough may be tapped a number of times. This will also let trapped air bubbles escape. It is not necessary to fill the trough completely. It is however necessary to ensure that the surface of the material is flat. The mass of the trough with the material is now measured, M_i. The trough is kept at a room temperature of 21 °C.

The suction probe should be ready at this stage for suction measurements. The saturation and calibration process should have been completed before starting the test. The tools necessary for volume change measurements (Figure 3.6) must be at the ready.

3.7.2 Measurements of mass, volume and suction

Measurements of mass and volume change are continually made throughout the drying process as described in Section 3.4. Taking measurements on an hourly or two hourly bases is sufficient. Measurements of mass are simply made with an accurate scale. Volume change is calculated with measurements of change in length and in height. Figure 3.19 shows how a spatula and vernier are used to measure the change in height of the material.

Measurements of suctions are made at shorter intervals, since for sample D the suctions rose to 350 kPa in less than 5 hours. The method used in measuring suctions was discussed in detail in Section 3.5. When two or more troughs are tested simultaneously, suction measurements should be taken after the minimum waiting time required and the probe removed and placed in water. The same should then

be carried out for the other troughs. When only one trough is tested, it is possible for the probe to be kept in contact with the material surface after the waiting time has passed. Measurements may then be taken selectively. It is then only necessary to remove the probe when measurements of mass and volume need to be made.

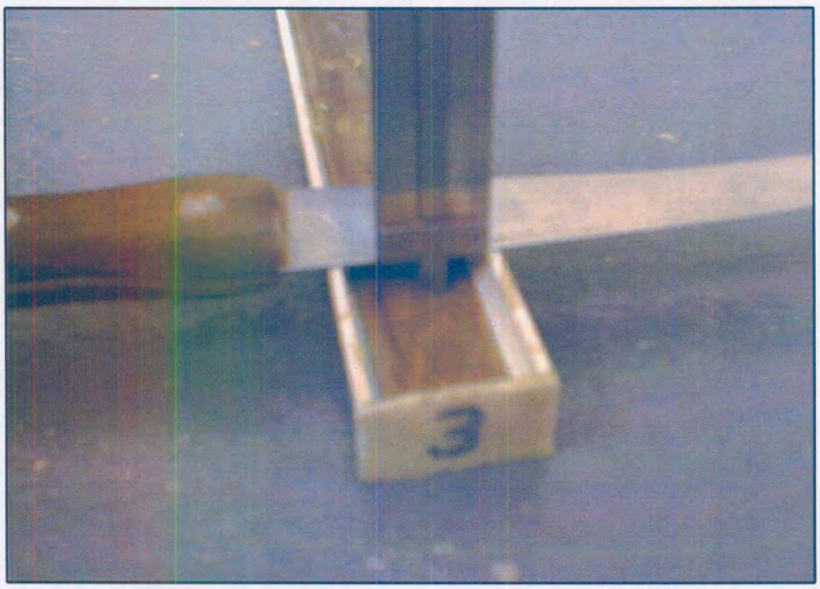

Figure 3.19: Measurement of change in height

When the drying time exceeds a working day, the trough may be placed in a desiccator overnight. It was found that this practise does not influence the measurements. When the material has dried out completely, the moisture content at every stage in the drying process may be calculated, w, as described in Section 3.4.

It is also more convenient to only measure mass and volume over the range where suctions are measured. The regression method described in the following section, shall also only be applied over the range where suctions were measured.

3.7.3 Regression of M and V and calculation of w, e, S, n and θ

Suction measurements need to be compared to the material's gravimetric moisture content, w, and volumetric moisture content, θ, at the time when the measurements of suction were made. However, measurements of mass, M, and volume, V, were made at different times, thus suction values may not

be compared to them directly. It is thus necessary to fit regression lines to the M and V data over time. The "add trendline" function in Microsoft Excel was used for this purpose. Generally, a 2nd order polynomial function was sufficient. The equation generated was then used to calculate the M and V values of the material at the same times when the measurements of suction were made. Figure 3.20 shows a regression line fitted to M data and Figure 3.21 shows a regression line fitted to V data. When the shrinkage limit is reached V will remain constant. The equation given in Figure 3.21 is used to obtain the turning point of the function. At the turning point the first derivative of the function is equal to zero. This equation is used to obtain the time at which the shrinkage limit is reached. To obtain the volume of the material at the shrinkage limit, the calculated time is simply substituted into the original equation.

Using Figure 3.21 as an example:

$$V = 31.823t^2 - 43.56t + 33.733$$

$$\frac{dV}{dt} = 63.646t - 43.56 = 0 \Rightarrow t = 0.684 = 16:25:33$$

$V = 18.827\ cm^3$ @ the shrinkage limit

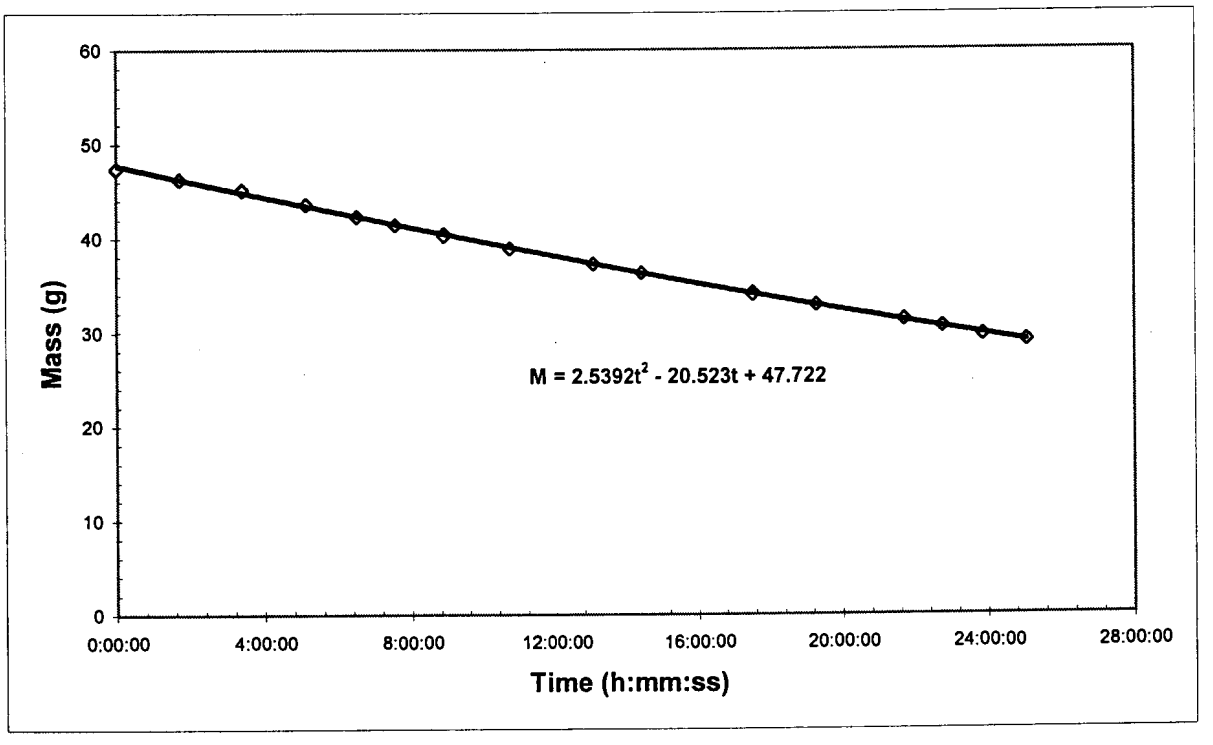

Figure 3.20: Regression of mass versus time data

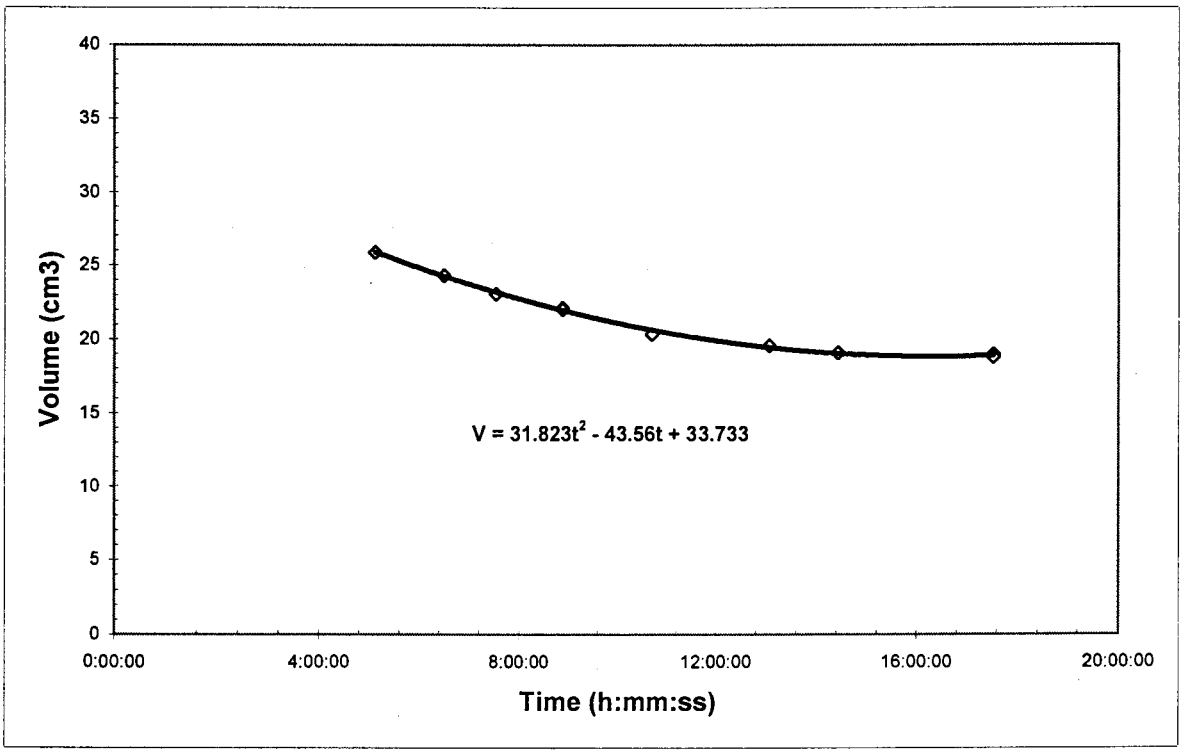

Figure 3.21: Regression of volume versus time data

The gravimetric moisture content, w, may be calculated using the mass of the trough and the material and the dry mass as explained in Section 3.4. With the w and volume, V, known for the material at a certain time, the void ratio, e, degree of saturation, S, porosity, n, and the volumetric water content, θ, may be calculated with the following equations (Craig, 1997):

$$e = \frac{(V.G_s.\rho_w)}{M_s} - 1 \qquad [3.11]$$

$$S = \frac{G_s.w}{e} \qquad [3.12]$$

$$n = \frac{e}{1+e} \qquad [3.13]$$

$$\theta = S.n \qquad [3.14]$$

3.7.4 Comparing the calculated values with suction

It is now possible to plot the calculated values against suction as well as gravimetric or volumetric moisture content against suction (SWCC). It is also now possible to compare the air-entry values obtained from the suction versus time data, the suction versus volumetric moisture content data, and from the turning point of the regression line. Various other values may also be compared with each other as will be shown in Chapters 4 and 5.

3.8 Field Measurements of Suction

The use of the suction probe for field suction measurements was also attempted. However it is deemed beyond the scope of this report. Further investigation into the field use of the probe is however still required. Preliminary testing however showed that the probe could effectively be used in the field. Testing was only conducted near the surface and it was clear that a similar stand to the one used during laboratory testing should be constructed to keep the probe upright. Figure 3.22 shows the in-situ measurement of suction at a tailings dam using the mid-plane suction probe.

Figure 3.22: In-situ measurement of suction using the mid plane suction probe

CHAPTER 4:

DIRECT MEASUREMENT OF PORE FLUID SUCTION IN GOLD MINE TAILINGS

4.1 Introduction

The aim of this chapter is to present the raw data obtained from the experimental programme discussed in Chapter 3. A discussion will follow on the presented data in Chapter 5. Data includes tables containing values for certain parameters and graphs representing the tabulated values.

This chapter is divided into various sections, each dealing with a certain material grading (Pay Dam Coarse and Fine), particle size range (Range A through Range E) or new samples created from particle size ranges (Sample A and Sample C) which was discussed in Section 3.6. The tables presented contain data comparing time, suction, gravimetric water content (w), void ratio (e), degree of saturation (S), volumetric water content (θ) and linear shrinkage (LS) of a sample of tailings undergoing desiccation. The graphs presented compare only the more relevant parameters. The time values represent the time since the first measurements of mass were made. The notation used to represent each sample is as follows: day-month-trough number. For example, a test started on the 3rd of January using trough number 4 would be labelled 3-1-4.

4.2 Pay Dam Coarse

Table 4.1 to 4.3 represents the data obtained from tests carried out on Pay Dam coarse tailings.
Figure 4.1 represents suction (on a logarithmic scale) versus time for the above samples.
Figure 4.2 represents gravimetric water content, w, versus suction (on a logarithmic scale).
Figure 4.3 represents void ratio, e, versus water content, w.
Figure 4.4 represents linear shrinkage, LS, versus suction.

Table 4.1: Test Data for Pay Dam Coarse Tailings (Sample 2-7-1)

Time (h:mm:ss)	Suction (kPa)	w -	e -	S -	θ -	LS (%)
4:31:00	5.9	0.32	0.88	0.99	0.46	0.00%
4:40:00	5.9	0.31	0.87	0.99	0.46	0.00%
5:05:00	10.5	0.30	0.84	0.98	0.45	0.00%
5:14:00	10.5	0.30	0.83	0.98	0.45	0.00%
5:39:00	16.3	0.29	0.81	0.98	0.44	0.16%
6:01:00	22.7	0.28	0.80	0.97	0.43	0.50%
6:27:00	30.2	0.27	0.78	0.95	0.42	0.86%
7:32:00	77.8	0.25	0.74	0.91	0.39	1.59%
7:48:00	95.5	0.24	0.73	0.90	0.38	1.74%
8:07:00	96.7	0.23	0.72	0.88	0.37	1.90%
8:30:00	110.7	0.22	0.72	0.85	0.36	2.06%
8:57:00	117.7	0.21	0.71	0.82	0.34	2.21%
9:30:00	120.4	0.20	0.70	0.78	0.32	2.34%
9:45:00	123.4	0.19	0.70	0.76	0.31	2.39%
10:05:00	126.4	0.19	0.70	0.73	0.30	2.42%
10:44:00	137.0	0.17	0.70	0.68	0.28	2.44%
11:18:00	153.3	0.16	0.70	0.63	0.26	2.44%
11:49:00	165.4	0.15	0.70	0.59	0.24	2.44%
12:16:00	185.4	0.14	0.70	0.55	0.23	2.44%
12:47:00	199.4	0.13	0.70	0.50	0.21	2.44%
13:21:00	234.2	0.12	0.70	0.46	0.19	2.44%
13:51:00	246.0	0.11	0.70	0.42	0.17	2.44%
14:24:00	287.6	0.10	0.70	0.37	0.15	2.44%
14:59:00	316.6	0.08	0.70	0.33	0.13	2.44%
15:33:00	383.3	0.07	0.70	0.28	0.12	2.44%

Table 4.2: Test Data for Pay Dam Coarse Tailings (Sample 2-7-2)

Time (h:mm:ss)	Suction (kPa)	w -	e -	S -	θ -	LS (%)
8:48:00	0.6	0.35	0.91	1.05	0.50	0.00%
9:18:00	1.2	0.34	0.88	1.05	0.49	0.00%
9:54:00	2.8	0.32	0.85	1.05	0.48	0.00%
10:39:00	6.0	0.31	0.81	1.05	0.47	0.00%
11:16:00	9.9	0.30	0.78	1.04	0.46	0.01%
11:48:00	15.6	0.29	0.76	1.03	0.45	0.23%
12:19:00	25.2	0.28	0.74	1.02	0.44	0.42%
12:32:00	32.4	0.27	0.73	1.02	0.43	0.49%
12:48:00	42.0	0.27	0.73	1.01	0.42	0.58%
13:03:00	50.4	0.26	0.72	1.00	0.42	0.66%
13:25:00	61.0	0.26	0.71	0.99	0.41	0.77%
13:48:00	78.2	0.25	0.70	0.98	0.40	0.87%
14:02:00	87.0	0.24	0.69	0.97	0.40	0.93%
14:20:00	91.3	0.24	0.68	0.95	0.39	1.00%
14:39:00	96.5	0.23	0.68	0.94	0.38	1.06%
15:10:00	104.2	0.22	0.67	0.91	0.37	1.15%
15:50:00	114.4	0.21	0.66	0.88	0.35	1.24%
16:40:00	119.9	0.20	0.65	0.83	0.33	1.31%
17:10:00	125.6	0.19	0.65	0.79	0.31	1.33%
17:48:00	130.4	0.18	0.65	0.75	0.29	1.33%
18:22:00	141.8	0.17	0.65	0.71	0.28	1.33%
18:55:00	150.4	0.16	0.65	0.67	0.26	1.33%
19:14:00	160.9	0.15	0.65	0.65	0.25	1.33%
19:34:00	168.4	0.15	0.65	0.62	0.24	1.33%
20:07:00	184.4	0.14	0.65	0.58	0.23	1.33%
20:42:00	203.0	0.13	0.65	0.55	0.21	1.33%
21:16:00	227.7	0.12	0.65	0.51	0.20	1.33%
21:38:00	246.3	0.11	0.65	0.48	0.19	1.33%
22:07:00	255.8	0.11	0.65	0.45	0.18	1.33%
22:43:00	297.2	0.10	0.65	0.41	0.16	1.33%
23:12:00	328.3	0.09	0.65	0.38	0.15	1.33%
23:27:00	342.0	0.09	0.65	0.37	0.14	1.33%
23:52:00	375.3	0.08	0.65	0.34	0.13	1.33%

Table 4.3: Test Data for Pay Dam Coarse Tailings (Sample 2-7-4)

Time (h:mm:ss)	Suction (kPa)	w -	e -	S -	θ -	LS (%)
10:10:00	2.2	0.36	0.92	1.06	0.51	0.00%
10:44:00	2.9	0.34	0.89	1.06	0.50	0.00%
11:23:00	6.0	0.33	0.86	1.05	0.49	0.00%
11:50:00	8.7	0.32	0.83	1.05	0.48	0.00%
12:43:00	17.2	0.30	0.79	1.04	0.46	0.26%
13:21:00	26.2	0.29	0.77	1.02	0.44	0.52%
13:51:00	40.4	0.28	0.75	1.01	0.43	0.70%
14:29:00	61.6	0.26	0.73	0.98	0.42	0.89%
15:03:00	82.5	0.25	0.72	0.96	0.40	1.02%
15:36:00	86.0	0.24	0.71	0.93	0.39	1.12%
15:56:00	91.1	0.23	0.70	0.92	0.38	1.17%
16:19:00	95.6	0.23	0.69	0.89	0.37	1.21%
16:55:00	102.7	0.21	0.69	0.86	0.35	1.24%
17:37:00	109.5	0.20	0.68	0.81	0.33	1.24%
18:19:00	116.0	0.19	0.68	0.76	0.31	1.24%
18:53:00	123.8	0.18	0.68	0.72	0.29	1.24%
19:27:00	140.4	0.17	0.68	0.67	0.27	1.24%
20:10:00	157.2	0.15	0.68	0.62	0.25	1.24%
20:35:00	170.1	0.15	0.68	0.59	0.24	1.24%
20:47:00	175.9	0.14	0.68	0.58	0.23	1.24%
21:05:00	189.4	0.14	0.68	0.55	0.22	1.24%
21:24:00	200.9	0.13	0.68	0.53	0.21	1.24%
21:53:00	219.0	0.12	0.68	0.50	0.20	1.24%
22:14:00	220.1	0.12	0.68	0.47	0.19	1.24%
22:19:00	223.8	0.12	0.68	0.47	0.19	1.24%
22:40:00	241.5	0.11	0.68	0.44	0.18	1.24%
23:06:00	265.7	0.10	0.68	0.41	0.17	1.24%
23:24:00	283.8	0.10	0.68	0.39	0.16	1.24%
23:49:00	313.2	0.09	0.68	0.36	0.15	1.24%
24:07:00	337.0	0.08	0.68	0.34	0.14	1.24%
24:17:00	351.5	0.08	0.68	0.33	0.13	1.24%
24:27:00	368.3	0.08	0.68	0.32	0.13	1.24%
24:35:00	380.9	0.08	0.68	0.31	0.13	1.24%

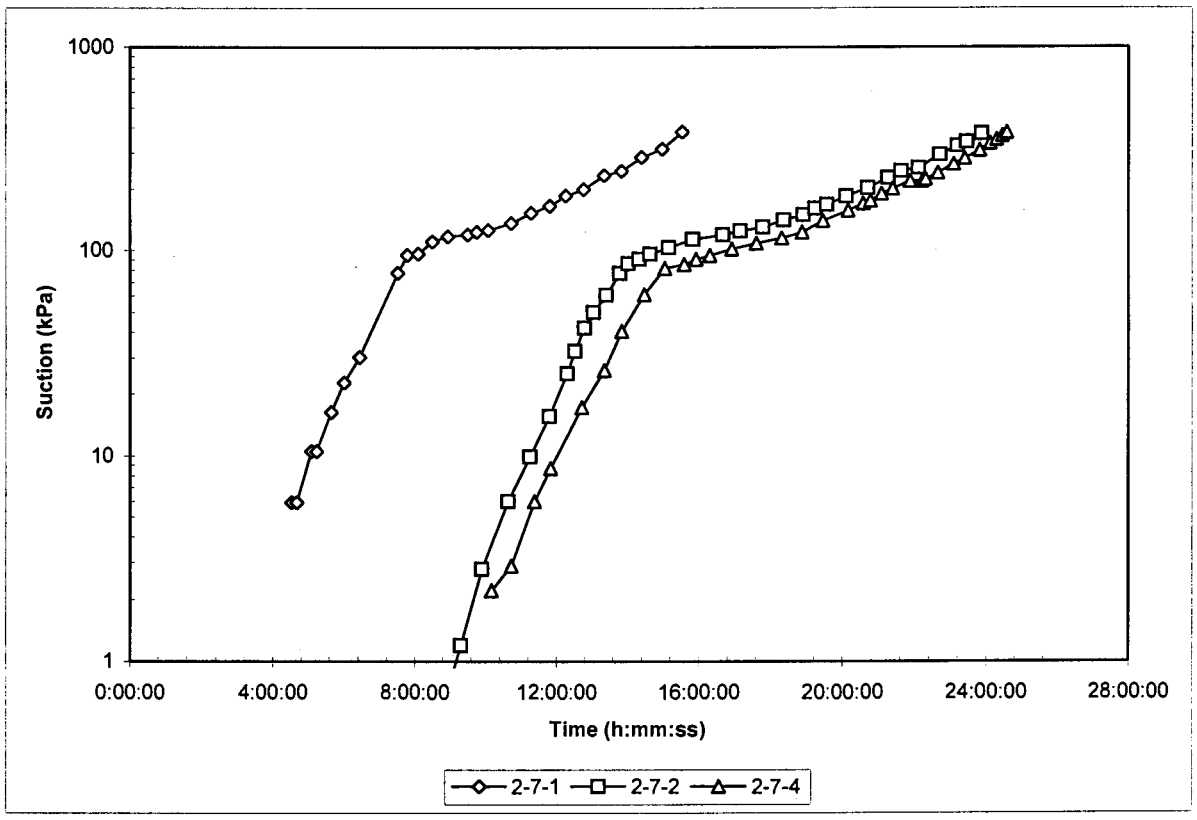

Figure 4.1: Suction versus time

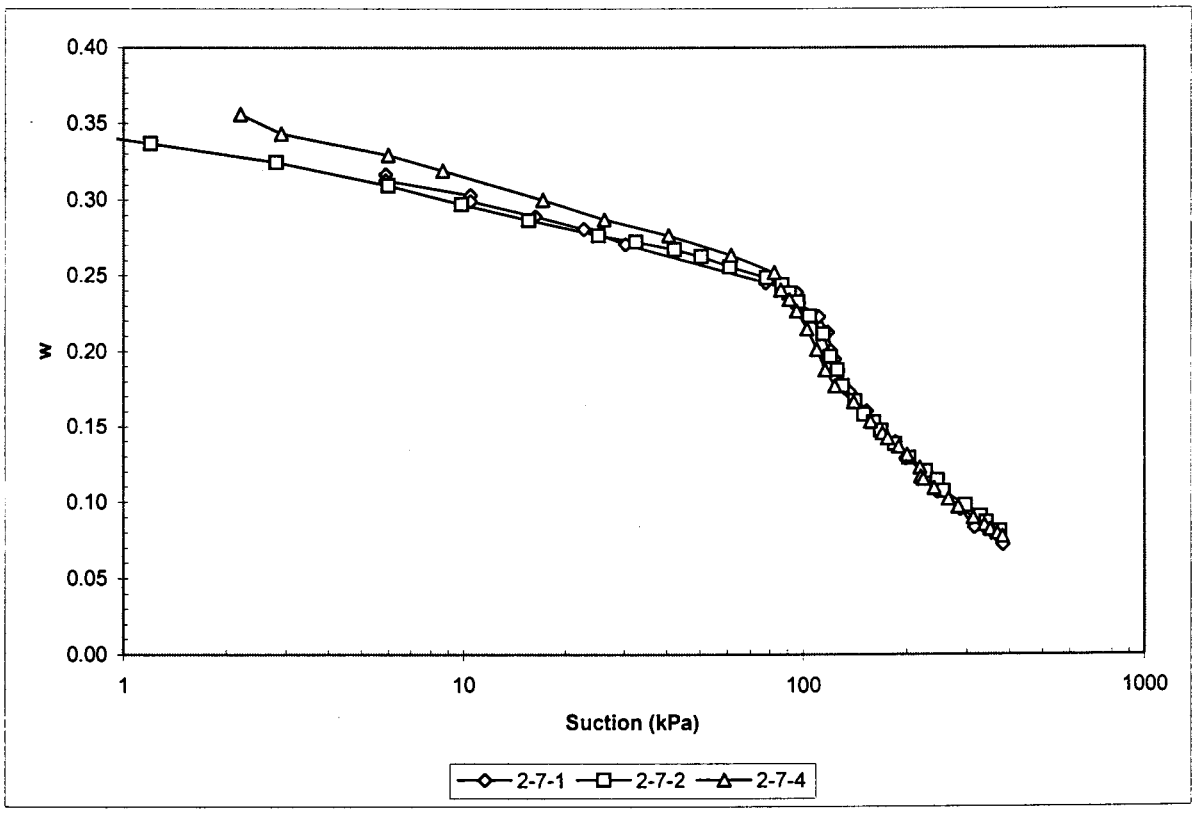

Figure 4.2: Moisture content, w, versus suction (SWCC)

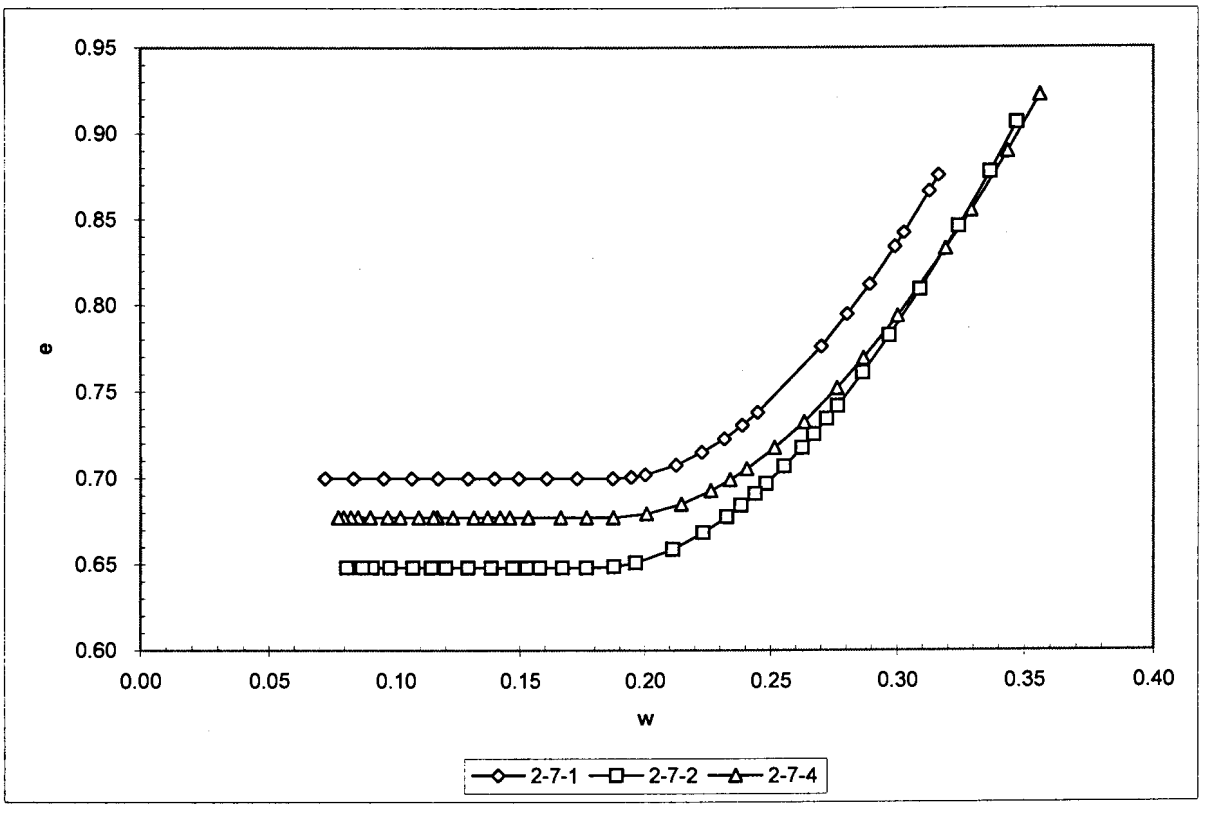

Figure 4.3: Void ratio, e, versus moisture content, w (shrinkage curve)

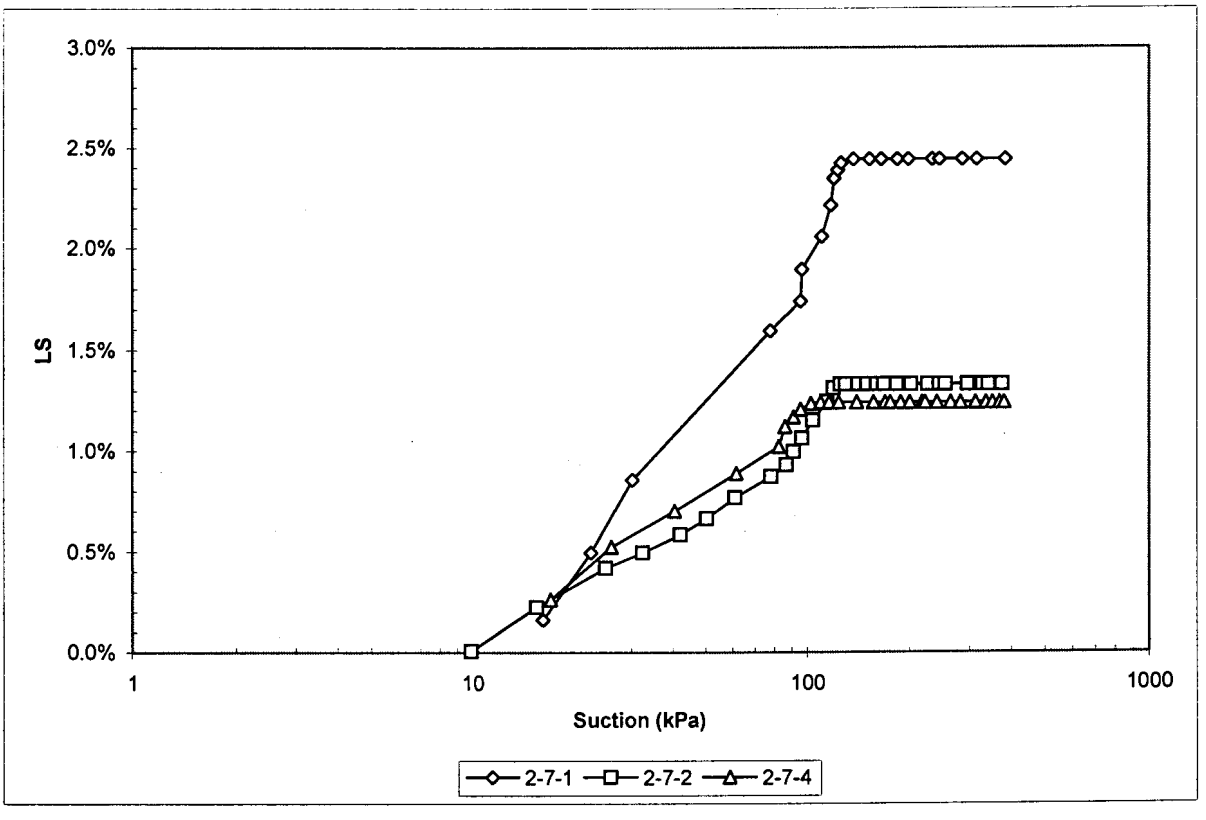

Figure 4.4: Linear shrinkage, LS, versus suction

4.3 Pay Dam Fine

Table 4.4 to 4.8 represents the data obtained from tests carried out on Pay Dam fine tailings.

Figure 4.5 represents suction (on a logarithmic scale) versus time for the above samples.

Figure 4.6 represents gravimetric water content, w, versus suction (on a logarithmic scale).

Figure 4.7 represents void ratio, e, versus water content, w.

Figure 4.8 represents linear shrinkage, LS, versus suction.

Table 4.4: Test Data for Pay Dam Fine Tailings (Sample 24-6-1)

Time (h:mm:ss)	Suction (kPa)	w -	e -	S -	θ -	LS (%)
15:59:00	9.3	0.54	1.53	0.96	0.58	0.40%
16:54:00	21.4	0.51	1.47	0.96	0.57	1.25%
17:15:00	31.1	0.50	1.44	0.96	0.56	1.54%
17:36:00	34.7	0.49	1.42	0.95	0.56	1.82%
18:10:00	47.5	0.48	1.38	0.95	0.55	2.23%
18:53:00	69.2	0.46	1.34	0.93	0.53	2.68%
19:19:00	82.1	0.44	1.31	0.92	0.52	2.92%
20:54:00	163.5	0.40	1.24	0.88	0.48	3.59%
21:20:00	193.0	0.38	1.22	0.86	0.47	3.71%
21:58:00	199.8	0.36	1.20	0.83	0.45	3.84%
22:28:00	207.5	0.35	1.18	0.81	0.44	3.91%
23:16:00	220.0	0.32	1.16	0.76	0.41	3.94%
23:40:00	230.0	0.31	1.15	0.74	0.40	3.94%
24:23:00	249.3	0.29	1.14	0.69	0.37	3.94%
24:56:00	258.2	0.27	1.13	0.66	0.35	3.94%
25:16:00	262.8	0.26	1.13	0.63	0.34	3.94%
26:01:00	290.0	0.24	1.12	0.58	0.31	3.94%
26:26:00	291.9	0.22	1.12	0.55	0.29	3.94%
27:18:00	317.0	0.19	1.12	0.48	0.25	3.94%
28:10:00	369.8	0.17	1.12	0.41	0.21	3.94%

Table 4.5: Test Data for Pay Dam Fine Tailings (Sample 24-6-2)

Time (h:mm:ss)	Suction (kPa)	w -	e -	S -	θ -	LS (%)
15:57:00	3.4	0.59	1.71	0.95	0.60	0.00%
16:54:00	5.6	0.57	1.64	0.95	0.59	0.00%
17:33:00	11.0	0.55	1.59	0.95	0.58	0.00%
18:10:00	14.3	0.54	1.54	0.95	0.58	0.48%
18:50:00	21.1	0.52	1.50	0.95	0.57	1.04%
19:15:00	23.8	0.51	1.47	0.95	0.56	1.36%
20:54:00	56.9	0.47	1.38	0.93	0.54	2.45%
21:22:00	67.5	0.45	1.35	0.92	0.53	2.70%
21:55:00	91.2	0.44	1.33	0.91	0.52	2.96%
22:22:00	124.9	0.43	1.31	0.90	0.51	3.15%
22:53:00	148.5	0.42	1.28	0.89	0.50	3.35%
23:49:00	187.8	0.39	1.25	0.86	0.48	3.62%
24:33:00	206.8	0.37	1.22	0.84	0.46	3.76%
25:10:00	214.5	0.36	1.20	0.81	0.44	3.84%
26:21:00	223.8	0.33	1.17	0.76	0.41	3.87%
27:45:00	254.3	0.29	1.14	0.69	0.37	3.87%
28:27:00	262.2	0.27	1.13	0.65	0.35	3.87%
29:47:00	302.2	0.23	1.12	0.57	0.30	3.87%
30:41:00	327.7	0.21	1.12	0.51	0.27	3.87%
30:57:00	339.6	0.20	1.12	0.49	0.26	3.87%

Table 4.6: Test Data for Pay Dam Fine Tailings (Sample 24-6-4)

Time (h:mm:ss)	Suction (kPa)	w -	e -	S -	θ -	LS (%)
18:48:00	4.9	0.60	1.64	1.01	0.63	0.00%
19:12:00	4.7	0.59	1.61	1.01	0.62	0.00%
20:52:00	14.6	0.54	1.48	1.01	0.60	0.41%
21:25:00	22.4	0.53	1.44	1.00	0.59	0.86%
21:53:00	27.6	0.52	1.41	1.00	0.59	1.21%
22:15:00	27.4	0.51	1.39	1.00	0.58	1.46%
22:44:00	42.1	0.49	1.36	0.99	0.57	1.78%
23:27:00	62.1	0.47	1.32	0.98	0.56	2.19%
23:58:00	78.7	0.46	1.30	0.97	0.55	2.44%
24:48:00	116.3	0.43	1.26	0.95	0.53	2.79%
25:31:00	151.9	0.42	1.23	0.93	0.51	3.02%
26:10:00	196.7	0.40	1.20	0.90	0.49	3.17%
27:10:00	204.2	0.37	1.17	0.86	0.47	3.30%
28:30:00	226.3	0.33	1.14	0.80	0.43	3.32%
29:18:00	241.3	0.31	1.13	0.76	0.40	3.32%
30:28:00	262.6	0.28	1.12	0.69	0.36	3.32%
30:55:00	267.1	0.27	1.12	0.66	0.35	3.32%
31:26:00	279.5	0.25	1.12	0.62	0.33	3.32%
32:04:00	293.5	0.24	1.12	0.58	0.31	3.32%
32:49:00	300.5	0.22	1.12	0.53	0.28	3.32%
33:09:00	305.9	0.21	1.12	0.51	0.27	3.32%

Table 4.7: Test Data for Pay Dam Fine Tailings (Sample 16-7-2)

Time (h:mm:ss)	Suction (kPa)	w -	e -	S -	θ -	LS (%)
6:12:00	0.3	0.61	1.54	1.08	0.65	0.00%
6:29:00	1.3	0.60	1.51	1.09	0.65	0.00%
6:53:00	1.9	0.59	1.47	1.10	0.65	0.00%
7:18:00	3.9	0.57	1.42	1.11	0.65	0.00%
7:41:00	4.3	0.56	1.38	1.11	0.65	0.00%
8:33:00	7.0	0.54	1.30	1.13	0.64	0.00%
9:28:00	15.0	0.51	1.22	1.14	0.63	0.00%
9:34:00	16.7	0.51	1.22	1.14	0.63	0.00%
9:44:00	18.9	0.50	1.20	1.15	0.63	0.00%
9:53:00	21.1	0.50	1.19	1.15	0.62	0.00%
10:42:00	32.4	0.47	1.13	1.15	0.61	0.46%
13:13:00	140.9	0.40	1.01	1.10	0.55	2.24%
13:54:00	190.3	0.38	0.98	1.07	0.53	2.56%
13:59:00	195.9	0.38	0.98	1.07	0.53	2.60%
14:05:00	202.6	0.38	0.98	1.06	0.53	2.64%
14:17:00	212.8	0.37	0.97	1.05	0.52	2.71%
14:44:00	228.5	0.36	0.96	1.03	0.50	2.87%
14:51:00	232.8	0.36	0.96	1.02	0.50	2.90%
15:05:00	239.4	0.35	0.96	1.01	0.49	2.97%
16:13:00	249.0	0.32	0.95	0.93	0.45	3.17%
17:28:00	270.7	0.29	0.95	0.83	0.41	3.20%
18:13:00	282.7	0.27	0.95	0.78	0.38	3.20%
19:13:00	307.3	0.24	0.95	0.70	0.34	3.20%
20:05:00	329.0	0.22	0.95	0.64	0.31	3.20%

Table 4.8: Test Data for Pay Dam Fine Tailings (Sample 16-7-3)

Time (h:mm:ss)	Suction (kPa)	w -	e -	S -	θ -	LS (%)
9:55:00	1.9	0.64	1.46	1.21	0.72	0.00%
10:05:00	3.1	0.64	1.44	1.21	0.72	0.00%
10:55:00	3.5	0.61	1.37	1.23	0.71	0.00%
11:01:00	4.0	0.61	1.36	1.23	0.71	0.00%
11:14:00	5.0	0.60	1.34	1.23	0.70	0.00%
13:16:00	11.7	0.54	1.19	1.24	0.67	0.00%
14:20:00	26.4	0.50	1.12	1.24	0.65	0.03%
14:25:00	29.0	0.50	1.11	1.23	0.65	0.07%
14:29:00	30.7	0.50	1.11	1.23	0.65	0.11%
15:10:00	46.3	0.48	1.07	1.22	0.63	0.44%
15:21:00	52.0	0.47	1.06	1.22	0.63	0.53%
15:30:00	57.6	0.47	1.05	1.22	0.62	0.59%
16:17:00	92.6	0.44	1.02	1.20	0.60	0.91%
16:26:00	101.8	0.44	1.01	1.19	0.60	0.97%
16:43:00	121.7	0.43	1.00	1.18	0.59	1.07%
16:51:00	132.3	0.43	0.99	1.18	0.59	1.11%
17:09:00	158.0	0.42	0.98	1.17	0.58	1.21%
18:06:00	222.0	0.39	0.95	1.12	0.55	1.45%
19:02:00	228.2	0.36	0.92	1.07	0.51	1.63%
19:55:00	238.4	0.33	0.91	1.01	0.48	1.72%
21:25:00	262.2	0.29	0.89	0.89	0.42	1.75%
21:47:00	270.2	0.28	0.89	0.86	0.41	1.75%
22:05:00	277.4	0.27	0.89	0.84	0.39	1.75%
22:22:00	281.9	0.26	0.89	0.81	0.38	1.75%
22:34:00	287.9	0.26	0.89	0.79	0.37	1.75%
22:55:00	301.3	0.25	0.89	0.76	0.36	1.75%
23:08:00	307.7	0.24	0.89	0.74	0.35	1.75%
23:26:00	316.3	0.23	0.89	0.72	0.34	1.75%
23:53:00	331.1	0.22	0.89	0.68	0.32	1.75%
24:12:00	342.3	0.21	0.89	0.65	0.31	1.75%
24:34:00	357.3	0.20	0.89	0.62	0.29	1.75%

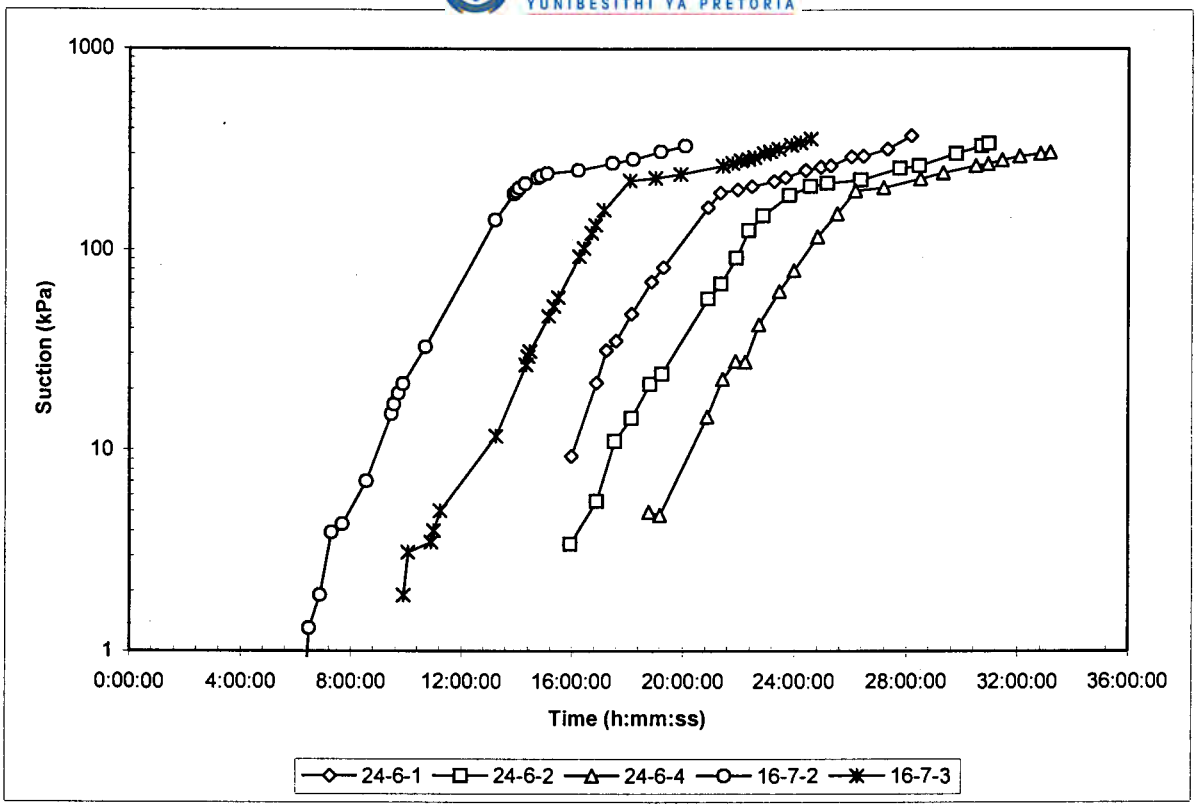

Figure 4.5: Suction versus time

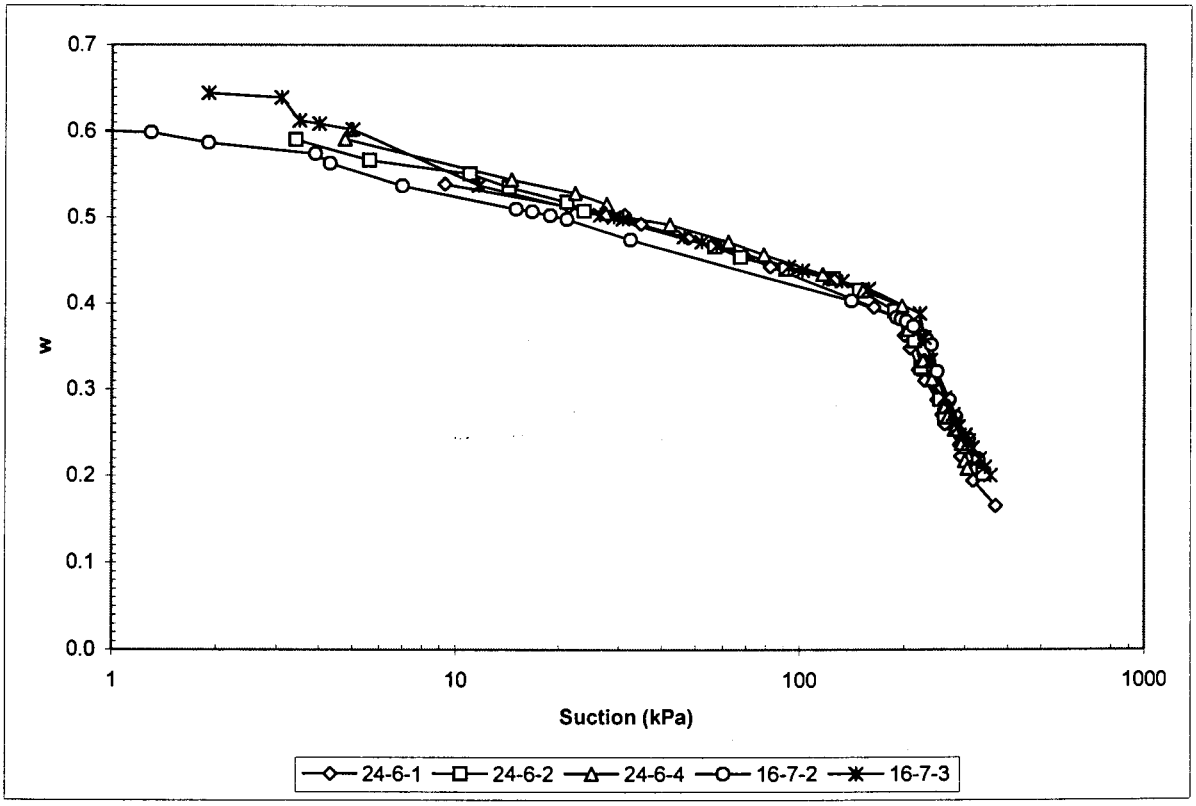

Figure 4.6: Moisture content, w, versus suction (SWCC)

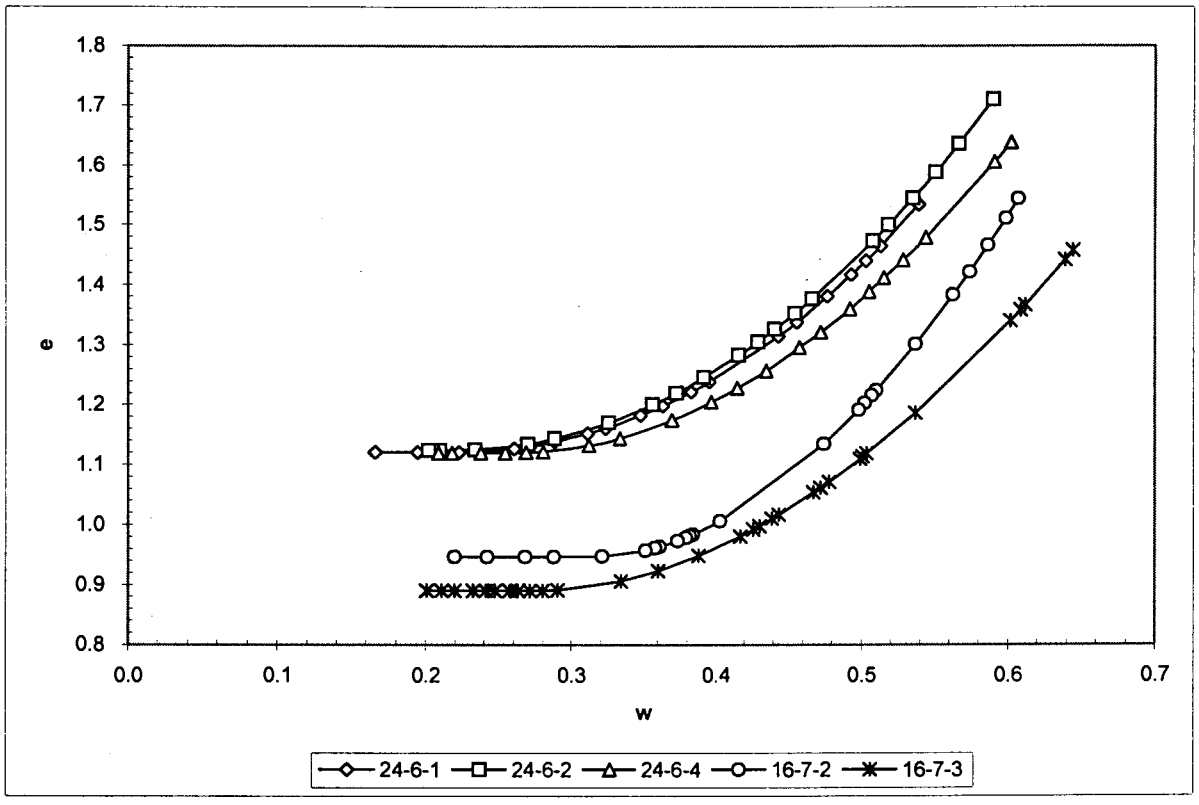

Figure 4.7: Void ratio, e, versus moisture content, w (shrinkage curve)

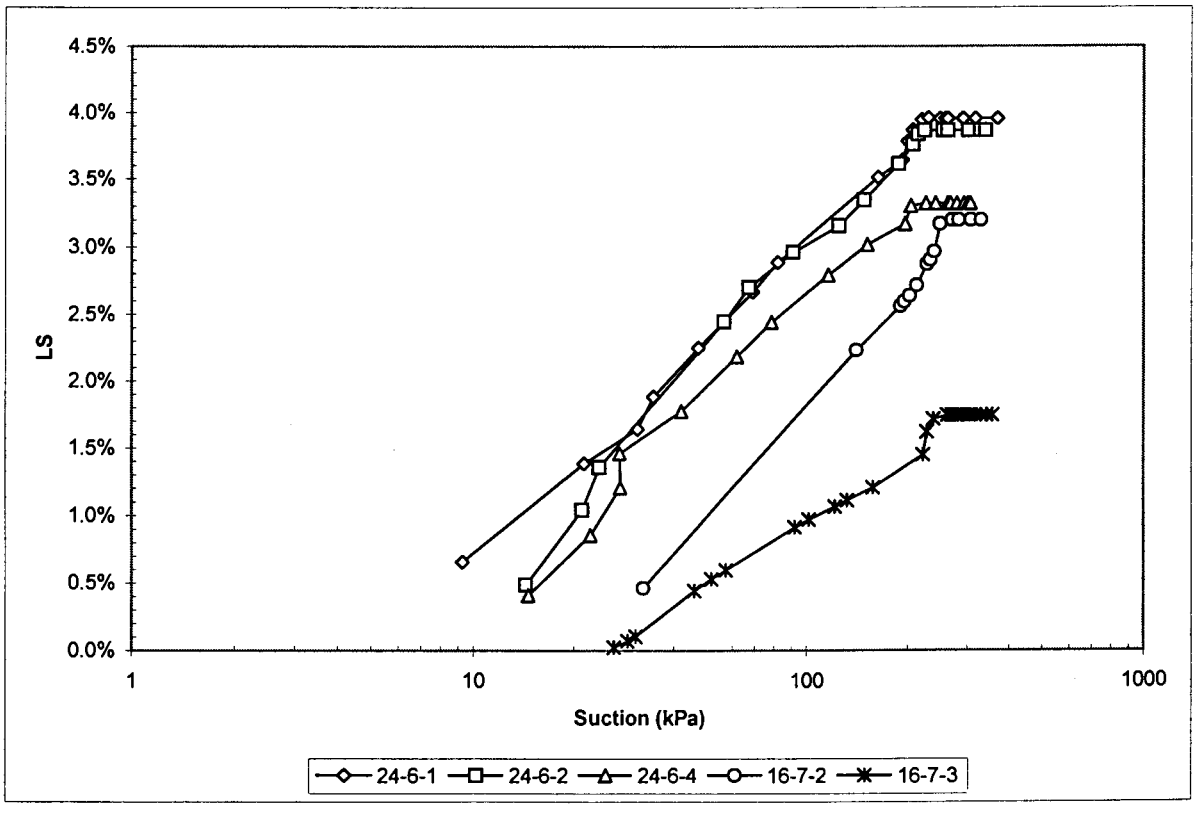

Figure 4.8: Linear shrinkage, LS, versus suction

Table 4.10: Test Data for Particle Size Range A (Sample 24-7-1)

Time (h:mm:ss)	Suction (kPa)	w -	e -	S -	θ -
0:45:00	0.4	0.24	0.57	1.16	0.42
0:49:00	1.4	0.24	0.57	1.16	0.42
0:53:00	2.4	0.24	0.57	1.15	0.42
0:57:00	3.2	0.24	0.57	1.14	0.42
1:00:00	3.7	0.24	0.57	1.14	0.41
1:05:00	4.5	0.24	0.57	1.13	0.41
1:11:00	5.4	0.23	0.57	1.12	0.41
1:15:00	6.0	0.23	0.57	1.11	0.40
1:19:00	6.8	0.23	0.57	1.10	0.40
1:25:00	7.4	0.23	0.57	1.09	0.40
1:35:00	6.9	0.22	0.57	1.07	0.39
1:40:00	7.4	0.22	0.57	1.06	0.39
1:46:00	7.7	0.22	0.57	1.05	0.38
1:51:00	8.0	0.22	0.57	1.04	0.38
1:57:00	8.1	0.22	0.57	1.03	0.38
2:03:00	8.3	0.21	0.57	1.02	0.37
2:12:00	8.8	0.21	0.57	1.01	0.37
2:24:00	9.0	0.21	0.57	0.98	0.36
2:30:00	9.1	0.20	0.57	0.97	0.35
2:47:00	8.1	0.20	0.57	0.94	0.34
2:53:00	8.8	0.19	0.57	0.93	0.34
2:59:00	9.1	0.19	0.57	0.92	0.34
3:05:00	9.5	0.19	0.57	0.91	0.33
3:13:00	9.8	0.19	0.57	0.90	0.33
3:23:00	10.2	0.18	0.57	0.88	0.32
3:34:00	10.7	0.18	0.57	0.86	0.31
3:44:00	10.8	0.18	0.57	0.84	0.31
3:54:00	11.1	0.17	0.57	0.82	0.30
4:04:00	11.3	0.17	0.57	0.81	0.29
4:19:00	11.4	0.16	0.57	0.78	0.28
4:33:00	11.6	0.16	0.57	0.75	0.27
6:01:00	9.4	0.12	0.57	0.60	0.22
6:10:00	10.6	0.12	0.57	0.58	0.21
6:22:00	11.8	0.12	0.57	0.56	0.20

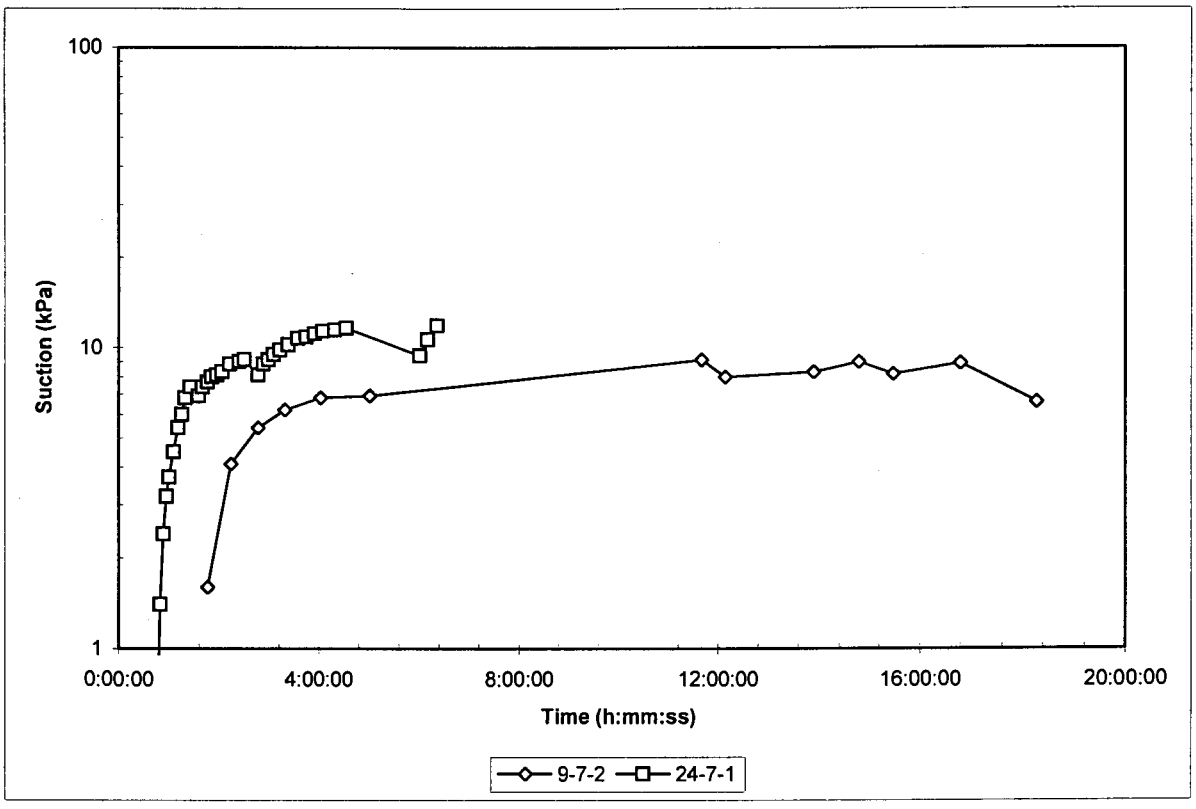

Figure 4.9: Suction versus time

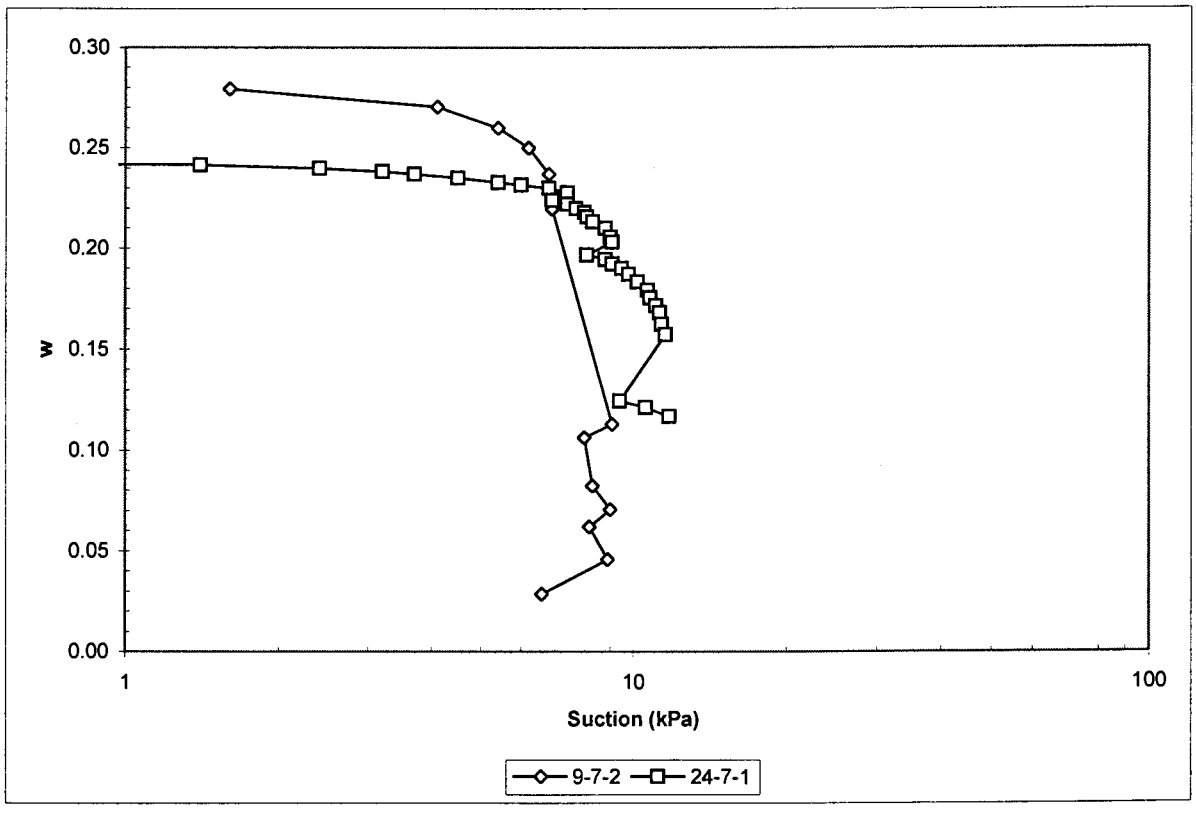

Figure 4.10: Moisture content, w, versus suction (SWCC)

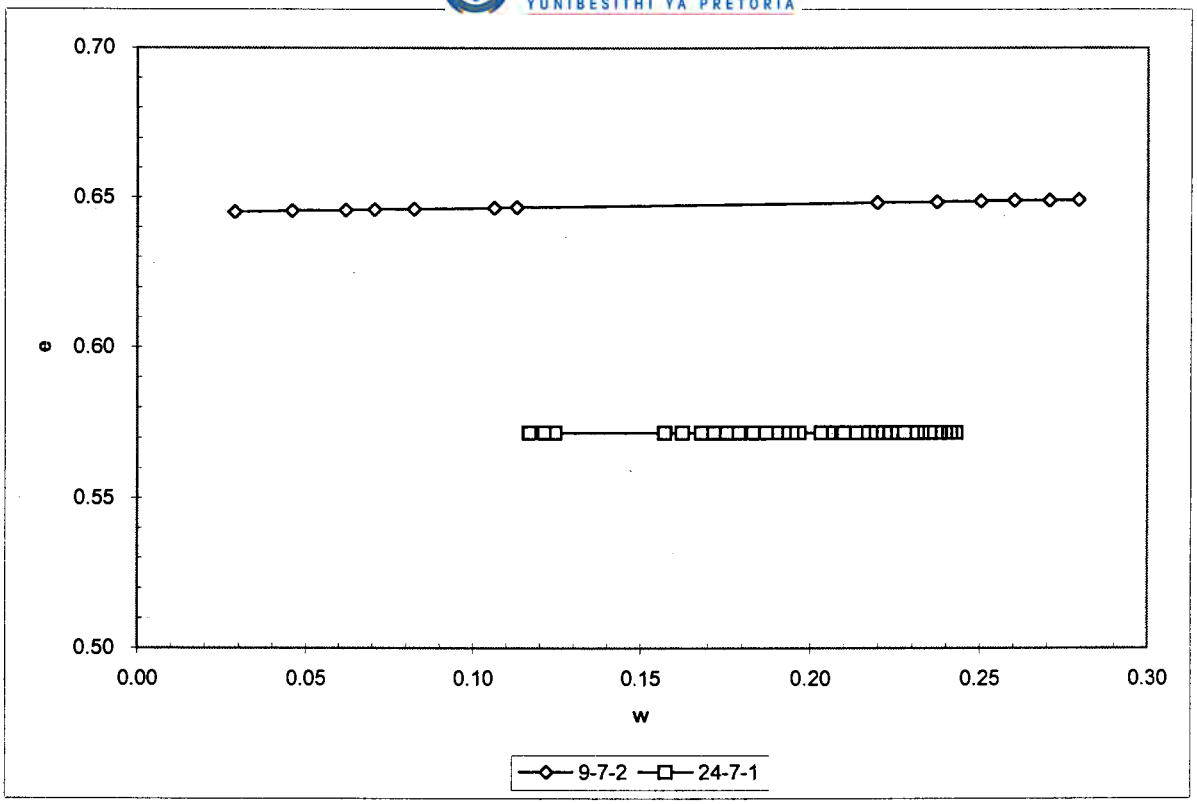

Figure 4.11: Void ratio, e, versus moisture content, w (shrinkage curve)

Table 4.12: Test Data for Particle Size Range B (Sample 9-7-4)

Time (h:mm:ss)	Suction (kPa)	w -	e -	S -	θ -
2:04:00	0.9	0.29	0.71	1.11	0.46
2:32:00	18.8	0.28	0.71	1.08	0.45
3:19:00	20.9	0.26	0.71	1.02	0.42
4:10:00	22.3	0.25	0.71	0.96	0.40
5:05:00	23.2	0.23	0.71	0.90	0.37
6:43:00	23.9	0.20	0.71	0.79	0.33
7:43:00	24.6	0.19	0.71	0.72	0.30
8:36:00	25.4	0.17	0.71	0.66	0.27
9:28:00	26.6	0.16	0.71	0.60	0.25
10:07:00	25.8	0.15	0.71	0.56	0.23
10:48:00	26.5	0.13	0.71	0.52	0.21
11:20:00	27.4	0.13	0.71	0.48	0.20
11:48:00	27.4	0.12	0.71	0.45	0.19
13:54:00	31.5	0.08	0.71	0.33	0.14
14:32:00	32.3	0.07	0.71	0.29	0.12
15:25:00	30.8	0.06	0.71	0.24	0.10
17:03:00	28.0	0.04	0.71	0.14	0.06
18:22:00	28.0	0.02	0.71	0.07	0.03

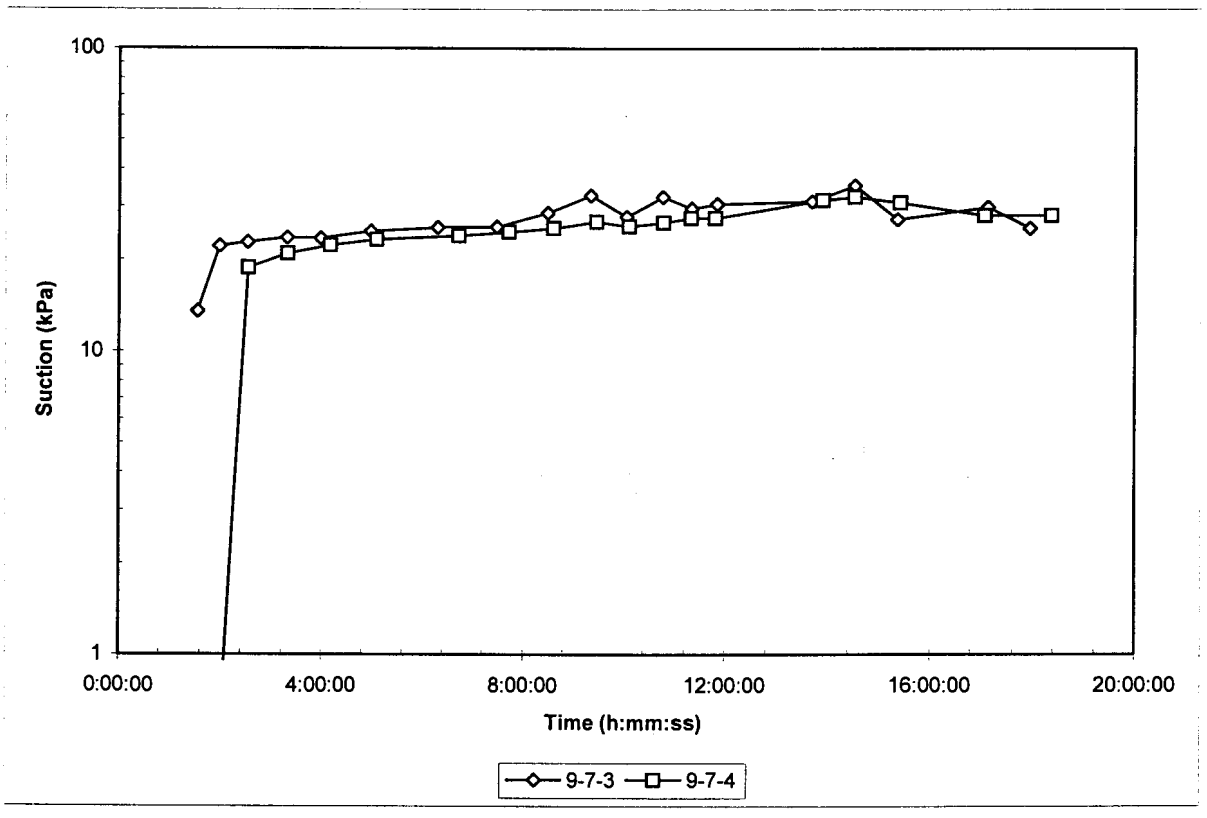

Figure 4.12: Suction versus time

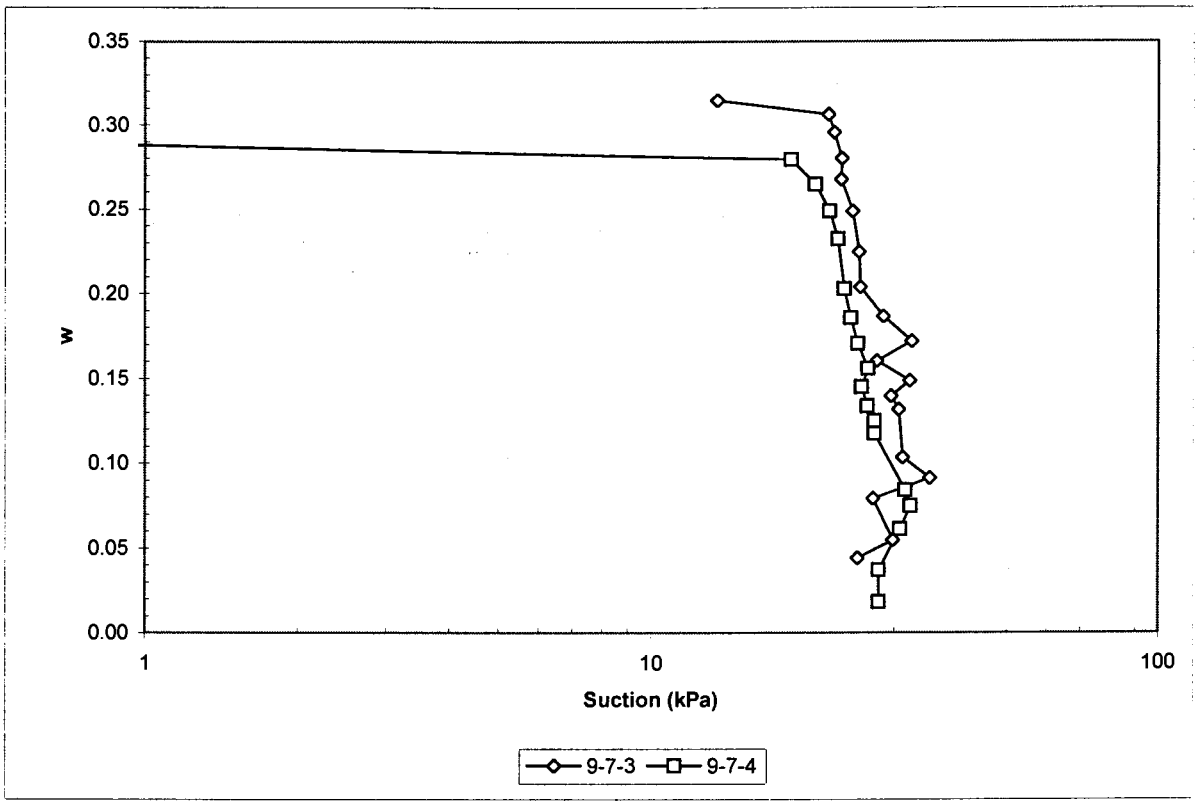

Figure 4.13: Moisture content, w, versus suction (SWCC)

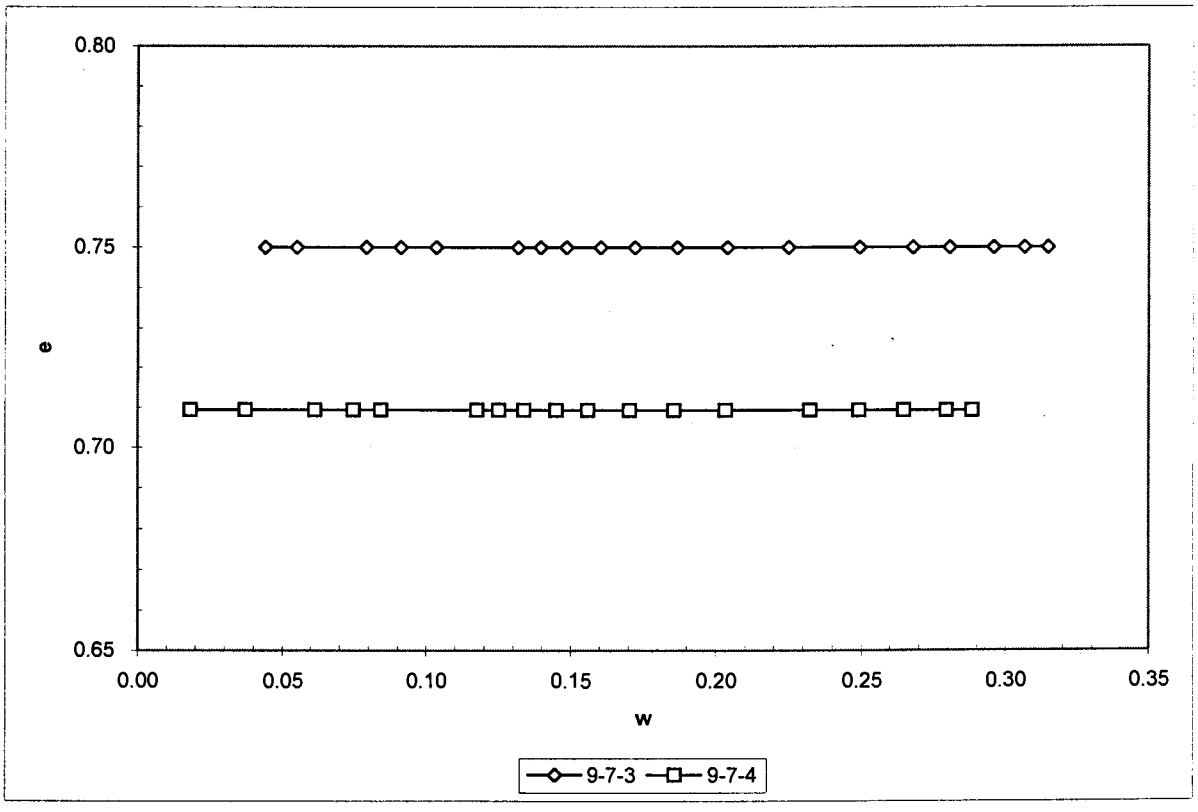

Figure 4.14: Void ratio, e, versus moisture content, w (shrinkage curve)

4.6 Particle Size Range C (6<20)

Table 4.13 to 4.14 represents the data obtained from tests carried out on Range C tailings.

Figure 4.15 represents suction (on a logarithmic scale) versus time for the above samples.

Figure 4.16 represents gravimetric water content, w, versus suction (on a logarithmic scale).

Figure 4.17 represents void ratio, e, versus water content, w.

Note: No linear shrinkage

Table 4.13: Test Data for Particle Size Range C (Sample 16-7-1)

Time (h:mm:ss)	Suction (kPa)	w -	e -	S -	θ -
1:38:00	16.1	0.34	0.79	1.18	0.52
1:41:00	23.1	0.34	0.79	1.18	0.52
1:43:00	28.7	0.34	0.79	1.17	0.52
1:58:00	87.4	0.33	0.79	1.15	0.50
2:24:00	89.8	0.32	0.79	1.10	0.48
3:24:00	96.0	0.29	0.79	0.99	0.44
3:45:00	97.2	0.27	0.79	0.96	0.42
4:14:00	97.8	0.26	0.79	0.91	0.40
5:32:00	105.6	0.22	0.79	0.78	0.34
8:03:00	117.9	0.15	0.79	0.53	0.23
8:42:00	120.8	0.14	0.79	0.47	0.21
10:43:00	149.0	0.08	0.79	0.29	0.13
12:46:00	377.7	0.03	0.79	0.11	0.05

Table 4.14: Test Data for Particle Size Range C (Sample 16-7-4)

Time (h:mm:ss)	Suction (kPa)	w -	e -	S -	θ -
2:35:00	7.0	0.31	0.67	1.27	0.51
2:38:00	10.6	0.31	0.67	1.27	0.51
2:42:00	17.9	0.31	0.67	1.26	0.51
2:47:00	32.5	0.31	0.67	1.25	0.50
2:52:00	51.5	0.31	0.67	1.25	0.50
2:56:00	67.1	0.30	0.67	1.24	0.50
2:58:00	75.6	0.30	0.67	1.24	0.50
3:01:00	83.3	0.30	0.67	1.23	0.50
3:03:00	86.4	0.30	0.67	1.23	0.49
3:05:00	88.5	0.30	0.67	1.23	0.49
3:07:00	90.6	0.30	0.67	1.22	0.49
3:27:00	97.8	0.29	0.67	1.19	0.48
5:14:00	111.2	0.25	0.67	1.03	0.42
6:19:00	113.6	0.23	0.67	0.94	0.38
8:15:00	117.3	0.19	0.67	0.77	0.31
10:52:00	130.7	0.14	0.67	0.56	0.22
13:16:00	165.1	0.09	0.67	0.37	0.15
13:31:00	170.0	0.09	0.67	0.35	0.14
14:10:00	182.4	0.07	0.67	0.30	0.12
14:23:00	190.7	0.07	0.67	0.28	0.11
15:03:00	198.2	0.06	0.67	0.23	0.09
15:08:00	211.4	0.05	0.67	0.22	0.09
15:13:00	219.5	0.05	0.67	0.22	0.09
15:23:00	238.2	0.05	0.67	0.20	0.08
15:34:00	274.2	0.05	0.67	0.19	0.08
15:42:00	300.9	0.04	0.67	0.18	0.07
15:48:00	323.1	0.04	0.67	0.17	0.07
15:54:00	347.7	0.04	0.67	0.16	0.07
15:58:00	363.4	0.04	0.67	0.16	0.06
16:01:00	384.0	0.04	0.67	0.16	0.06

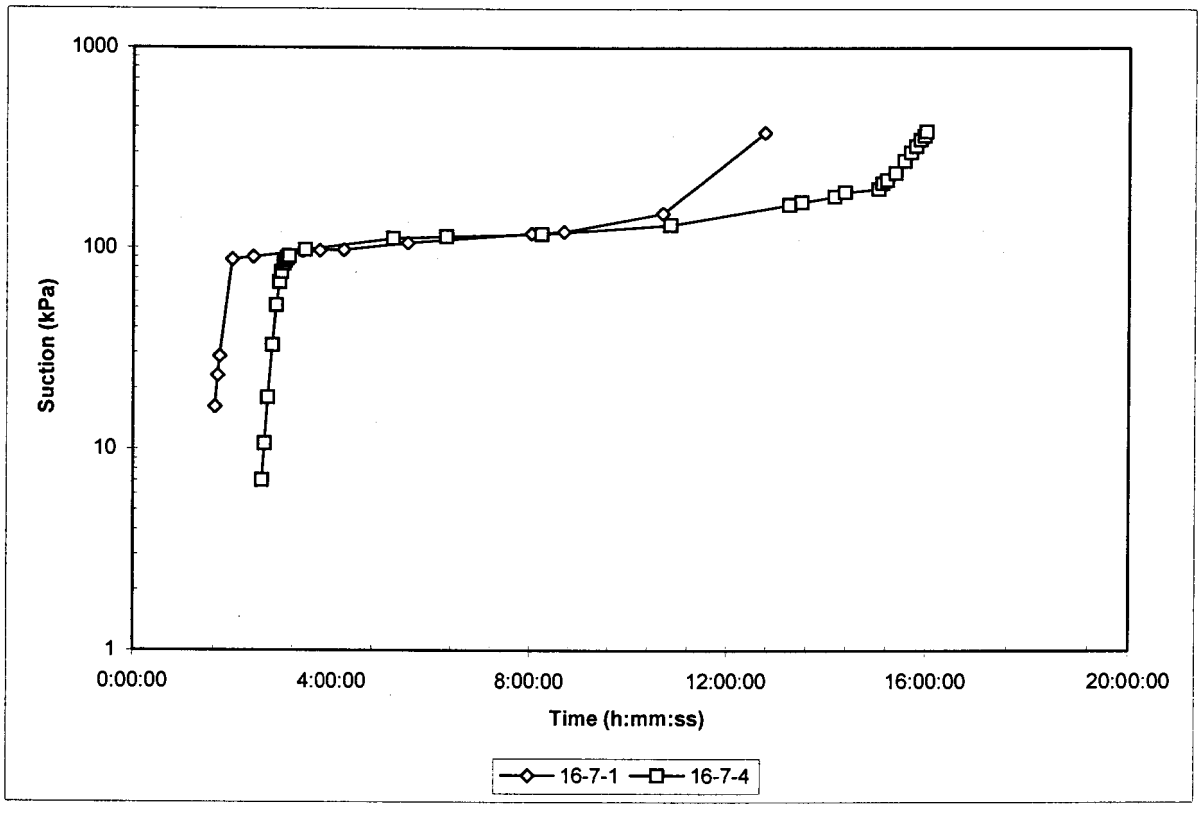

Figure 4.15: Suction versus time

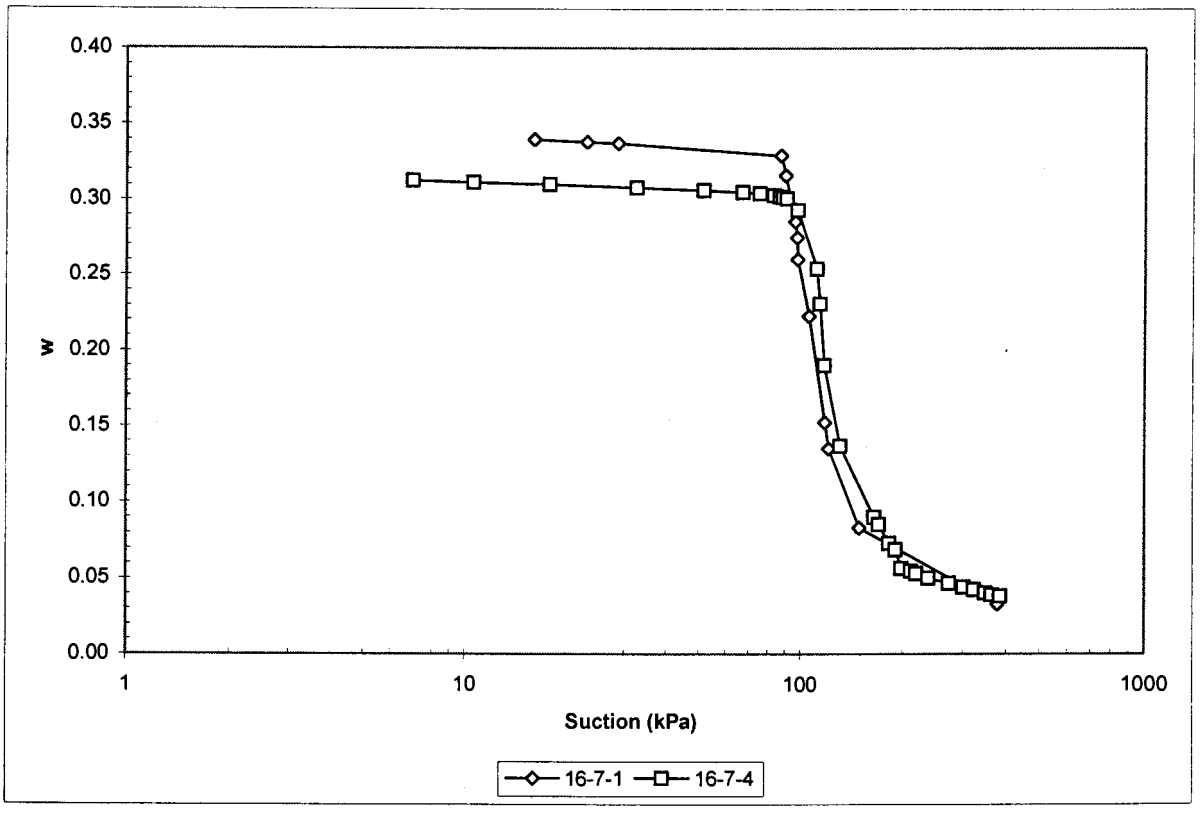

Figure 4.16: Moisture content, w, versus suction (SWCC)

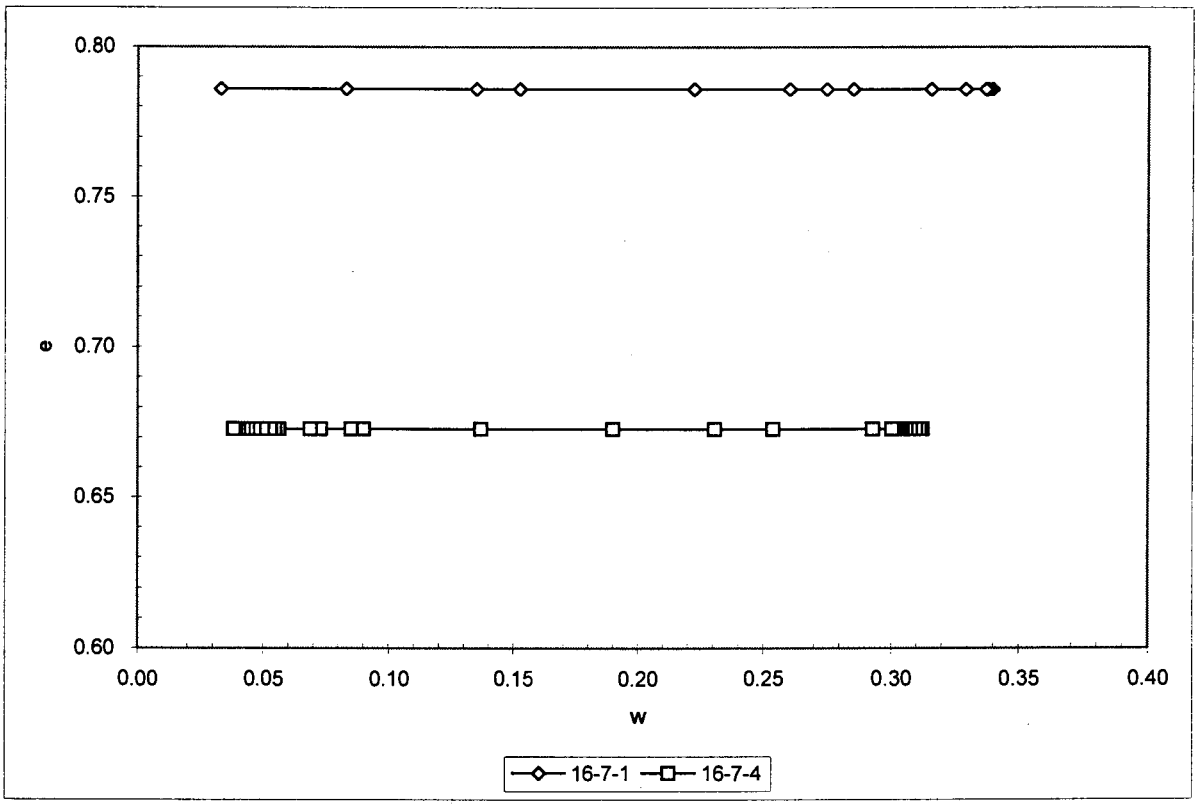

Figure 4.17: Void ratio, e, versus moisture content, w (shrinkage curve)

4.7 Particle Size Range D (2<6)

Table 4.15 to 4.16 represents the data obtained from tests carried out on Range D tailings.

Figure 4.18 represents suction (on a logarithmic scale) versus time for the above samples.

Figure 4.19 represents gravimetric water content, w, versus suction (on a logarithmic scale).

Figure 4.20 represents void ratio, e, versus water content, w.

Figure 4.21 represents linear shrinkage, LS, versus suction.

Table 4.15: Test Data for Particle Size Range D (Sample 2-8-2)

Time (h:mm:ss)	Suction (kPa)	w -	e -	S -	θ -	LS (%)
6:30:00	5.0	0.42	0.76	1.50	0.65	0.00%
6:55:00	23.1	0.40	0.73	1.51	0.64	0.00%
7:14:00	42.2	0.40	0.72	1.51	0.63	0.00%
7:33:00	80.7	0.39	0.70	1.51	0.62	0.30%
7:52:00	126.3	0.38	0.69	1.50	0.61	0.69%
8:12:00	201.8	0.37	0.68	1.49	0.60	1.02%
8:34:00	297.4	0.36	0.67	1.46	0.59	1.29%
9:02:00	339.6	0.34	0.66	1.42	0.57	1.48%
9:32:00	340.2	0.33	0.66	1.36	0.54	1.52%
9:59:00	350.5	0.32	0.66	1.31	0.52	1.52%
10:25:00	357.1	0.31	0.66	1.26	0.50	1.52%
10:54:00	358.0	0.29	0.66	1.21	0.48	1.52%
11:35:00	368.0	0.27	0.66	1.13	0.45	1.52%

Table 4.16: Test Data for Particle Size Range D (Sample 2-8-3)

Time (h:mm:ss)	Suction (kPa)	w -	e -	S -	θ -	LS (%)
6:47:00	5.6	0.39	0.74	1.44	0.61	0.00%
7:09:00	25.4	0.38	0.72	1.44	0.60	0.00%
7:27:00	48.1	0.37	0.71	1.43	0.60	0.00%
7:47:00	90.1	0.36	0.70	1.42	0.59	0.30%
8:07:00	149.1	0.35	0.69	1.41	0.57	0.57%
8:26:00	235.4	0.35	0.68	1.39	0.56	0.78%
8:51:00	331.6	0.33	0.67	1.36	0.55	0.99%
9:22:00	345.2	0.32	0.67	1.31	0.53	1.13%
9:48:00	351.6	0.31	0.67	1.26	0.51	1.16%
10:17:00	355.3	0.30	0.67	1.21	0.49	1.16%
10:44:00	365.6	0.28	0.67	1.16	0.47	1.16%
11:19:00	367.6	0.27	0.67	1.10	0.44	1.16%
11:53:00	382.2	0.25	0.67	1.03	0.42	1.16%

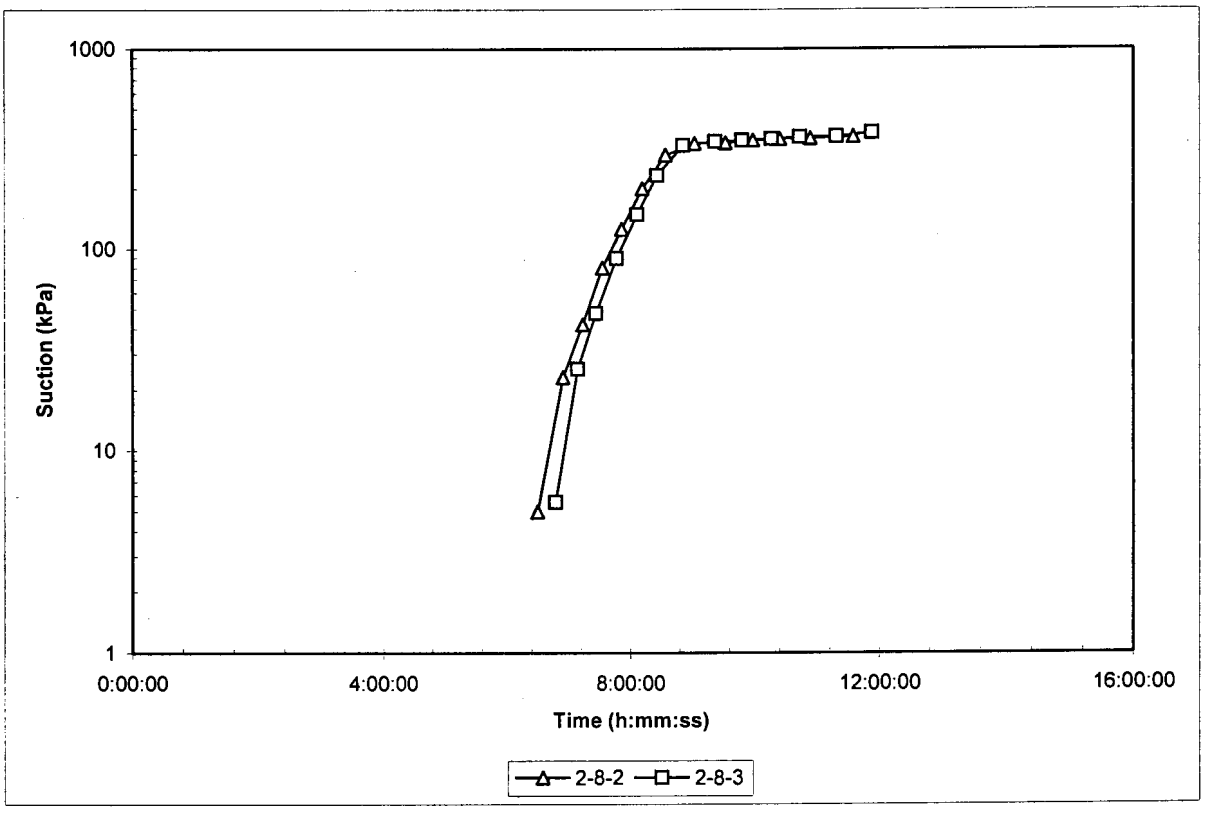

Figure 4.18: Suction versus time

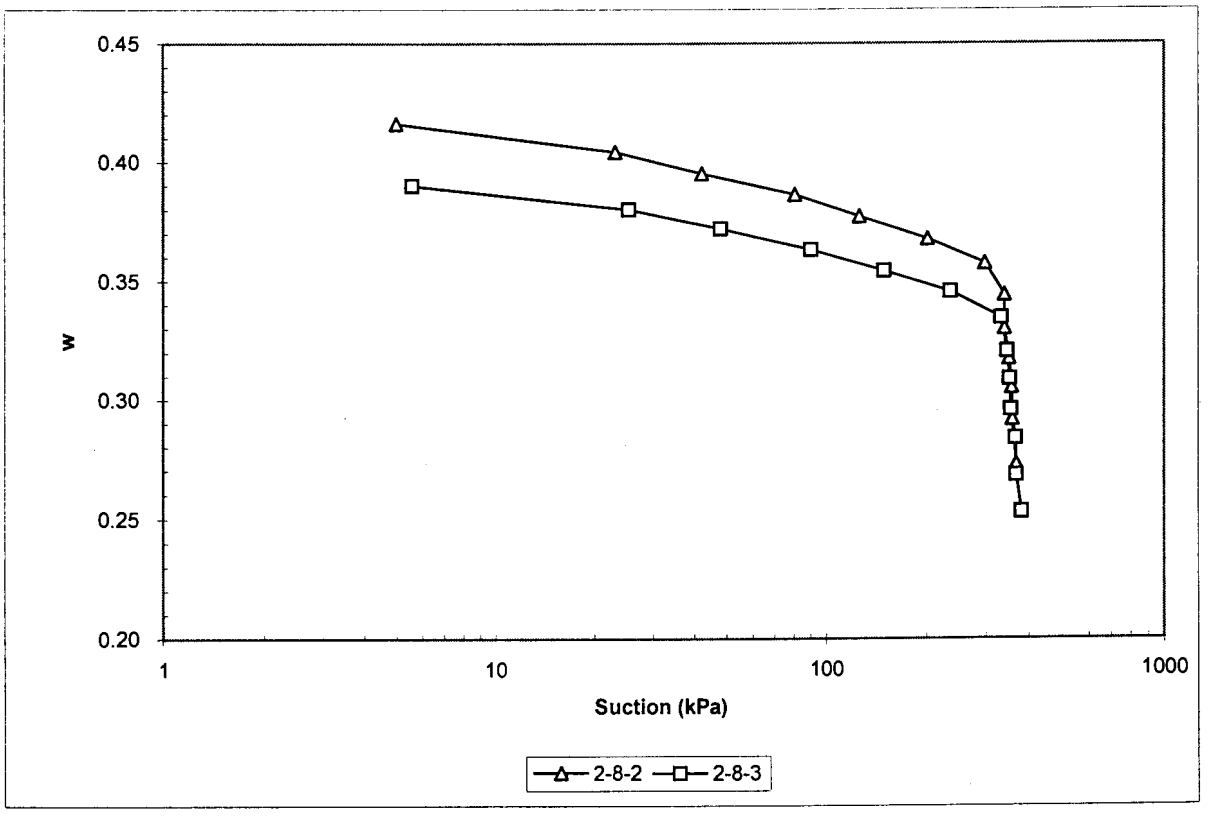

Figure 4.19: Moisture content, w, versus suction (SWCC)

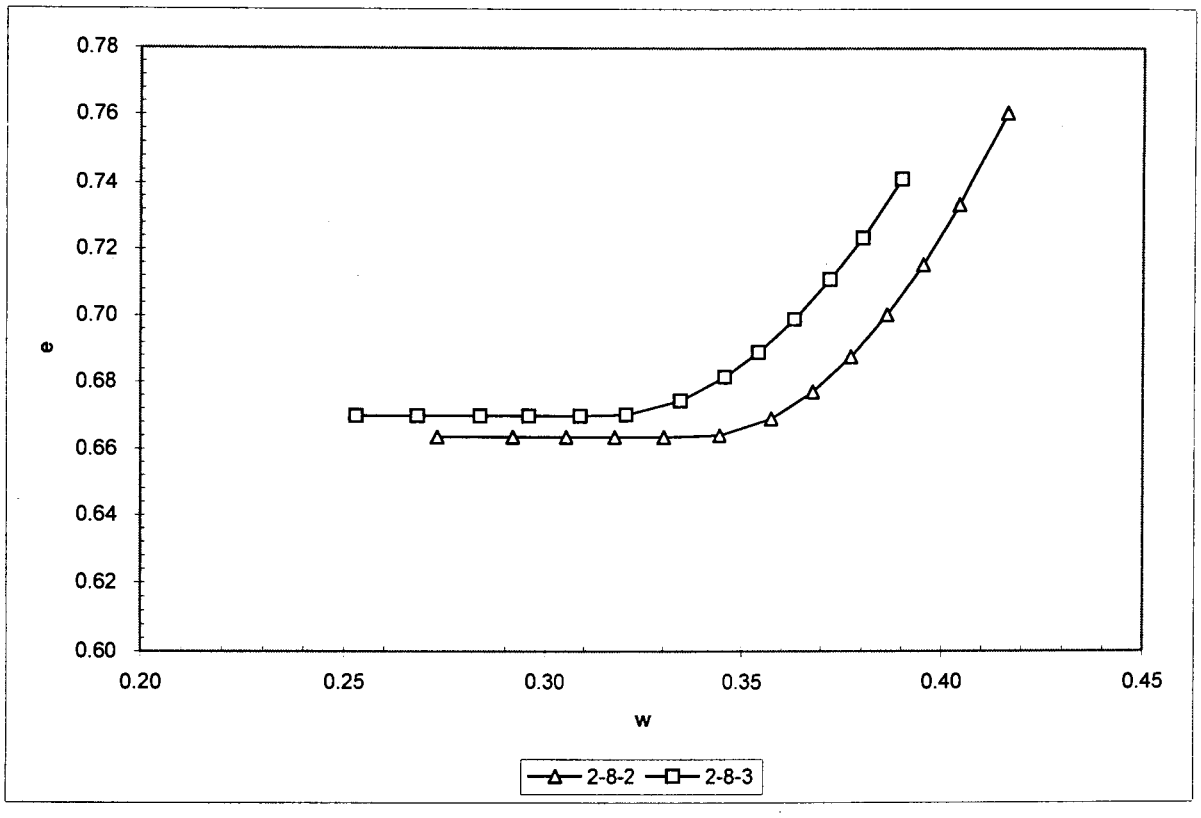

Figure 4.20: Void ratio, e, versus moisture content, w (shrinkage curve)

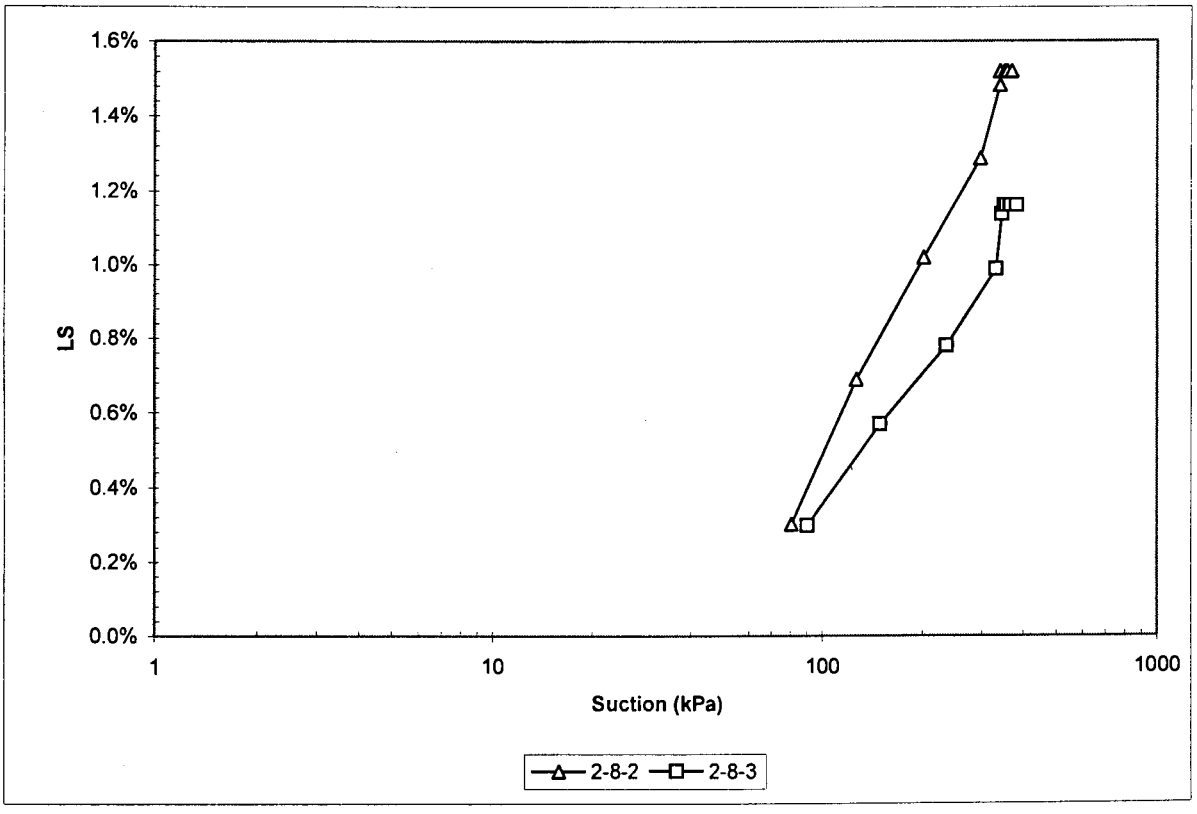

Figure 4.21: Linear shrinkage, LS, versus suction

4.8 Particle Size Range E (<2)

Table 4.17 represents the data obtained from a test carried out on Range E tailings.

Figure 4.22 represents suction (on a logarithmic scale) versus time for the above samples.

Figure 4.23 represents gravimetric water content, w, versus suction (on a logarithmic scale).

Figure 4.24 represents void ratio, e, versus water content, w.

Figure 4.25 represents linear shrinkage, LS, versus suction.

Table 4.17: Test Data for Particle Size Range E (Sample 15-8-3)

Time (h:mm:ss)	Suction (kPa)	w -	e -	S -	θ -	LS (%)
5:34:00	1.0	0.46	1.39	0.91	0.53	0.00%
5:42:00	1.5	0.46	1.38	0.91	0.53	0.00%
5:50:00	3.0	0.46	1.38	0.91	0.53	0.00%
5:58:00	5.1	0.45	1.37	0.90	0.52	0.00%
6:32:00	12.7	0.44	1.34	0.89	0.51	0.00%
6:40:00	19.4	0.43	1.33	0.89	0.51	0.00%
6:49:00	26.7	0.43	1.33	0.89	0.50	0.00%
7:03:00	36.0	0.42	1.32	0.88	0.50	0.00%
7:09:00	46.7	0.42	1.31	0.88	0.50	0.01%
7:17:00	60.6	0.42	1.31	0.87	0.49	0.05%
7:25:00	77.2	0.41	1.30	0.87	0.49	0.10%
7:41:00	118.6	0.40	1.29	0.86	0.48	0.26%
7:46:00	138.3	0.40	1.29	0.86	0.48	0.32%
7:50:00	151.8	0.40	1.28	0.85	0.48	0.37%
7:56:00	173.1	0.40	1.28	0.85	0.48	0.46%
8:04:00	202.3	0.39	1.28	0.85	0.47	0.60%
8:23:00	284.4	0.39	1.27	0.83	0.47	0.99%
8:25:00	299.4	0.38	1.26	0.83	0.47	1.03%
8:27:00	316.1	0.38	1.26	0.83	0.46	1.08%
8:29:00	330.0	0.38	1.26	0.83	0.46	1.13%
8:31:00	341.2	0.38	1.26	0.83	0.46	1.18%
8:33:00	354.7	0.38	1.26	0.83	0.46	1.23%

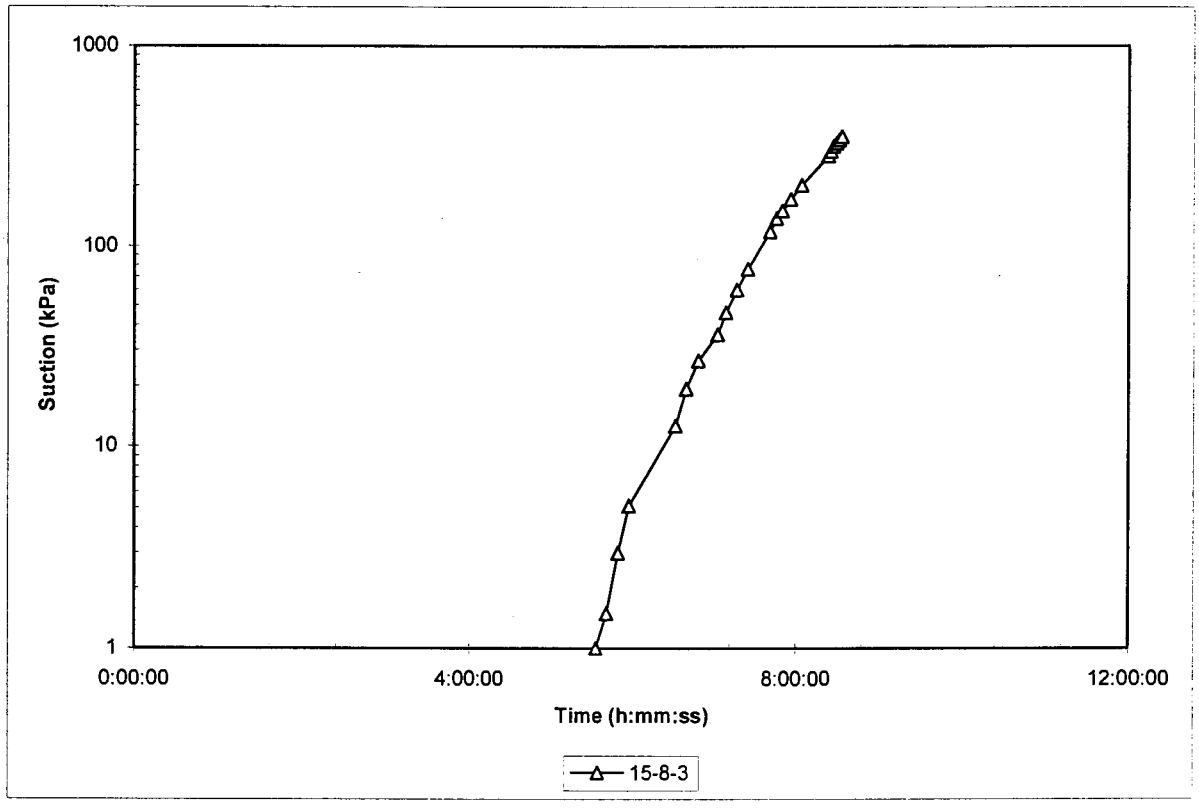

Figure 4.22: Suction versus time

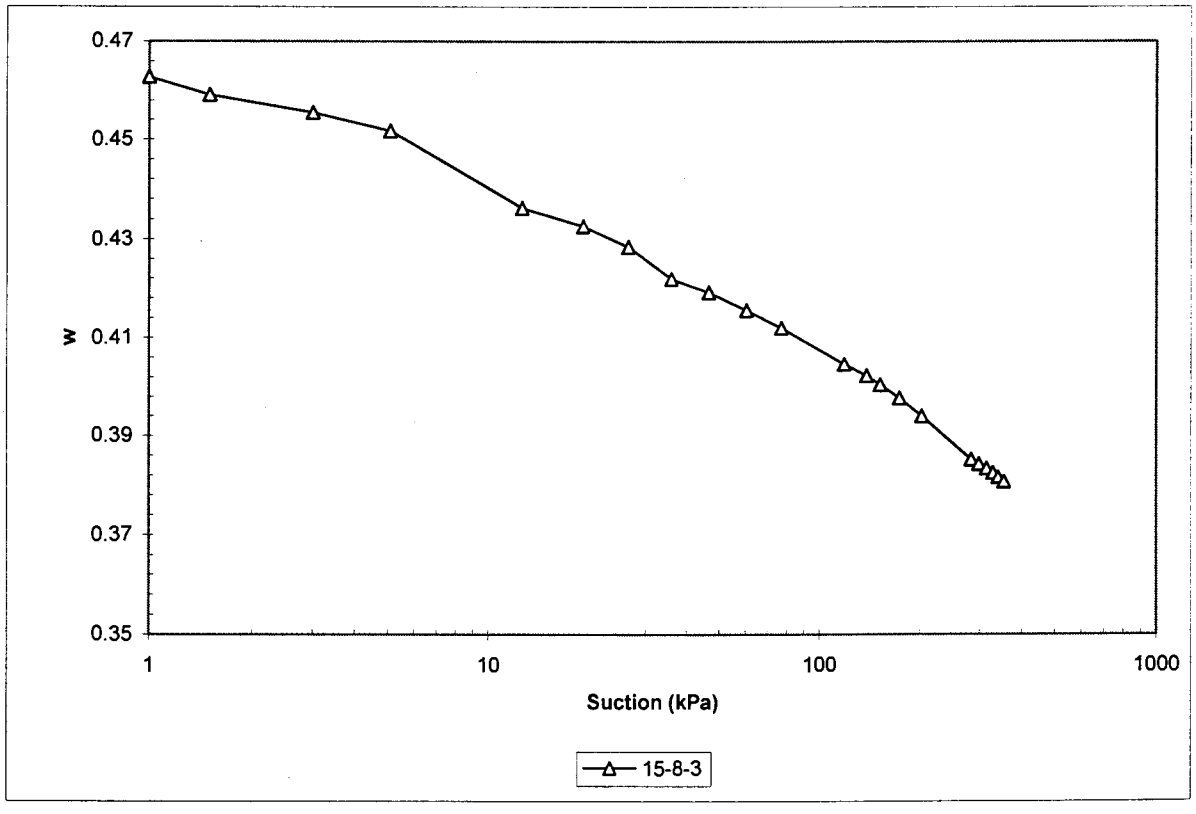

Figure 4.23: Moisture content, w, versus suction (SWCC)

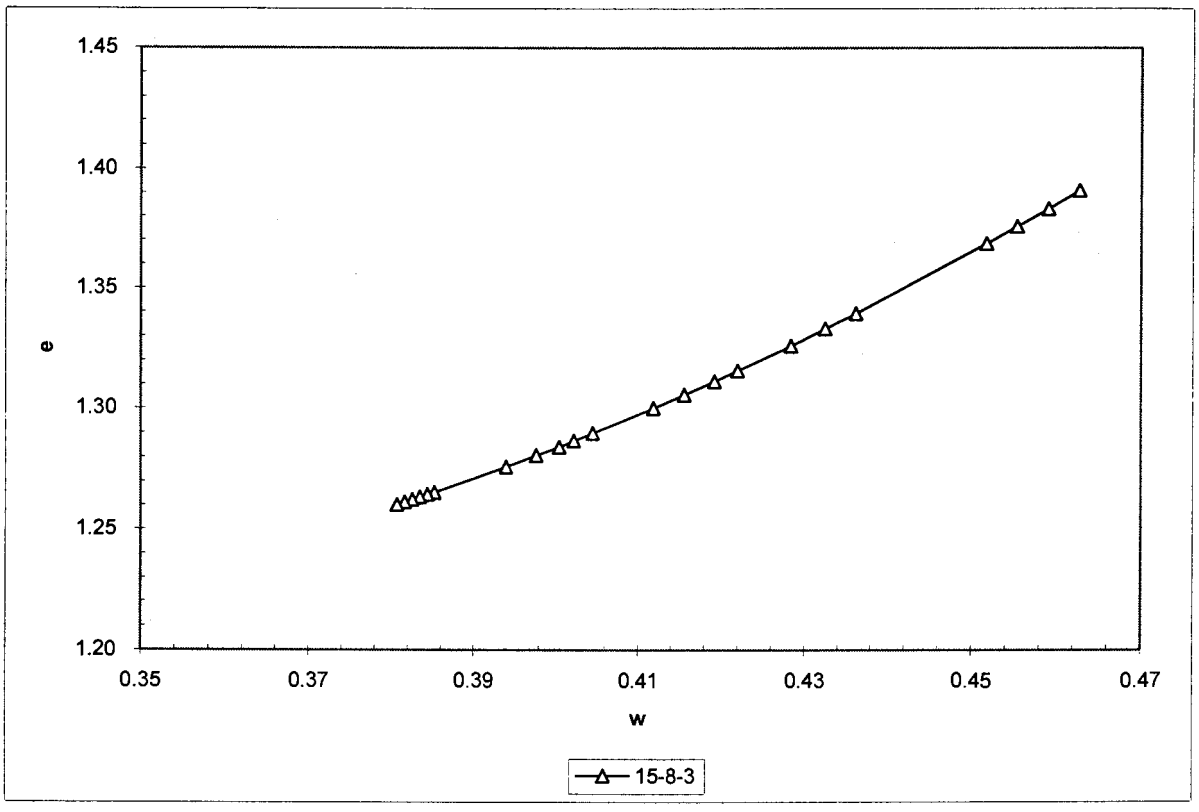

Figure 4.24: Void ratio, e, versus moisture content, w (shrinkage curve)

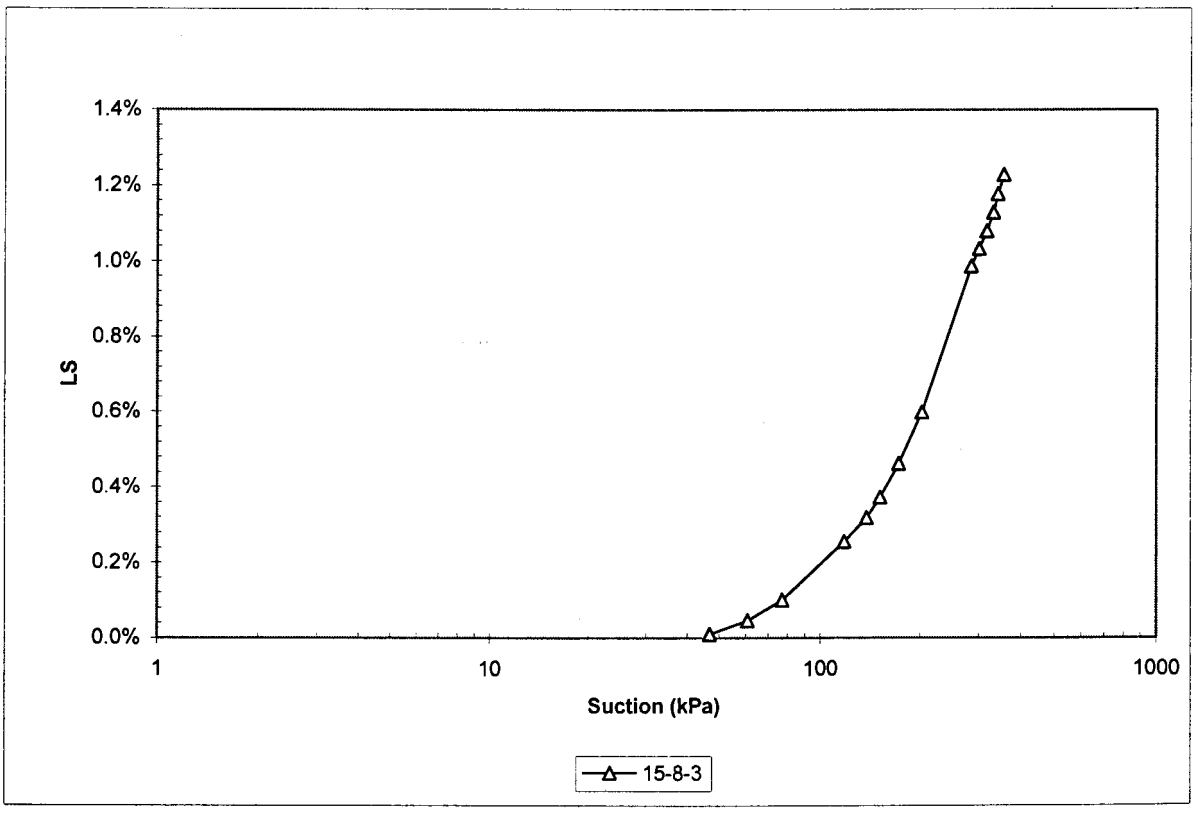

Figure 4.25: Linear shrinkage, LS, versus suction

4.9 New Sample A

Table 4.18 represents the data obtained from a test carried out on Sample A tailings.

Figure 4.26 represents suction (on a logarithmic scale) versus time for the above samples.

Figure 4.27 represents gravimetric water content, w, versus suction (on a logarithmic scale).

Figure 4.28 represents void ratio, e, versus water content, w.

Figure 4.29 represents linear shrinkage, LS, versus suction.

Table 4.18: Test Data for New Sample A (Sample 20-8-2)

Time (h:mm:ss)	Suction (kPa)	w -	e -	S -	θ -	LS (%)
5:31:00	5.8	0.20	0.44	1.24	0.38	0.00%
5:48:00	27.3	0.20	0.44	1.23	0.38	0.00%
6:06:00	44.6	0.19	0.43	1.22	0.37	0.11%
6:21:00	67.2	0.19	0.43	1.21	0.36	0.33%
6:43:00	87.6	0.18	0.42	1.20	0.35	0.43%
7:02:00	89.2	0.18	0.42	1.18	0.35	0.45%
7:21:00	90.8	0.17	0.41	1.16	0.34	0.48%
7:39:00	91.4	0.17	0.41	1.14	0.33	0.49%
7:55:00	95.7	0.17	0.41	1.12	0.32	0.51%
8:12:00	99.5	0.16	0.40	1.10	0.32	0.52%
8:26:00	105.7	0.16	0.40	1.08	0.31	0.53%
8:43:00	110.9	0.15	0.40	1.06	0.30	0.54%
9:01:00	115.7	0.15	0.40	1.03	0.29	0.55%
9:26:00	123.7	0.14	0.40	0.99	0.28	0.56%
9:57:00	138.5	0.14	0.40	0.93	0.27	0.57%
10:15:00	142.1	0.13	0.40	0.90	0.26	0.57%
10:31:00	146.9	0.13	0.40	0.88	0.25	0.57%
10:49:00	155.1	0.12	0.40	0.85	0.24	0.57%
11:11:00	161.3	0.12	0.40	0.81	0.23	0.57%
11:38:00	176.0	0.11	0.40	0.77	0.22	0.57%
12:07:00	188.0	0.10	0.40	0.72	0.20	0.57%
12:30:00	202.0	0.10	0.40	0.68	0.19	0.57%
12:36:00	206.9	0.10	0.40	0.67	0.19	0.57%
12:42:00	211.0	0.10	0.40	0.66	0.19	0.57%
12:51:00	231.6	0.09	0.40	0.64	0.18	0.57%
12:56:00	236.7	0.09	0.40	0.63	0.18	0.57%
13:08:00	246.5	0.09	0.40	0.61	0.18	0.57%
13:20:00	257.0	0.09	0.40	0.59	0.17	0.57%
13:39:00	272.7	0.08	0.40	0.56	0.16	0.57%
13:56:00	279.6	0.08	0.40	0.53	0.15	0.57%
14:01:00	284.5	0.08	0.40	0.53	0.15	0.57%
14:09:00	291.1	0.07	0.40	0.51	0.15	0.57%
14:25:00	305.7	0.07	0.40	0.49	0.14	0.57%
14:36:00	319.6	0.07	0.40	0.47	0.13	0.57%
14:51:00	324.4	0.06	0.40	0.44	0.13	0.57%
14:58:00	331.6	0.06	0.40	0.43	0.12	0.57%
15:07:00	341.3	0.06	0.40	0.42	0.12	0.57%
15:15:00	353.5	0.06	0.40	0.40	0.11	0.57%

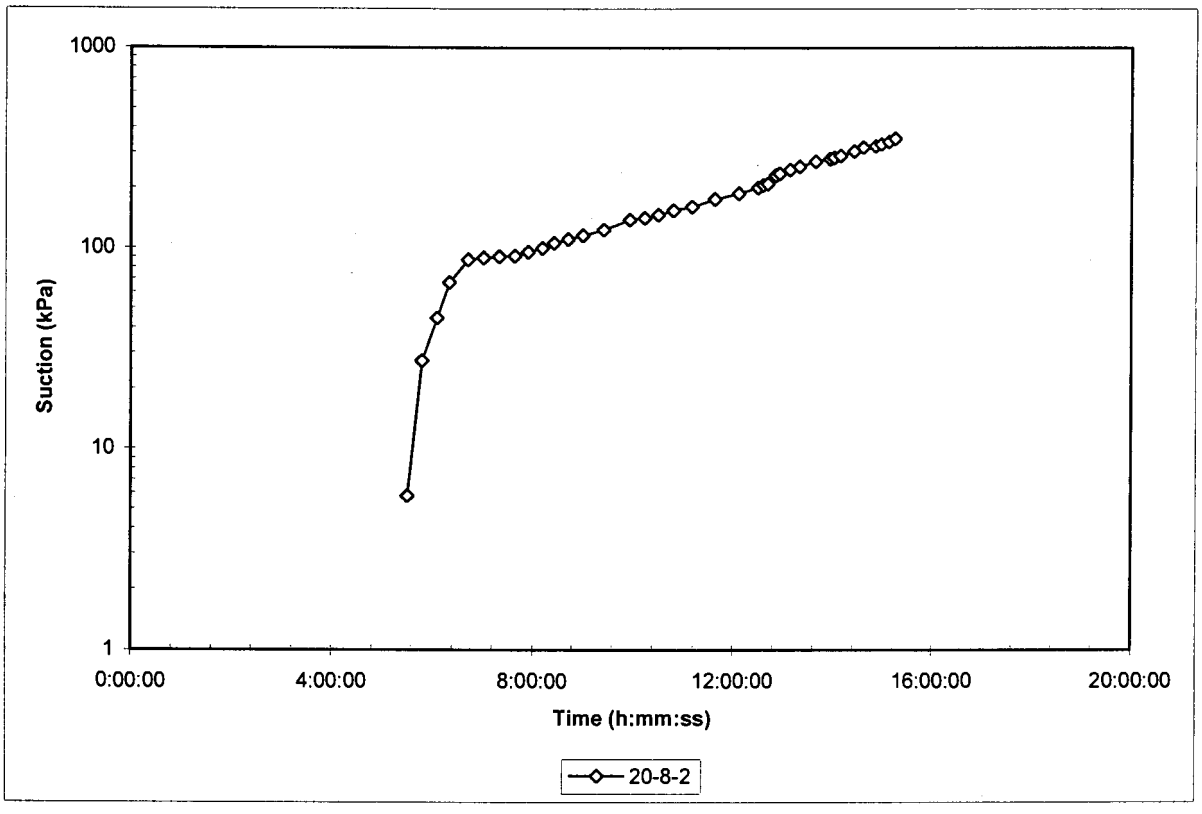

Figure 4.26: Suction versus time

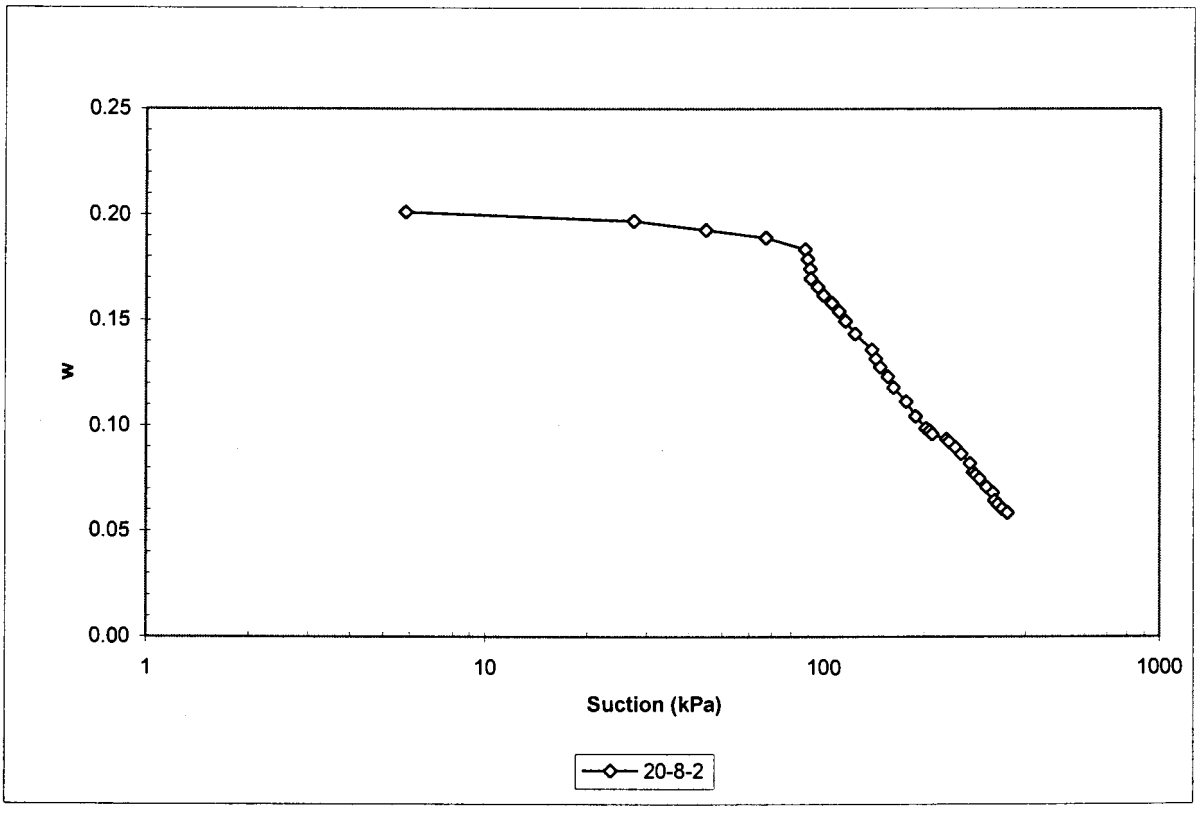

Figure 4.27: Moisture content, w, versus suction (SWCC)

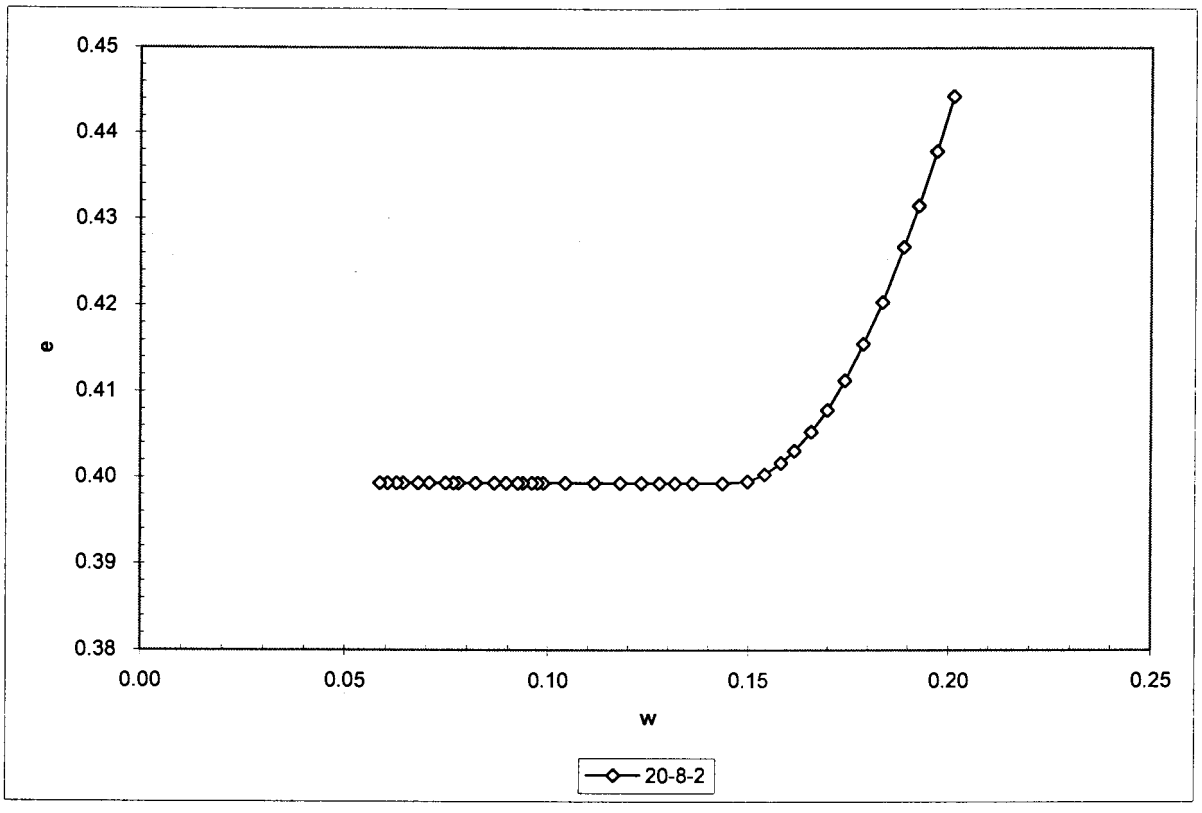

Figure 4.28: Void ratio, e, versus moisture content, w (shrinkage curve)

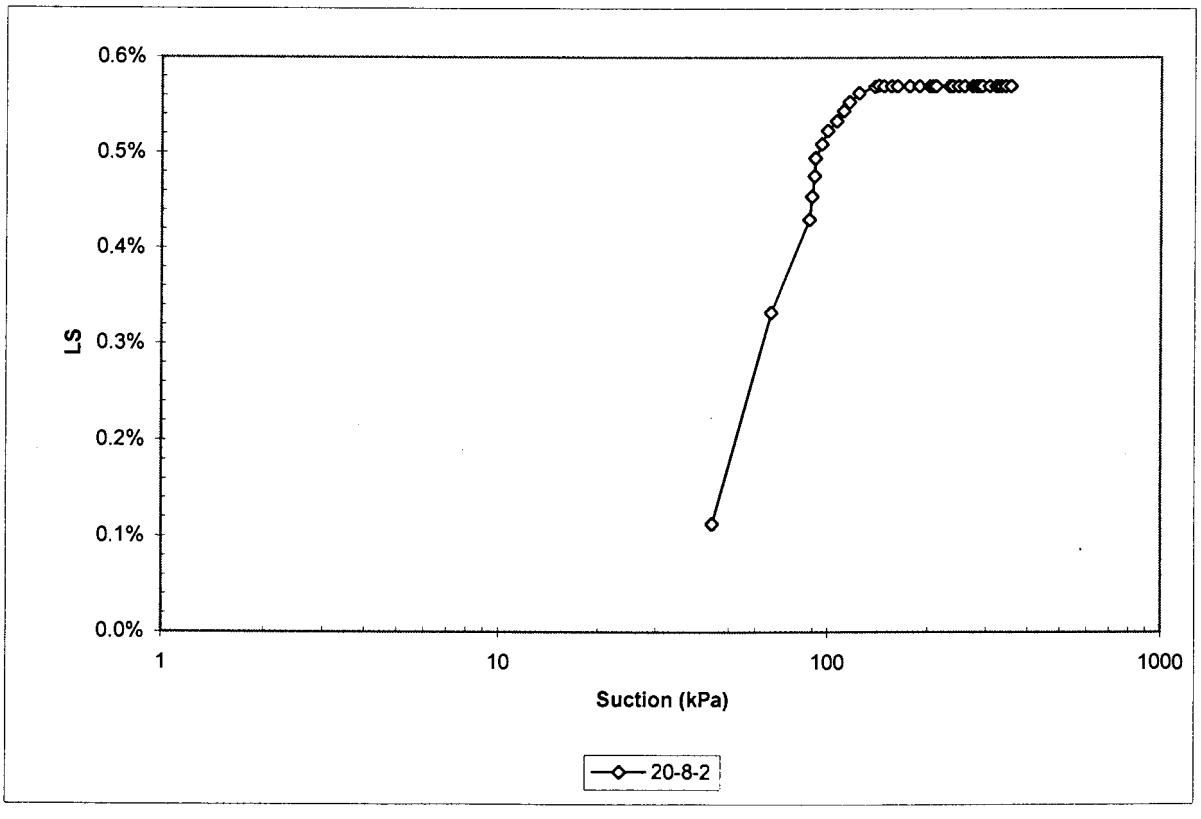

Figure 4.29: Linear shrinkage, LS, versus suction

4.10 New Sample C

Table 4.19 represents the data obtained from a test carried out on Sample C tailings.

Figure 4.30 represents suction (on a logarithmic scale) versus time for the above samples.

Figure 4.31 represents gravimetric water content, w, versus suction (on a logarithmic scale).

Figure 4.32 represents void ratio, e, versus water content, w.

Figure 4.33 represents linear shrinkage, LS, versus suction.

Table 4.19: Test Data for New Sample C (Sample 20-8-1)

Time (h:mm:ss)	Suction (kPa)	w -	e -	S -	θ -	LS (%)
5:41:00	19.1	0.23	0.57	1.10	0.40	0.00%
5:57:00	31.7	0.22	0.56	1.09	0.39	0.00%
6:14:00	55.0	0.22	0.55	1.08	0.38	0.00%
6:32:00	56.3	0.21	0.55	1.07	0.38	0.04%
6:50:00	94.3	0.21	0.54	1.05	0.37	0.25%
7:08:00	108.0	0.20	0.53	1.04	0.36	0.42%
7:28:00	117.3	0.20	0.53	1.02	0.35	0.57%
7:45:00	123.8	0.19	0.52	1.00	0.34	0.66%
8:03:00	128.7	0.19	0.52	0.99	0.34	0.73%
8:20:00	145.4	0.18	0.51	0.97	0.33	0.76%
8:39:00	156.4	0.18	0.51	0.94	0.32	0.76%
8:52:00	173.4	0.17	0.51	0.93	0.31	0.76%
9:11:00	190.2	0.17	0.50	0.90	0.30	0.76%
9:29:00	205.4	0.16	0.50	0.88	0.29	0.76%
9:47:00	218.7	0.15	0.50	0.85	0.28	0.76%
10:13:00	247.6	0.15	0.50	0.81	0.27	0.76%
10:44:00	272.0	0.14	0.50	0.76	0.25	0.76%
11:01:00	278.8	0.13	0.50	0.73	0.24	0.76%
11:18:00	297.7	0.13	0.50	0.70	0.23	0.76%
11:34:00	300.4	0.12	0.50	0.68	0.23	0.76%
12:01:00	315.3	0.12	0.50	0.63	0.21	0.76%
12:30:00	331.9	0.11	0.50	0.59	0.20	0.76%
12:57:00	354.2	0.10	0.50	0.54	0.18	0.76%

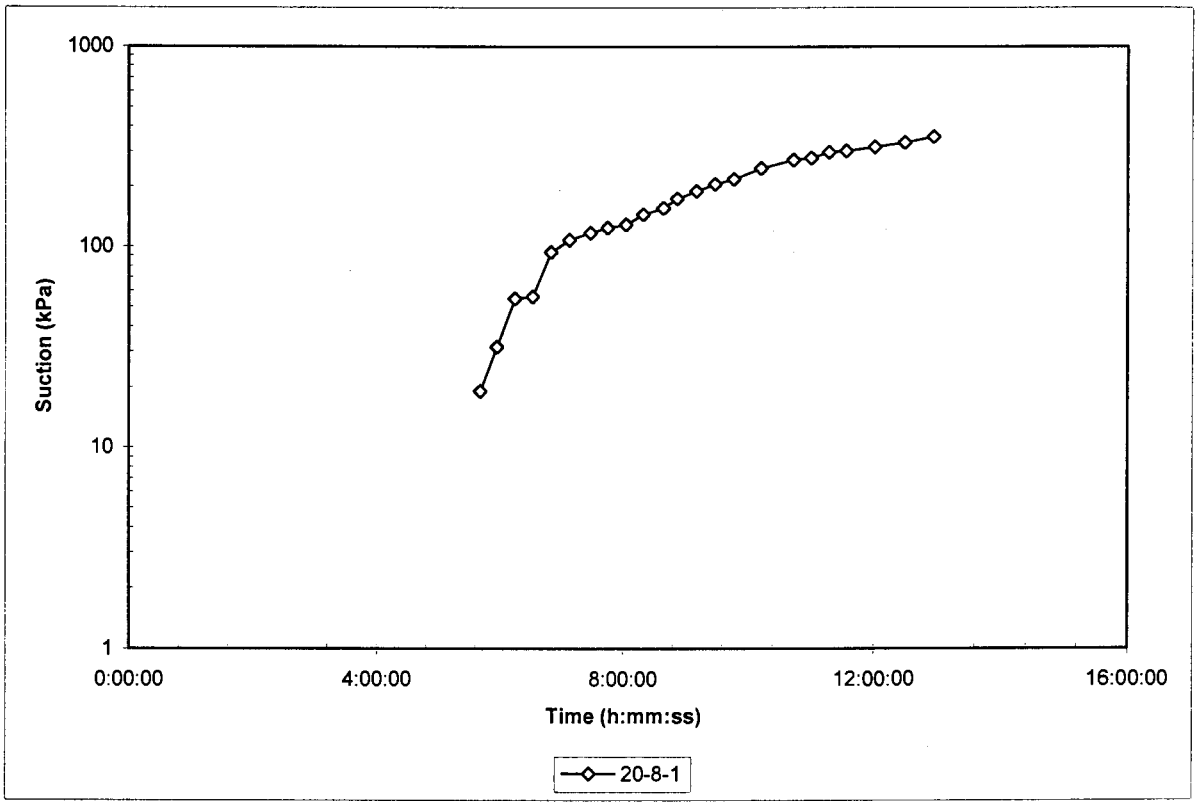

Figure 4.30: Suction versus time

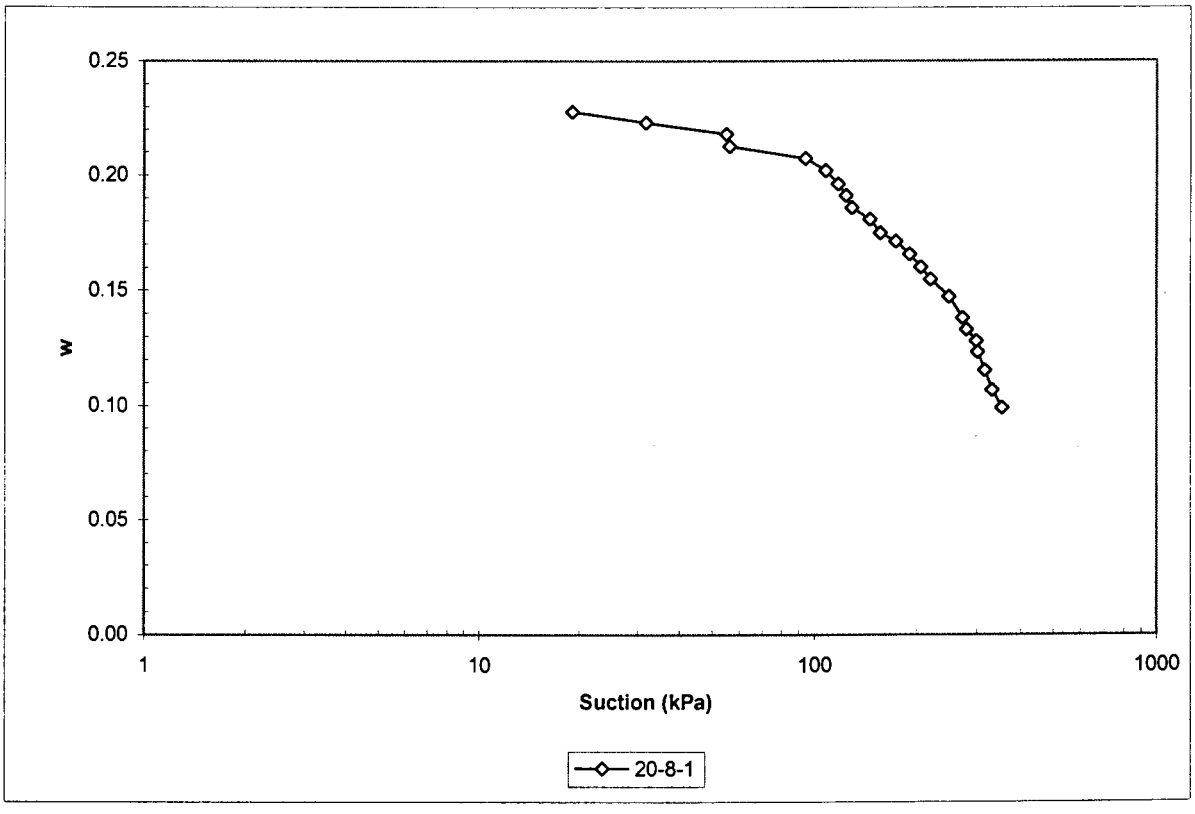

Figure 4.31: Moisture content, w, versus suction (SWCC)

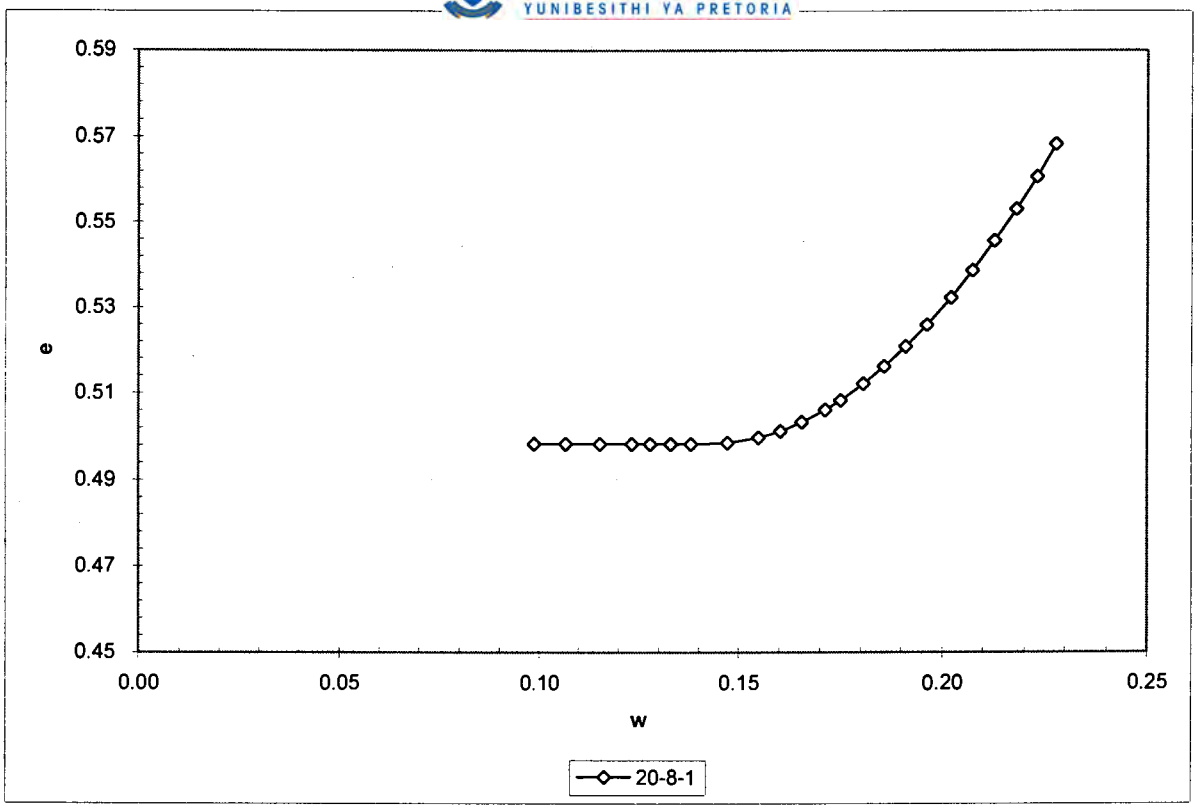

Figure 4.32: Void ratio, e, versus moisture content, w (shrinkage curve)

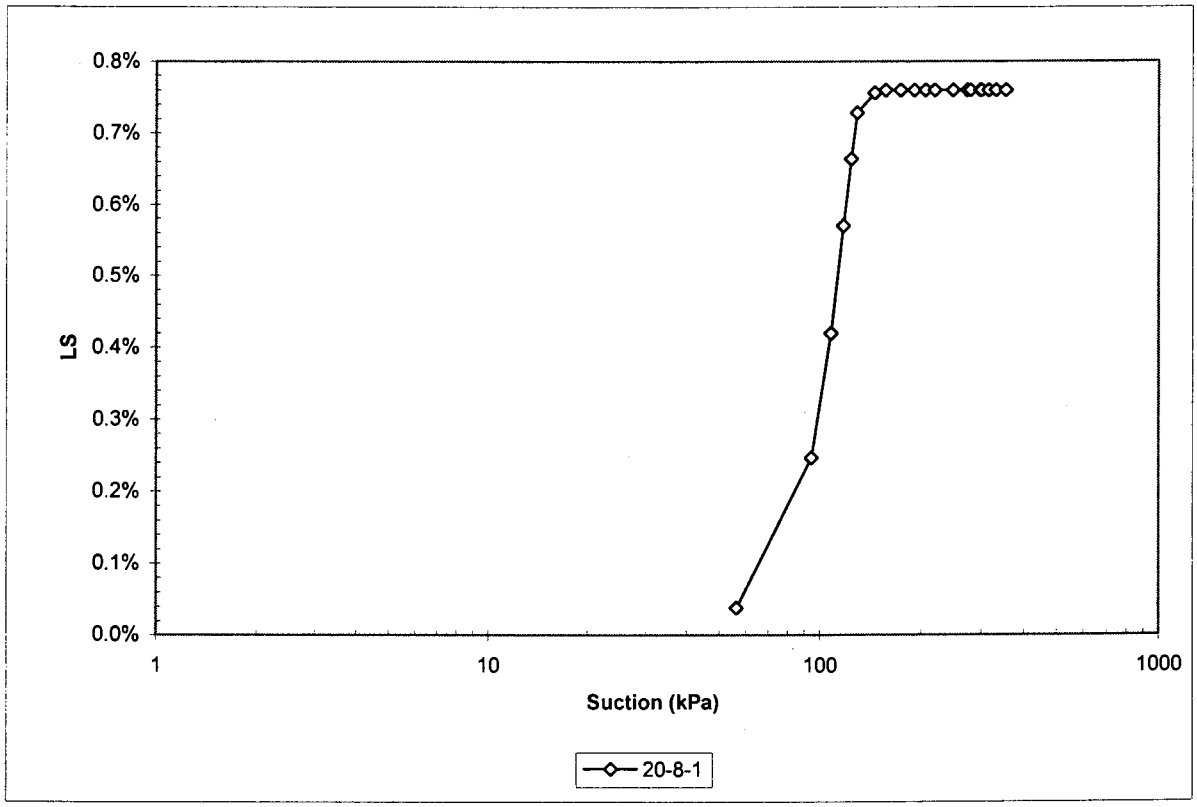

Figure 4.33: Linear shrinkage, LS, versus suction

CHAPTER 5:

DISCUSSION

5.1 Shortcomings

The test method described in Chapter 3 does have some shortcomings as was evident from the results given in Chapter 4. The first of these is the fact that initially the moisture content of the material at the surface will be lower than the material at the bottom of the trough. At the start of the test moisture loss can only occur from the top surface of the material as the body of the trough prevents moisture loss from the other surfaces. The suctions measured will then be slightly higher at the lower moisture content. The moisture content calculated would be an average value for the whole sample, which will be slightly more than the moisture content at the surface. As the material dries and it undergoes shrinkage, the material moves away from the sides of the trough, allowing moisture loss to occur at all surfaces except at the very bottom where the material rests on the inside of the trough. This will cause a near even distribution of moisture content throughout the depth of the sample. The initial error however, is assumed to be insignificant due to the fact that the depth of the trough is small i.e. the sample is very thin, resulting in a small difference between the average moisture content and the surface moisture content.

The second shortcoming is clear from the high degrees of saturation calculated at saturation in Chapter 4. The maximum degree of saturation, S, that can occur is unity, however some of the calculated degrees of saturation exceeds this value, some even reaching 1.5 (Particle Size Range D, Sample 2-8-2). This was found to be due to inaccurate measurements of change in depth of the material inside the trough (hence volume change). This usually happened with the fine silt and clay material that distort completely during drying (Figure 5.1) making depth measurements very difficult. Inaccurate measurements of volume change will result in inaccurate calculations of degree of saturation, void ratio (e) and volumetric water content (θ). A degree of saturation in excess of unity will result in a lower void ratio and higher volumetric water content. It was therefore decided to force degrees of saturation to unity at saturation (it is assumed that material in a slurry consistency will be fully saturated). The manner in which this was done was to divide the calculated degrees of saturation with the maximum value. Void ratio was then calculated from S with the following equation:

$$e = \frac{w.G_s}{S} \qquad [5.1]$$

Where:

w = gravimetric water content

G_s = specific gravity of material = 2.74

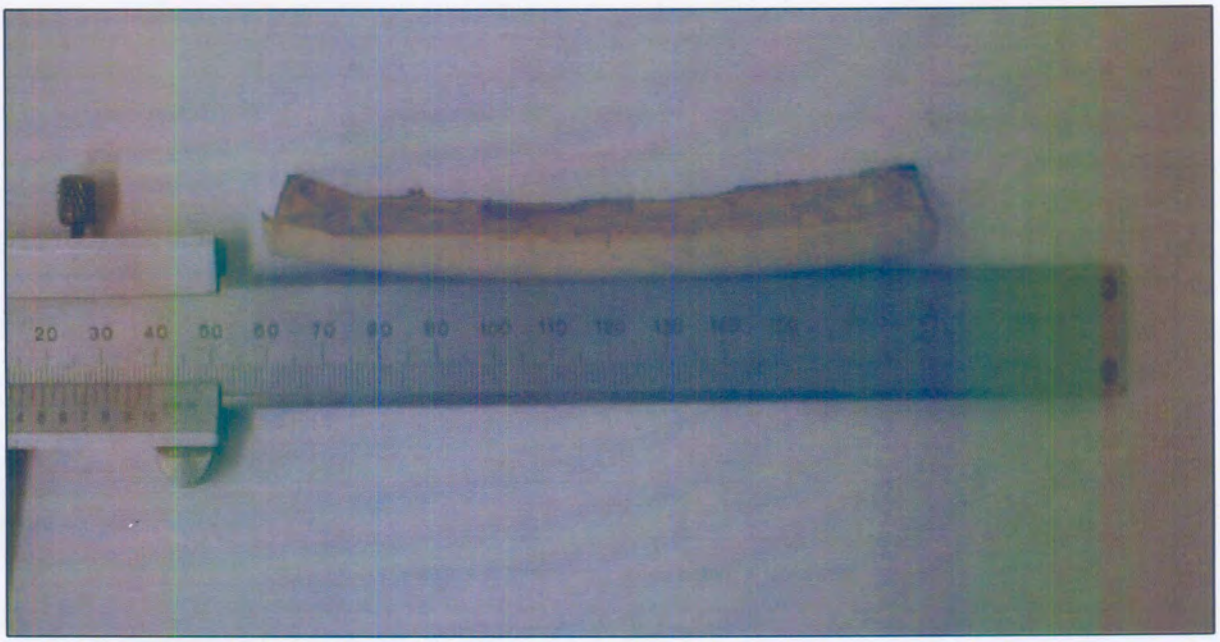

Figure 5.1: Distortion of clayey sample

An example of forcing S to unity is shown in Table 5.1. The maximum calculated value of S on Particle Size Range D, Sample 2-8-2 was 1.51. Each of the calculated values of S is then divided by 1.51 to force the initial degrees of saturation to unity. New values for e and θ are then calculated.

Table 5.1: Corrected values for S, e and θ on Particle Size Range D, Sample 2-8-2

Time (h:mm:ss)	Suction (kPa)	w -	S -	e -	θ -	LS (%)
6:30:00	5.0	0.42	1.00	1.14	0.53	0.00%
6:55:00	23.1	0.40	1.00	1.11	0.53	0.00%
7:14:00	42.2	0.40	1.00	1.08	0.52	0.00%
7:33:00	80.7	0.39	1.00	1.06	0.51	0.30%
7:52:00	126.3	0.38	0.99	1.04	0.51	0.69%
8:12:00	201.8	0.37	0.98	1.03	0.50	1.02%
8:34:00	297.4	0.36	0.97	1.01	0.49	1.29%
9:02:00	339.6	0.34	0.94	1.01	0.47	1.48%
9:32:00	340.2	0.33	0.90	1.00	0.45	1.52%
9:59:00	350.5	0.32	0.87	1.00	0.43	1.52%
10:25:00	357.1	0.31	0.83	1.00	0.42	1.52%
10:54:00	358.0	0.29	0.80	1.00	0.40	1.52%
11:35:00	368.0	0.27	0.74	1.00	0.37	1.52%

Comparing Table 5.1 with Table 4.16, it is clear that a lower S results in a higher e and a lower θ. It was decided to apply this correction to all of the data even though poor volume measurements did not feature for all the samples. Appendix A contains the corrected data for all the samples listed in Chapter 4. This correction will however have no effect on suction, w and LS.

The third shortcoming deals with the suction probe. Hydraulic contact between the probe and the sample is essential to ensure accurate measurements of suction. This was found to be quite difficult to obtain with the coarser samples (Particle size ranges A and B) as was clear from the dips in Figures 4.9 and 4.12. The reason for this is the fact that a good hydraulic contact is difficult to obtain on samples that are very dry. Particle size ranges A and B are very porous and causes the probe to "daylight" to the atmosphere. This causes the probe's ceramic to dry out on its own. For the rest of the samples hydraulic contact was not a problem, except that sufficient time should be allowed for equilibrium (response time) to be reached when the samples become very dry.

It should also be kept in mind that the experimental work was only conducted on samples from Pay Dam and Mizpah. In no way should the results from the experimental programme be extrapolated to tailings or soil from other locations. Further testing regarding this aspect is required. The investigation also assumes that the method used to obtain the particle size ranges accurately separated the different size ranges.

5.2 Suction versus Time

5.2.1 Pay Dam coarse and fine

The suction versus time graphs for Pay Dam coarse and fine tailings (Figures 4.1 and 4.5) are plotted on a semi-logarithmic scale. This enhances the visual occurrence of the kink shown in the above-mentioned figures. The shapes of the curves in the figures are all similar. There is an initial linear part up to a kink from where the curve progresses in a non-linear fashion. In Figure 4.1 the kinks for all three curves for the coarse tailings occurs at a suction of about 90 kPa. In Figure 4.5 the kinks for the 24-6 samples occur at about 195 kPa, and for the 16-7 samples at about 220 kPa. This difference was because the 24-6 samples were prepared with tap water, while the 16-7 samples were prepared with distilled water (all the other samples were prepared with distilled water).

Figure 5.2 shows a comparison between Pay Dam coarse and fine tailings (only one representative sample from each were taken). It is clear that the coarse tailings reaches its kink faster than the fine tailings. It is also clear from the graph that the finer the material, the higher the kink will take place. Thus the position of the kink is dependent on the material grading.

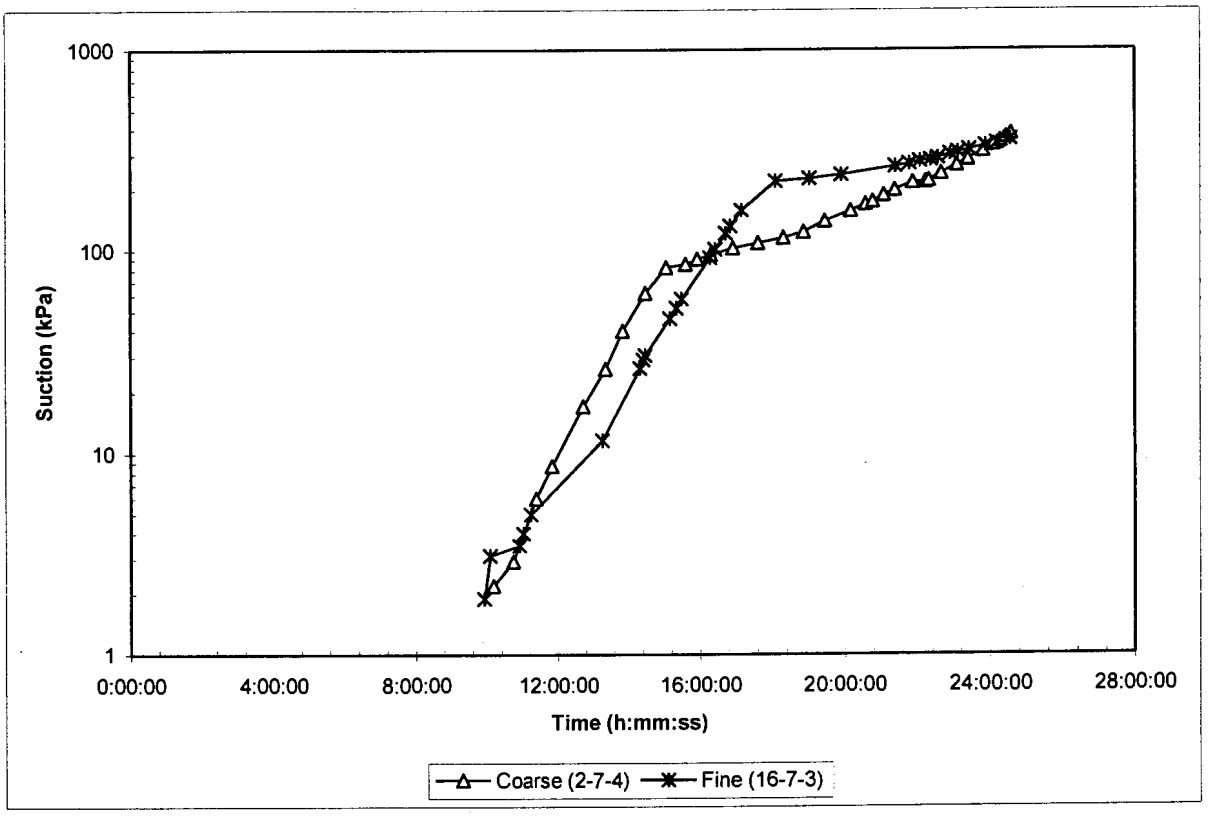

Figure 5.2: Suction versus time for samples from Pay Dam coarse and fine tailings

The above may now be compared with results obtained from Luyt (2001) presented in Figure 5.3. The graph shows that the coarse tailings dry out faster than the fine tailings, and that the kink for the fine tailings is higher than for the coarse tailings. However, the graph does not show the position of the kink accurately. The superiority of the above graph and hence test method over the method proposed by Luyt (2001) is clear, especially regarding testing time (28 hours versus 280 hours).

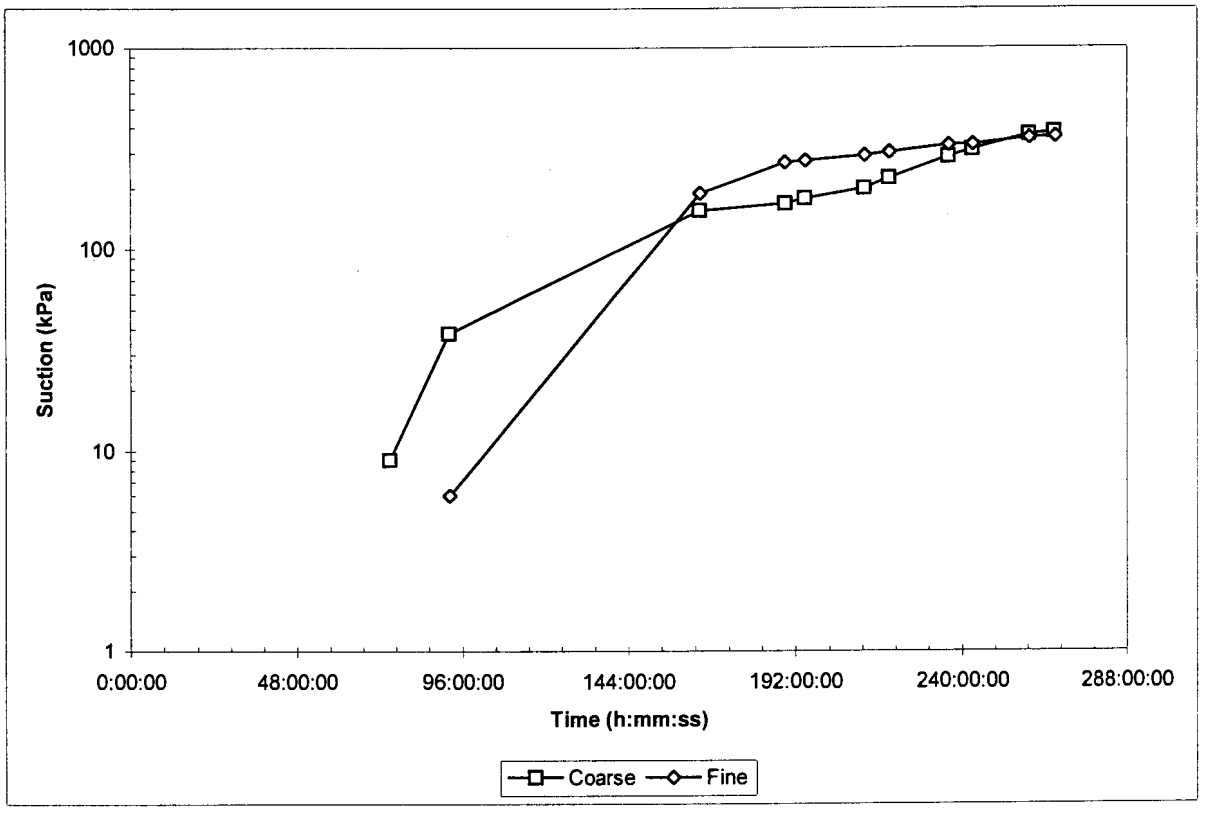

Figure 5.3: Suction versus time for samples from Pay Dam (after Luyt, 2001)

5.2.2 Particle size ranges A through E

The suction versus time curves for the five particles size ranges (PSR) from the Mizpah whole tailings were presented in Figures 4.9, 4.12, 4.15, 4.18 and 4.22. As for the Pay Dam coarse and fine samples, a kink is again apparent in all the graphs except for the PSR E graphs. For PSR A, the kink occurs at an average suction of 7 kPa, for PSR B at an average of 21 kPa, for the PSR C at an average of 89 kPa and for the PSR D at an average of 315 kPa. One sample was selected from each PSR and plotted in Figure 5.3 for comparison.

From Figure 5.4 it is again clear that the suction versus time curves in a semi-logarithmic plot consists of two parts: an initial near linear part up to a kink from where the curve progresses in a non-linear fashion. The figure also shows that the finer the material the higher the kink.

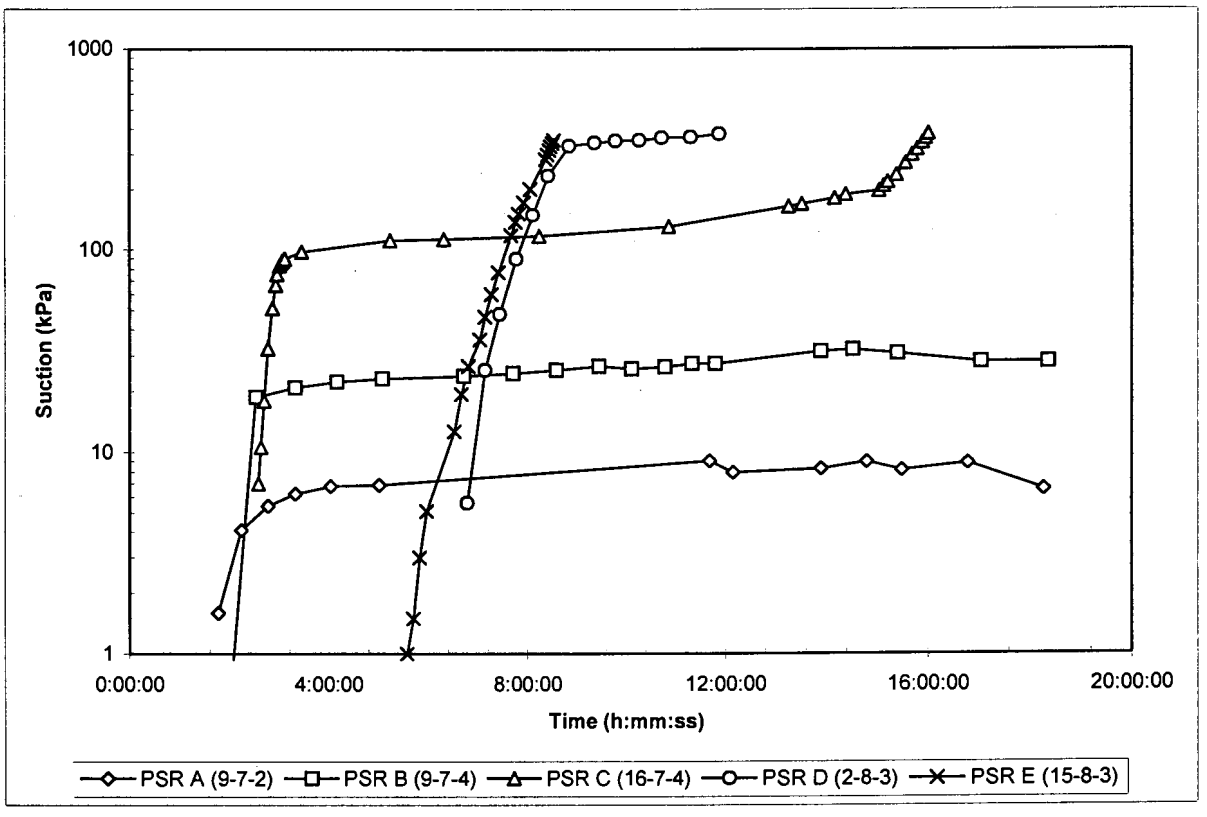

Figure 5.4: Suction versus time for the Mizpah whole particle size ranges

5.2.3 New samples A and C

The suction versus time curves for the new samples (NS) A and C created from the Mizpah particle size ranges were presented in Figures 4.26 and 4.30. Again, a kink is clearly visible in both graphs. The kink for the NS A sample occurs at 87.6 kPa and for the NS C sample at 94.3 kPa. The two curves are compared in Figure 5.5. NS C was created to correspond with the grading for the Pay Dam coarse tailings. NS A was created to correspond with the grading for BE tailings from Aubertin et al (1998). It is slightly coarser than NS A. The figure is again consistent with the previous results: the slightly finer material shows a kink at a slightly higher suction.

The results obtained from testing on Pay Dam coarse and fine, Mizpah whole particle size ranges and new samples created from the particle size ranges showed very similar characteristics regarding the shape of the curves and the occurrence of a kink. It is clear that the grading of the material controls the position of the kink. The reason for the occurrence of this phenomenon should now be investigated.

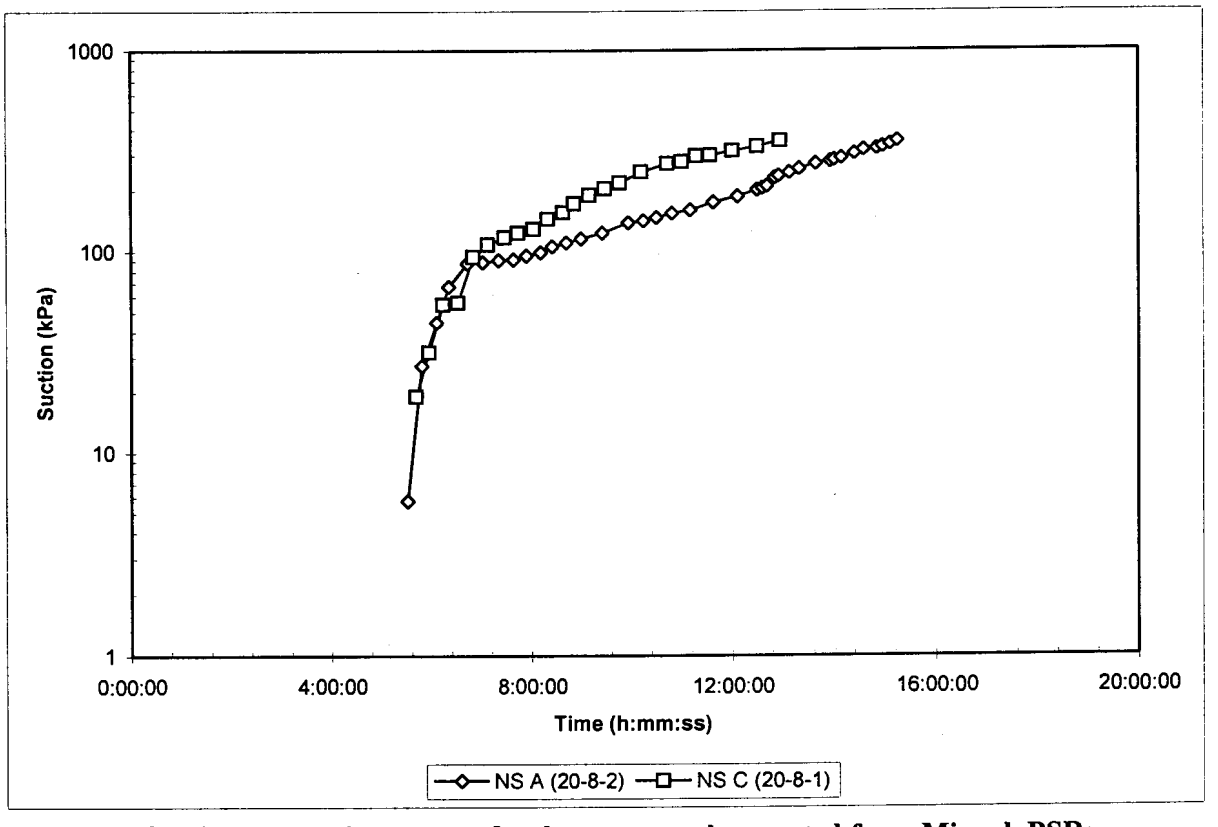

Figure 5.5: Suction versus time curves for the new samples created from Mizpah PSRs

5.3 Soil-Water Characteristic Curves

5.3.1 Pay Dam coarse and fine

The soil-water characteristic curves (SWCCs) for Pay Dam coarse and fine tailings were presented in Figures 4.2 and 4.6. The shapes of the curves in these figures are all similar. There is an initial linear part up to a kink from where the curve progresses in a non-linear fashion. The SWCC was discussed in Section 2.4. It was shown that this kink corresponds to the air-entry value (AEV) of the sample, thus the kink discussed in Section 5.2 is in actual fact the AEV. From Figure 4.1 and 4.2 it is clear that the AEV for the coarse tailings occurs at a suction of about 90 kPa. From Figure 4.5 and 4.6 it is clear that the AEV for the 24-6 samples occur at about 195 kPa, and for the 16-7 samples at about 220 kPa.

Figure 5.6 shows a comparison between Pay Dam coarse and fine tailings (only one representative sample from each were taken). The figure shows that the SWCC is linear up to the AEV from where it progresses non-linearly. It also shows that the AEV for a finer material is higher than for a coarser

material, and that the corresponding moisture contents, w, at a certain suction value is higher for a finer material than for a coarser material. Due to the fact that the suction probe can only measure suctions up to about 350 kPa, the residual suction value cannot be determined from Figure 5.6. Figure 5.6 also shows the SWCC for both the coarse and fine Pay Dam tailings obtained by Luyt (2001). The shapes of the curves are very similar; however there were not enough measurements of suction made during the initial stages to accurately pinpoint the AEV.

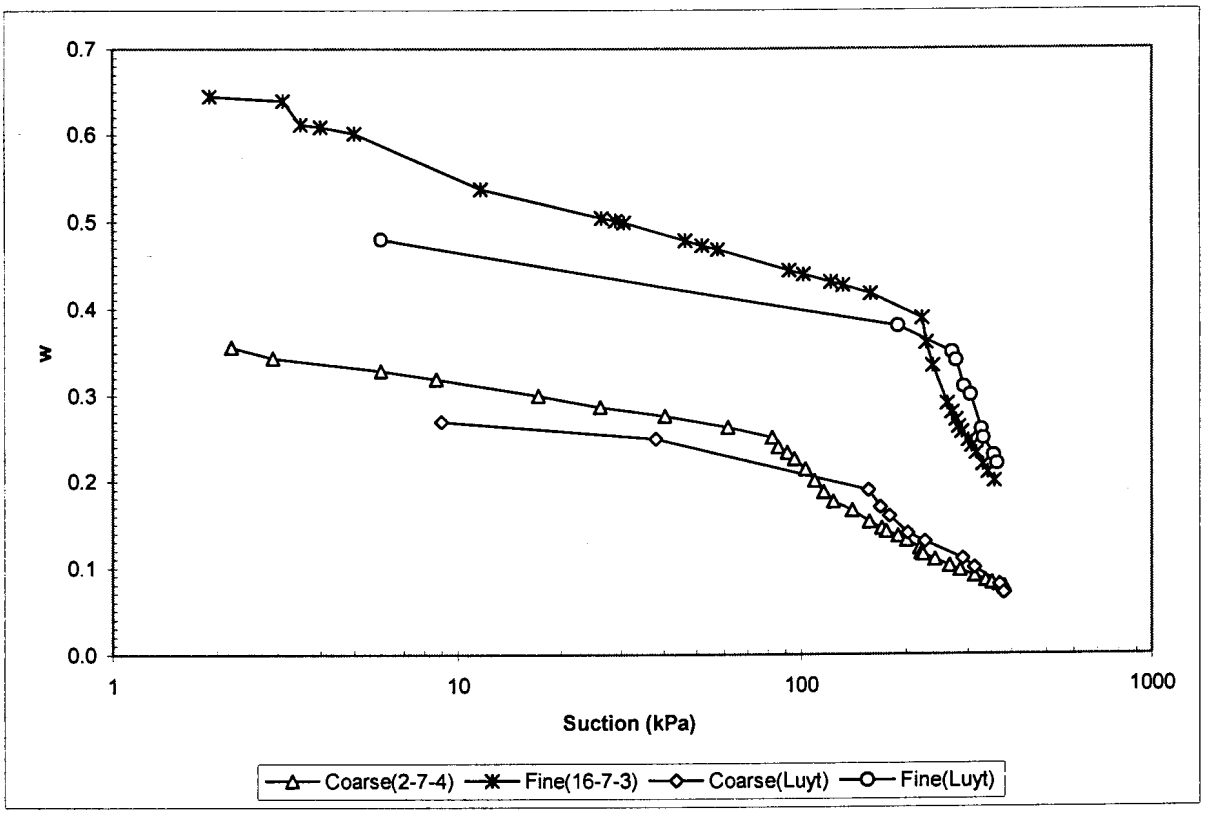

Figure 5.6: SWCCs for Pay Dam coarse and fine

5.3.2 Particle size ranges A through E

The SWCCs for the particle size ranges A through E were presented in Figures 4.10, 4.13, 4.16, 4.19 and 4.23. Again, the shapes of the curves are very similar, except for particle size range (PSR) E. There is an initial near linear part up to the AEV, from where the curve progresses in a non-linear fashion. PSR E does not show the position of the AEV as the test was terminated around 350 kPa. It is thus clear that the AEV for PSR E is in excess of 350 kPa. From the above-mentioned figures and from the corresponding suction versus time graphs, it is obvious that the AEV for PSR A is around 7

kPa, for PSR B around 21 kPa, for PSR C around 89 kPa, for PSR D around 315 kPa and in excess of 350 kPa for PSR E.

Figure 5.7 shows a comparison between the five different particle size ranges (only one representative sample from each were taken). It is again clear that the finer the material, the higher the water content of the sample at a certain suction, and the higher the AEV. It is interesting to note that the AEV for PSR A through D are approximately equally spaced horizontally on the graph.

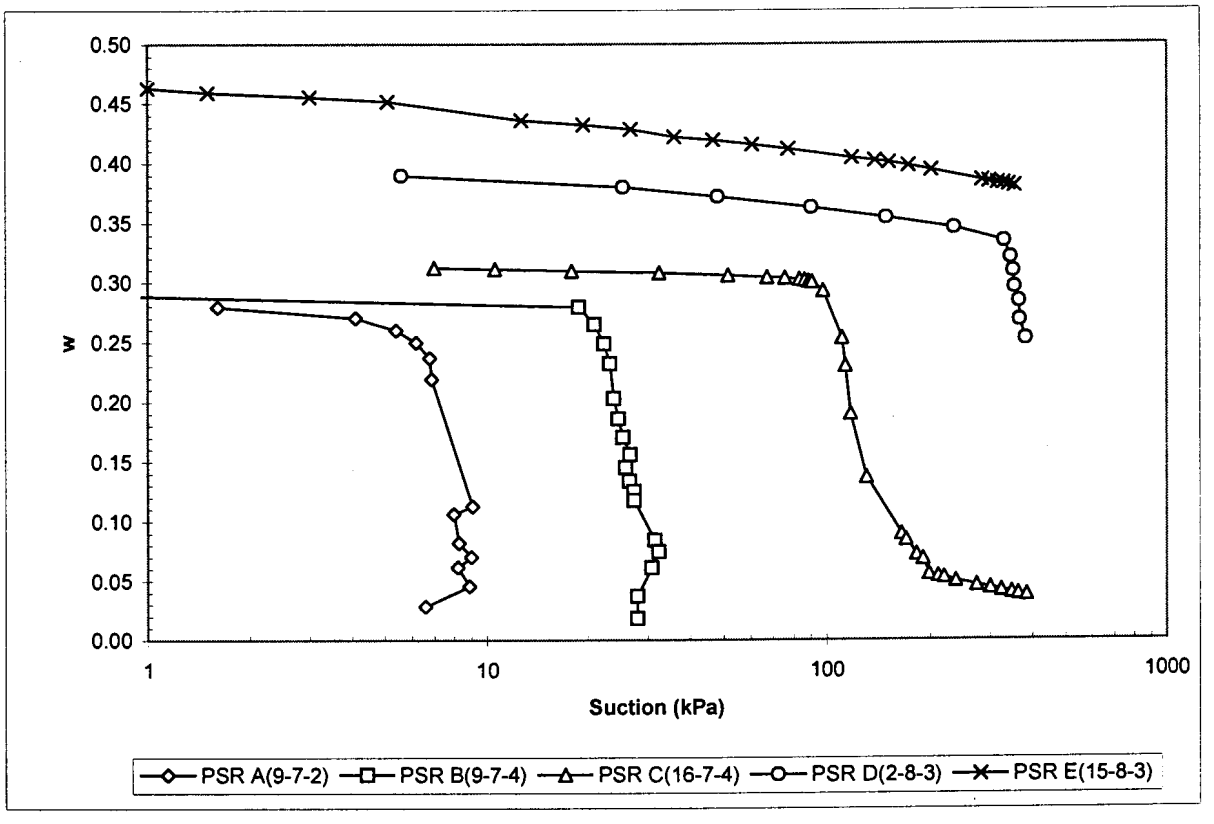

Figure 5.7: SWCCs for particle size ranges A through E

5.3.3 New samples A and C

The SWCCs for the new samples A and C created from the Mizpah particle size ranges were presented in Figures 4.27 and 4.31. As was mentioned in Section 3.6.3, new sample (NS) C was created to have the same particle size range percentages as the coarse tailings from Pay Dam, thus it can be expected that the SWCC for both samples would be very similar. NS A was created to closely represent sample BE from Aubertin et al (1998). It is slightly coarser than the NS C sample.

The NS A and C samples together with the representative Pay Dam coarse sample are presented in Figure 5.8. The NS A sample has an AEV of 87.6 kPa, the NS C sample an AEV of 94.3 kPa and the Pay Dam coarse sample an AEV of 82.5 kPa. The AEVs for the three samples are virtually identical, owing to the similarity in grading. The curves for the NS C and Pay Dam coarse samples however, do not overlap. This is probably due to the fact that although the particle size range percentages are the same, the grading within these ranges are not. This can be seen in the grading curves for Pay Dam coarse and Mizpah whole tailings in Figure 3.17.

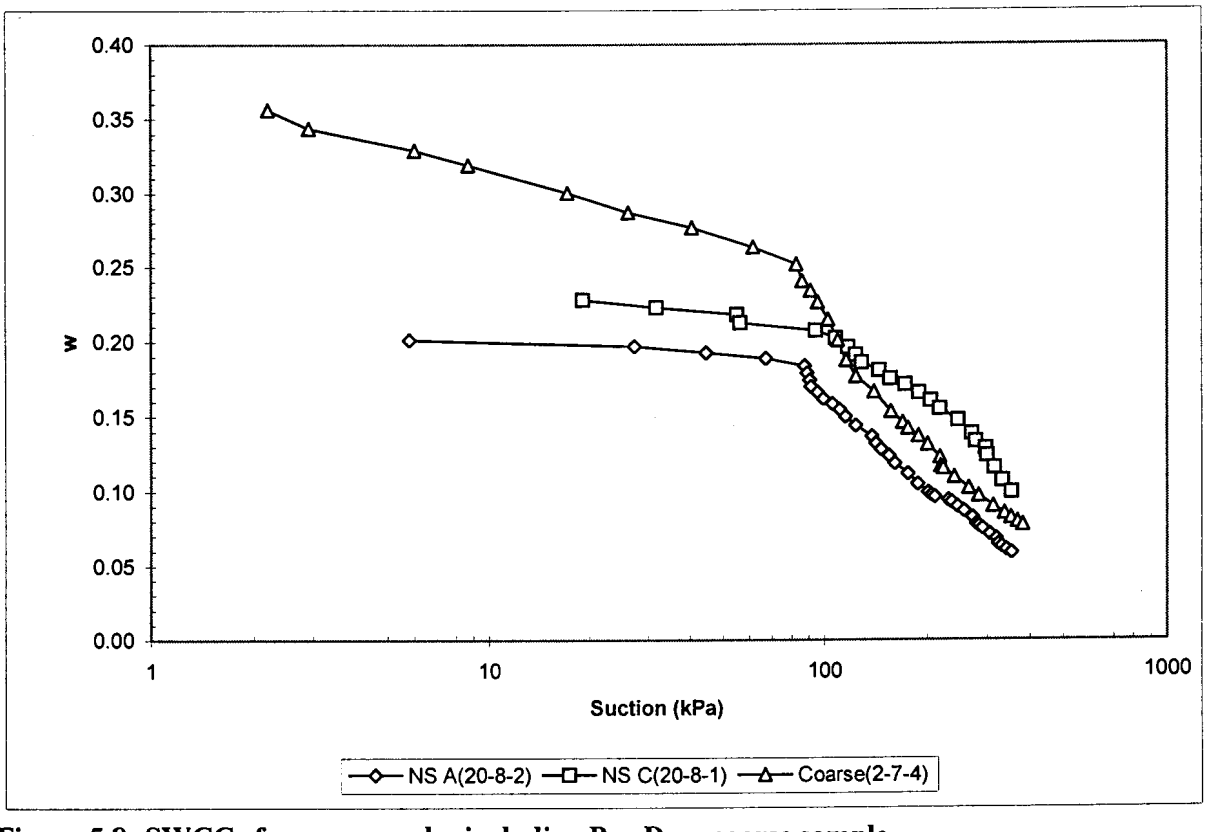

Figure 5.8: SWCCs for new samples including Pay Dam coarse sample

Aubertin et al (1998) presented the SWCC data as volumetric water content, θ, versus suction. Figure 5.9 presents the data from Figure 5.8 as volumetric water content versus suction (using the corrected values for θ as given in Appendix A). Included in the figure are the results taken from Aubertin et al (1998). According to the graph, the AEV for BE tailings lies somewhere between 15 and 40 kPa. This is much lower than the value for the NS A tailings. The results for the BE tailings does however raise some questions. The spread of results are poor. The reliability of the graph is questionable.

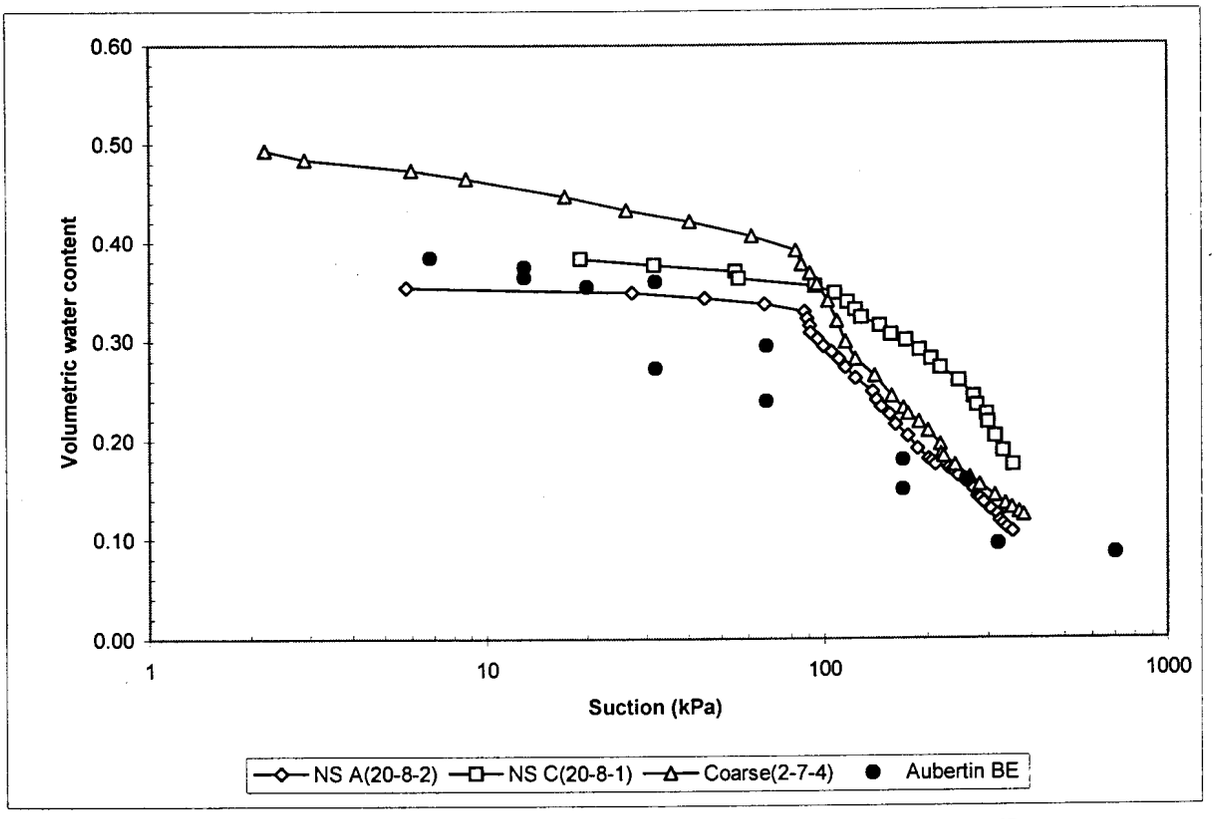

Figure 5.9: SWCCs for new samples including Pay Dam coarse and Aubertin BE

5.4 Air-Entry Value

5.4.1 Pay Dam coarse and fine

Values for the air-entry value (AEV) have already been determined from Figures 5.2 and 5.6 for the coarse and fine tailings from Pay Dam. It was stated in Section 2.4.2 that the AEV corresponds to the shrinkage limit (SL) for a particular material. Various other methods of obtaining the AEV were also discussed. With the AEV already determined, the opportunity arose to investigate the applicability and accuracy of the various methods.

The shrinkage curves for the representative samples from Pay Dam are shown in Figure 5.10. The SL corresponds to the moisture content, w, when the void ratio, e, reaches a constant value (no more volume change). From Figure 5.6 the AEV for the coarse and fine samples are respectively 82.5 kPa and 222.0 kPa at moisture contents of 0.25 and 0.39. To find the SL a straight line is drawn through the initial part of the shrinkage curve and another through the horizontal part. A vertical line is drawn

through the intersection of the two straight lines and the intersection with the w axis corresponds to the SL. This is shown in Figure 5.10. The SL for the coarse tailings is 0.26 and for the fine tailings 0.40. These values correspond very well with the w at the AEV from Figure 5.6.

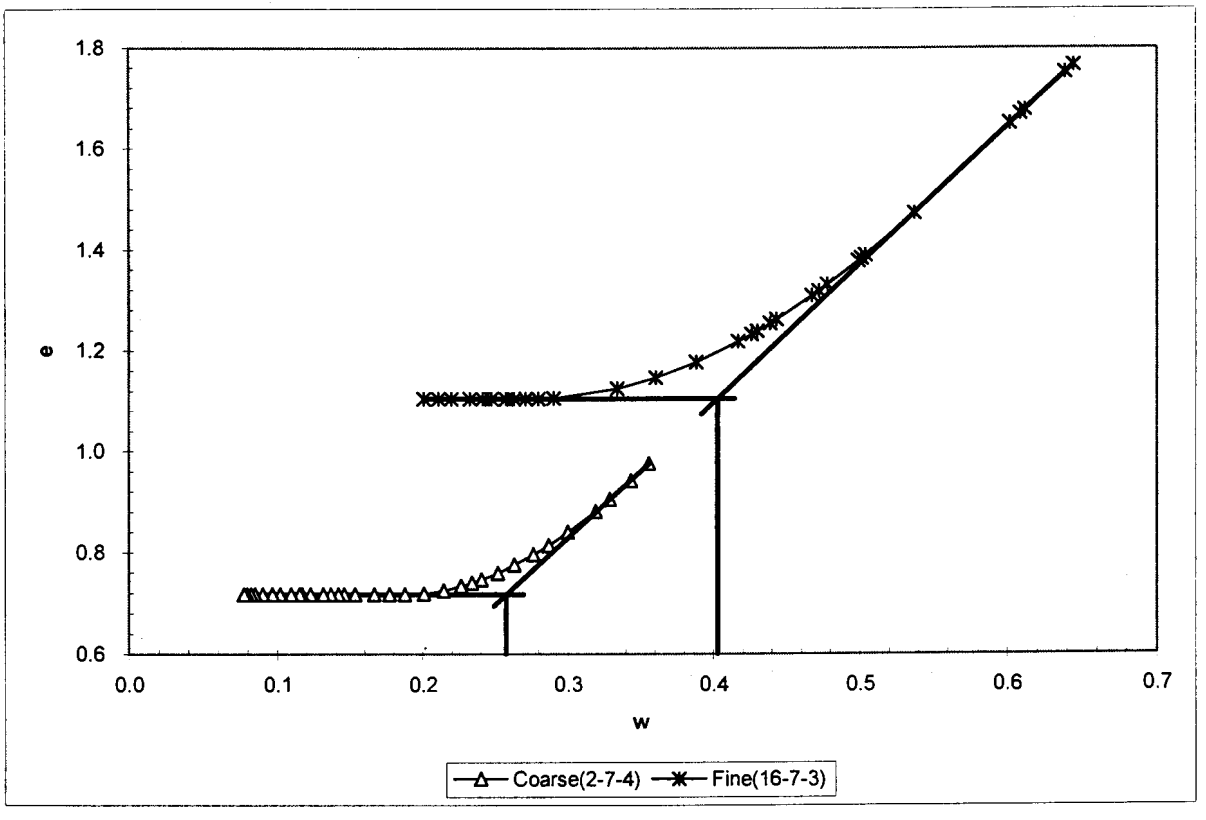

Figure 5.10: Use of shrinkage curves to find the SL for Pay Dam coarse and fine samples

Table 5.2 lists the various parameter values at the AEV for all the Pay Dam coarse and fine (where distilled water was used) samples tested. The similarities between the various parameters at the AEV are immediately apparent. S, e and θ are the corrected values from Appendix A.

Table 5.2: AEV information for Pay Dam coarse and fine tailings

Sample -	AEV (kPa)	w -	S -	e -	θ -	LS (%)
Coarse (2-7-1)	95.5	0.24	0.90	0.72	0.38	1.74%
Coarse (2-7-2)	87.0	0.24	0.92	0.73	0.39	0.93%
Coarse (2-7-4)	82.5	0.25	0.91	0.76	0.39	1.02%
Fine (16-7-2)	212.8	0.37	0.92	1.12	0.48	2.71%
Fine (16-7-3)	222.0	0.39	0.90	1.18	0.49	1.45%

The first method of obtaining the AEV discussed in Section 2.4.2 is the one proposed by Brooks and Corey (1964). This method assumes that the initial part of the SWCC is horizontal. Figures 5.6, 5.7 and 5.8 however, show that the initial part of the curve is not horizontal. The residual value of the volumetric water content is also needed, which could not be determined with the adopted test method. The use of the Brooks and Corey method is thus not applicable when the full SWCC is not known.

The second method of obtaining the AEV was proposed by Aubertin et al (1998). It was stated that the AEV is equal to the suction at an S of 0.9. The average value of S at the AEV in Table 5.2 is 0.91. This compares very well. No prediction of the AEV however, can be made with this method.

The third method is an estimation of the AEV knowing only some basic properties of the material (Aubertin et al, 1998). The equation incorporates a constant b (equal to 4 mm^2 according to Aubertin et al, 1998), the void ratio, e, and the diameter for which 10% by weight passes a sieve having an opening size D (in mm).

$$AEV = \frac{b}{e.D_{10}} \cdot \frac{\gamma_w}{1000} \qquad [5.1]$$

It was found that a b-value of 4 mm^2 is incorrect. It was decided to calculate the b-value using Equation 5.1 and Table 5.2 for the various samples. The results are presented in Table 5.3. The Pay Dam coarse tailings have a D_{10} of 0.002 mm and the fine tailings a D_{10} of 0.0017 mm. The table clearly shows that if a b-value of 4 mm^2 should be used, the predicted AEV would be erroneous. Thus there is a need for a method of predicting the AEV for a certain material.

Table 5.3: Calculation of the b-value for Pay Dam tailings

Sample	AEV (kPa)	e -	b-value (mm^2)
Coarse (2-7-1)	95.5	0.72	14.09
Coarse (2-7-2)	87.0	0.73	12.88
Coarse (2-7-4)	82.5	0.76	12.77
Fine (16-7-2)	212.8	1.12	41.14
Fine (16-7-3)	222.0	1.18	45.29

5.4.2 Particle size ranges A through E

Values for the AEV have already been determined from Figures 5.4 and 5.7 for the Mizpah whole particle size ranges A through D (AEV for PSR E was not reached). The shrinkage limits for PSR A through C could not be determined from the shrinkage curves given in Figures 4.11, 4.14 and 4.17 due to the fact that the curves are horizontal lines (no volume change).

The representative samples for the particle size ranges are shown in Figure 5.11. It is clear that the only SL that may be calculated using the method described in Section 5.4.1, is for PSR D. The w at AEV from Figure 5.7 for PSR D is at 0.33, while the SL calculated from Figure 5.11 is 0.35. Again the results of the two methods of obtaining the SL are very similar. Both figures also show that the SL and hence AEV for the PSR E sample have not yet been reached.

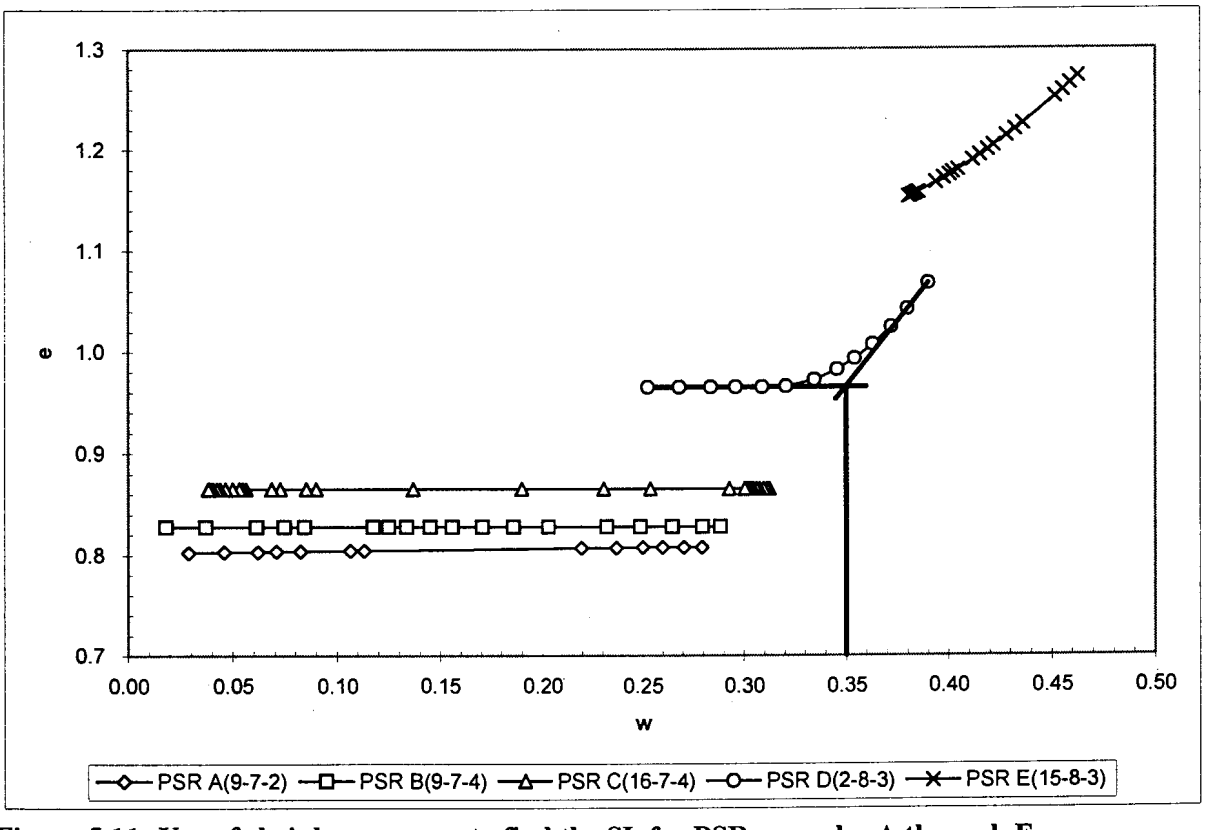

Figure 5.11: Use of shrinkage curves to find the SL for PSRs samples A through E

Table 5.4 lists the AEV information for the particle size range samples. The AEVs for each PSR compares well. It is also shown that the parameter values increases with the AEV for each finer PSR. S, e and θ are the corrected values from Appendix A. It is interesting to note that the S at the AEV

increases, as the PSR gets progressively finer. For PSR A the average S 0.87, for PSR B 0.95, for PSR C 0.95 and for PSR D 0.96, which is not equal to the 0.9 value proposed by Aubertin et al (1998).

Table 5.4: AEV information for Mizpah particle size ranges

Sample -	AEV (kPa)	w -	S -	e -	θ -	LS (%)
PSR A (9-7-2)	6.2	0.25	0.85	0.81	0.38	-
PSR A (24-7-1)	6.9	0.22	0.89	0.69	0.36	-
PSR B (9-7-3)	22.2	0.31	0.97	0.87	0.45	-
PSR B (9-7-4)	18.8	0.28	0.93	0.83	0.42	-
PSR C (16-7-1)	87.4	0.33	0.95	0.95	0.46	-
PSR C (16-7-4)	90.6	0.30	0.95	0.87	0.44	-
PSR D (2-8-2)	297.4	0.36	0.97	1.01	0.49	1.29%
PSR D (2-8-3)	331.6	0.33	0.94	0.97	0.46	0.99%

Table 5.5 shows the results from calculating the b-value using Equation 5.1 and Table 5.4. The D_{10} values for the PSRs were obtained by linear interpolation of the grading curve for Mizpah whole tailings. For example: PSR B has a maximum particle size of 0.063 mm and a minimum of 0.02 mm. By interpolating between these two values, D_{10} is calculated as 0.0243 mm. The calculated b-values are much larger than the proposed value of 4 mm^2. It is apparent that the finer the material, the higher the b-value. The question that needs to be asked is whether the AEVs for the PSRs can be used to predict the AEV for other samples with known gradings. This question shall be answered at a later stage.

Table 5.5: Calculation of the b-value for Mizpah PSRs

Sample -	AEV (kPa)	e -	D_{10} (mm)	b-value (mm^2)
PSR A (9-7-2)	6.2	0.81	0.0699	35.66
PSR A (24-7-1)	6.9	0.69	0.0699	33.85
PSR B (9-7-3)	22.2	0.87	0.0243	47.84
PSR B (9-7-4)	18.8	0.83	0.0243	38.55
PSR C (16-7-1)	87.4	0.95	0.0074	62.74
PSR C (16-7-4)	90.6	0.87	0.0074	59.13
PSR D (2-8-2)	297.4	1.01	0.0024	73.72
PSR D (2-8-3)	331.6	0.97	0.0024	78.85

5.4.3 New samples A and C

Values for the AEV have already been determined for the new samples A and C from Figures 5.5 and 5.8. The representative samples are shown in Figure 5.12. The w at the AEV from Figure 5.8 for NS A is at 0.18, while the SL calculated from Figure 5.12 is 0.17. For NS C the w at AEV is 0.21, while the SL is determined as 0.18. Again the results of the two methods of obtaining the SL are very similar.

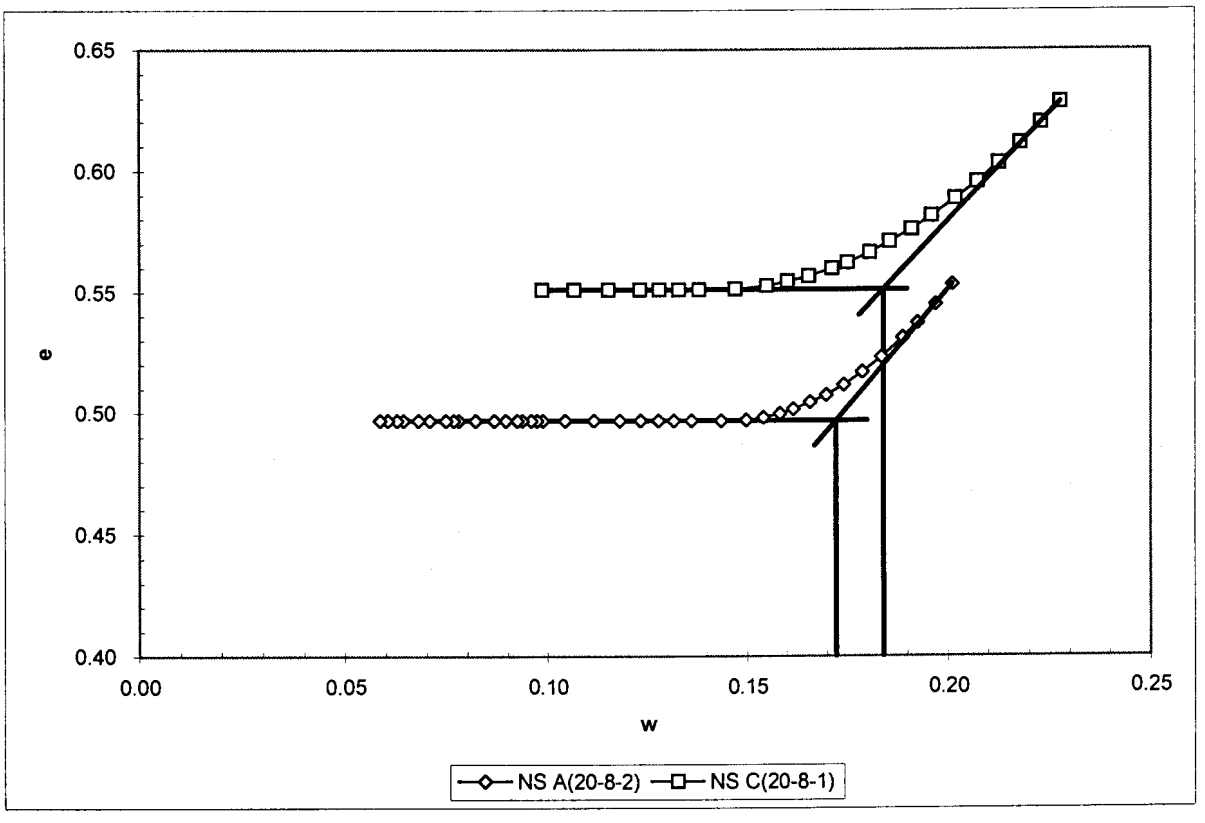

Figure 5.12: Use of shrinkage curves to find the SL for new samples A and C

Table 5.6 lists the AEV information for the new samples. S, e and θ are the corrected values from Appendix A. The NS C sample is slightly finer than the NS A sample, thus it is expected that the parameter values should be very similar, which is indeed the case. The values of S is equal to about 0.95 for both samples, which is higher than the 0.9 value proposed by Aubertin et al (1998).

Table 5.6: AEV information for the new samples

Sample -	AEV (kPa)	w -	S -	e -	θ -	LS (%)
NS A (20-8-2)	87.6	0.18	0.96	0.52	0.33	0.43%
NS C (20-8-1)	94.3	0.21	0.95	0.60	0.36	0.25%

The D_{10} values for the new samples were obtained by interpolation of the PSR percentages for the new samples given in Table 3.1. NS A has a D_{10} of 0.004 mm, while NS C has a D_{10} of 0.00227 mm. Again it is apparent that the calculated b-values exceeds 4 mm^2.

Table 5.7: Calculation of the b-value for the new samples

Sample -	AEV (kPa)	e -	D_{10} (mm)	b-value (mm^2)
NS A (20-8-2)	87.6	0.52	0.00400	18.69
NS C (20-8-1)	94.3	0.60	0.00227	13.00

5.5 Linear Shrinkage

5.5.1 Pay Dam coarse and fine

The linear shrinkage (LS) versus suction curves for the Pay Dam coarse and fine samples were presented in Figures 4.4 and 4.8. The curve is reproduced using the selected samples in Figure 5.13. The final amount of LS is highly variable as was shown in Figure 4.8. The final amount of LS for the fine tailings is more than for the coarse tailings as can be expected because of the higher clay content in the fine tailings. Figure 5.13 does however show an interesting characteristic: LS starts at a suction of about 10 kPa for both the coarse and fine tailings. Thus it would be fairly safe to say that when the first signs of cracking appears on a newly deposited layer of tailings on the Pay Dam tailings dam, the suctions is in excess of 10 kPa throughout the depth of cracking.

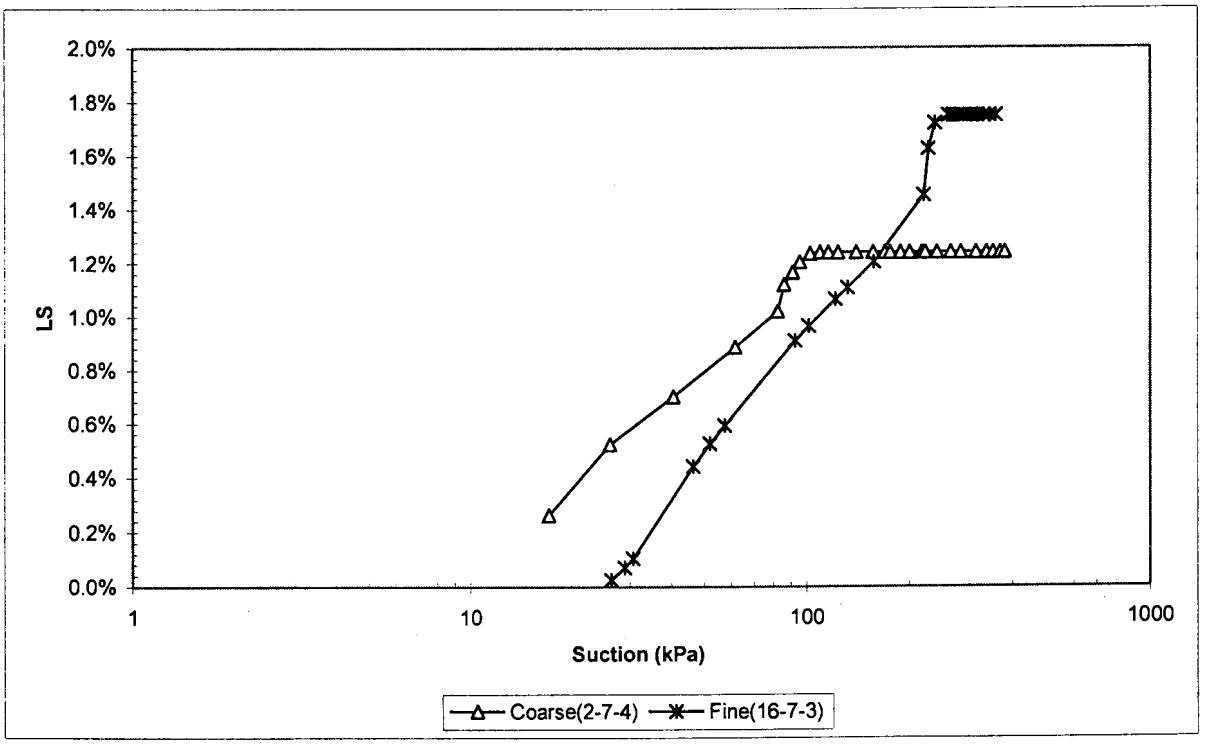

Figure 5.13: Linear shrinkage versus suction curves for Pay Dam coarse and fine tailings

5.5.2 Particle size ranges A through E

The only PSRs that showed linear shrinkage (LS) were the fine silt PSR D samples and clay PSR E sample. The LS versus suction curves for these samples were presented in Figures 4.21 and 4.25. The selected representative samples are presented in Figure 5.14. It is interesting to note that LS starts at a suction of about 50 kPa for both samples.

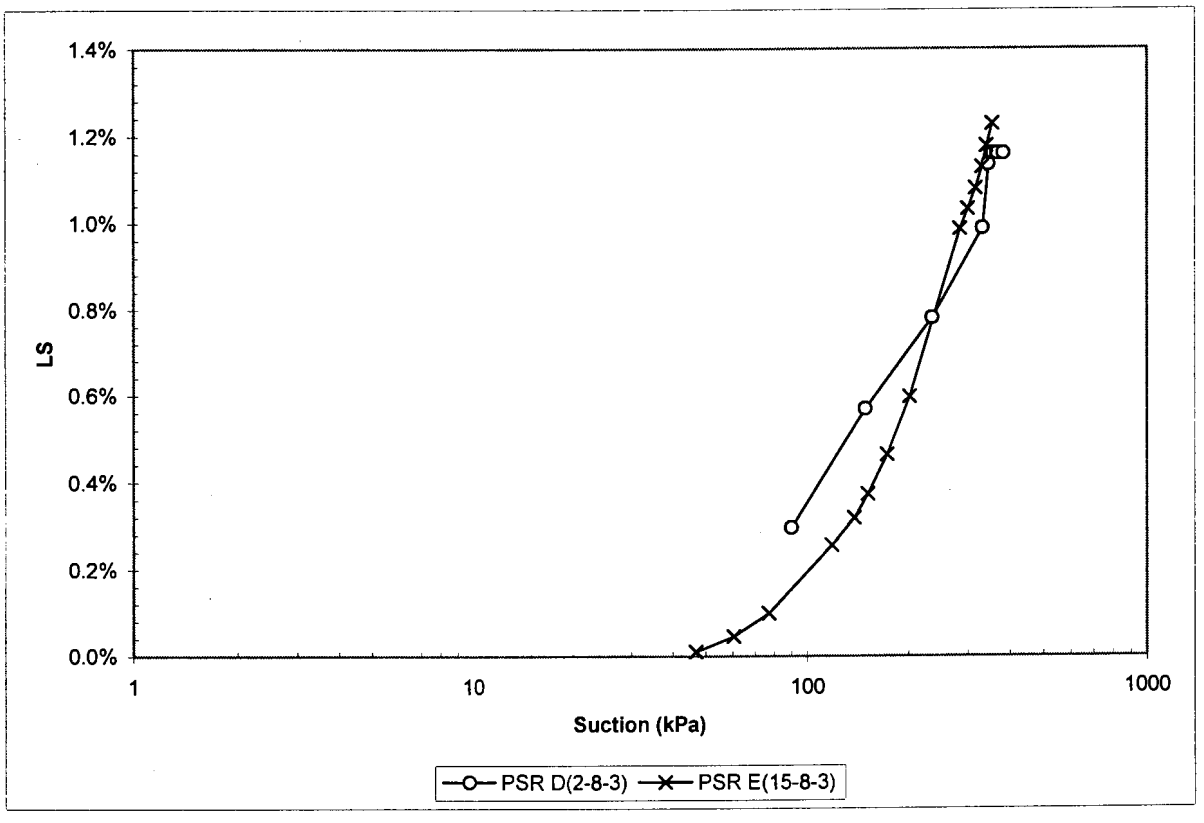

Figure 5.14: Linear shrinkage versus suction curves for PSRs D and E

5.5.3 New samples A and C

The linear shrinkage versus suction curves for both new samples A and C were presented in Figures 4.29 and 4.33. Both samples are presented in Figure 5.15 for comparison. Again, it seems as though the first signs of LS starts at a suction of about 50 kPa.

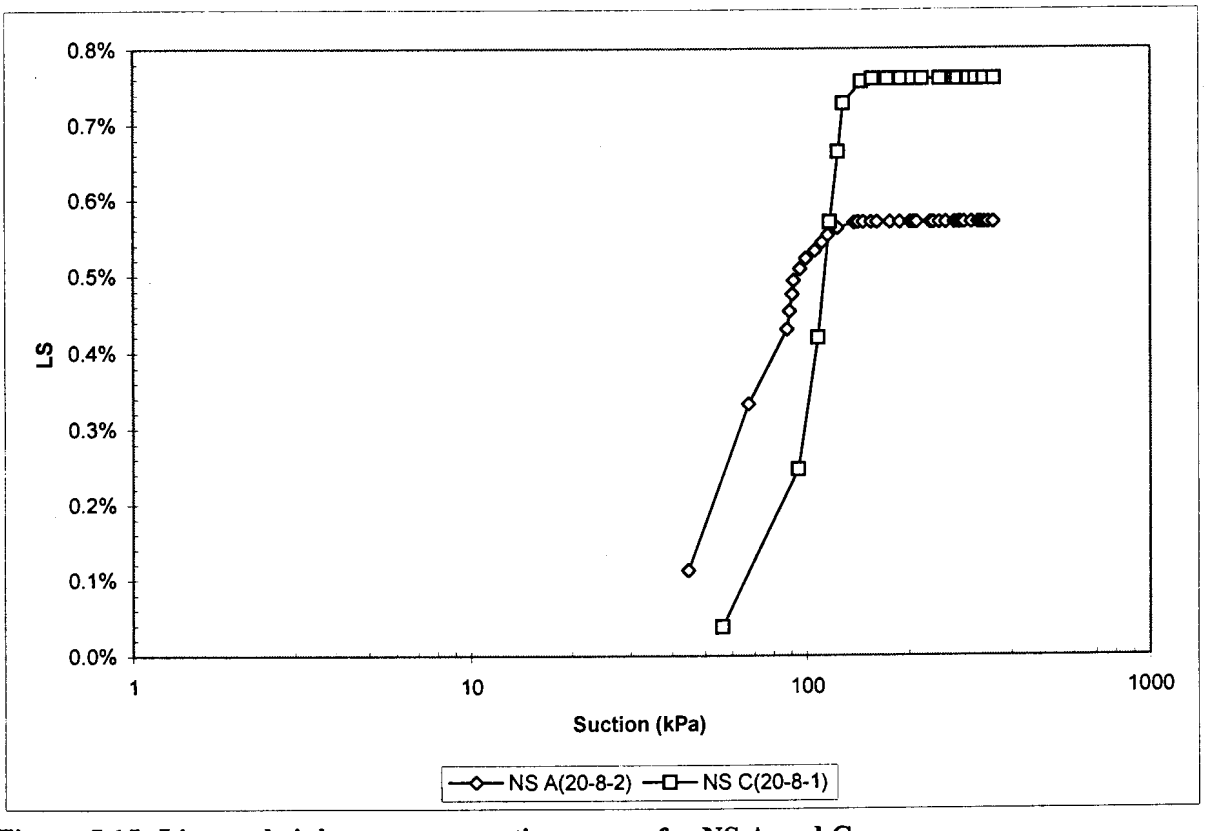

Figure 5.15: Linear shrinkage versus suction curves for NS A and C

5.6 Air-Entry Value Prediction

5.6.1 Introduction

Air-entry values for the various samples tested were determined in Section 5.4. It was shown that the AEV could be fairly easily determined with the proposed test method by using graphs of suction versus time and soil-water characteristic curves. The moisture content at the AEV was also shown to be the same as the shrinkage limit. The results were compared with other more conventional methods used to determine the AEV. The only method that was found to be reasonable accurate was the one proposed by Aubertin et al (1998), where the AEV is taken to be equal to the suction at a degree of saturation of 0.9. There is a need, however, to being able to predict the AEV before any testing has been completed on a particular material. The AEV does not exclusively depend on the particle sizes of a material, but also on the density of the material. This section aims at developing a method of obtaining a prediction of the AEV using the results for the Mizpah particle size ranges.

5.6.2 Particle size ranges and new samples

Table 5.8 lists the average parameter values (corrected) at the AEV determined for the Mizpah particle size ranges discussed in Section 5.4. It is clear that the finer the particle size ranges, the higher the AEV and parameter values. The AEV for PSR E could however not be determined due to the limited range of the suction probe.

Table 5.8: Average parameter values at the AEV for Mizpah particle size ranges

PSR -	AEV (kPa)	w -	S -	e -	θ -
A	6.6	0.24	0.87	0.75	0.37
B	20.5	0.29	0.95	0.85	0.43
C	89.0	0.31	0.95	0.91	0.45
D	314.5	0.35	0.95	0.99	0.48

The PSRs were combined in certain percentages to develop new samples A and C. Table 5.9 lists the parameter values (corrected) at the AEV determined for the new samples. NS A is slightly coarser than NS C, which is evident from the table (lower values).

Table 5.9: Parameter values at the AEV for the new samples

NS -	AEV (kPa)	w -	S -	e -	θ -
A	87.6	0.18	0.96	0.52	0.33
C	94.3	0.21	0.95	0.60	0.36

5.6.3 AEV prediction

The percentages of the PSRs used to create the new samples were given in Table 3.1. If the AEV and percentage of each PSR is multiplied and the results added, the answer should closely approximate the AEV determined for NS A and C. This assumption together with the "goal seek" function within Microsoft Excel is used to determine the AEV for PSR E. The AEV for PSR E was thus changed until the combined AEV equalled the required AEV. Table 5.10 and 5.11 shows the results of the calculation of the AEV for PSR E.

Table 5.10: Calculation of the AEV for PSR E using data for NS A

PSR -	AEV (kPa)	P (%)	AEV*P (kPa)
A	6.6	30%	2.0
B	20.5	34%	7.0
C	89.0	21%	18.7
D	314.5	10%	31.5
E	570.5	5%	28.5
		100%	87.6

Table 5.11: Calculation of the AEV for PSR E using data for NS C

PSR -	AEV (kPa)	P (%)	AEV*P (kPa)
A	6.6	27%	1.8
B	20.5	28%	5.7
C	89.0	21%	18.7
D	314.5	15%	47.2
E	232.5	9%	20.9
		100%	94.3

The tables show that there is a large difference in the calculated AEV for PSR E. The average of these two values is approximately equal to 400 kPa. This value shall now be adopted as the AEV for PSR E. Table 5.12 presents the results of AEV calculations using the average value on the fine Pay Dam tailings, NS A and NS C (same as Pay Dam coarse) samples. The real values are the average AEVs obtained from the test results, and the predicted values are the results of AEV calculations using the same method as in Tables 5.10 and 5.11 with the AEV for PSR E equal to 400 kPa.

Table 5.12: Prediction of the AEV

Sample	Real AEV (kPa)	Predicted AEV (kPa)	Accuracy (%)
Fine	217.4	201.0	-8.2%
NS A	87.6	79.1	-10.7%
NS C	94.3	109.4	+13.8%

The table indicated that the accuracy of the adopted AEV prediction method is about ten percent above or below the real value. This method does only take into account particle size, while it is well known that the AEV also depends on the density (void ratio) of the material. The AEV for PSR E might also be inaccurate. However, this method is only a prediction of the real value, and it is assumed that the results will be reasonably accurate.

5.7 Soil-Water Characteristic Curve Prediction

5.7.1 Theoretical curves

Prediction of the SWCC can be made with the use of several proposed models (For example Van Genuchten, 1980 and Fredlund and Xing, 1994). These were discussed in Section 2.4.3. These models uses an initial horizontal line almost up to the AEV (See Figure 2.10), however, it is clear from Section 5.3 that this initial line, during which the sample is still completely saturated, is not horizontal. Thus it can be expected that the theoretical curves are not accurate in the initial stages of a drying curve while the sample is still saturated. This section aims at developing a new method of accurately predicting the SWCC up to the AEV knowing only some basic properties of a soil.

5.7.2 Mizpah particle size ranges

The SWCCs for the representative samples of each PSR were presented in Figure 5.7. Each curve can be divided into two parts (except for PSR E): an initial linear part up to the AEV, and a second non-linear part. The "trendline" function within Microsoft Excel was used to fit functions to the data presented in Figure 5.7 up to the AEV. These are shown in Figure 5.16. All the lines are logarithmic (linear on logarithmic scale) up to the AEV. Table 5.13 presents the functions used to represent the SWCCs for the PSRs up to the AEV, together with the suction and moisture content at the AEV. These values are about the same as the values presented in Table 5.4.

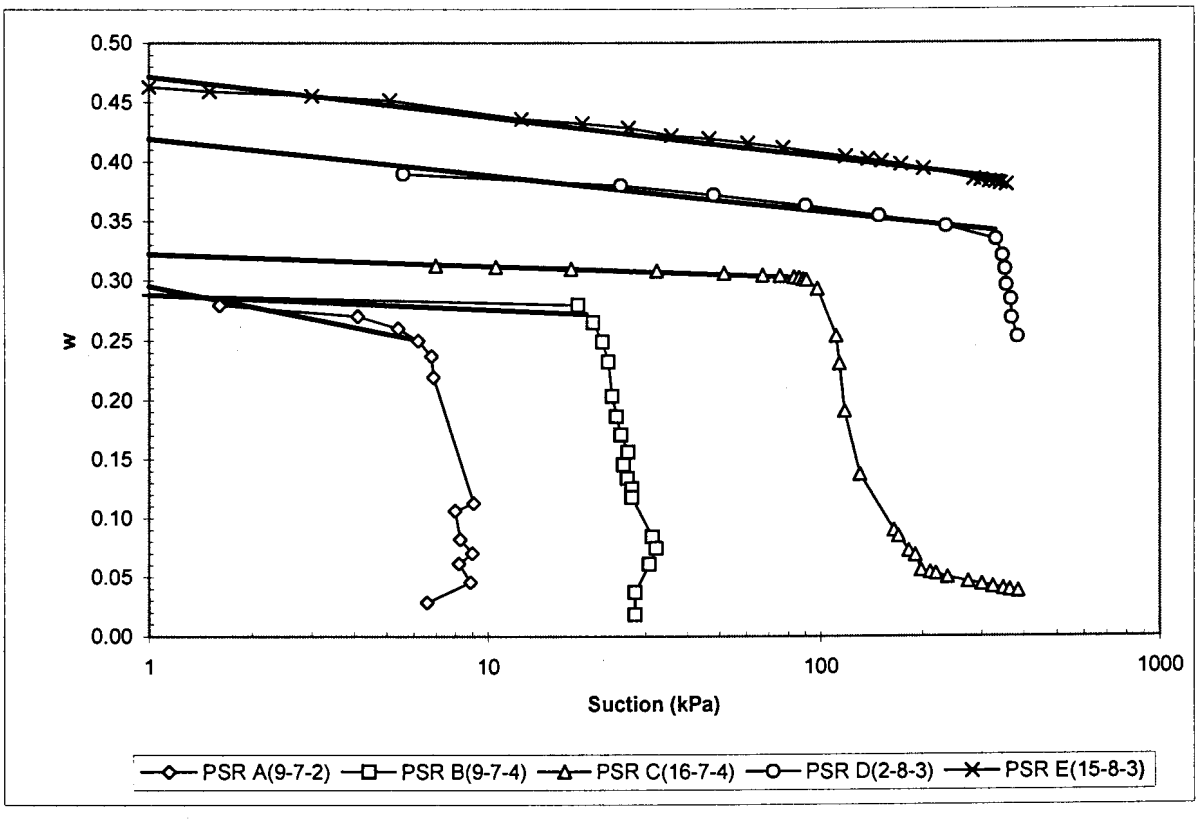

Figure 5.16: Trendlines fitted to SWCCs for particle size ranges

Table 5.13: Functions used to represent PSR SWCCs

PSR	Function	AEV (kPa)	w at AEV
A	w = -0.0245 ln(Suction) + 0.2952	6	0.25
B	w = -0.0054 ln(Suction) + 0.2882	20	0.27
C	w = -0.0043 ln(Suction) + 0.3218	91	0.30
D	w = -0.0133 ln(Suction) + 0.4193	330	0.34
E	w = -0.0146 ln(Suction) + 0.4713	-	-

5.7.3 SWCC prediction

The above may now be used to predict the SWCC up to the AEV for NS A and C, knowing only the percentages of each PSR within the sample. These percentages for NS A and C were specified in Tables 5.10 and 5.11. The method of predicting the AEV for the samples was discussed in Section 5.6.3. Using these and incorporating the functions in Table 5.13, a prediction may be made of the SWCC up to the AEV.

The moisture content, w, at any suction value may be calculated for any PSR using the functions presented in Table 5.13. For example, Table 5.14 shows the moisture contents calculated for each PSR at a suction of 10 kPa using the functions. Also presented are the individual percentages within NS A and C. Multiplying these percentages with the individual moisture contents and adding the results can predict the w at a suction of 10 kPa for NS A and C. Since the initial part of the SWCC is linear up to the AEV, it is only necessary to calculate the w at a suction of 1 kPa and at the AEV. The results of this method are presented in Figure 5.17. As may be seen, the predicted lines are not very accurate.

Table 5.14: Example of predicting the w for NS A and C at a suction of 10 kPa

PSR	w	NS A % (%)	NS C % (%)	w for NS A	w for NS C
A	0.24	30%	27%	0.07	0.06
B	0.28	34%	28%	0.09	0.08
C	0.31	21%	21%	0.07	0.07
D	0.39	10%	15%	0.04	0.06
E	0.44	5%	9%	0.02	0.04
		100%	100%	0.29	0.30

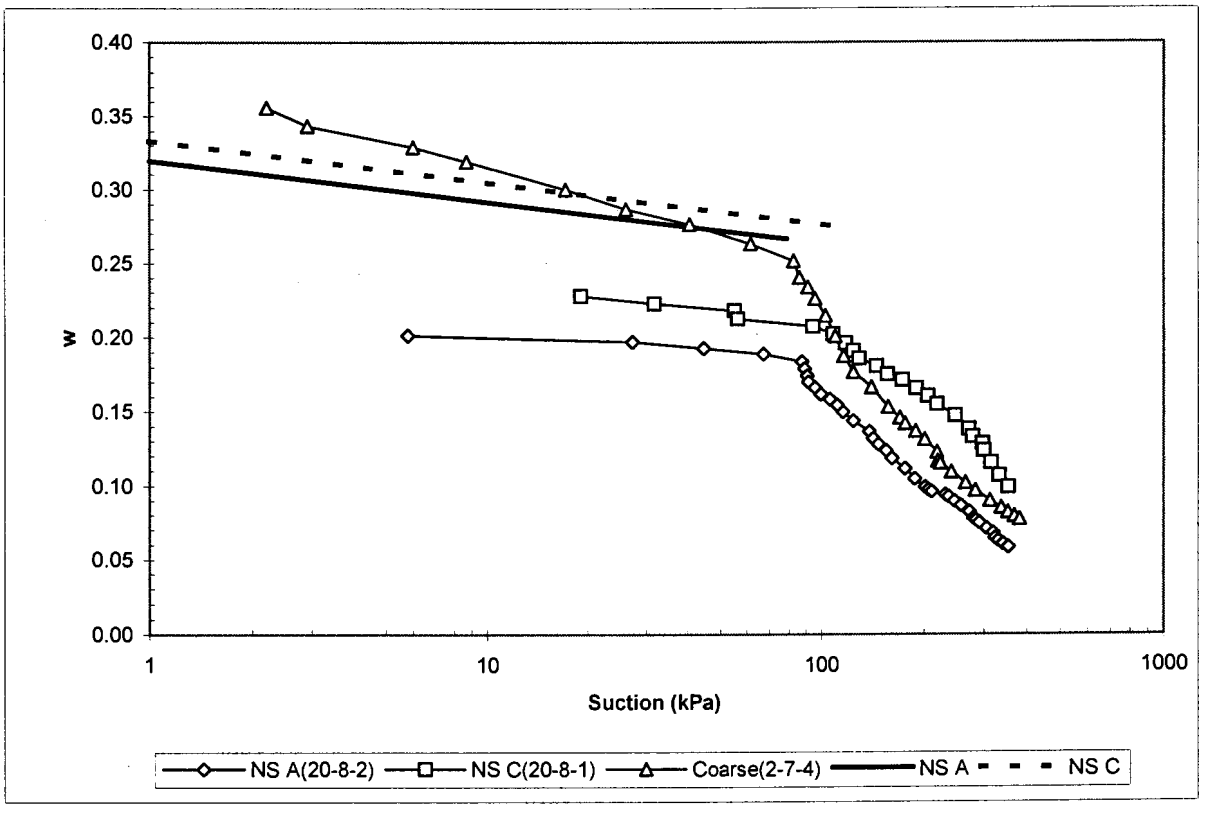

Figure 5.17: Results of the SWCC prediction method up to the AEV

5.8 Void Ratio versus Suction

5.8.1 Pay Dam coarse and fine

Effective stress is equal to the total stress, σ, minus the pore water pressure, u_w. The samples inside the trough have no stress acting on it except the stress caused by the build-up of suctions. Thus the effective stress for a sample is equal to the suction acting on it. The results obtained from the experimental programme may be represented in the compression plane (void ratio, e, or specific volume, υ, versus suction on a semi-logarithmic scale). The sample will undergo isotropic compression up to the AEV while it is still saturated and normally consolidated. This is evident from the straight line fitted to the data up to the AEV in Figure 5.18. Thus the data may be used to calculate the slope of the normally consolidated line ($-\lambda$), together with the value of υ ($\upsilon = e + 1$) when the effective stress (suction) is equal to 1 kPa (N). Table 5.15 lists the values of λ and N determined for the representative Pay Dam coarse and fine samples.

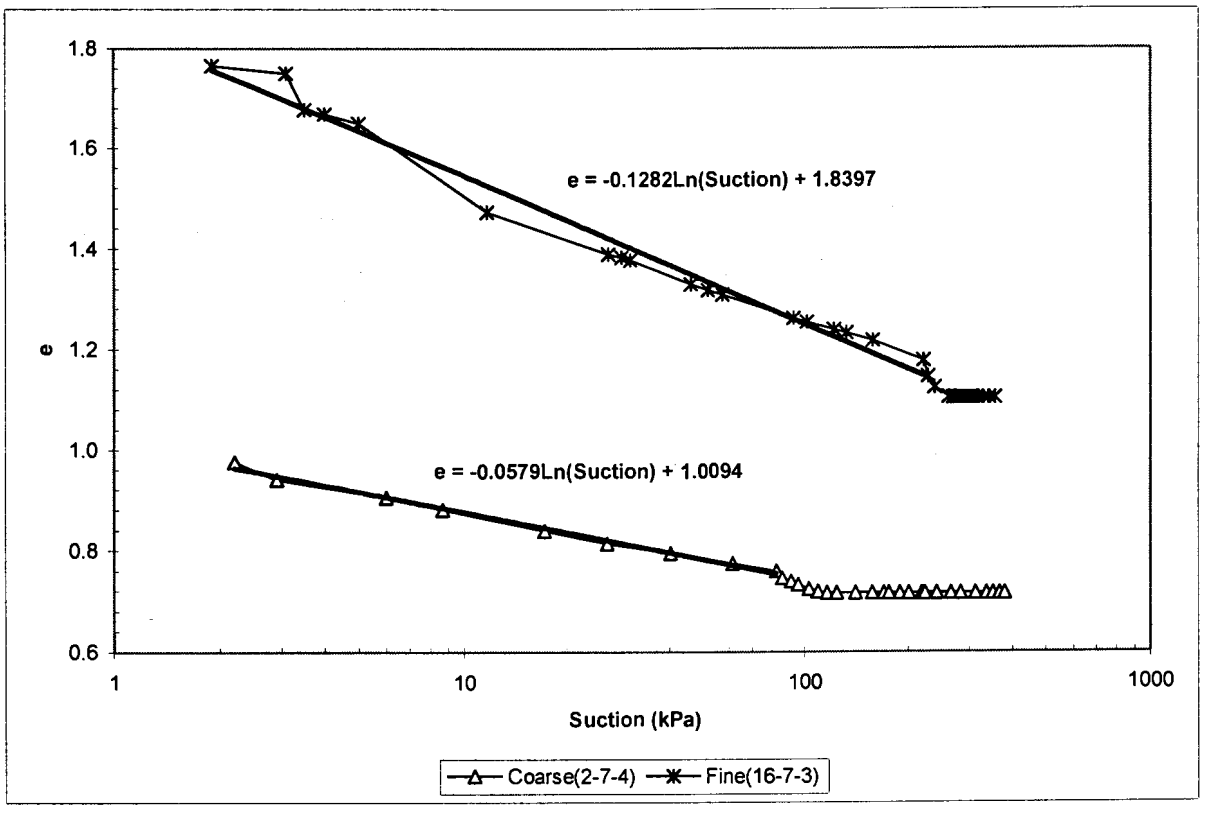

Figure 5.18: Compression plane for Pay Dam coarse and fine

Table 5.15: Compression plane parameters for Pay Dam coarse and fine

Sample	λ	N
	-	-
Coarse(2-7-4)	0.0579	2.0094
Fine(16-7-3)	0.1282	2.8397

5.8.2 Particle size ranges A through E

The results from the experimental programme for the Mizpah PSRs A through E are presented in the compression plane in Figure 5.19. Again the straight lines up to the AEV are evident, and the compression plane parameters λ and N are listed in Table 5.16.

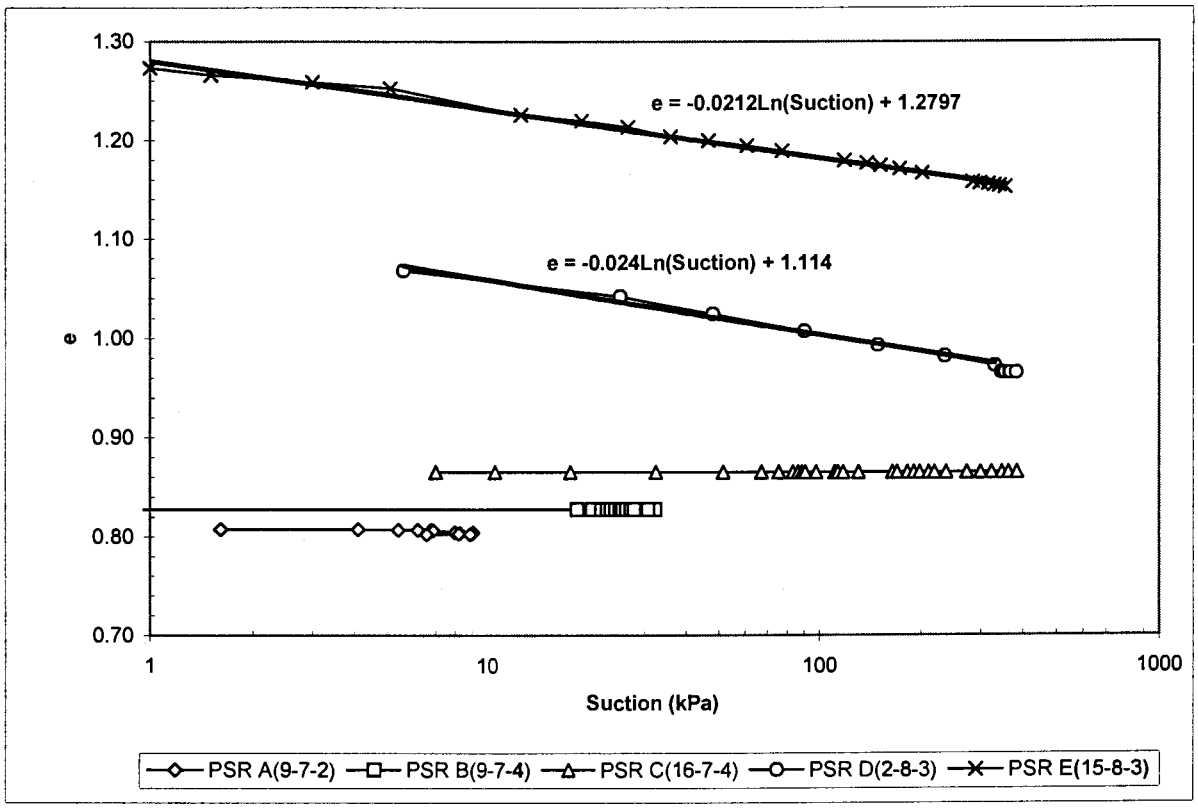

Figure 5.19: Compression plane for Mizpah PSRs

Table 5.16: Compression plane parameters for Mizpah PSRs

Sample -	λ -	N -
PSR A (9-7-2)	0	1.81
PSR B (9-7-4)	0	1.83
PSR C (16-7-4)	0	1.87
PSR D (2-8-3)	0.024	2.114
PSR E (15-8-3)	0.0212	2.2797

5.8.3 New samples A and C

The results from the experimental programme for NS A and C are presented in the compression plane in Figure 5.20. Again the straight lines up to the AEV are evident, and the compression plane parameters λ and N are listed in Table 5.17. NS C, which was created to resemble the grading for Pay Dam coarse, does not compare well regarding the parameter values.

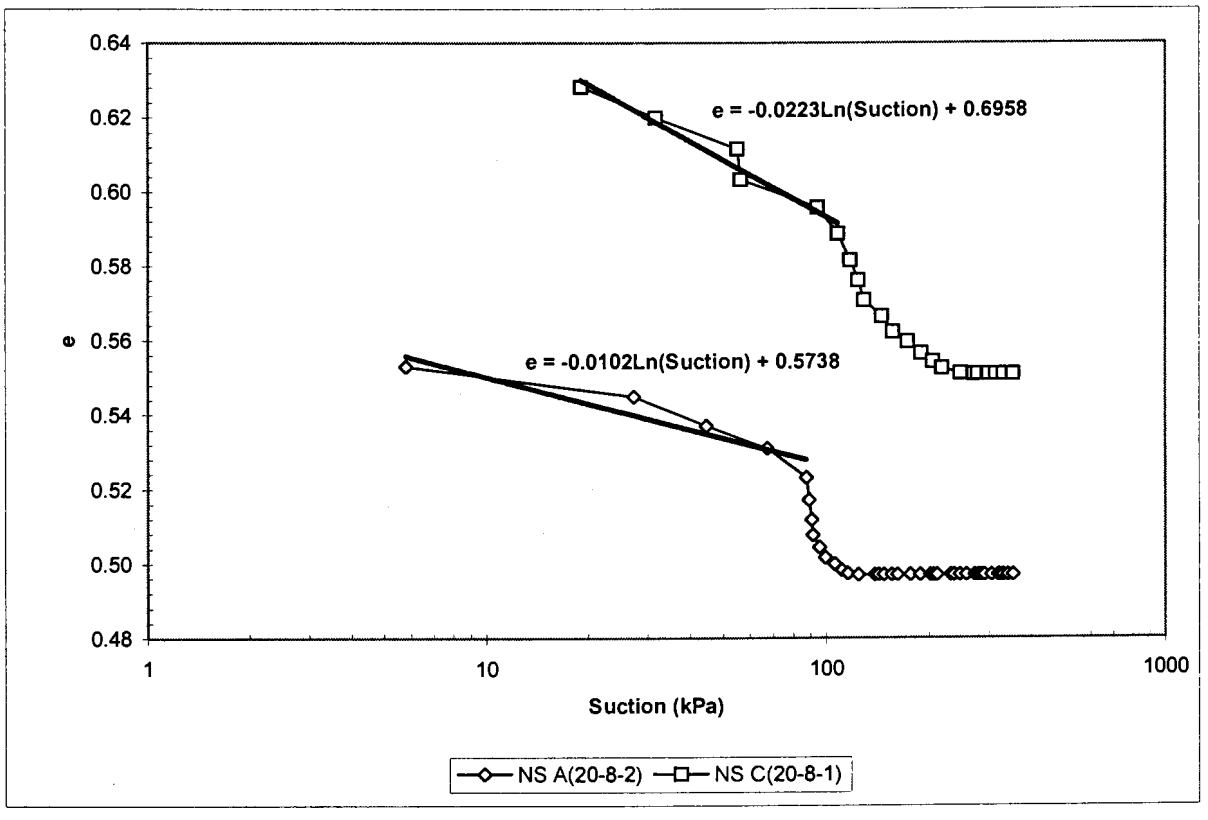

Figure 5.20: Compression plane for NS A and C

Table 5.17: Compression plane parameters for NS A and C

Sample	λ	N
NS A (20-8-2)	0.0102	1.5738
NS C (20-8-1)	0.0223	1.6958

5.9 The Mid-Plane Suction Probe

The preceding sections proved that the mid-plane suction probe is an invaluable tool in unsaturated soil mechanics. Combined with an adequate test method, like the one proposed, the parameters that may be obtained are numerous. The probe has unlimited potential, not only in the laboratory, but also in the field. Further testing regarding the field use of the probe is therefore recommended.

CHAPTER 6:

CONCLUSIONS

6.1 Summary of Conclusions from Experimental Programme

- Graphs of suction versus time and the soil-water characteristic curves showed the occurrence of clear kinks in semi-logarithmic plots. It was fond that these kinks correspond to the air-entry value of the sample. As can be expected, the finer and denser the material, the higher the air-entry value.

- It was found that the moisture content at the air-entry value corresponds to the shrinkage limit. The shrinkage limit was calculated using a graphical technique. Thus it is concluded that when the material reaches its air-entry value, the material will remain at a constant volume.

- Various methods of obtaining the air-entry value were compared with the results from the experimental programme. It was found that conventional methods tend to be inaccurate. The position of the kink in the graphs of suction versus time and the soil-water characteristic curves is an accurate method of determining the air-entry value. The use of the suction versus time graphs is a quick an easy way of determining the air-entry value due to the fact that only measurements of time and suction are necessary.

- During the proposed tests on particle size ranges from Mizpah tailings dam, it was found that linear shrinkage only took place in fine silt and clay tailings. Thus it may be concluded that cracking shall only develop on the tailings dam is sufficient percentages of fine silt and clay are present within the in-situ tailings.

- Results from the proposed tests on the Pay Dam coarse and fine tailings showed that the first signs of linear shrinkage in both samples started to develop when the suctions reached about 10 kPa. Test work on the Mizpah particle size ranges and new samples showed the same phenomena, except that linear shrinkage started when suctions reached about 50 kPa.

- Various methods of predicting the air-entry value were compared with the results from the experimental programme. The inaccuracies encountered with these methods lead to the development of a new method. The new method of predicting the air-entry value incorporates the results from the Mizpah particle size ranges. It was found that the new method has an accuracy of about 10 % when predictions were made, even though the method only incorporates material grading.

- There exist various models of predicting the soil-water characteristic curve. It was shown that these models tend to differ from the experimental results in the initial part of the curve up to the air-entry value. Furthermore, these models incorporate fitting parameters that can only be obtained through experimental work, or through comparison with parameters used for similar material. A new method of predicting the soil-water characteristic curve up to the air-entry value was developed, knowing only the grading of the material. Although the results were inaccurate, the method shows promise and should in future incorporate material density.

- The results from the experimental programme showed that the data may be used to determine the critical state parameters λ and N. The data plotted in the compression plane showed that the material behaves normally consolidated up to the air-entry value.

- The results from the experimental programme showed that the tailings act saturated up to the air-entry value.

- The vast amount of parameters and information gained through the use of the proposed test method clearly indicates its effectiveness in studying the performance and characteristics of a material drying from saturation. The results also indicated the effectiveness of the mid-plane suction probe for the direct measurement of suction.

6.2 Conclusions in Reference to Research Objectives

- The mid-plane suction probe was found to be an invaluable instrument for the measurement of suctions directly. The response time of the probe is dependent on the grading of the material and the quality of the hydraulic bond between the probe and the material. Generally the probe has an accurate response time of between 1 and 5 minutes.

- A test method was developed in which the gold tailings samples are initially slurried and poured into a shrinkage trough. Continuous measurements of time, mass, volume and suction are made while the samples are allowed to air-dry. The results are then transformed into other soil mechanics parameters and compared with suction.

- Tests on Pay Dam coarse and fine tailings clearly indicated that a finer material would have a higher air-entry value.

- Tests on Mizpah particle size ranges clearly showed that suctions are primarily controlled by medium silt and smaller particle size ranges.

CHAPTER 7:

REFERENCES

Aitchison, G.D. Butler, P.F. and Gurr, C.G. 1950. Techniques Associated with the Use of Gypsum Block Soil Moisture Meters. *Australian Journal of Applied Science.* Noble N.S. (Ed.), pp 56-71.

Aubertin, A. Ricard, J. and Chapuis, R.P. 1998. A Predictive Model for the Water Retention Curve: Application to Tailings from Hard-Rock Mines. *Canadian Geotechnical Journal,* Vol.35, pp 55-69.

Barbour, S.L. 1998. Nineteenth Canadian Geotechnical Colloquium: The Soil-Water Characteristic Curve: A Historical Perspective. *Canadian Geotechnical Journal,* Vol.35, pp 873-894.

Bear, J. 1972. *Dynamics of Fluids in Porous Media.* Dover Publications, New York.

Benson, C.H. and Daniel, D.E. 1990. Influence of Clods on Hydraulic Conductivity of Compacted Clay. *Journal of Geotechnical Engineering,* ASCE, Vol.116, pp 1231-1248.

Blight, G.E. 1997. Destructive Mudflows as a Consequence of Tailings Dyke Failures. *Proceedings of the Institution of Civil Engineers: Geotechnical Engineering,* Vol.125, pp 9-18.

Blight, G.E. 1980. *The Mechanics of Unsaturated Soils.* Notes for a series of lectures delivered as part of Course 270C at the University of California, Berkeley.

Brooks, R.H. and Corey, A.T. 1964. Hydraulic Properties of Porous Media. *Colorado State University Hydrology Paper,* Vol.27, No.3, March.

BS1377. 1990. Methods of Testing Soils for Civil Engineering Purposes. *British Standards Institution,* London.

Chandler, R.J. and Gutierrez, C.I. 1986. The Filter Paper Method of Suction Measurement. *Geotechnique,* Vol.36, pp 265-268.

Chou, P.C. and Pagano, N.J. 1967. *Elasticity,* Toronto: Van Nostrand, 290 pp.

Craig, R.F. 1997. *Soil Mechanics.* E & FN Spon. 6th Edition. Chapman and Hall, London.

Edlefsen, N.E. and Anderson, A.B.C. 1943. Thermodynamics of Soil Moisture. *Hilgardia,* Vol.15, pp 31-298.

Fredlund, D.G. 1964. *Comparison of Soil Suction and One-Dimensional Consolidation Characteristics of a Highly Plastic Clay.* National Resources Council Technical Report, No.245.v, Division of Building Resources, Ottawa, Ontario, Canada, 26 pp.

Fredlund, D.G. 1979. Second Canadian Geotechnical Colloquium: Appropriate Concepts and Technology for Unsaturated Soils. *Canadian Geotechnical Journal,* Vol.16, No.1, pp 121-139.

Fredlund, D.G. and Morgenstern, N.R. 1977. Stress State Variables for Unsaturated Soils. *ASCE Journal Geotechnical Engineering Division GT5,* Vol.103, pp 447-466.

Fredlund, D.G. and Rahardjo, H. 1987. *Soil Mechanics Principles for Highway Engineering in Arid Regions.* Transportations Res. Record 1137, pp 1-11.

Fredlund, D.G. and Rahardjo, H. 1993. *Soil Mechanics for Unsaturated Soils,* 1st Ed., John Wiley and Sons, Inc.

Fredlund, D.G. Vanapalli, S.K. Xing, A. and Pufahl, D.E. 1995. Predicting the Shear Strength Function for Unsaturated Soils using the Soil-Water Characteristic Curve. *Proceedings of the 1st International Conference on Unsaturated Soils,* Vol. 2, Paris, Alonso, A.A. and Delarge, P. (Ed.), pp 63-69.

Fredlund, D.G. and Xing, A. 1994. Equations for the Soil-Water Characteristic Curve. *Canadian Geotechnical Journal,* Vol.31, No.4, pp 521-532.

Fung, Y.C. 1977. *A First Course in Continuum Mechanics,* 2nd Ed., Englewood Cliffs, NJ: Prentice-Hall, 340 pp.

Head, K.H. 1984. Soil Classification and Compaction Tests. *Manual of Soil Laboratory Testing.* Vol.1. Pentech Press, London.

Ho, D.Y.F. 1979. *Measurement of Soil Suction Using the Filter Paper Technique*. Internal Report, IR-11, Transportation and Geotechnical Group, Department of Civil Engineering, University of Saskatchewan, Saskatoon, Sask., Canada, 90 pp.

Holtz, R.D. and Kovacs, W.D. 1981. *An Introduction to Geotechnical Engineering.* Prentice Hall, New York.

Huang, S.Y. 1994. *Evaluation and Laboratory Measurement of the Coefficient of Permeability in Deformable, Unsaturated Soils*. Ph.D. Dissertation, Department of Civil Engineering, University of Saskatchewan, Saskatoon.

Koorevaar, P. Menelik, G. and Dirksen, C. 1983. *Elements of Soil Physics,* Amsterdam, The Netherlands: Elsevier, 228 pp.

Kovacs, G. 1981. *Seepage Hydraulics*. Elsevier Science Publishers, Amsterdam.

Lapierre, C. Leroueil, S. and Locat, J. 1989. Mercury Intrusion and Permeability of Louisville Clay. *Proceedings of the 42nd Geotechnical Conference*, Winnipeg, October. Canadian Geotechnical Society, pp 103-119.

Luyt, A.J. 2001. *Measurement of Suction Pressures in Mine Tailings*. BEng Project Report. University of Pretoria.

Matyas, E.L. and Radhakrishna, H.S. 1968. Volume Change Characteristics of Partially Saturated Soils. *Geotechnique*, Vol.18, No.4, pp 432-448.

McKeen, R.G. 1981. *Suction Studies: Filter Paper Method.* Design of Airport Pavements for Expansive Soils: Final Report (No.DOT/FAA/RD-81/25), U.S. Department of Transportation, FAA, Systems Research and Development Service, Washington, DC.

McPhail, G.I. and Wagener, J.C. 1989. Disposal of Residues. *The Extractive Metallurgy of Gold in South Africa.* The Chamber of Mines in South Africa, pp 655-707.

Rawlins, S.L. and Dalton, F.N. 1967. Psychrometric Measurement of Soil Water Potential without Precise Temperature Control. *Proceedings of the Soil Science Society of America,* Vol.31, pp 297-301.

Richards, B.G. 1965. Measurement of the Free Energy of Soil Moisture by the Psychrometric Technique Using Thermistors. *Moisture Equilibria and Moisture Changes in Soils Beneath Covered Areas, A Symposium in Print,* Australia: Butterworths, pp 39-46.

Ridley, A.M. 1993. *The Measurement of Soil Moisture Suction.* PhD Thesis. University of London.

Ridley, A.M. and Burland, J.B. 1993. A New Instrument for the Measurement of Soil Moisture Suction. *Geotechnique,* Vol.43, No.2, pp 321-324.

Ridley, A.M. Patel, A.R. and Marsland, F. 1998. Tensiometers: Their Use for Civil Engineering Purposes. *Proceedings of the 1st International Conference on Site Characterisation,* Atlanta, Robertson P.K. and Mayne P.W. (Ed.), A.A. Balkema, pp 851-856.

Sattler, P. and Fredlund, D.G. 1989. Use of Thermal Conductivity Sensors to Measure Matric Suction in the Laboratory. *Canadian Geotechnical Journal,* Vol.26, pp 491-498.

Schofield, R. 1935. The pF of the Water in Soil. *Trans. 3rd International Congress on Soil Science,* Vol.2, pp 37-48.

Stokes, Sir G.G. 1891. *Mathematical and Physical Paper III.* Cambridge University Press, Cambridge.

Taylor, D.W. 1948. *Fundamentals of Soil Mechanics,* New York: Wiley, 700 pp.

Terzaghi, K. 1936. The Shear Resistance of Saturated Soils. *Procedures of 1st International Conference on Soil Mechanics and Foundation Engineering,* Cambridge, MA, Vol.1, pp 54-56.

Theron, M. 2000. *Soil Suction in Mine Tailings.* MSc Dissertation. University of Pretoria.

Van Genuchten, M. Th. 1980. A Closed-Form Equation for Predicting the Hydraulic Conductivity of Unsaturated Soils. *Soil Science Society of America Journal,* Vol.44, pp 892-898.

Vanapalli, S.K. 1994. *Simple Test Procedures and their Interpretation in Evaluating the Shear Strength of an Unsaturated Soil.* Ph.D. Thesis. University of Saskatchewan.

Vermeulen, N.J. 2001. *The Composition and State of Gold Tailings.* Ph.D. Thesis. University of Pretoria.

Vick, S.G. 1983. *Planning, Design and Analysis of Tailings Dams.* Wiley Series in Geotechnical Engineering, New York.

Wagener, F. 1997. *The Merriespruit Slimes Dam Failure: Overview and Lessons Learnt.* SAICE Journal, Vol.39, No.3, pp 11-15.

APPENDIX A:

CORRECTED VALUES FOR S, e AND θ

A.1 Pay Dam Coarse

Table A.1 to A.3 represents the data obtained from tests carried out on Pay Dam coarse tailings.

Figure A.1 represents void ratio, e, versus water content, w. (C = corrected)

Table A.1: Corrected Test Data for Pay Dam Coarse Tailings (Sample 2-7-1)

Time (h:mm:ss)	Suction (kPa)	w -	S -	e -	θ -	LS (%)
4:31:00	5.9	0.32	1.00	0.87	0.46	0.00%
4:40:00	5.9	0.31	1.00	0.86	0.46	0.00%
5:05:00	10.5	0.30	0.99	0.83	0.45	0.00%
5:14:00	10.5	0.30	0.99	0.83	0.45	0.00%
5:39:00	16.3	0.29	0.98	0.80	0.44	0.16%
6:01:00	22.7	0.28	0.98	0.79	0.43	0.50%
6:27:00	30.2	0.27	0.96	0.77	0.42	0.86%
7:32:00	77.8	0.25	0.92	0.73	0.39	1.59%
7:48:00	95.5	0.24	0.90	0.72	0.38	1.74%
8:07:00	96.7	0.23	0.89	0.72	0.37	1.90%
8:30:00	110.7	0.22	0.86	0.71	0.36	2.06%
8:57:00	117.7	0.21	0.83	0.70	0.34	2.21%
9:30:00	120.4	0.20	0.79	0.70	0.32	2.34%
9:45:00	123.4	0.19	0.77	0.69	0.31	2.39%
10:05:00	126.4	0.19	0.74	0.69	0.30	2.42%
10:44:00	137.0	0.17	0.68	0.69	0.28	2.44%
11:18:00	153.3	0.16	0.63	0.69	0.26	2.44%
11:49:00	165.4	0.15	0.59	0.69	0.24	2.44%
12:16:00	185.4	0.14	0.55	0.69	0.23	2.44%
12:47:00	199.4	0.13	0.51	0.69	0.21	2.44%
13:21:00	234.2	0.12	0.46	0.69	0.19	2.44%
13:51:00	246.0	0.11	0.42	0.69	0.17	2.44%
14:24:00	287.6	0.10	0.38	0.69	0.15	2.44%
14:59:00	316.6	0.08	0.33	0.69	0.13	2.44%
15:33:00	383.3	0.07	0.28	0.69	0.12	2.44%

Table A.2: Corrected Test Data for Pay Dam Coarse Tailings (Sample 2-7-2)

Time (h:mm:ss)	Suction (kPa)	w -	S -	e -	θ -	LS (%)
8:48:00	0.6	0.35	1.00	0.95	0.49	0.00%
9:18:00	1.2	0.34	1.00	0.92	0.48	0.00%
9:54:00	2.8	0.32	1.00	0.89	0.47	0.00%
10:39:00	6.0	0.31	1.00	0.85	0.46	0.00%
11:16:00	9.9	0.30	0.99	0.82	0.45	0.01%
11:48:00	15.6	0.29	0.98	0.80	0.44	0.23%
12:19:00	25.2	0.28	0.97	0.78	0.43	0.42%
12:32:00	32.4	0.27	0.97	0.77	0.42	0.49%
12:48:00	42.0	0.27	0.96	0.76	0.42	0.58%
13:03:00	50.4	0.26	0.95	0.75	0.41	0.66%
13:25:00	61.0	0.26	0.94	0.74	0.40	0.77%
13:48:00	78.2	0.25	0.93	0.73	0.39	0.87%
14:02:00	87.0	0.24	0.92	0.73	0.39	0.93%
14:20:00	91.3	0.24	0.91	0.72	0.38	1.00%
14:39:00	96.5	0.23	0.90	0.71	0.37	1.06%
15:10:00	104.2	0.22	0.87	0.70	0.36	1.15%
15:50:00	114.4	0.21	0.84	0.69	0.34	1.24%
16:40:00	119.9	0.20	0.79	0.68	0.32	1.31%
17:10:00	125.6	0.19	0.75	0.68	0.31	1.33%
17:48:00	130.4	0.18	0.71	0.68	0.29	1.33%
18:22:00	141.8	0.17	0.67	0.68	0.27	1.33%
18:55:00	150.4	0.16	0.64	0.68	0.26	1.33%
19:14:00	160.9	0.15	0.61	0.68	0.25	1.33%
19:34:00	168.4	0.15	0.59	0.68	0.24	1.33%
20:07:00	184.4	0.14	0.56	0.68	0.23	1.33%
20:42:00	203.0	0.13	0.52	0.68	0.21	1.33%
21:16:00	227.7	0.12	0.48	0.68	0.20	1.33%
21:38:00	246.3	0.11	0.46	0.68	0.19	1.33%
22:07:00	255.8	0.11	0.43	0.68	0.17	1.33%
22:43:00	297.2	0.10	0.39	0.68	0.16	1.33%
23:12:00	328.3	0.09	0.36	0.68	0.15	1.33%
23:27:00	342.0	0.09	0.35	0.68	0.14	1.33%
23:52:00	375.3	0.08	0.33	0.68	0.13	1.33%

Table A.3: Corrected Test Data for Pay Dam Coarse Tailings (Sample 2-7-4)

Time (h:mm:ss)	Suction (kPa)	w -	S -	e -	θ -	LS (%)
10:10:00	2.2	0.36	1.00	0.98	0.49	0.00%
10:44:00	2.9	0.34	1.00	0.94	0.48	0.00%
11:23:00	6.0	0.33	1.00	0.90	0.47	0.00%
11:50:00	8.7	0.32	0.99	0.88	0.47	0.00%
12:43:00	17.2	0.30	0.98	0.84	0.45	0.26%
13:21:00	26.2	0.29	0.97	0.81	0.43	0.52%
13:51:00	40.4	0.28	0.95	0.80	0.42	0.70%
14:29:00	61.6	0.26	0.93	0.78	0.41	0.89%
15:03:00	82.5	0.25	0.91	0.76	0.39	1.02%
15:36:00	86.0	0.24	0.88	0.75	0.38	1.12%
15:56:00	91.1	0.23	0.87	0.74	0.37	1.17%
16:19:00	95.6	0.23	0.85	0.73	0.36	1.21%
16:55:00	102.7	0.21	0.81	0.72	0.34	1.24%
17:37:00	109.5	0.20	0.77	0.72	0.32	1.24%
18:19:00	116.0	0.19	0.72	0.72	0.30	1.24%
18:53:00	123.8	0.18	0.68	0.72	0.28	1.24%
19:27:00	140.4	0.17	0.64	0.72	0.27	1.24%
20:10:00	157.2	0.15	0.59	0.72	0.24	1.24%
20:35:00	170.1	0.15	0.56	0.72	0.23	1.24%
20:47:00	175.9	0.14	0.54	0.72	0.23	1.24%
21:05:00	189.4	0.14	0.52	0.72	0.22	1.24%
21:24:00	200.9	0.13	0.50	0.72	0.21	1.24%
21:53:00	219.0	0.12	0.47	0.72	0.20	1.24%
22:14:00	220.1	0.12	0.45	0.72	0.19	1.24%
22:19:00	223.8	0.12	0.44	0.72	0.18	1.24%
22:40:00	241.5	0.11	0.42	0.72	0.17	1.24%
23:06:00	265.7	0.10	0.39	0.72	0.16	1.24%
23:24:00	283.8	0.10	0.37	0.72	0.15	1.24%
23:49:00	313.2	0.09	0.34	0.72	0.14	1.24%
24:07:00	337.0	0.08	0.32	0.72	0.14	1.24%
24:17:00	351.5	0.08	0.31	0.72	0.13	1.24%
24:27:00	368.3	0.08	0.30	0.72	0.13	1.24%
24:35:00	380.9	0.08	0.30	0.72	0.12	1.24%

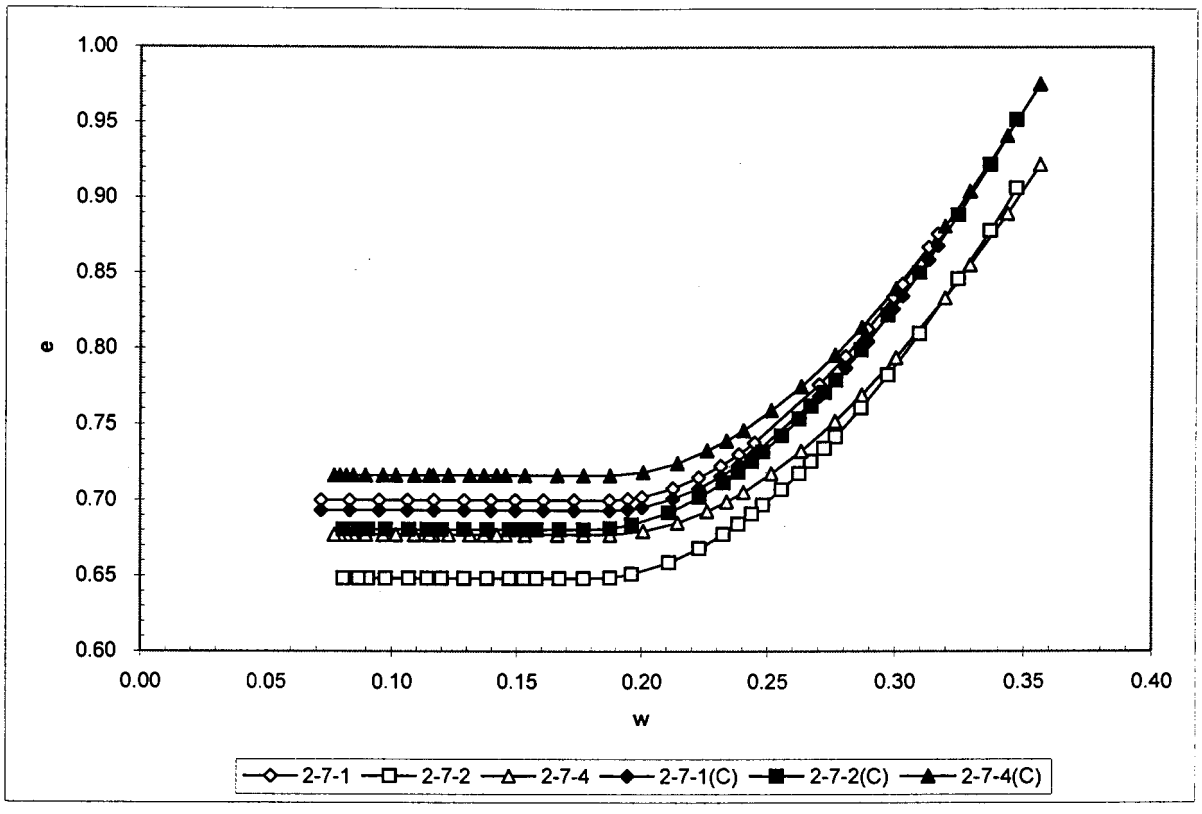

Figure A.1: Void ratio, e, versus moisture content, w (shrinkage curve)

A.2 Pay Dam Fine

Table A.4 to A.8 represents the data obtained from tests carried out on Pay Dam fine tailings.

Figure A.2 represents void ratio, e, versus water content, w.

Table A.4: Corrected Test Data for Pay Dam Fine Tailings (Sample 24-6-1)

Time (h:mm:ss)	Suction (kPa)	w -	S -	e -	θ -	LS (%)
15:59:00	9.3	0.54	1.00	1.47	0.60	0.40%
16:54:00	21.4	0.51	1.00	1.41	0.58	1.25%
17:15:00	31.1	0.50	1.00	1.38	0.58	1.54%
17:36:00	34.7	0.49	0.99	1.36	0.57	1.82%
18:10:00	47.5	0.48	0.98	1.33	0.56	2.23%
18:53:00	69.2	0.46	0.97	1.29	0.55	2.68%
19:19:00	82.1	0.44	0.96	1.26	0.54	2.92%
20:54:00	163.5	0.40	0.91	1.19	0.50	3.59%
21:20:00	193.0	0.38	0.89	1.17	0.48	3.71%
21:58:00	199.8	0.36	0.87	1.15	0.46	3.84%
22:28:00	207.5	0.35	0.84	1.14	0.45	3.91%
23:16:00	220.0	0.32	0.80	1.11	0.42	3.94%
23:40:00	230.0	0.31	0.77	1.11	0.40	3.94%
24:23:00	249.3	0.29	0.72	1.09	0.38	3.94%
24:56:00	258.2	0.27	0.68	1.09	0.36	3.94%
25:16:00	262.8	0.26	0.66	1.08	0.34	3.94%
26:01:00	290.0	0.24	0.60	1.08	0.31	3.94%
26:26:00	291.9	0.22	0.57	1.08	0.29	3.94%
27:18:00	317.0	0.19	0.50	1.08	0.26	3.94%
28:10:00	369.8	0.17	0.42	1.08	0.22	3.94%

Table A.5: Corrected Test Data for Pay Dam Fine Tailings (Sample 24-6-2)

Time (h:mm:ss)	Suction (kPa)	w -	S -	e -	θ -	LS (%)
15:57:00	3.4	0.59	1.00	1.62	0.62	0.00%
16:54:00	5.6	0.57	1.00	1.55	0.61	0.00%
17:33:00	11.0	0.55	1.00	1.51	0.60	0.00%
18:10:00	14.3	0.54	1.00	1.47	0.59	0.48%
18:50:00	21.1	0.52	1.00	1.42	0.59	1.04%
19:15:00	23.8	0.51	0.99	1.40	0.58	1.36%
20:54:00	56.9	0.47	0.98	1.31	0.55	2.45%
21:22:00	67.5	0.45	0.97	1.29	0.55	2.70%
21:55:00	91.2	0.44	0.96	1.26	0.53	2.96%
22:22:00	124.9	0.43	0.95	1.24	0.52	3.15%
22:53:00	148.5	0.42	0.94	1.22	0.51	3.35%
23:49:00	187.8	0.39	0.91	1.18	0.49	3.62%
24:33:00	206.8	0.37	0.88	1.16	0.47	3.76%
25:10:00	214.5	0.36	0.86	1.14	0.46	3.84%
26:21:00	223.8	0.33	0.80	1.11	0.42	3.87%
27:45:00	254.3	0.29	0.73	1.09	0.38	3.87%
28:27:00	262.2	0.27	0.69	1.08	0.36	3.87%
29:47:00	302.2	0.23	0.60	1.07	0.31	3.87%
30:41:00	327.7	0.21	0.54	1.07	0.28	3.87%
30:57:00	339.6	0.20	0.52	1.07	0.27	3.87%

Table A.6: Corrected Test Data for Pay Dam Fine Tailings (Sample 24-6-4)

Time (h:mm:ss)	Suction (kPa)	w -	S -	e -	θ -	LS (%)
18:48:00	4.9	0.60	1.00	1.65	0.62	0.00%
19:12:00	4.7	0.59	1.00	1.62	0.62	0.00%
20:52:00	14.6	0.54	1.00	1.49	0.60	0.41%
21:25:00	22.4	0.53	1.00	1.45	0.59	0.86%
21:53:00	27.6	0.52	0.99	1.42	0.58	1.21%
22:15:00	27.4	0.51	0.99	1.40	0.58	1.46%
22:44:00	42.1	0.49	0.98	1.37	0.57	1.78%
23:27:00	62.1	0.47	0.97	1.33	0.55	2.19%
23:58:00	78.7	0.46	0.96	1.31	0.54	2.44%
24:48:00	116.3	0.43	0.94	1.27	0.53	2.79%
25:31:00	151.9	0.42	0.92	1.24	0.51	3.02%
26:10:00	196.7	0.40	0.90	1.22	0.49	3.17%
27:10:00	204.2	0.37	0.86	1.18	0.46	3.30%
28:30:00	226.3	0.33	0.79	1.15	0.42	3.32%
29:18:00	241.3	0.31	0.75	1.14	0.40	3.32%
30:28:00	262.6	0.28	0.68	1.13	0.36	3.32%
30:55:00	267.1	0.27	0.65	1.13	0.35	3.32%
31:26:00	279.5	0.25	0.62	1.13	0.33	3.32%
32:04:00	293.5	0.24	0.58	1.13	0.31	3.32%
32:49:00	300.5	0.22	0.53	1.13	0.28	3.32%
33:09:00	305.9	0.21	0.51	1.13	0.27	3.32%

Table A.7: Corrected Test Data for Pay Dam Fine Tailings (Sample 16-7-2)

Time (h:mm:ss)	Suction (kPa)	w -	S -	e -	θ -	LS (%)
6:12:00	0.3	0.61	1.00	1.66	0.62	0.00%
6:29:00	1.3	0.60	1.00	1.64	0.62	0.00%
6:53:00	1.9	0.59	1.00	1.61	0.62	0.00%
7:18:00	3.9	0.57	1.00	1.57	0.61	0.00%
7:41:00	4.3	0.56	1.00	1.54	0.61	0.00%
8:33:00	7.0	0.54	1.00	1.47	0.60	0.00%
9:28:00	15.0	0.51	1.00	1.40	0.58	0.00%
9:34:00	16.7	0.51	1.00	1.39	0.58	0.00%
9:44:00	18.9	0.50	1.00	1.38	0.58	0.00%
9:53:00	21.1	0.50	1.00	1.37	0.58	0.00%
10:42:00	32.4	0.47	1.00	1.30	0.57	0.46%
13:13:00	140.9	0.40	0.96	1.15	0.51	2.24%
13:54:00	190.3	0.38	0.93	1.13	0.50	2.56%
13:59:00	195.9	0.38	0.93	1.12	0.49	2.60%
14:05:00	202.6	0.38	0.93	1.12	0.49	2.64%
14:17:00	212.8	0.37	0.92	1.12	0.48	2.71%
14:44:00	228.5	0.36	0.90	1.10	0.47	2.87%
14:51:00	232.8	0.36	0.89	1.10	0.47	2.90%
15:05:00	239.4	0.35	0.88	1.10	0.46	2.97%
16:13:00	249.0	0.32	0.81	1.09	0.42	3.17%
17:28:00	270.7	0.29	0.73	1.09	0.38	3.20%
18:13:00	282.7	0.27	0.68	1.09	0.35	3.20%
19:13:00	307.3	0.24	0.61	1.09	0.32	3.20%
20:05:00	329.0	0.22	0.55	1.09	0.29	3.20%

Table A.8: Corrected Test Data for Pay Dam Fine Tailings (Sample 16-7-3)

Time (h:mm:ss)	Suction (kPa)	w -	S -	e -	θ -	LS (%)
9:55:00	1.9	0.64	1.00	1.77	0.64	0.00%
10:05:00	3.1	0.64	1.00	1.75	0.64	0.00%
10:55:00	3.5	0.61	1.00	1.68	0.63	0.00%
11:01:00	4.0	0.61	1.00	1.67	0.63	0.00%
11:14:00	5.0	0.60	1.00	1.65	0.62	0.00%
13:16:00	11.7	0.54	1.00	1.47	0.60	0.00%
14:20:00	26.4	0.50	0.99	1.39	0.58	0.03%
14:25:00	29.0	0.50	0.99	1.38	0.58	0.07%
14:29:00	30.7	0.50	0.99	1.38	0.58	0.11%
15:10:00	46.3	0.48	0.99	1.33	0.56	0.44%
15:21:00	52.0	0.47	0.98	1.32	0.56	0.53%
15:30:00	57.6	0.47	0.98	1.31	0.56	0.59%
16:17:00	92.6	0.44	0.96	1.26	0.54	0.91%
16:26:00	101.8	0.44	0.96	1.25	0.53	0.97%
16:43:00	121.7	0.43	0.95	1.24	0.53	1.07%
16:51:00	132.3	0.43	0.95	1.23	0.52	1.11%
17:09:00	158.0	0.42	0.94	1.22	0.52	1.21%
18:06:00	222.0	0.39	0.90	1.18	0.49	1.45%
19:02:00	228.2	0.36	0.86	1.15	0.46	1.63%
19:55:00	238.4	0.33	0.81	1.13	0.43	1.72%
21:25:00	262.2	0.29	0.72	1.11	0.38	1.75%
21:47:00	270.2	0.28	0.69	1.10	0.36	1.75%
22:05:00	277.4	0.27	0.67	1.10	0.35	1.75%
22:22:00	281.9	0.26	0.65	1.10	0.34	1.75%
22:34:00	287.9	0.26	0.64	1.10	0.34	1.75%
22:55:00	301.3	0.25	0.61	1.10	0.32	1.75%
23:08:00	307.7	0.24	0.60	1.10	0.31	1.75%
23:26:00	316.3	0.23	0.58	1.10	0.30	1.75%
23:53:00	331.1	0.22	0.55	1.10	0.29	1.75%
24:12:00	342.3	0.21	0.52	1.10	0.27	1.75%
24:34:00	357.3	0.20	0.50	1.10	0.26	1.75%

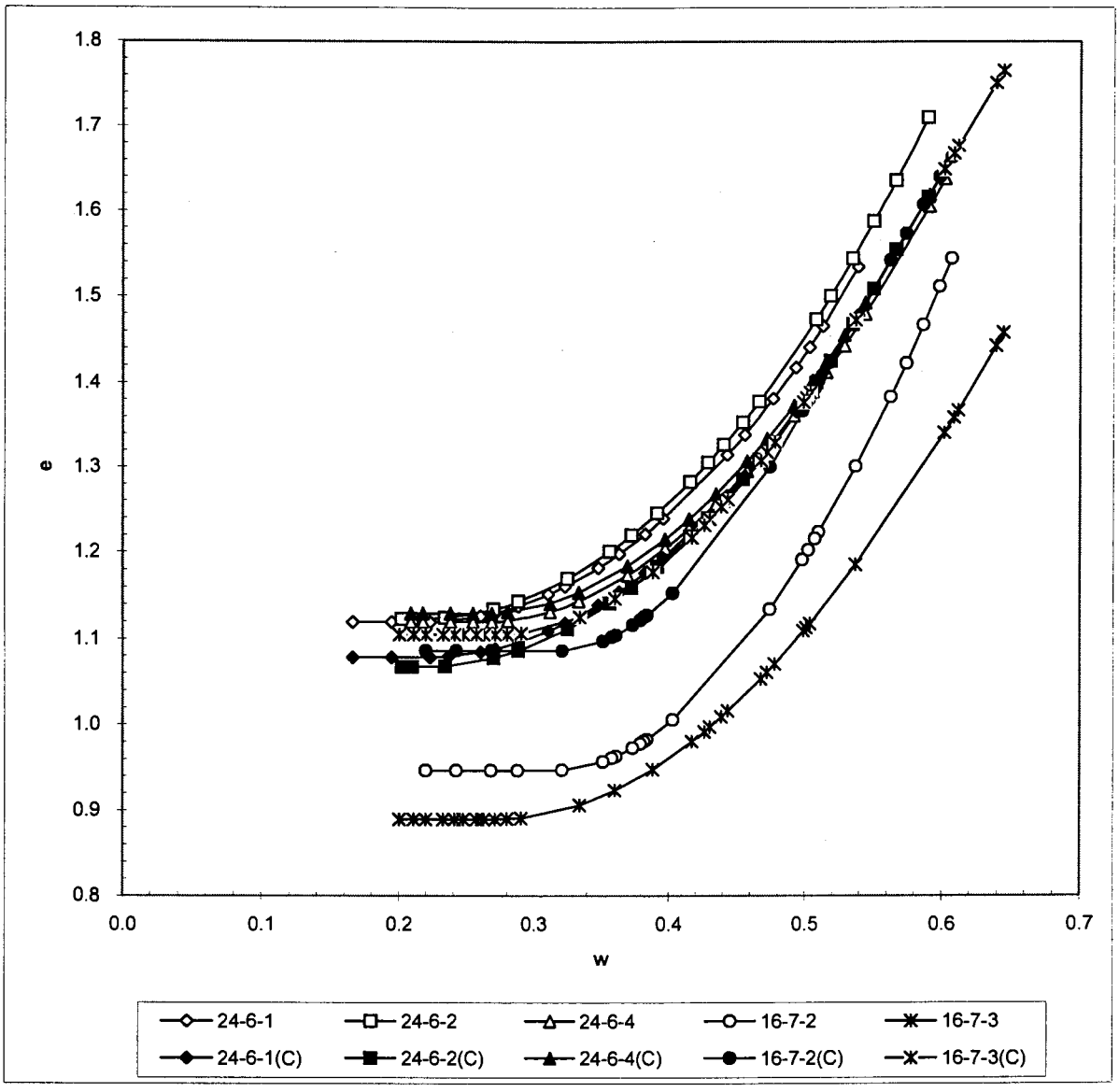

Figure A.2: Void ratio, e, versus moisture content, w (shrinkage curve)

A.3 Particle Size Range A (>63)

Table A.9 to A.10 represents the data obtained from tests carried out on Range A tailings.

Figure A.3 represents void ratio, e, versus water content, w.

Table A.9: Corrected Test Data for Particle Size Range A (Sample 9-7-2)

Time (h:mm:ss)	Suction (kPa)	w -	S -	e -	θ -
1:46:00	1.6	0.28	0.95	0.81	0.42
2:14:00	4.1	0.27	0.92	0.81	0.41
2:47:00	5.4	0.26	0.88	0.81	0.39
3:19:00	6.2	0.25	0.85	0.81	0.38
4:02:00	6.8	0.24	0.81	0.81	0.36
5:01:00	6.9	0.22	0.75	0.81	0.33
11:41:00	9.1	0.11	0.38	0.80	0.17
12:09:00	8.0	0.11	0.36	0.80	0.16
13:54:00	8.3	0.08	0.28	0.80	0.13
14:48:00	9.0	0.07	0.24	0.80	0.11
15:29:00	8.2	0.06	0.21	0.80	0.09
16:48:00	8.9	0.05	0.16	0.80	0.07
18:17:00	6.6	0.03	0.10	0.80	0.04

Table A.10: Corrected Test Data for Particle Size Range A (Sample 24-7-1)

Time (h:mm:ss)	Suction (kPa)	w -	S -	e -	θ -
0:45:00	0.4	0.24	0.97	0.69	0.39
0:49:00	1.4	0.24	0.96	0.69	0.39
0:53:00	2.4	0.24	0.95	0.69	0.39
0:57:00	3.2	0.24	0.95	0.69	0.39
1:00:00	3.7	0.24	0.94	0.69	0.38
1:05:00	4.5	0.24	0.94	0.69	0.38
1:11:00	5.4	0.23	0.93	0.69	0.38
1:15:00	6.0	0.23	0.92	0.69	0.38
1:19:00	6.8	0.23	0.92	0.69	0.37
1:25:00	7.4	0.23	0.91	0.69	0.37
1:35:00	6.9	0.22	0.89	0.69	0.36
1:40:00	7.4	0.22	0.88	0.69	0.36
1:46:00	7.7	0.22	0.87	0.69	0.36
1:51:00	8.0	0.22	0.87	0.69	0.35
1:57:00	8.1	0.22	0.86	0.69	0.35
2:03:00	8.3	0.21	0.85	0.69	0.35
2:12:00	8.8	0.21	0.84	0.69	0.34
2:24:00	9.0	0.21	0.82	0.69	0.33
2:30:00	9.1	0.20	0.81	0.69	0.33
2:47:00	8.1	0.20	0.78	0.69	0.32
2:53:00	8.8	0.19	0.77	0.69	0.32
2:59:00	9.1	0.19	0.77	0.69	0.31
3:05:00	9.5	0.19	0.76	0.69	0.31
3:13:00	9.8	0.19	0.74	0.69	0.30
3:23:00	10.2	0.18	0.73	0.69	0.30
3:34:00	10.7	0.18	0.71	0.69	0.29
3:44:00	10.8	0.18	0.70	0.69	0.28
3:54:00	11.1	0.17	0.68	0.69	0.28
4:04:00	11.3	0.17	0.67	0.69	0.27
4:19:00	11.4	0.16	0.65	0.69	0.26
4:33:00	11.6	0.16	0.63	0.69	0.26
6:01:00	9.4	0.12	0.50	0.69	0.20
6:10:00	10.6	0.12	0.48	0.69	0.20
6:22:00	11.8	0.12	0.47	0.69	0.19

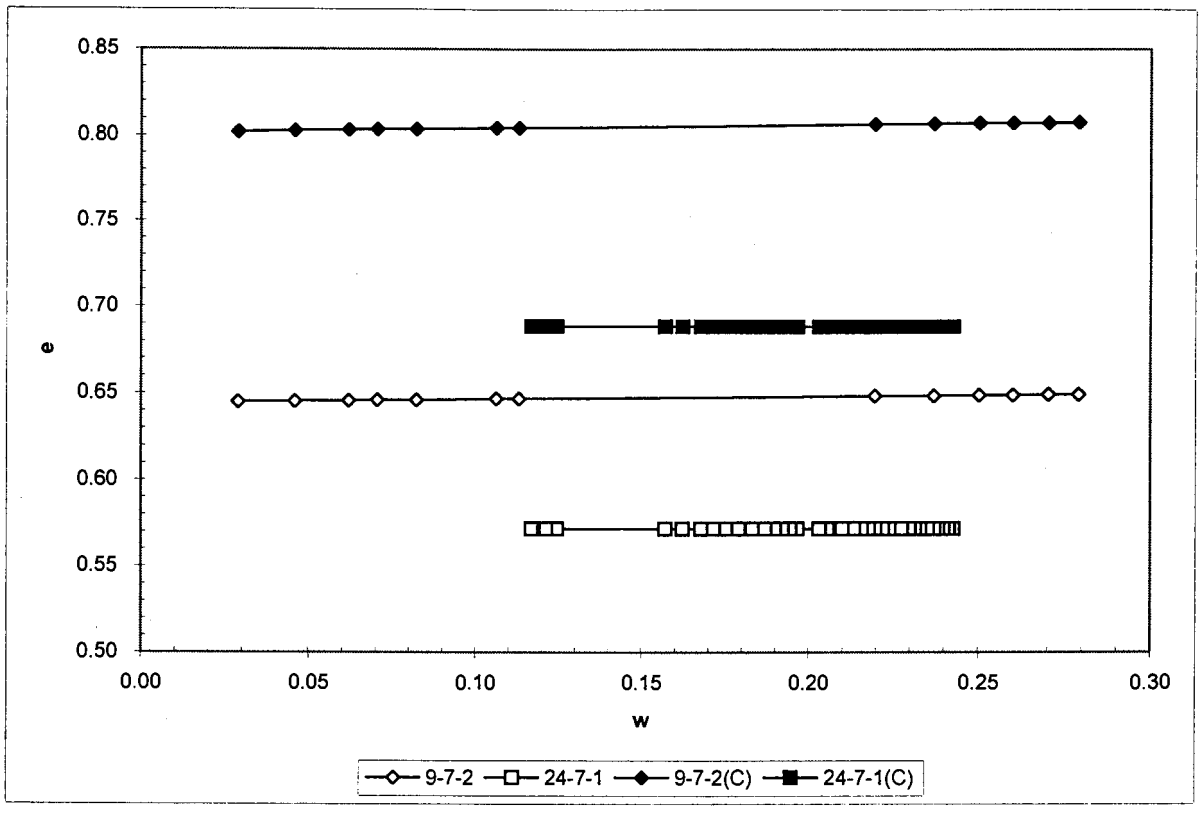

Figure A.3: Void ratio, e, versus moisture content, w (shrinkage curve)

A.4 Particle Size Range B (20<63)

Table A.11 to A.12 represents the data obtained from tests carried out on Range B tailings.

Figure A.4 represents void ratio, e, versus water content, w.

Table A.11: Corrected Test Data for Particle Size Range B (Sample 9-7-3)

Time (h:mm:ss)	Suction (kPa)	w -	S -	e -	θ -
1:33:00	13.5	0.31	0.99	0.87	0.46
1:58:00	22.2	0.31	0.97	0.87	0.45
2:31:00	22.8	0.30	0.93	0.87	0.43
3:18:00	23.6	0.28	0.88	0.87	0.41
3:58:00	23.5	0.27	0.84	0.87	0.39
4:58:00	24.8	0.25	0.79	0.87	0.37
6:18:00	25.5	0.23	0.71	0.87	0.33
7:29:00	25.7	0.20	0.64	0.87	0.30
8:29:00	28.5	0.19	0.59	0.87	0.27
9:21:00	32.5	0.17	0.54	0.87	0.25
10:04:00	27.7	0.16	0.51	0.87	0.23
10:47:00	32.2	0.15	0.47	0.87	0.22
11:21:00	29.6	0.14	0.44	0.87	0.20
11:51:00	30.6	0.13	0.42	0.87	0.19
13:42:00	31.2	0.10	0.33	0.87	0.15
14:32:00	35.2	0.09	0.29	0.87	0.13
15:22:00	27.2	0.08	0.25	0.87	0.12
17:07:00	29.8	0.05	0.17	0.87	0.08
17:56:00	25.4	0.04	0.14	0.87	0.06

Table A.12: Corrected Test Data for Particle Size Range B (Sample 9-7-4)

Time (h:mm:ss)	Suction (kPa)	w -	S -	e -	θ -
2:04:00	0.9	0.29	0.95	0.83	0.43
2:32:00	18.8	0.28	0.93	0.83	0.42
3:19:00	20.9	0.26	0.88	0.83	0.40
4:10:00	22.3	0.25	0.82	0.83	0.37
5:05:00	23.2	0.23	0.77	0.83	0.35
6:43:00	23.9	0.20	0.67	0.83	0.30
7:43:00	24.6	0.19	0.61	0.83	0.28
8:36:00	25.4	0.17	0.56	0.83	0.26
9:28:00	26.6	0.16	0.52	0.83	0.23
10:07:00	25.8	0.15	0.48	0.83	0.22
10:48:00	26.5	0.13	0.44	0.83	0.20
11:20:00	27.4	0.13	0.41	0.83	0.19
11:48:00	27.4	0.12	0.39	0.83	0.18
13:54:00	31.5	0.08	0.28	0.83	0.13
14:32:00	32.3	0.07	0.25	0.83	0.11
15:25:00	30.8	0.06	0.20	0.83	0.09
17:03:00	28.0	0.04	0.12	0.83	0.06
18:22:00	28.0	0.02	0.06	0.83	0.03

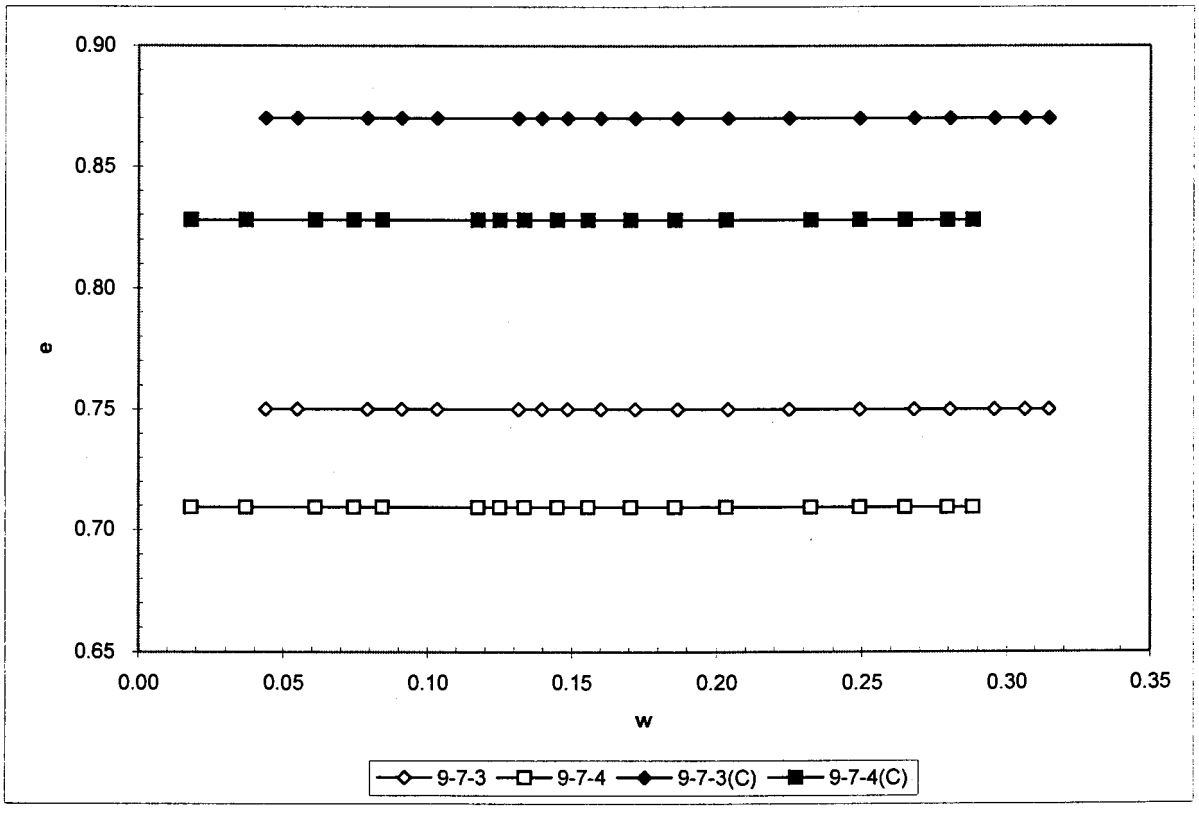

Figure A.4: Void ratio, e, versus moisture content, w (shrinkage curve)

A.5 Particle Size Range C (6<20)

Table A.13 to A.14 represents the data obtained from tests carried out on Range C tailings.

Figure A.5 represents void ratio, e, versus water content, w.

Table A.13: Corrected Test Data for Particle Size Range C (Sample 16-7-1)

Time (h:mm:ss)	Suction (kPa)	w -	S -	e -	θ -
1:38:00	16.1	0.34	0.98	0.95	0.48
1:41:00	23.1	0.34	0.97	0.95	0.47
1:43:00	28.7	0.34	0.97	0.95	0.47
1:58:00	87.4	0.33	0.95	0.95	0.46
2:24:00	89.8	0.32	0.91	0.95	0.44
3:24:00	96.0	0.29	0.82	0.95	0.40
3:45:00	97.2	0.27	0.79	0.95	0.39
4:14:00	97.8	0.26	0.75	0.95	0.37
5:32:00	105.6	0.22	0.64	0.95	0.31
8:03:00	117.9	0.15	0.44	0.95	0.21
8:42:00	120.8	0.14	0.39	0.95	0.19
10:43:00	149.0	0.08	0.24	0.95	0.12
12:46:00	377.7	0.03	0.09	0.95	0.05

Table A.14: Corrected Test Data for Particle Size Range C (Sample 16-7-4)

Time (h:mm:ss)	Suction (kPa)	w -	S -	e -	θ -
2:35:00	7.0	0.31	0.99	0.87	0.46
2:38:00	10.6	0.31	0.99	0.87	0.46
2:42:00	17.9	0.31	0.98	0.87	0.46
2:47:00	32.5	0.31	0.98	0.87	0.45
2:52:00	51.5	0.31	0.97	0.87	0.45
2:56:00	67.1	0.30	0.96	0.87	0.45
2:58:00	75.6	0.30	0.96	0.87	0.45
3:01:00	83.3	0.30	0.96	0.87	0.44
3:03:00	86.4	0.30	0.96	0.87	0.44
3:05:00	88.5	0.30	0.95	0.87	0.44
3:07:00	90.6	0.30	0.95	0.87	0.44
3:27:00	97.8	0.29	0.93	0.87	0.43
5:14:00	111.2	0.25	0.80	0.87	0.37
6:19:00	113.6	0.23	0.73	0.87	0.34
8:15:00	117.3	0.19	0.60	0.87	0.28
10:52:00	130.7	0.14	0.43	0.87	0.20
13:16:00	165.1	0.09	0.28	0.87	0.13
13:31:00	170.0	0.09	0.27	0.87	0.12
14:10:00	182.4	0.07	0.23	0.87	0.11
14:23:00	190.7	0.07	0.22	0.87	0.10
15:03:00	198.2	0.06	0.18	0.87	0.08
15:08:00	211.4	0.05	0.17	0.87	0.08
15:13:00	219.5	0.05	0.17	0.87	0.08
15:23:00	238.2	0.05	0.16	0.87	0.07
15:34:00	274.2	0.05	0.15	0.87	0.07
15:42:00	300.9	0.04	0.14	0.87	0.06
15:48:00	323.1	0.04	0.13	0.87	0.06
15:54:00	347.7	0.04	0.13	0.87	0.06
15:58:00	363.4	0.04	0.12	0.87	0.06
16:01:00	384.0	0.04	0.12	0.87	0.06

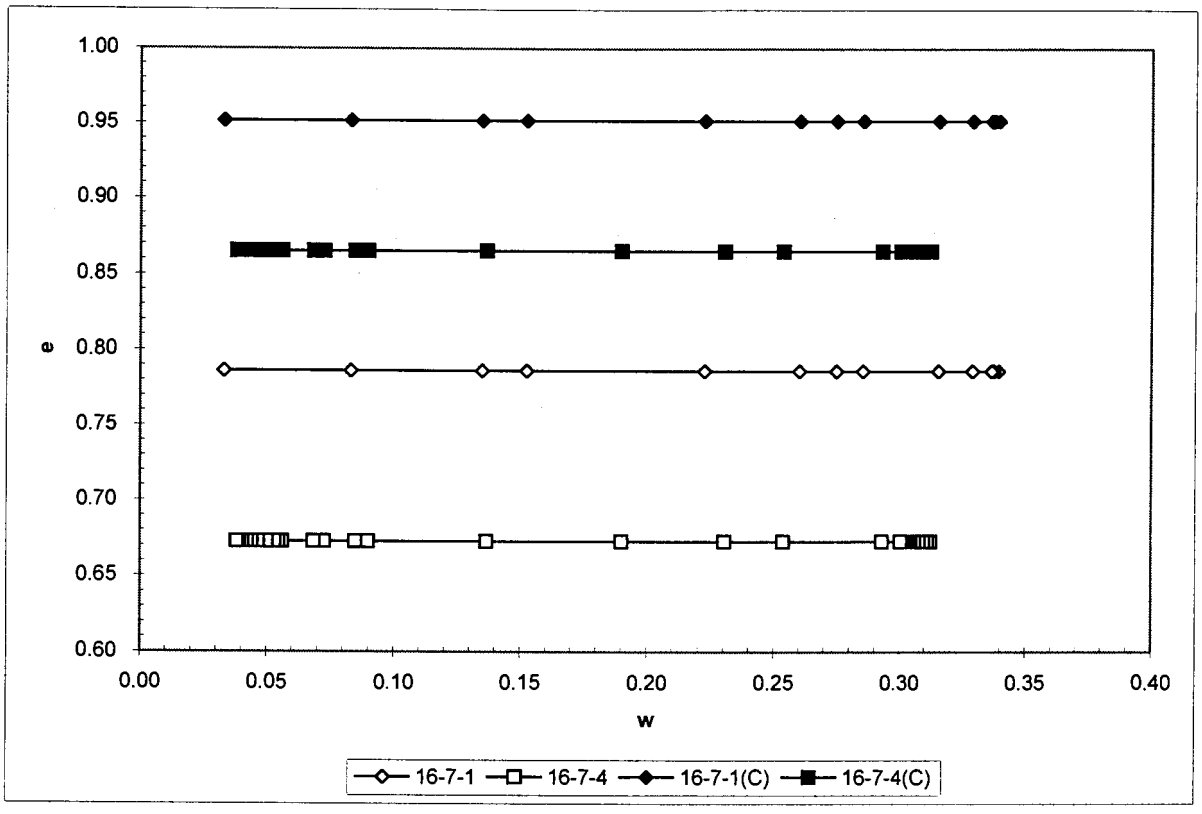

Figure A.5: Void ratio, e, versus moisture content, w (shrinkage curve)

A.6 Particle Size Range D (2<6)

Table A.15 to A.16 represents the data obtained from tests carried out on Range D tailings.

Figure A.6 represents void ratio, e, versus water content, w.

Table A.15: Corrected Test Data for Particle Size Range D (Sample 2-8-2)

Time (h:mm:ss)	Suction (kPa)	w -	S -	e -	θ -	LS (%)
6:30:00	5.0	0.42	1.00	1.14	0.53	0.00%
6:55:00	23.1	0.40	1.00	1.11	0.53	0.00%
7:14:00	42.2	0.40	1.00	1.08	0.52	0.00%
7:33:00	80.7	0.39	1.00	1.06	0.51	0.30%
7:52:00	126.3	0.38	0.99	1.04	0.51	0.69%
8:12:00	201.8	0.37	0.98	1.03	0.50	1.02%
8:34:00	297.4	0.36	0.97	1.01	0.49	1.29%
9:02:00	339.6	0.34	0.94	1.01	0.47	1.48%
9:32:00	340.2	0.33	0.90	1.00	0.45	1.52%
9:59:00	350.5	0.32	0.87	1.00	0.43	1.52%
10:25:00	357.1	0.31	0.83	1.00	0.42	1.52%
10:54:00	358.0	0.29	0.80	1.00	0.40	1.52%
11:35:00	368.0	0.27	0.74	1.00	0.37	1.52%

Table A.16: Corrected Test Data for Particle Size Range D (Sample 2-8-3)

Time (h:mm:ss)	Suction (kPa)	w -	S -	e -	θ -	LS (%)
6:47:00	5.6	0.39	1.00	1.07	0.52	0.00%
7:09:00	25.4	0.38	1.00	1.04	0.51	0.00%
7:27:00	48.1	0.37	1.00	1.02	0.50	0.00%
7:47:00	90.1	0.36	0.99	1.01	0.50	0.30%
8:07:00	149.1	0.35	0.98	0.99	0.49	0.57%
8:26:00	235.4	0.35	0.96	0.98	0.48	0.78%
8:51:00	331.6	0.33	0.94	0.97	0.46	0.99%
9:22:00	345.2	0.32	0.91	0.97	0.45	1.13%
9:48:00	351.6	0.31	0.88	0.97	0.43	1.16%
10:17:00	355.3	0.30	0.84	0.97	0.41	1.16%
10:44:00	365.6	0.28	0.81	0.97	0.40	1.16%
11:19:00	367.6	0.27	0.76	0.97	0.37	1.16%
11:53:00	382.2	0.25	0.72	0.97	0.35	1.16%

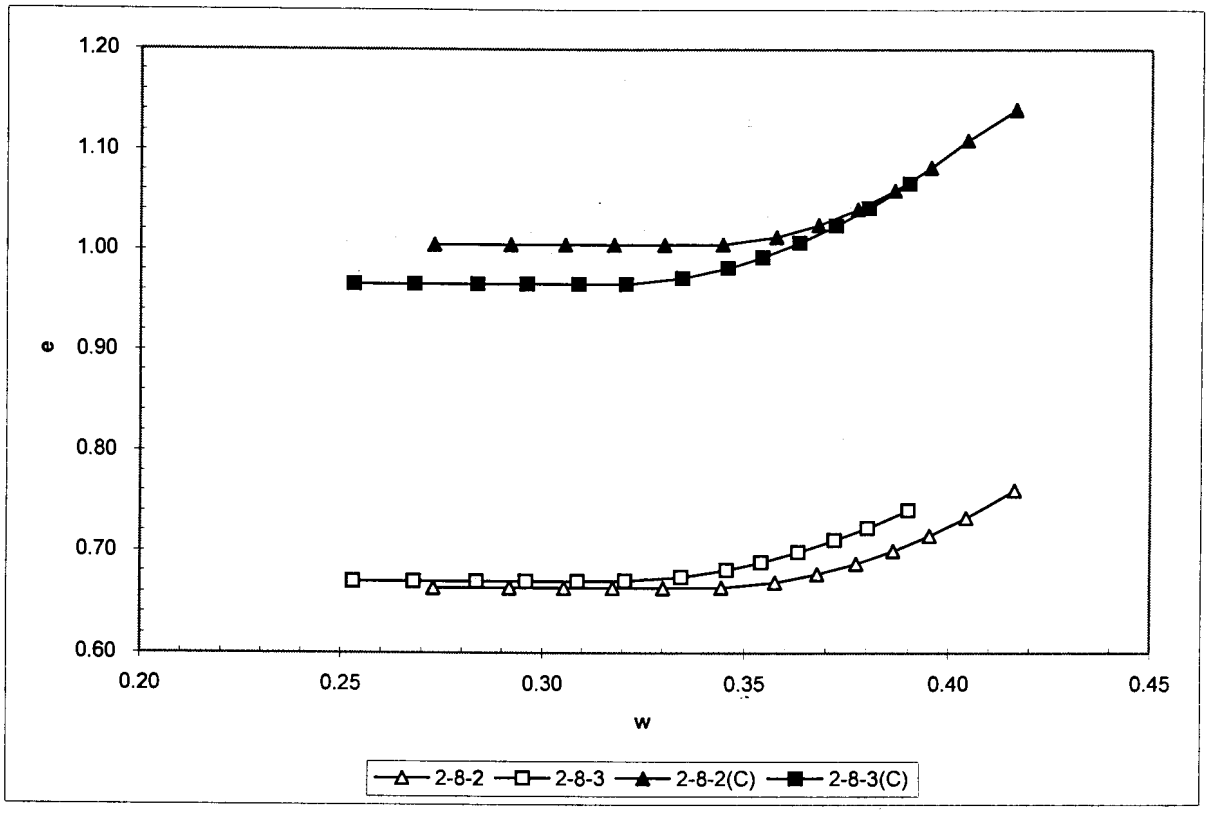

Figure A.6: Void ratio, e, versus moisture content, w (shrinkage curve)

A.7 Particle Size Range E (<2)

Table A.7 represents the data obtained from a test carried out on Range E tailings.

Figure A.7 represents void ratio, e, versus water content, w.

Table A.17: Corrected Test Data for Particle Size Range E (Sample 15-8-3)

Time (h:mm:ss)	Suction (kPa)	w -	S -	e -	θ -	LS (%)
5:34:00	1.0	0.46	1.00	1.27	0.56	0.00%
5:42:00	1.5	0.46	0.99	1.27	0.56	0.00%
5:50:00	3.0	0.46	0.99	1.26	0.55	0.00%
5:58:00	5.1	0.45	0.99	1.25	0.55	0.00%
6:32:00	12.7	0.44	0.98	1.23	0.54	0.00%
6:40:00	19.4	0.43	0.97	1.22	0.53	0.00%
6:49:00	26.7	0.43	0.97	1.21	0.53	0.00%
7:03:00	36.0	0.42	0.96	1.20	0.52	0.00%
7:09:00	46.7	0.42	0.96	1.20	0.52	0.01%
7:17:00	60.6	0.42	0.95	1.19	0.52	0.05%
7:25:00	77.2	0.41	0.95	1.19	0.52	0.10%
7:41:00	118.6	0.40	0.94	1.18	0.51	0.26%
7:46:00	138.3	0.40	0.94	1.18	0.51	0.32%
7:50:00	151.8	0.40	0.93	1.17	0.50	0.37%
7:56:00	173.1	0.40	0.93	1.17	0.50	0.46%
8:04:00	202.3	0.39	0.92	1.17	0.50	0.60%
8:23:00	284.4	0.39	0.91	1.16	0.49	0.99%
8:25:00	299.4	0.38	0.91	1.16	0.49	1.03%
8:27:00	316.1	0.38	0.91	1.16	0.49	1.08%
8:29:00	330.0	0.38	0.91	1.15	0.49	1.13%
8:31:00	341.2	0.38	0.91	1.15	0.49	1.18%
8:33:00	354.7	0.38	0.90	1.15	0.48	1.23%

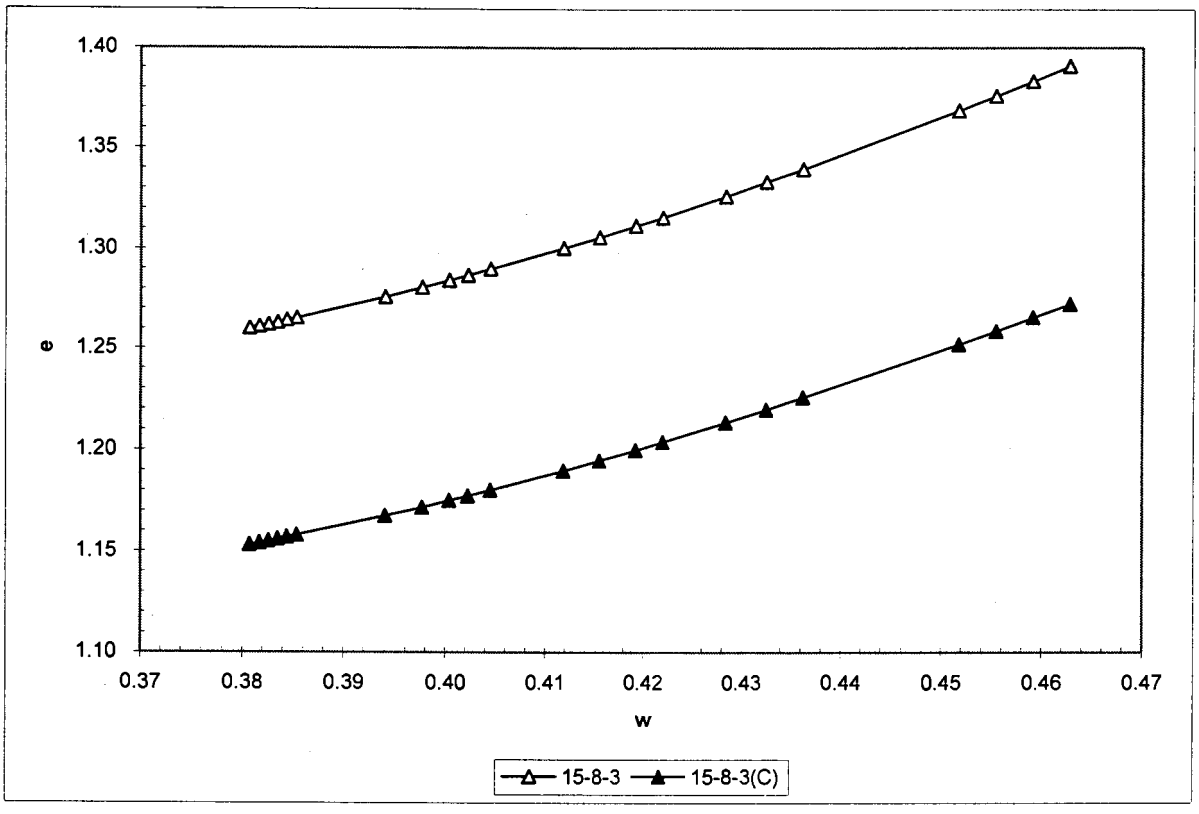

Figure A.7: Void ratio, e, versus moisture content, w (shrinkage curve)

A.8 New Sample A

Table A.18 represents the data obtained from a test carried out on Sample A tailings.

Figure A.8 represents void ratio, e, versus water content, w.

Table A.18: Corrected Test Data for New Sample A (Sample 20-8-2)

Time (h:mm:ss)	Suction (kPa)	w -	S -	e -	θ -	LS (%)
5:31:00	5.8	0.20	1.00	0.55	0.35	0.00%
5:48:00	27.3	0.20	0.99	0.54	0.35	0.00%
6:06:00	44.6	0.19	0.98	0.54	0.34	0.11%
6:21:00	67.2	0.19	0.97	0.53	0.34	0.33%
6:43:00	87.6	0.18	0.96	0.52	0.33	0.43%
7:02:00	89.2	0.18	0.95	0.52	0.32	0.45%
7:21:00	90.8	0.17	0.93	0.51	0.32	0.48%
7:39:00	91.4	0.17	0.92	0.51	0.31	0.49%
7:55:00	95.7	0.17	0.90	0.50	0.30	0.51%
8:12:00	99.5	0.16	0.88	0.50	0.30	0.52%
8:26:00	105.7	0.16	0.87	0.50	0.29	0.53%
8:43:00	110.9	0.15	0.85	0.50	0.28	0.54%
9:01:00	115.7	0.15	0.83	0.50	0.27	0.55%
9:26:00	123.7	0.14	0.79	0.50	0.26	0.56%
9:57:00	138.5	0.14	0.75	0.50	0.25	0.57%
10:15:00	142.1	0.13	0.73	0.50	0.24	0.57%
10:31:00	146.9	0.13	0.70	0.50	0.23	0.57%
10:49:00	155.1	0.12	0.68	0.50	0.23	0.57%
11:11:00	161.3	0.12	0.65	0.50	0.22	0.57%
11:38:00	176.0	0.11	0.61	0.50	0.20	0.57%
12:07:00	188.0	0.10	0.58	0.50	0.19	0.57%
12:30:00	202.0	0.10	0.54	0.50	0.18	0.57%
12:36:00	206.9	0.10	0.54	0.50	0.18	0.57%
12:42:00	211.0	0.10	0.53	0.50	0.18	0.57%
12:51:00	231.6	0.09	0.52	0.50	0.17	0.57%
12:56:00	236.7	0.09	0.51	0.50	0.17	0.57%
13:08:00	246.5	0.09	0.49	0.50	0.16	0.57%
13:20:00	257.0	0.09	0.48	0.50	0.16	0.57%
13:39:00	272.7	0.08	0.45	0.50	0.15	0.57%
13:56:00	279.6	0.08	0.43	0.50	0.14	0.57%
14:01:00	284.5	0.08	0.42	0.50	0.14	0.57%
14:09:00	291.1	0.07	0.41	0.50	0.14	0.57%
14:25:00	305.7	0.07	0.39	0.50	0.13	0.57%
14:36:00	319.6	0.07	0.38	0.50	0.12	0.57%
14:51:00	324.4	0.06	0.36	0.50	0.12	0.57%
14:58:00	331.6	0.06	0.35	0.50	0.11	0.57%
15:07:00	341.3	0.06	0.33	0.50	0.11	0.57%
15:15:00	353.5	0.06	0.32	0.50	0.11	0.57%

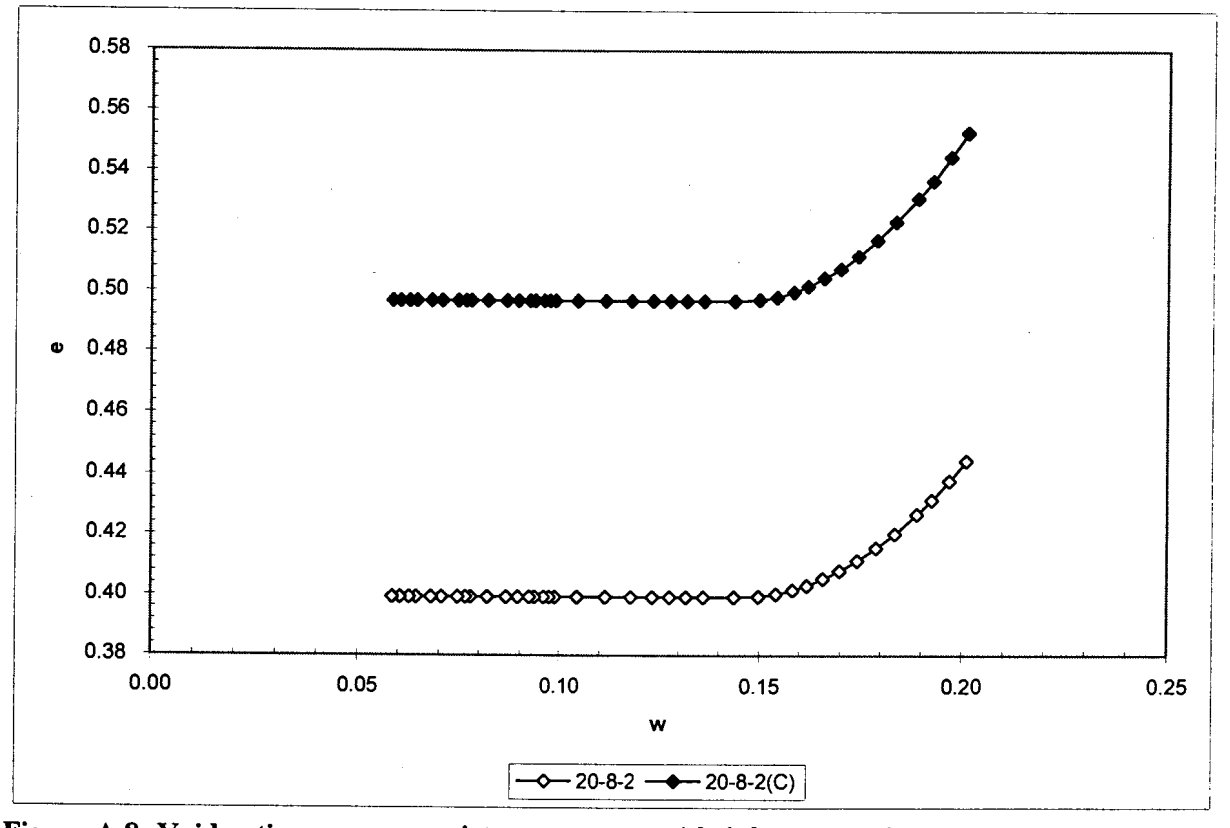

Figure A.8: Void ratio, e, versus moisture content, w (shrinkage curve)

A.9 New Sample C

Table A.19 represents the data obtained from a test carried out on Sample C tailings.

Figure A.9 represents void ratio, e, versus water content, w.

Table A.19: Corrected Test Data for New Sample C (Sample 20-8-1)

Time (h:mm:ss)	Suction (kPa)	w -	S -	e -	θ -	LS (%)
5:41:00	19.1	0.23	0.99	0.63	0.38	0.00%
5:57:00	31.7	0.22	0.99	0.62	0.38	0.00%
6:14:00	55.0	0.22	0.98	0.61	0.37	0.00%
6:32:00	56.3	0.21	0.97	0.60	0.36	0.04%
6:50:00	94.3	0.21	0.95	0.60	0.36	0.25%
7:08:00	108.0	0.20	0.94	0.59	0.35	0.42%
7:28:00	117.3	0.20	0.92	0.58	0.34	0.57%
7:45:00	123.8	0.19	0.91	0.58	0.33	0.66%
8:03:00	128.7	0.19	0.89	0.57	0.32	0.73%
8:20:00	145.4	0.18	0.87	0.57	0.32	0.76%
8:39:00	156.4	0.18	0.85	0.56	0.31	0.76%
8:52:00	173.4	0.17	0.84	0.56	0.30	0.76%
9:11:00	190.2	0.17	0.82	0.56	0.29	0.76%
9:29:00	205.4	0.16	0.79	0.55	0.28	0.76%
9:47:00	218.7	0.15	0.77	0.55	0.27	0.76%
10:13:00	247.6	0.15	0.73	0.55	0.26	0.76%
10:44:00	272.0	0.14	0.69	0.55	0.24	0.76%
11:01:00	278.8	0.13	0.66	0.55	0.24	0.76%
11:18:00	297.7	0.13	0.64	0.55	0.23	0.76%
11:34:00	300.4	0.12	0.61	0.55	0.22	0.76%
12:01:00	315.3	0.12	0.57	0.55	0.20	0.76%
12:30:00	331.9	0.11	0.53	0.55	0.19	0.76%
12:57:00	354.2	0.10	0.49	0.55	0.17	0.76%

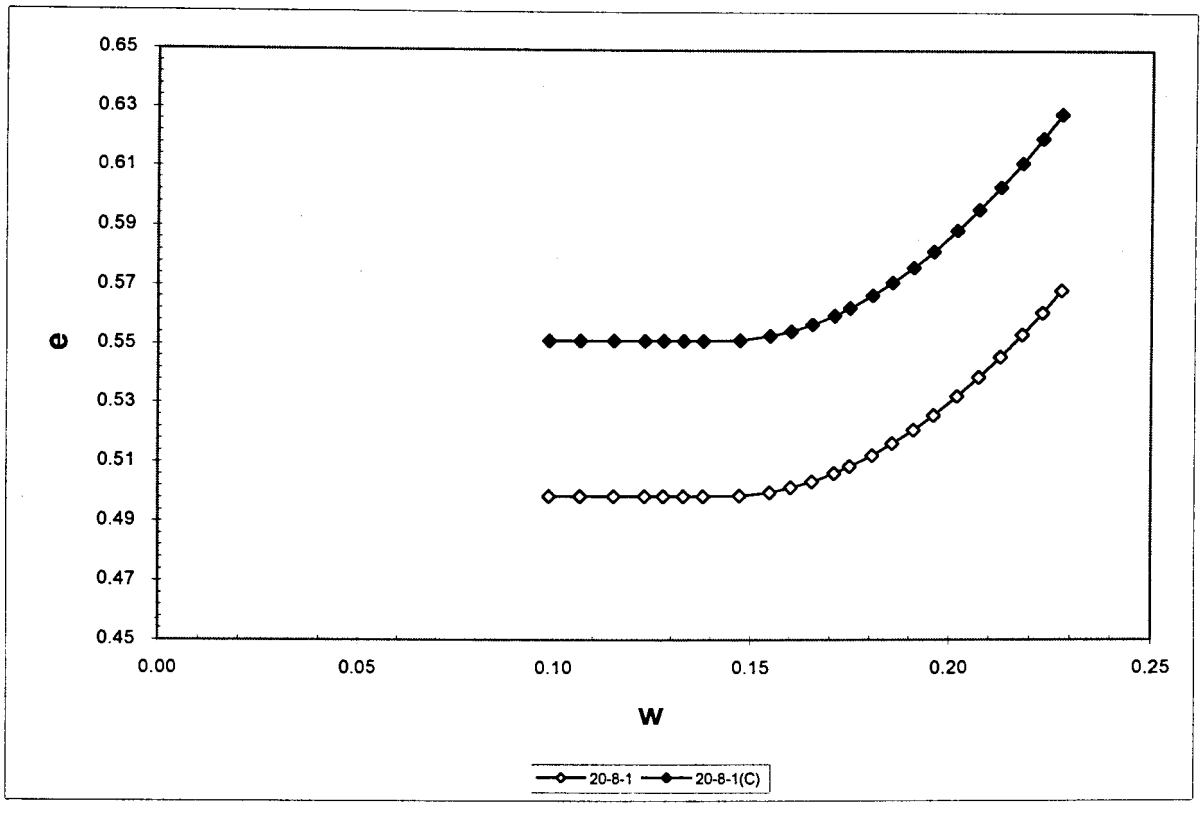

Figure A.9: Void ratio, e, versus moisture content, w (shrinkage curve)